K-ELECTRON CAPTURE TO POSITRON EMISSION RATIOS IN ALLOWED TRANSITIONS

MARGARET L. FITZPATRICK

DEPARTMENT OF NATURAL PHILOSOPHY

UNIVERSITY OF GLASGOW

Presented as a thesis for the degree of Ph.D.
in the University of Glasgow, November 1973.

C O N T E N T S

PREFACE

This thesis describes measurements of the K/β^+ ratios for the decays of ^{30}P and ^{91}Mo to the ground states of ^{30}Si and ^{91}Nb, respectively, and the ft values of the weak transitions to excited states of these nuclei. It also contains a review of all available experimental values of K/β^+ and ϵ/β^+ ratios for allowed transitions.

The work was carried out at the Kelvin Laboratory, University of Glasgow, between October 1969 and October 1973, excluding the period from October 1971 to January 1972.

The first chapter contains an introduction to beta decay theory. Orbital electron capture, particularly K-capture, is considered and a theoretical expression given for the ratio of K-electron capture to positron emission for allowed transitions.

The following chapter examines the agreement between experimental and theoretical values of the K/β^+ ratio for nuclei with $Z \lesssim 15$. The review of K/β^+ measurements in this region was carried out in collaboration with Dr K. W. D. Ledingham and Dr J. Y. Gourlay. The measurement of the K/β^+ for ^{30}P ratio described in this chapter was performed by Dr Gourlay and Dr Ledingham together with Dr J. G. Lynch. The present author assisted in the analysis of some of the data. A description of the ^{30}P experiment is included since it is typical of the low Z K/β^+ measurements and demonstrates the experimental techniques applicable in this region. The experimental K/β^+ ratios for the low Z region are compared with theoretical K/β^+ ratios calculated by the author and Dr Gourlay employing published tables of Fermi functions.

The measurement of the intensity of the weak transition of ^{30}P to the 2.23 MeV level in ^{30}Si is described in appendix 1. This work was carried out by Dr Gourlay, Dr Ledingham, Dr Lynch and the author and was a development of observations made during the ^{30}P K/β^+ measurement. The presence of a 680 keV peak seen in the gamma ray spectra from ^{30}P was attributed by the author to the summing of a 511 keV positron annihilation gamma ray with its backscattered partner.

A review of all available K/β^+ and ϵ/β^+ measurements for nuclei with $Z > 15$ is contained in chapter 3 and appendix 2. The author was solely responsible for the review of the experimental evidence. Comparison of these ratios with theoretical ratios shows a discrepancy between experiment and theory which is more pronounced at high values of Z.

The measurement of the total K/β^+ ratio for ^{91}Mo is described in chapter 4. This experiment was undertaken as a result of the apparent disagreement between experiment and theory revealed in the previous chapter. The experimental work was carried out jointly by the author and Dr Ledingham with assistance from Dr Lynch, Dr Gourlay and Mr M. Campbell. The author is solely responsible for the analysis of the data but must acknowledge the assistance given by Dr Gourlay in connection with the development of computer programs.

The following chapter examines the weak transitions from ^{91}Mo to excited states in the daughter nucleus, and log ft values for these transitions are calculated. The measurements of the efficiency of the Ge(Li) detector employed in this study of the gamma ray spectrum of ^{91}Mo were carried out by Mr Campbell. A value of the K/β^+ ratio for the decay of ^{91}Mo to the ground state of ^{91}Nb is derived from the total K/β^+ ratio

obtained in the previous chapter using the intensities of the weak transitions to excited states.

Chapter 6 compares the experimental and theoretical K/β^+ ratios for ^{91}Mo. A fairly large discrepancy between these ratios is observed. This is in agreement with the general trend observed in all the measurements considered in chapter 3. However, the existence of some exceptions to this general trend (e.g. ^{89}Zr and ^{111}Sn) and the possibility of systematics errors, particularly in the group of results around $Z = 60$, indicates the need for at least one accurate measurement of a K/β^+ ratio in the region above $Z = 30$. The experience gained from the ^{91}Mo experiment has been used in the choice of ^{120}Sb as a suitable isotope for a precision K/β^+ measurement.

PUBLICATIONS

The ratio of K-capture to positron emission in the decay of ^{30}P.

K. W. D. Ledingham, J. Y. Gourlay, J. L. Campbell,
M. L. Fitzpatrick, J. G. Lynch and J. McDonald.
Nucl. Phys. A 170 (1971) 663.

The weak positron transition in the decay of ^{30}P.

J. Y. Gourlay, K. W. D. Ledingham, M. L. Fitzpatrick
and J. G. Lynch.
J. Phys. A 6 (1973) 415.

K-electron capture to positron emission ratios in allowed transitions - a critical analysis.

M. L. Fitzpatrick, K. W. D. Ledingham, J. Y. Gourlay and
J. G. Lynch.
J. Phys. A 6 (1973) 713.

An earlier verison of this paper appeared in the proceedings of the Atlanta Conference on Inner Shell Ionisation Phenomena, April 1972, p. 2013.

ACKNOWLEDGMENTS

The author wishes to express her gratitude to Professor G. R. Bishop for his interest and assistance during the course of this work. In addition, the author thanks Professor J. C. Gunn and Professor P. I. Dee for their support.

The research was performed under the supervision of Dr K. W. D. Ledingham whose useful advice and encouragement the author gratefully acknowledges.

Considerable assistance was given by Dr J. Y. Gourlay, particularly in connection with the writing and development of computer programs.

The author would also like to thank Dr J. G. Lynch and Mr M. Campbell for their help during the ^{91}Mo experiment.

Much constructive advice was given by Dr W. P. S. Meikle whose diligent reading of the manuscript was of great assistance to the author.

The author's parents must be thanked for their continued kindness and support.

Assistance with drawing and photographing many of the diagrams was given by Mrs E. A. Taylor and the thesis was carefully typed by Mrs M. Shepherd.

During the first part of the work the author was in receipt of an SRC research studentship and was later given financial support by the University of Glasgow.

CHAPTER 1

INTRODUCTION

Measurements of the ratio of K-electron capture to positron emission (K/β^+) for allowed transitions have played an important part in the development of beta decay theory. Comparison of experimental and theoretical values of K/β^+ ratios has yielded information about the relative magnitudes of the five basic interactions, scalar (S), vector (V), tensor (T), axial vector (A) and pseudoscalar (P), which can contribute to the beta decay process (Joshi and Lewis, 1961, and Scobie and Lewis, 1957). Since the theoretical K/β^+ ratio depends on the K-shell electron wavefunction this comparison of experimental and theoretical ratios has also been used to test the K-shell wavefunctions or corrections to these wavefunctions arising from imperfect atomic overlap and electron exchange (Bahcall, 1965).

Beta Decay

The first successful beta decay theory was proposed by Fermi (1934) and is based on the assumption that beta decay is an exact analogue of the electromagnetic interaction. In the electromagnetic case a change of the atomic state leads to the emission of photons while in the beta interaction a change of the nuclear state leads to the emission of leptons (i.e. electrons, neutrinos and their corresponding antiparticles). The effect of beta decay in a nucleus can be represented by the following processes

$$n \rightarrow p + e^- + \bar{\nu} \qquad \text{electron emission } (\beta^-)$$

$$p \rightarrow n + e^+ + \nu \qquad \text{positron emission } (\beta^+)$$

where n, p, e^-, e^+, ν and $\bar{\nu}$ represent a neutron, proton, electron,

positron, neutrino and antineutrino, respectively. The extension of the theory to include electron capture can be made by taking into account the Dirac theory where the creation of a particle can be regarded as equivalent to the annihilation of the corresponding antiparticle. Thus positron emission is equivalent to the capture of an electron by a proton

$$p + e^- \longrightarrow n + \nu \qquad \text{electron capture.}$$

The theory of beta decay was developed by Yukawa and Sakata (1936), Bethe and Bacher (1936) and Møller (1937) to include the electron capture process.

Since the interaction responsible for beta decay is very weak, first order perturbation theory can be used to calculate the transition probability, T, from an initial state i to a final state f giving

$$T = \frac{2\pi}{\hbar} \left| \mathcal{H}_{if} \right|^2 \frac{dN}{dW} \qquad \text{equation (1)}$$

where $\mathcal{H}_{if}$ is the matrix element of the interaction responsible for the transition and dN/dW is the energy density of final available states. $\mathcal{H}_{if}$ can be written as

$$\mathcal{H}_{if} = \int H \, d\tau$$

where H is the beta decay interaction density.

The electromagnetic interaction can be described by the interaction of a current with a vector potential, the strength of the interaction being given by the elementary charge e. By analogy, in beta decay the current associated with the neutron-proton transition is given by

$$\psi_p^* \gamma_\mu \psi_n$$

where ψ_p and ψ_n are the wavefunctions of the proton and neutron, respec-

where ψ_p and ψ_n are the wavefunctions of the proton and neutron, respec-

Operator O_i	Relativistic transformation properties of $\psi_a^* \, O_i \, \psi_b$
1	Scalar (S)
γ_5	Pseudoscalar (P)
γ_μ	Vector (V)
$\gamma_\mu \gamma_5$	Axial Vector (A)
$\gamma_\mu \gamma_\rho$	Tensor (T)

TABLE 1.1

tively, and γ_μ is a four-vector defined by

$$\gamma_\mu = (-i\beta\alpha_x, -i\beta\alpha_y, -i\beta\alpha_z, \beta)$$

where α and β are the Dirac matrices (Schopper 1966). The symmetry of $p + e^- \rightarrow n + \nu$ in the nucleons and leptons suggests the form

$$\psi_e^* \gamma_\mu \psi_\nu$$

for the vector potential of the emitted lepton field. The resultant Hamiltonian is of the form

$$H = \frac{g}{\sqrt{2}} \left[(\psi_p^* \gamma_\mu \psi_n)(\psi_e^* \gamma_\mu \psi_\nu) + (\psi_n^* \gamma_\mu \psi_p)(\psi_\nu^* \gamma_\mu \psi_e) \right]$$

where g, the coupling constant, determines the strength of the interaction and the second term, which is the hermitian conjugate of the first, is added to ensure that the energy eigenvalues are real. The first term describes processes like

$$n + \nu \rightarrow p + e^-$$

and $n \rightarrow p + e^- + \bar{\nu}$

and the second term describes processes like

$$p + e^- \rightarrow n + \nu$$

and $p \rightarrow n + e^+ + \nu$

Terms of the form $\psi_a^* \gamma_\mu \psi_b$ can be generalised to $\psi_a^* O_i \psi_b$, where the O_i are various combinations of the γ matrices. There are only five distinct combinations and they can be grouped according to their properties under a Lorentz transformation (see table 1.1).

Five different interaction densities can, therefore, be formed

$$H_i = g_i \left[(\psi_p^* O_i \psi_n)(\psi_e^* O_i \psi_\nu) + \text{hermitian conjugate} \right]$$

with i = S, P, V, A and T (Konopinski and Langer, 1953). The general interaction is a linear combination of all five interactions

$$H = \sum_i g_i H_i = g \sum_i C_i H_i$$

where $g_i = gC_i$.

Since the scalar and pseudoscalar terms, and also the vector and axial vector terms, transform in the same way apart from a difference in sign, an equivalent set of interaction densities is given by

$$H_i' = g_i \left[(\psi_f^* O_i \psi_n)(\psi_e^* O_i \gamma_5 \psi_\nu) + \text{hermitian conjugate} \right]$$

Thus H may assume the more general form

$$H = g \sum_i (C_i H_i + C_i' H_i') \qquad \text{equation (2).}$$

This general beta decay Hamiltonian is not invariant with respect to space inversion, i.e. it does not conserve parity. C and C' are the coupling constants of the parity-conserving and parity-nonconserving interactions, respectively.

In 1956, Lee and Yang examined all previous experimental results on weak interactions and concluded that there was no evidence for or against parity conservation. They showed that the question of parity conservation in beta decay could be settled only by forming a pseudoscalar from experimentally measured quantities. The reason is that only pseudoscalars contain terms of the form CC', representing interference between the parity-conserving and parity-nonconserving interactions. One of the experiments suggested by Lee and Yang was a measurement of the angular distribution of the electrons from the beta decays of polarized nuclei. The quantity $\underline{p} \cdot \underline{\sigma}$, where $\underline{p}$ is the momentum of the electron and $\underline{\sigma}$ is the nuclear spin, is a pseudoscalar since, under the parity operation, $\underline{p} \rightarrow -\underline{p}$ and $\underline{\sigma} \rightarrow \underline{\sigma}$. Therefore, an asymmetry in the angular distribution would prove that parity is

not conserved in beta decay.

Wu et al. (1957) measured the angular distribution of the electrons from the beta decay of polarized ^{60}Co nuclei and found that the electrons were emitted preferentially in the direction opposite to that of the ^{60}Co nuclear spin. This shows that parity is not conserved and the most general form of the beta decay Hamiltonian is, therefore, given by equation (2).

Allowed Beta Decay

Since the neutrino has practically no interaction with matter (e.g. Reines and Cowan, 1959) it can be represented by a plane wave

$$\psi_\nu \sim \exp(ik_\nu.r)$$

where k_ν is the wave vector of the neutrino ($k_\nu\hbar = q$ = neutrino momentum). The wavefunction of the electron can also be represented by a plane wave if the distortion of the wavefunction by the nuclear charge is neglected

$$\psi_e \sim \exp(ik_e.r).$$

In the calculation of the transition matrix elements, integration over only the nuclear volume is required since the nuclear wavefunctions are zero outside the nucleus. The lepton wavefunctions are, therefore, required only for $0 \leq r \leq R$ (R = nuclear radius $\sim 10^{-12}$ cm). For 1 MeV electrons and neutrinos $(k_e + k_\nu)R \sim 0.1$. The transition probability, therefore, contains terms

$$\exp\left[i(k_e + k_\nu).r\right]$$

which can be expanded as a series of terms corresponding to different orbital angular momenta of the leptons, consecutive terms in the expansion differing by a factor $(k_e + k_\nu)^2R^2$. The terms, therefore,

ΔI	Parity change	Type of transition
0, ± 1	No	Allowed
0, ± 1	Yes	First forbidden
± 2	Yes	Unique first forbidden
± 2	No	Second forbidden
± 3	No	Unique second forbidden
± 3	Yes	Third forbidden
± 4	Yes	Unique third forbidden
± 4	No	Fourth forbidden

TABLE 1.2

decrease rapidly with increasing angular momentum.

Transitions in which the leptons do not carry away orbital angular momentum are called allowed. These are described by taking only the first term in the expansion. The allowed decays are divided into Fermi decays, in which the leptons are emitted with their spins anti-parallel, and the Gamow-Teller decays, in which the leptons have parallel spins. Thus in Fermi decays the total angular momentum removed by the leptons is zero and in Gamow-Teller decays the leptons carry away one unit of angular momentum. There is no change in parity between the initial and final nuclear states in allowed transitions since the leptons do not remove any orbital angular momentum.

Transitions associated with higher terms in the expansion are called forbidden. The selection rules for allowed and forbidden transitions are shown in table 1.2.

For allowed decays, the scalar (S) and vector (V) interactions can both give rise to Fermi decays while the tensor (T) and axial vector (A) interactions can give rise to Gamow-Teller decays. The pseudo-scalar (P) interaction does not contribute to allowed decays since it requires a parity change. The possibility of interference between the S and V interactions and, separately, between the T and A interactions is described by the Fierz interference term, b (Fierz, 1937).

$$b = \frac{(C_S C_V + C_S' C_V')\left|M_F\right|^2 + (C_T C_A + C_T' C_A')\left|M_{GT}\right|^2}{(C_S^2 + C_V^2 + C_S'^2 + C_V'^2)\left|M_F\right|^2 + (C_T^2 + C_A^2 + C_T'^2 + C_A'^2)\left|M_{GT}\right|^2}$$

where M_F and M_{GT} are the Fermi and Gamow-Teller matrix elements, respectively (e.g. Lee and Yang, 1956) and the nuclear matrix element

M is defined by

$$|M|^2 = C_F |M_F|^2 + C_{GT} |M_{GT}|^2 .$$

A comparison of experimental and theoretical K/β^+ ratios can be used to determine the magnitude of b since

$$b = \frac{R - R_o}{R_o + R\langle 1/W \rangle}$$

where $\langle 1/W \rangle$ is the average of 1/W (W is the energy of the beta particle). R and R_o are the experimental and theoretical values of the K/β^+ ratio, R_o being calculated assuming b = 0.

The evidence from a comparison of experimental and theoretical K/β^+ ratios indicates that b is very small. Sherr and Miller (1954) found b to have a value of -0.02 ± 0.04 for ^{22}Na. This is a pure Gamow-Teller transition and, therefore, the Fierz interference term describes here interference between the T and A interactions only. Drever et al. (1956) also determined b for a pure Gamow-Teller decay, ^{18}F, by measuring the K/β^+ ratio and they found b = 0.008 ± 0.04. Konijn et al. (1958/59) measured the K/β^+ ratios for the decays of ^{22}Na, ^{48}V, ^{52}Mn, ^{58}Co and ^{57}Ni and obtained a mean value of -0.007 ± 0.010 for b. From a measurement of the K/β^+ ratio for ^{11}C, a predominantly Fermi decay, Scobie and Lewis (1957) estimated b to be 0.03 ± 0.10.

Lee and Yang (1957), Landau (1957), and Salam (1957) introduced a two-component neutrino theory which required the neutrino rest mass to be zero and the spin to be either parallel or anti-parallel to the direction of motion. ψ_ν can be written as

$$\psi_\nu = \tfrac{1}{2}(1 + \gamma_5)\psi_\nu + \tfrac{1}{2}(1 - \gamma_5)\psi_\nu$$

The first term $\frac{1}{2}(1 + \gamma_5)$ is the projection operator for left-handed

particles (i.e. particles with spin opposite to the direction of motion) and $\frac{1}{2}(1 - \gamma_5)$ is the projection operator for right-handed particles. It was shown experimentally by Goldhaber et al. (1958) that the neutrino is left-handed (i.e. has negative helicity), and, therefore, ψ_ν can be replaced by

$$\tfrac{1}{2}(1 + \gamma_5)\,\psi_\nu$$

Experimental evidence indicates that electrons emitted in beta decay have negative helicity and positrons have positive helicity (Frauenfelder et al., 1957, Frauenfelder and Steffen, 1965). Thus ψ_e can be replaced by

$$\tfrac{1}{2}(1 + \gamma_5)\,\psi_e = a\,\psi_e$$

where $a = \frac{1}{2}(1 + \gamma_5)$ and $a^* = \frac{1}{2}(1 - \gamma_5)$.

Feynman and Gell-Mann (1958) suggest applying the same rule to the wave-functions of all the particles in the beta decay giving an interaction of the form

$$\sum_i C_i \left\{(a\psi_p)^*\, O_i\, a\psi_n\right\}\left\{(a\psi_e)^*\, O_i\, a\psi_\nu\right\}$$

Since $(a\psi)^* = \psi^* a^*$ each term contains $a^* O_i a$. For the S, T and P interactions this reduces to zero and only the V and A terms can exist. This is known as the V-A theory of beta decay. In this theory the Fierz interference term b is identically equal to zero.

Electron-neutrino correlation measurements (e.g. Johnson et al., 1963 and Carlson, 1963) have shown that any contribution to beta decay from the scalar and tensor interactions is very small. The experimental results are in very good agreement with a pure V-A interaction and the coupling constants C_F and C_{GT} can, therefore, be identified with C_V and C_A, respectively.

The form of dN/dW, the energy density of available final states, can be determined from the assumption that the energy of the transition is shared statistically among the decay products, i.e. the probability of a decay leading to a given group of final states is proportional to the number of these states.

The probability of emission of an electron with energy in the range W to W + dW per unit time is

$$N(W)dW = \frac{g^2}{2\pi^3} |M|^2 F(\mp Z,W) pW(W_o - W)^2 \, dW \qquad \text{equation (3)}$$

where p = electron momentum in units of $m_o c$

$W = \sqrt{p^2 + 1}$ = total electron energy in units of $m_o c^2$

W_o = maximum value of W

$W_o - W$ = neutrino energy (or momentum) in units of $m_o c^2$ (or $m_o c$)

Z = atomic number of daughter nucleus.

The Fermi function, $F(\mp Z,W)$ takes into account the distortion of the wavefunction of the emitted beta particle by the nuclear charge. The minus and plus signs refer to β^+ and β^- emission, respectively. Tables of Fermi functions including the effects of finite size of the nucleus and the screening of the nucleus by the orbital electrons have been published by Behrens and Jänecke (1969).

The probability that a nucleus undergoes an allowed beta decay per unit time is given by λ where

$$\lambda = \int_1^{W_o} N(W)dW$$

$$= \frac{g^2}{2\pi^3} |M|^2 f(Z,W_o)$$

with $$f(Z,W_o) = \int_1^{W_o} pW(W_o - W)^2 F(\mp Z,W)dW.$$

This assumes that the nuclear matrix element M does not depend on W.

The half life t of a transition is given by

$$t = \frac{\ln 2}{\lambda}$$

Therefore,

$$f(Z,W_o)t = \frac{2\pi^3 \ln 2}{g^2|M|^2}$$

This quantity, ft, is called the comparative half life. The ft values for allowed transitions are found to fall into two groups, one with log ft values in the region from about 4.0 to 7.0 and the other with log ft values around 3.5. The transitions in this latter group are called superallowed. For these transitions the nuclear matrix element M, which measures the overlap of the initial and final nuclear wavefunctions, is large due to the similarity of these wavefunctions. The mirror transitions ($N - Z = \pm 1$ for both initial and final nuclei) fall into this category. The $0^+ - 0^+$ transitions are also superallowed. For these transitions only the Fermi matrix element can contribute according to the selection rules, therefore

$$|M|^2 = C_V^2 \, |M_F|^2.$$

Since the matrix element M_F is equal to $\sqrt{2}$ (Schopper, 1966) the value of the vector coupling constant can be found from the ft value for a $0^+ - 0^+$ transition.

From equation (3) it is apparent that a graph of $\left[N(W)/F(\mp Z,W)pW\right]^{\frac{1}{2}}$ against W should be a straight line. This graph is known as a Kurie plot and extrapolation of the line can be used to determine the β particle end point energy, W_o.

Orbital Electron Capture

Orbital electron capture was first detected experimentally by Alvarez (1937, 1938). He observed titanium K x-rays emitted during the atomic rearrangement following the capture of K-shell electrons in ^{48}V.

The main difference between orbital electron capture and β emission lies in the fact that the electron wavefunction for electron capture corresponds to a bound atomic state compared with the free particle wavefunction for β emission. Therefore, for capture from a given shell, the electron energy has a unique value.

The energy (q) available to the neutrino in electron capture from the n^{th} shell for a nuclear mass difference W_o is

$$q = W_o + W_n = W_o + 1 - B$$

where B is the atomic binding energy of the captured electron and $W_n = 1 - B$ is the total energy of an electron in the n^{th} shell. All energies are given here in units of $m_o c^2$.

The probability of K-electron capture in an allowed decay is

$$\lambda_k = \frac{g^2}{4\pi^2} |M|^2 q^2 g_K^2$$

where g_K is the large component of the Dirac K-electron wavefunction evaluated at the nuclear radius. Graphical representations of K and L shell electron radial wavefunctions, taking into account screening and finite nuclear size, were published by Brysk and Rose (1955, 1958). Band et al. (1956, 1958) calculated wavefunctions for K and L capture by integrating the Dirac equation with a uniform charge distribution inside the nucleus and a Thomas-Fermi-Dirac potential outside the nucleus. L_1/K electron capture ratios were obtained by Winter (1968)

using analytical Hartree-Fock wavefunctions. The results he obtained are in good agreement with Band et al. but not with Brysk and Rose. Suslov (1968) and Zyrianova and Suslov (1968) obtained electron radial wavefunctions by numerical integration of the Dirac equation using a nonrelativistic Hartree-Fock-Slater potential for $13 \leq Z \leq 73$ and a relativistic potential for $74 \leq Z \leq 98$. Finite nuclear size was included by treating the nucleus as a uniformly charged sphere. Behrens and Jänecke (1969) give tables of electron radial wavefunctions, at the nuclear radius, of K, L and M electrons for all values of Z. The wavefunctions were calculated by integrating the Dirac equation with a uniform charge distribution inside the nucleus and with a Hartree-Fock potential ($Z \leq 36$) or a Thomas-Fermi-Dirac potential ($Z > 36$) outside the nucleus. Electron radial wavefunctions have also been calculated by Martin and Blichert-Toft (1970) by solving the Dirac equation with a Hartree self-consistent potential.

K-Electron Capture to Positron Emission Ratios

For an allowed transition in which positron emission is energetically possible, electron capture is also a possible decay process and the ratio of K-electron capture to positron emission is given by

$$K/\beta^+ = \frac{\pi (W_o + W_K)^2 g_K^2}{2\int_1^{W_o} pW(W_o - W)^2 F(-Z,W)dW} \qquad \text{equation (4)}$$

This ratio is independent of the nuclear matrix element M and depends on the K-electron wavefunction, g_K. In the calculations of theoretical K/β^+ ratios in this thesis, the electron radial wavefunctions, the Fermi functions and electron binding energies given by Behrens and Jänecke (1969) have been used.

Corrections to the Theoretical K/β^+ Ratio

Benoist-Gueutal (1950, 1953) and Odiot and Daudel (1956) showed that, for an exact treatment of electron capture processes, it is necessary to include corrections due to an exchange interaction between the captured electron and electrons in other shells. This arises because of the indistinguishability of the atomic electrons, which means that it is not possible to identify the electron which disappears in K-capture with an electron initially present in the K-shell of the parent nucleus. Also, since the nuclear charge changes by one unit as a result of electron capture, the initial and final atomic states do not overlap perfectly.

Bahcall (1962, 1963 a, b, c and 1965) has calculated the effect of exchange and imperfect atomic overlap on electron capture probabilities for a range of values of Z. The calculations of Benoist-Gueutal and Odiot and Daudel were complicated by the fact that an infinite number of final states must be taken into account. Bahcall showed (1963 c), by explicit calculation of one-electron overlap integrals using Hartree-Fock wavefunctions, that the inner atomic electrons are almost inert (i.e. the overlap integrals are approximately unity) if they are not captured. He also showed that the probability of an outer electron (i.e. outside the 3s shell) in the initial atom jumping to an inner level in the final atom is very small. It follows that the atomic state vectors can be separated into two practically independent parts, one representing the inner electrons and the other representing the outer electrons. The outer electron states form an almost complete set since the only states in the final atom not available to the outer electrons are the few inner electron states.

Bahcall's corrections to K-electron capture arise from the fact that a vacancy in the K-shell of the final atom can occur in three experimentally indistinguishable ways.

(1) annihilation of a 1s electron in the initial atom with the 2s and 3s electrons appearing in the 2s' and 3s' states in the final atom

(2) annihilation of a 2s electron with a 1s electron jumping into the 2s' state in the final atom

(3) annihilation of a 3s electron with a 1s electron jumping into the final 3s' state.

Therefore, the amplitude for the production of a hole in the final 1s' shell is

$$f(1s') = \langle 2s' \mid 2s \rangle \langle 3s' \mid 3s \rangle \ \psi_{1s}(0)$$
$$- \langle 2s' \mid 1s \rangle \langle 3s' \mid 3s \rangle \ \psi_{2s}(0)$$
$$- \langle 3s' \mid 1s \rangle \langle 2s' \mid 2s \rangle \ \psi_{3s}(0)$$

where the atomic matrix elements $\langle ns' \mid ms \rangle$ represent the overlap of the ms wavefunction of an electron in the initial atom with the ns' wavefunction of an electron in the finalatom. The integrals of the type $\langle ms' \mid ms \rangle$ are called overlap integrals while those of the type $\langle ns' \mid ms \rangle$ are called exchange integrals. The $\psi_{ms}(0)$ are one-electron wavefunctions evaluated at the nucleus.

In the theory without exchange and overlap corrections

$$f(1s') = \psi_{1s}(0)$$

The exchange-overlap correction to K-electron capture is B_K, defined by

$$B_K = \left| \frac{f(1s')}{\psi_{1s}(0)} \right|^2$$

The integrals $\langle ns' \mid ms \rangle$ were evaluated by Bahcall using the analytic Hartree-Fock wavefunctions of Watson and Freeman (1961). According to Bahcall, his calculations of B_K are not valid for values of $Z < 15$ and the fact that B_K tends to unity as Z increases reflects the increasing similarity of the initial and final atoms. Bahcall gives the following formula which can be used to calculate values of B_K with an accuracy of about 2 per cent

$$B_K = 1 - 0.929Z^{-1} + 20.98Z^{-2} - 316.5Z^{-3}$$

The effect of these exchange-overlap corrections on K/β^+ ratios is given by

$$(K/\beta^+)_{\text{corrected}} = (K/\beta^+)^\circ \, B_K$$

where $(K/\beta^+)^\circ$ is the usual uncorrected theoretical K-electron capture to positron emission ratio.

Similar exchange-overlap corrections must be made to L_1 and M_1 capture. For example, in the case of L_1 capture, the amplitude for the production of a hole in the final 2s' shell is

$$\begin{aligned} f(2s') = {} & \langle 1s' \mid 1s \rangle \langle 3s' \mid 3s \rangle \psi_{2s}(0) \\ & - \langle 1s' \mid 2s \rangle \langle 3s' \mid 3s \rangle \psi_{1s}(0) \\ & - \langle 3s' \mid 2s \rangle \langle 1s' \mid 1s \rangle \psi_{3s}(0) \end{aligned}$$

and in the theory without corrections

$$f(2s') = \psi_{2s}(0)$$

The exchange-overlap correction to L_1-capture is

$$B_{L_1} = \left| \frac{f(2s')}{\psi_{2s}(0)} \right|^2$$

The exchange-overlap correction to L_1/K capture ratios is

Z	Bahcall	Suslov	Faessler et al.	Martin and Blichert-Toft	Vatai
13				0.975	0.987
14	0.924	0.9231		0.976	0.988
15	0.939	0.9391		0.977	0.988
16	0.947	0.9479		0.978	0.988
17	0.954	0.9542		0.979	0.988
18	0.959	0.9589	0.960	0.980	0.988
19	0.963	0.9600		0.981	0.988
20	0.966	0.9650		0.982	0.989
21	0.969	0.9667		0.982	0.989
22	0.970	0.9690		0.982	0.989
23	0.973	0.9710	0.973	0.983	0.990
24	0.974	0.9742		0.984	0.990
25	0.976	0.9731		0.985	0.990
26	0.977	0.9759		0.985	0.991
27	0.978	0.9770		0.986	0.991
28	0.980	0.9783		0.986	0.991
29	0.981	0.9800		0.986	0.991
30	0.981	0.9794		0.987	0.991
31	0.981	0.9800		0.987	0.992
32	0.982	0.9805		0.988	0.992

TABLE 1.3 - EXCHANGE CORRECTIONS B_K

$$X^{L/K} = \frac{B_{L_1}}{B_K}$$

and the corrected theoretical L_1/K capture ratio is

$$(L_1/K)_{corrected} = (L_1/K)^o \, X^{L/K}$$

where $(L_1/K)^o$ is the uncorrected theoretical ratio.

It has been pointed out (Zyrianova and Suslov, 1968, and Fink, 1968) that Bahcall's exchange-overlap corrections to L_1/K and M_1/L_1 capture ratios result in theoretical values which are a few percent larger than experiment.

The Watson-Freeman wavefunctions used by Bahcall do not take into account relativistic and nuclear size effects. However, Bahcall estimates that these effects are relatively unimportant for exchange-overlap corrections.

Suslov (1970) obtained relativistic estimates of exchange-overlap effects in electron capture. He used wavefunctions obtained by numerical integration of the Dirac equation, with a non-relativistic self-consistent Hartree-Fock-Slater potential for $13 \leq Z \leq 73$, and an analogous relativistic potential for $Z > 74$. The finite size of the nucleus was included by considering the nucleus to be a uniformly charged sphere.

The values of B_K obtained by Suslov are very similar to those obtained by Bahcall (Table 1.3). Bahcall has calculated B_K only for $14 \leq Z \leq 37$. Suslov's calculations extend up to $Z = 98$, but are not shown for every value of Z above 40 since they change very little with Z in this region.

Faessler et al. (1970) recalculated the Bahcall corrections for

Z	Bahcall	Suslov	Faessler et al.	Martin and Blichert-Toft	Vatai
33	0.982	0.9810		0.988	0.992
34	0.983	0.9817		0.988	0.992
35	0.983	0.9822		0.989	0.992
36	0.984	0.9826		0.989	0.992
37	0.984	0.9831		0.989	0.993
38		0.9835		0.990	
39		0.9840		0.990	
40		0.9844		0.990	
50		0.9878		0.991	
60		0.9888		0.992	
70		0.9896		0.992	
80		0.9898		0.992	
90		0.9899		0.992	

TABLE 1.3 (continued)

EXCHANGE CORRECTIONS B_K

light atoms using the Hartree-Fock-Slater functions of Herman and Skillman (1963) and the Hartree-Fock functions of Froese (1965, 1969). The latter calculation was carried out only for Z = 4, 18 and 23. The values of B_K obtained with the Herman-Skillman wavefunctions are also shown in table 1.3 and are seen to be in good agreement with Bahcall.

In Bahcall's calculations the electron wavefunctions of the ground states of the initial and final atoms were used. However, Vatai (1968) pointed out that, after electron capture, the final atom is in an excited state with a vacancy in one of the inner shells.

Vatai (1970) examined the approximations made in Bahcall's calculations of exchange-overlap corrections to electron capture. He noted that, in these calculations, the disappearance of a proton charge had been taken into account but that the disappearance of the captured electron's charge had been neglected. Due to the screening effect before capture, the actual change in potential during the capture process is less than the change which would be caused by the removal of the proton charge alone. The effect of the exchange-overlap corrections calculated by Vatai is, therefore, smaller than that due to Bahcall's corrections. Vatai used the analytic one-electron wavefunctions of Watson and Freeman (1960, 1961) to describe the initial state and as a basis for the calculation of the wavefunctions of the final state by first order perturbation theory.

The values of B_K calculated by Vatai are shown in table 1.3. Vatai has calculated B_K for $13 \leq Z \leq 37$ and also gives expressions which can be used to extrapolate the results into the regions below Z = 13 and above Z = 37. It is clear that, for all values of Z, the values of B_K

given by Vatai are larger than those given by Bahcall, Suslov and Faessler et al.

Faessler et al. (1970) have also recalculated exchange-overlap corrections taking into account the fact that the final atom is left in an excited state, as suggested by Vatai (1968). They do not give values of B_K calculated in this way but their values of $X^{L/K}$, the exchange-overlap correction to L_1/K ratios, are in fairly good agreement with those of Vatai and are smaller than the corresponding corrections given by Bahcall.

Exchange-overlap corrections have also been calculated by Martin and Blichert-Toft (1970) using wavefunctions obtained by solving the Dirac equation with a Hartree self-consistent potential. The values of B_K which they obtained are shown in table 1.3.

The values of B_K calculated by those various authors fall into two groups, with one group based on Bahcall's theory of exchange and overlap and the other based on Vatai's. The disagreement between the two sets of results is most pronounced at low values of Z. The lowest value of Z for which the two theories can be directly compared is Z = 14. Vatai gives a formula which may be used to extrapolate his results to lower values of Z but Bahcall gives no such extrapolation.

A comparison of experimental and theoretical K/β^+ ratios for isotopes with low atomic number is given in chapter 2 where the question of exchange-overlap corrections to K-electron capture is considered.

CHAPTER 2

K-ELECTRON CAPTURE TO POSITRON EMISSION RATIOS FOR LIGHT ISOTOPES

The importance of measurements of K/β^+ ratios for allowed transitions in the low Z region in giving information about the magnitude of exchange-overlap corrections has been described in chapter 1. This chapter describes the techniques used to measure K/β^+ ratios in this region and also reviews all available experimental results.

TECHNIQUES FOR MEASURING K/β^+ RATIOS FOR LOW Z NUCLEI

1 Direct Measurements

K-electron capture is observed experimentally by the detection of the K x-rays and Auger electrons emitted when the K shell vacancies produced by orbital electron capture are filled.

Detectors with external sources are not suitable for observing K-capture events in low Z nuclei because the energy of these events (K x-rays and Auger electrons) is so low that absorption in the detector window is a limiting factor. Internal source proportional counters (Drever et al. 1956) and scintillation counters (McCann and Smith 1969) have been used successfully to detect K-capture events.

For light isotopes the K/β^+ ratio is generally very small (e.g. $K/\beta^+ = 0.00168$ for ^{13}N) and it is difficult to detect the low intensity, low energy K-capture events against the high background caused by the positrons. To overcome this difficulty a proportional counter, with an internal gaseous source, surrounded by an anti-coincidence counter has been used for many K/β^+ measurements. One such counter, known as the plastic counter (Moljk et al. 1958), consists of a central proportional counter surrounded by a plastic

scintillation counter. In this arrangement the gaseous source is mixed with the normal proportional counter filling gas. Both the positrons and electron capture events are detected in the central counter but only the positrons have sufficient energy to be detected in the outer counter. If events from the proportional counter are taken in anti-coincidence with those from the surrounding plastic scintillator the resulting spectrum consists mainly of an electron capture peak. The K/β^+ ratio can then be calculated from the total counting rate of positrons plus K-capture events in the proportional counter and the number of K-events in the anti-coincidence spectrum.

A similar type of detector, the multiwire counter (Scobie and Lewis, 1957), consisting of a central proportional counter surrounded by a ring of proportional counters, has also been used to measure K/β^+ ratios for light isotopes.

Since the half lives of many of the light isotopes of interest are short, continuous production of the source during the measurement is desirable. For this reason the plastic counter was modified to allow a continuous flow of the gaseous source through the central proportional counter (Campbell et al. 1967).

This method cannot, of course, be used for nuclei of which no suitable gaseous form exists. For these isotopes it may be possible to grow NaI (Tl) crystals with a trace of the radioactive source. This technique has been applied to ^{22}Na (McCann and Smith 1969).

2 Indirect Measurements

For β^+ decays which are followed by the emission of a gamma ray

Isotope	K/β^+	Technique	Reference
^{11}C	$(1.9 \pm 0.3) \times 10^{-3}$	(a) Multiwire counter (b) Plastic counter	Scobie & Lewis 1957
^{11}C	$(2.30 \,^{+\,0.14}_{-\,0.11}) \times 10^{-3}$	Plastic counter with continuous gas flow	Campbell et al. 1967
^{13}N	$(1.68 \pm 0.12) \times 10^{-3}$	Plastic counter with continuous gas flow	Ledingham et al. 1963
^{15}O	$(1.07 \pm 0.06) \times 10^{-3}$	Plastic counter with continuous gas flow	Leiper & Drever 1972
^{18}F	$(3.00 \pm 0.18) \times 10^{-2}$	Proportional counter with gaseous source	Drever et al. 1956
^{19}Ne	$(9.6 \pm 0.3) \times 10^{-4}$	Plastic counter with continuous gas glow	Leiper & Drever 1972
^{22}Na	0.105 ± 0.009	NaI(Tl) crystal with internal source	McCann & Smith 1969
^{30}P	$(1.24 \pm 0.04) \times 10^{-3}$	Plastic counter with continuous gas flow	Ledingham et al. 1971

TABLE 2.1

SUMMARY OF K/β^+ MEASUREMENTS FOR LIGHT ISOTOPES

the K/β^+ ratio can be found indirectly by the measurement of the ratio of total electron capture to positron emission (ϵ/β^+). Since the number of gamma rays emitted is equal to the total number of decays (i.e. positrons plus electron capture events), the ϵ/β^+ ratio can be measured by a coincidence technique. The number of gamma rays (N_γ) and the number of coincidences between positrons and gamma rays (N_c) in the same time interval give the ϵ/β^+ ratio.

$$\epsilon/\beta^+ = \frac{N_\gamma - N_c}{N_c}$$

The total electron capture rate can be expressed as the sum of the separate shell captures. Thus,

$$\epsilon/\beta^+ = \frac{K + L + M + \ldots}{\beta^+}$$

$$= (K/\beta^+)\left[1 + \frac{L}{K} + \frac{M}{L}\cdot\frac{L}{K} + \ldots \right]$$

The K/β^+ ratio can be calculated from the measured ϵ/β^+ ratio if the L/K, M/L, etc electron capture ratios are known. Since there are few experimental values of L/K, M/L etc known, calculated values of these ratios must be used to obtain the K/β^+ ratio. Calculation of these ratios is described in chapter 3. At this point it is sufficient to note that in regions where exchange-overlap corrections are not negligible (i.e. the low Z region), the calculated L/K, M/L ratios must be corrected for these effects. Therefore, it is clear that K/β^+ ratios derived in this way cannot be used to give information about exchange-overlap effects.

In this chapter only low Z isotopes are considered and, hence, only direct K/β^+ measurements are described. In the following chapter, however, higher Z isotopes are discussed and, since exchange-overlap

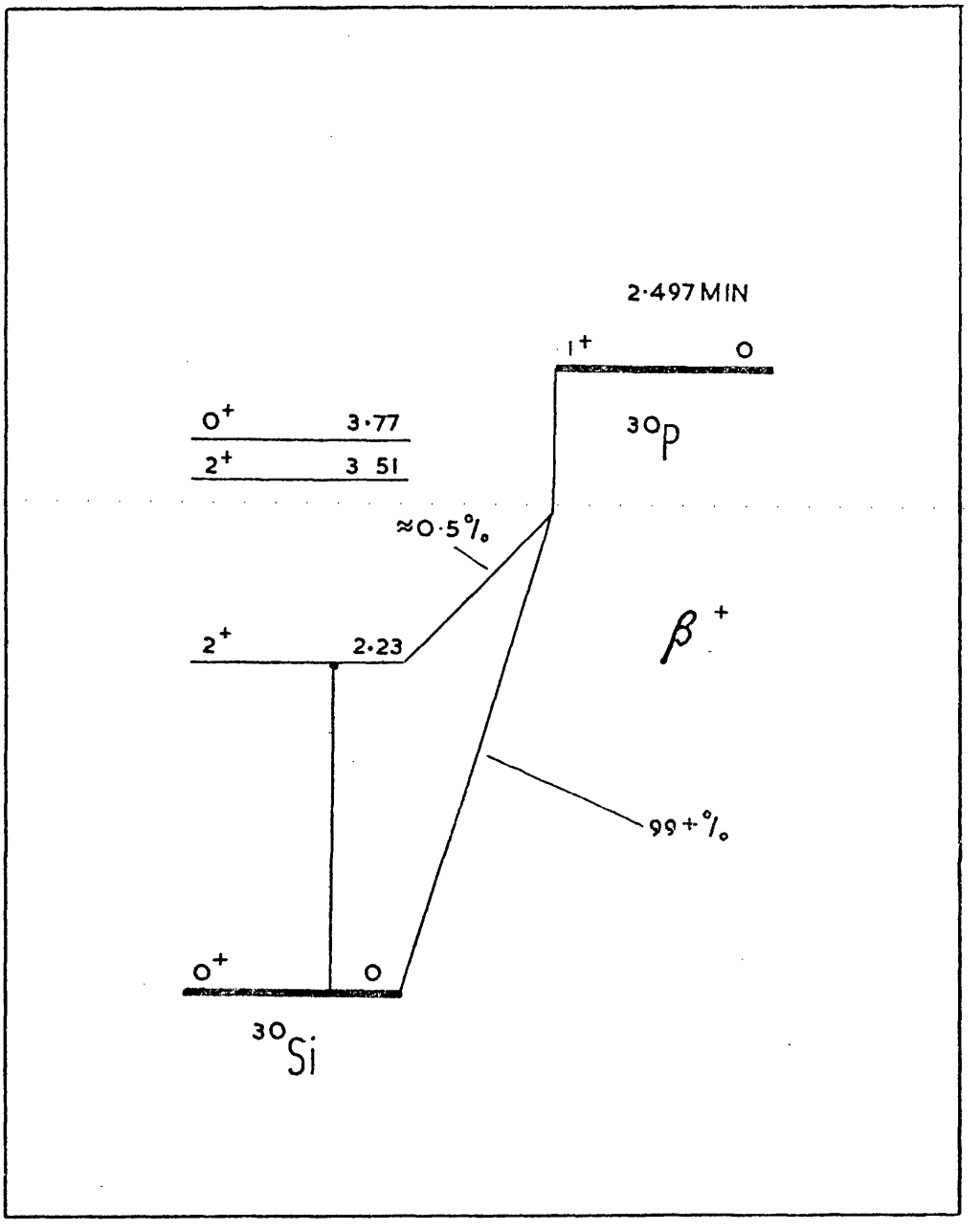

FIG 2-1

effects are smaller for such isotopes, accurate K/β^+ ratios can be derived from ϵ/β^+ measurements.

REVIEW OF PREVIOUS MEASUREMENTS OF K/β^+ RATIOS FOR LOW Z NUCLEI

Table 2.1 reviews all K/β^+ measurements for light nuclei ($Z \leq 15$). There have been several measurements of the ϵ/β^+ ratio for ^{22}Na but because of the uncertainty in the exchange-overlap corrections for this isotope only the direct K/β^+ measurement of McCann and Smith (1969) is given in table 2.1.

One of these K/β^+ measurements (viz. ^{30}P) is now described in some detail as it is typical of the measurements made in the low Z region. The present author was not involved in the actual experiment but assisted in the analysis of the data.

MEASUREMENT OF THE K/β^+ RATIO FOR ^{30}P

^{30}P is known to decay by positron emission with a half life of 2.497 ± 0.005 min. (McDonald et al. 1963). The decay is mainly a ground state-ground state, allowed Gamow-Teller transition but a weak positron branch to the first excited state of ^{30}Si has been reported (Morinaga and Bleuler 1956). The decay scheme is shown in figure 2.1.

Electron capture from the K-shell of phosphorus results in the emission of x-rays or Auger electrons with total energies equal to the K-shell binding energy in silicon (1.838 keV). A proportional counter with a gaseous source of ^{30}P was, therefore, used to detect these low energy K-capture events. There are few gaseous compounds

PLASTIC COUNTER

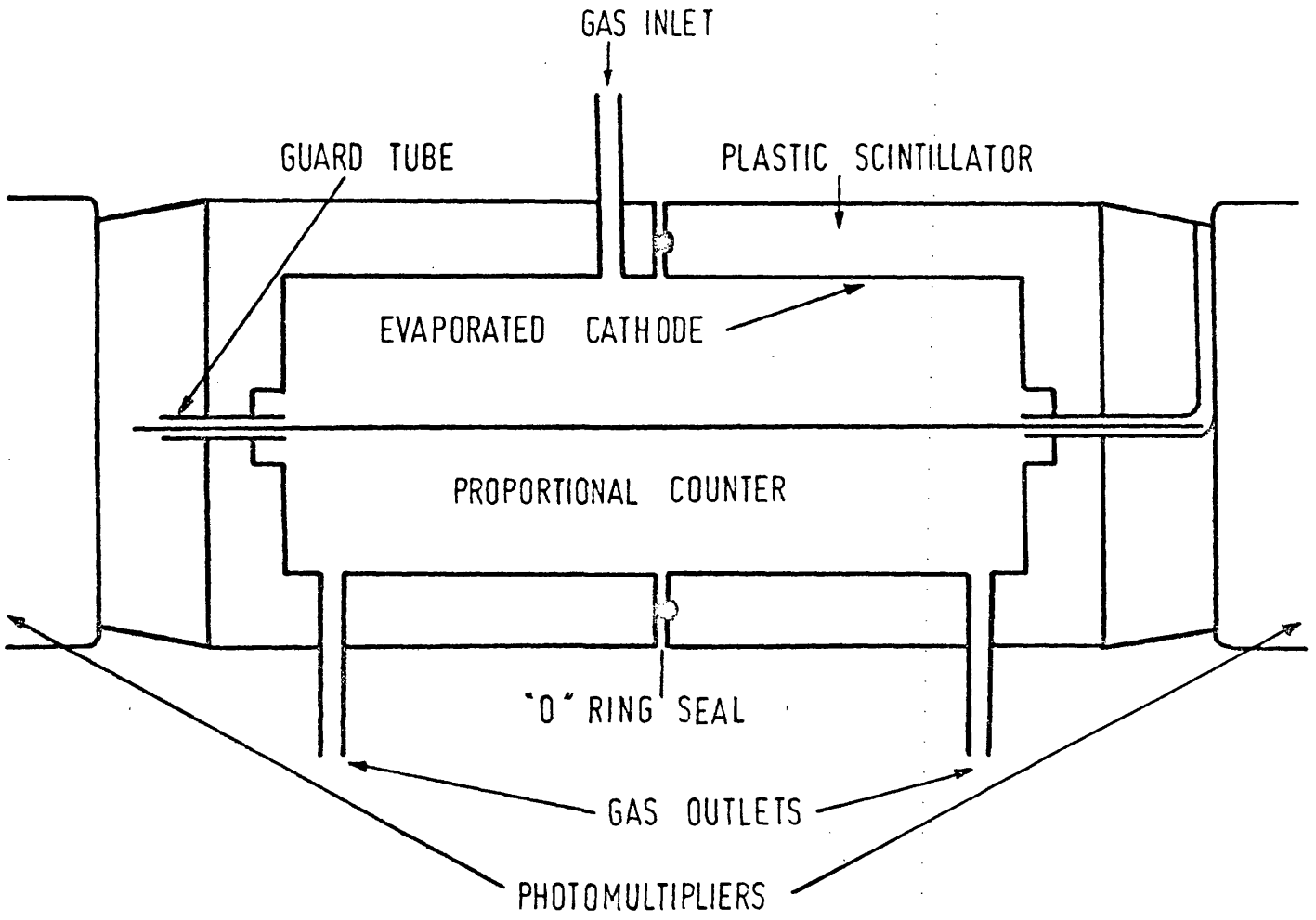

FIG 2-2

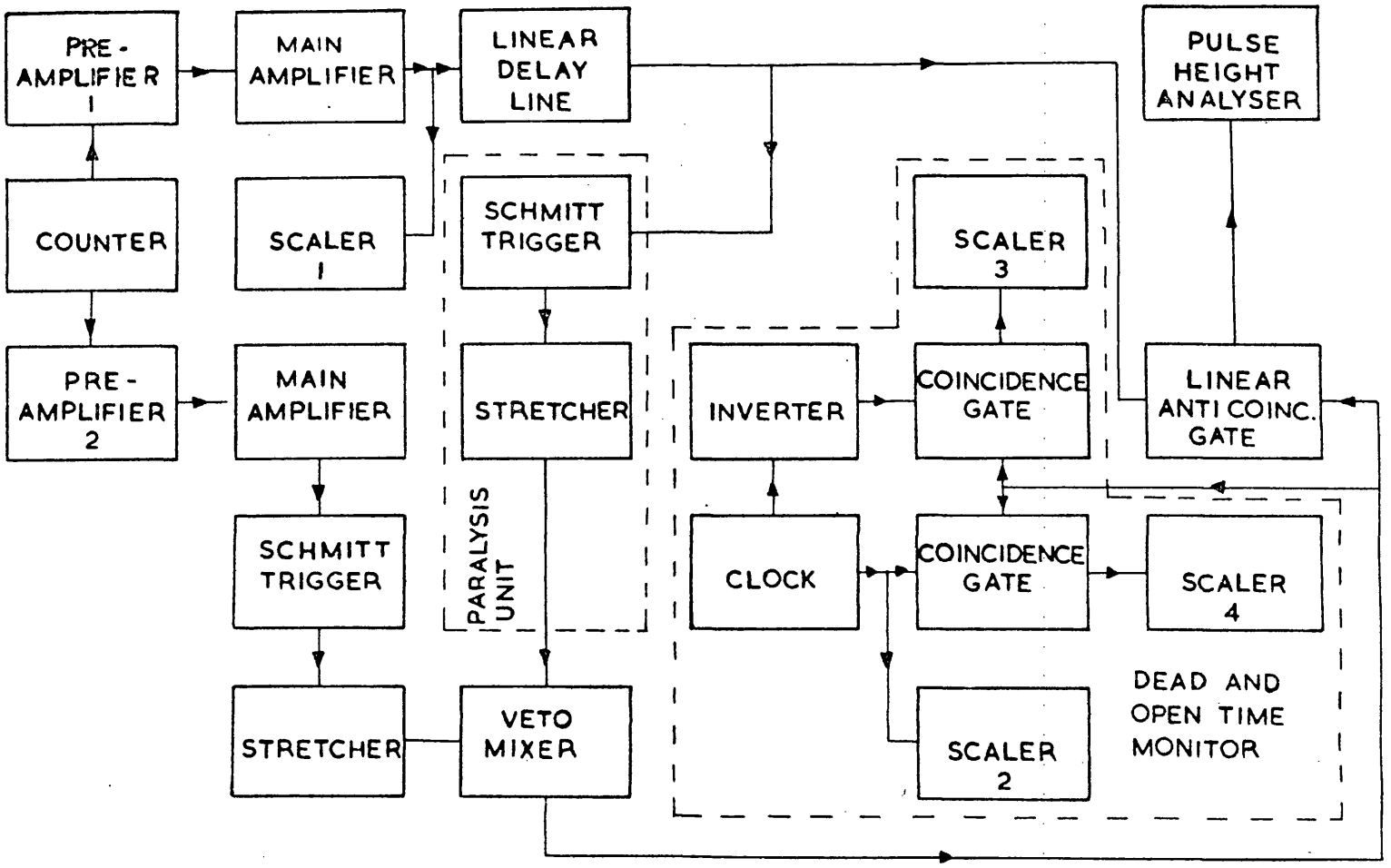

FIG. 2.-3 ELECTRONIC ARRANGEMENT

of phosphorus but phosphine, PH_3, was chosen because it had previously been used in a proportional counter (Pahor et al. 1968).

The counter used was the plastic counter described earlier in this chapter. Since the half life of the source was fairly short the continuous gas flow system was employed. A diagram of the counter is shown in figure 2.2. A block diagram of the electronic arrangement is shown in figure 2.3, and has been described in detail by Campbell et al. (1967).

Phosphine of minimum purity 99.5 per cent flowed at about 1 ml/min from a high pressure cylinder through fine bore copper tubing (1 mm in diameter) a distance of 30 metres to a copper irradiation vessel of volume 9 ml placed in a 100 MeV bremsstrahlung beam from the Kelvin Laboratory electron linear accelerator. ^{30}P was produced by the reaction

$$^{31}P(\gamma, n)\ ^{30}P$$

on the 100 per cent abundant ^{31}P isotope in the phosphine. The irradiated phosphine then passed through a further 5 metres of copper tubing before mixing with proportional counter filling gas (argon plus 10 per cent methane) flowing at a rate of about 200 ml/min. The combined gases flowed through 30 metres of tubing to the counter from which they were released to the atmosphere. The flow rates were chosen so that the concentration of phosphine was less than 1 per cent of the argon-methane mixture, since higher concentrations were found to degrade the resolution of the counter, and so that the ^{30}P decayed by several half lives between entering and leaving the counter. The total number of decays, i.e. positrons plus capture events, was recorded on scaler 1 and the number of K-capture events was obtained

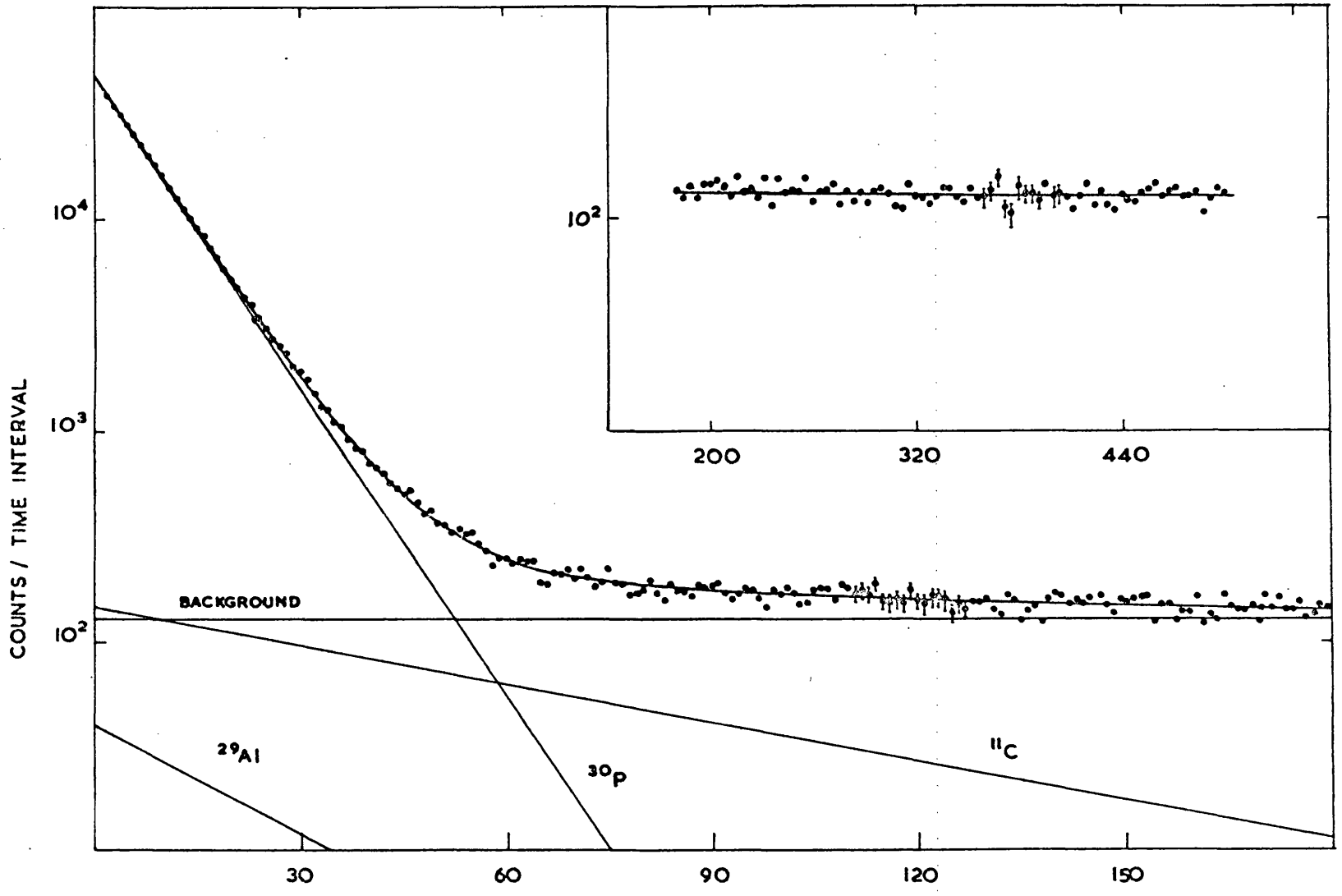
COUNTS / TIME INTERVAL
10^4
10^3
10^2
10^2
200
320
440
BACKGROUND
^{29}Al
^{30}P
^{11}C
30
60
90
120
150
TIME (ARBITRARY UNITS)

FIG 2-4

from the K-peak in the anti-coincidence spectrum. Hence the K/β^+ ratio was evaluated.

The purity of the source was checked by measuring the half life. The irradiated gas was sealed in the counter and the activity measured as a function of time using the multiscale facility of a multichannel analyser. The counting time was 25 secs/channel and the activity was monitored for four hours. A graph of the data obtained is shown in figure 2.4. The data points were fitted to an expression of the form

$$Y = Ae^{-\lambda_1 t} + Be^{-\lambda_2 t} + Ce^{-\lambda_3 t} + D$$

by a least squares computer program, Minuit. This is a minimisation procedure based on a method developed by Rosenbrock (1960). The parameters A, B, C, D, λ_1, λ_2 and λ_3 were varied by the program to give the best fit to the data. The dominant activity was found to be due to an activity with a half life of 2.48 ± 0.03 min. Activities with half lives of about 7 min and 20 ± 4 min attributed to ^{29}Al and ^{11}C were present to less than 0.5 per cent of the ^{30}P activity. This analysis was carried out by Dr J. Y. Gourlay.

The total number of events recorded on scaler 1 amounted to approximately 1.8×10^7. The number of background events in the same time interval was approximately 1.2×10^5. These numbers have to be corrected to take into account events which were not recorded due to the finite triggering level (1.5V) on the input to scaler 1. The correction factor was obtained by measuring the pulse height spectrum from the central counter. This is shown in figure 2.5. The scaler threshold on this graph corresponds to a pulse height of 1.5 volts.

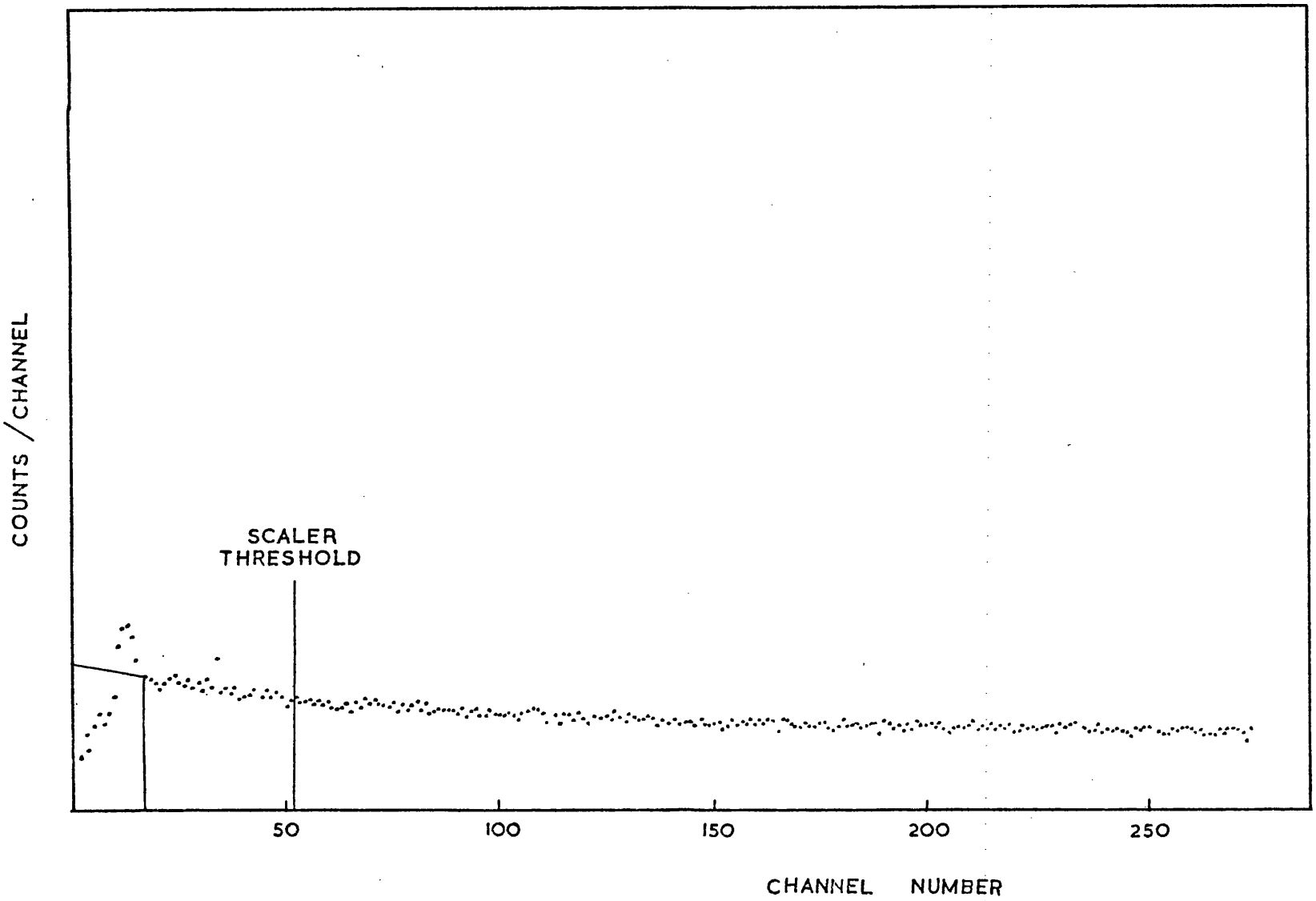
COUNTS /CHANNEL
SCALER
THRESHOLD
50
100
150
200
250
CHANNEL NUMBER

FIG 2-5

The number of pulses in the region below this threshold level represents the correction which has to be made to the scaler reading. It is apparent that the spectrum in the first few channels is not as smoothly varying as in the remaining channels of the analyser. The lower level discriminator on the analyser was set to a non-zero value causing a drop in the number of pulses in the first few channels. The spectrum was extrapolated into the distorted region as shown in figure 2.5 and the total number of pulses below the scaler threshold found. The correction amounted to (10.6 ± 0.7) per cent of the total number of events recorded.

A further correction of 0.4 per cent was applied to the total number of positrons to account for the impurities in the source.

The estimation of the number of K-capture events was more difficult since the K-peak was superimposed on a continuous spectrum of pulses arising principally from positrons of energy less than the threshold of the anti-coincidence gate (50 keV). Figure 2.6 shows a typical K-peak.

Two independent methods were used to estimate the number of counts in the K-peak. The first consisted of fitting a smoothly varying function to the points on either side of the peak. This curve was interpolated under the peak and used to represent the continuum in this region. The number of K-capture events was found by subtracting this background from the data points. Since the shape of the continuum is not known theoretically, several smoothly varying functions were fitted to the data around the peak using the Minuit program. The best fits to the data were obtained using either exponential or hyperbolic

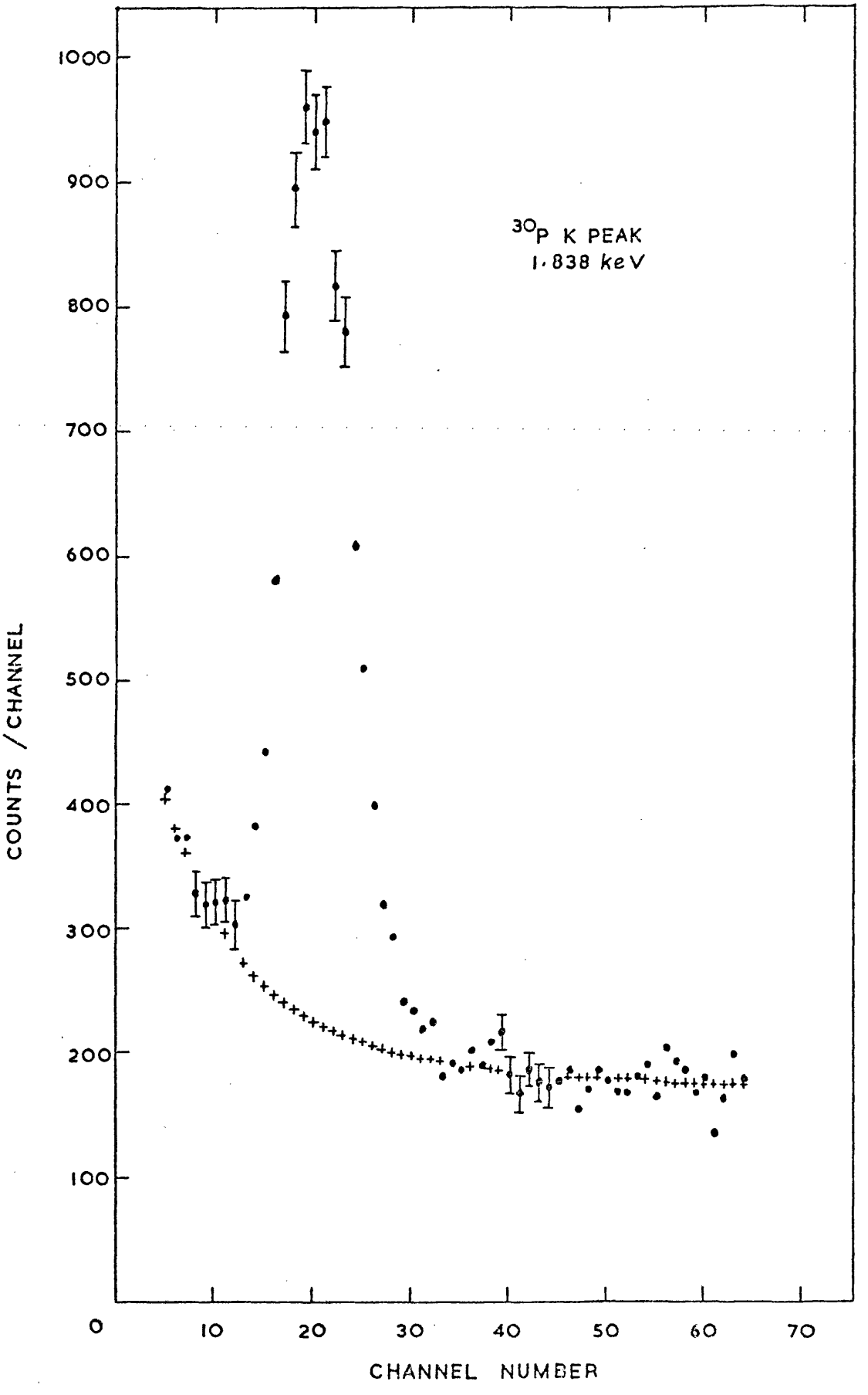
^{30}P K PEAK
1.838 keV
COUNTS / CHANNEL
CHANNEL NUMBER
0
100
200
300
400
500
600
700
800
900
1000
10
20
30
40
50
60
70

FIG 2-6

functions. Shown in figure 2.6 is a fit to the expression

$$Ae^{-Bx} + Ce^{-Dx} + E.$$

The fitted spectra were subtracted from the data points to give the number of K-capture events.

The second method of estimating the area of the K-capture peak is based on the assumption that the pulse height distributions produced in a proportional counter by monoenergetic radiations have a Poisson shape (Campbell and Ledingham, 1966). Poisson distributions of variable width, height and mean position were fitted to the K-peaks using the Minuit program. These peaks were then subtracted from the data and the resulting spectra examined. If smoothly varying spectra, without peaks or troughs, were produced by this technique the areas under the Poisson peaks were taken as the number of K-capture events.

The values of the K/β^+ ratio obtained by the two methods described were $(1.25 \pm 0.04) \times 10^{-3}$ and $(1.21 \pm 0.06) \times 10^{-3}$. The mean of the two values was found by weighting each result in inverse proportion to the square of its error. The standard error of the weighted mean (2.4 per cent) was taken as a measure of the systematic error in the estimation of the number of K-capture events.

The experimental errors are summarised as follows:

(i) 2.4 per cent systematic, 1 per cent statistical in the determination of the number of K-capture events.

(ii) 0.7 per cent systematic error in the number of positron events. This error comes from the extrapolation into the region below the scaler threshold.

These errors were added in quadrature and a final result of

$$(1.24 \pm 0.04) \times 10^{-3}$$

was obtained for the K/β^+ ratio of ^{30}P.

Calculation of Theoretical K/β^+ Ratios

The theoretical values of the K/β^+ ratios were calculated using the expression given in chapter 1 (equation 4). The values of positron end point energies used were taken from tables given by Wapstra and Gove (1971). The values of electron radial wave functions (g_K) and the K-shell binding energies of Behrens and Jänecke (1969) were used. As already mentioned in chapter 1 these authors also give tables of Fermi functions calculated for a nucleus of finite size with a uniform charge distribution inside the nucleus and taking into account the effect of the screening of the nuclear charge by the orbital electrons.

The values of the Fermi functions are given in these tables for various values of p_e, the electron momentum, and were interpolated by the author and Dr Gourlay using Bessel's formula (Massey and Kestelman, 1964) to obtain values at momentum intervals of 0.1 $m_o c$. The difference between the interpolated values obtained using the second order formula and the fourth order formula was, on average, about 1 part in 70 000. The fourth order formula was, therefore, considered to be satisfactory and was used throughout to find interpolated values of the Fermi function over the total positron range for each nucleus.

These interpolated values of the Fermi function were then used to calculate the denominator of equation 4 by numerical integration

Isotope	Maximum β^+ kinetic energy (keV)	$(K/\beta^+)_{expt}$	$(K/\beta^+)_{theor}$	$(B_K)_{expt}$
^{11}C	960.2 ± 1.0	$(2.30 \,^{+\,0.14}_{-\,0.11}) \times 10^{-3}$	$(2.32 \pm 0.01) \times 10^{-3}$	$0.993 \,^{+\,0.061}_{-\,0.048}$
^{13}N	1198.5 ± 0.9	$(1.68 \pm 0.12) \times 10^{-3}$	$(1.939 \pm 0.006) \times 10^{-3}$	0.866 ± 0.067
^{15}O	1737.2 ± 0.9	$(1.07 \pm 0.06) \times 10^{-3}$	$(0.969 \pm 0.002) \times 10^{-3}$	1.104 ± 0.062
^{18}F	633.3 ± 0.9	$(3.00 \pm 0.18) \times 10^{-2}$	$(3.31 \pm 0.02) \times 10^{-2}$	0.906 ± 0.055
^{19}Ne	2216.2 ± 0.9	$(9.6 \pm 0.3) \times 10^{-4}$	$(9.75 \pm 0.02) \times 10^{-4}$	0.985 ± 0.031
^{22}Na	545.7 ± 0.5	0.105 ± 0.009	0.1073 ± 0.0004	0.979 ± 0.084
^{30}P	3205.4 ± 2.6	$(1.24 \pm 0.04) \times 10^{-3}$	$(1.286 \pm 0.005) \times 10^{-3}$	0.964 ± 0.031

TABLE 2.2

COMPARISON OF EXPERIMENTAL AND THEORETICAL K/β^+ RATIOS FOR LIGHT ISOTOPES

using Simpson's rule. The numerical integration was estimated (Massey and Kestelman, 1964) to be accurate to better than 0.3 per cent.

Comparison of Experimental and Theoretical K/β^+ Ratios

Table 2.2 shows the positron end point energies taken from Wapstra and Gove (1971) and the theoretical K/β^+ ratios calculated as described above. The errors quoted for the theoretical ratios are due solely to the uncertainties in the end point energies. For ^{11}C only the more recent result due to Campbell et al. (1967) has been included.

The last column of table 2.2 shows the values of $(B_K)_{expt}$ defined by

$$(B_K)_{expt} = \frac{(K/\beta^+)_{expt}}{(K/\beta^+)_{theory}}$$

In figure 2.7 these values are compared with the theoretical values of B_K calculated by Bahcall (1963a, 1963c, 1965) and Vatai (1970). One of the main differences between these two theories of overlap-exchange corrections is that the final state wave functions used by Vatai take into account the disappearance of the charge distribution of the captured electron as well as the disappearance of the proton charge while Bahcall's do not. Due to the screening effect before capture the actual change in the atomic potential during capture is much less than that caused by the disappearance of a proton alone. Therefore, the corrections calculated by Vatai are smaller than those of Bahcall. Vatai gives numerical values of B_K for $Z = 13$ to 37 and an expression which can be used to extrapolate the results down to $Z = 6$. However for $6 \leq Z \leq 10$ the

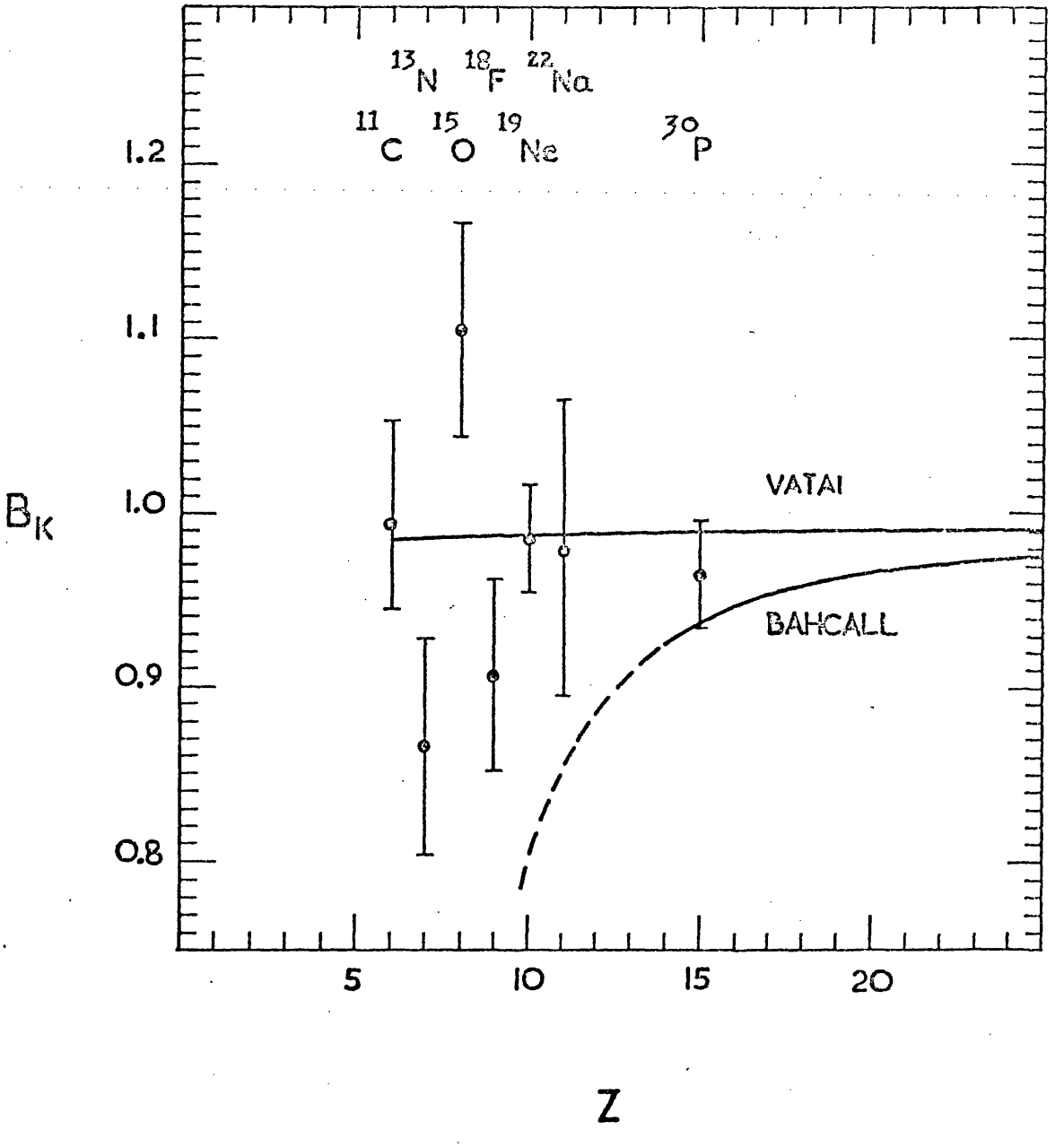
13 N
18 F
22 Na
11 C
15 O
19 Ne
30 P
1.2
1.1
1.0
0.9
0.8
B_K
VATAI
BAHCALL
5
10
15
20
Z

FIG 2-7

correct value of B_K is expected to be higher than the extrapolated value because of the absence of 3s electrons in this region. Bahcall also gives numerical values of B_K for Z = 14 to 37. In figure 2.7 Bahcall's results have been extrapolated to lower values of Z using an expression given by Bahcall (1963c). However, it must be pointed out that Bahcall does not claim that his theory is valid for values of Z less than 14.

It can be seen from figure 2.7 that the experimental results indicate that exchange-overlap corrections to K/β^+ ratios are small (i.e. $(B_K)_{expt} \simeq 1$) and are, therefore, in better agreement with Vatai's calculations. However, since Bahcall's results have been calculated explicitly only for values of $Z \geq 14$ the only point at which the two theories can be directly compared is at Z = 15 (i.e. ^{30}P) where, although not conclusive, the result slightly favours Vatai's corrections.

In conclusion, it appears that exchange-overlap corrections to K/β^+ ratios are small but the present experimental evidence is not accurate enough to allow precise estimates of the magnitudes of these corrections. The required experimental accuracy of about 1 per cent or better is outside the range of present techniques for measuring K/β^+ ratios for light isotopes.

CHAPTER 3

REVIEW OF EXPERIMENTAL K/β^+ AND ϵ/β^+ RATIOS FOR ALLOWED TRANSITIONS

Following the work on K/β^+ ratios for light isotopes, it was decided to extend the comparison of experimental and theoretical K/β^+ ratios to higher values of Z, above the region where exchange-overlap corrections to K-capture are important.

The techniques for measuring K/β^+ ratios for low Z nuclei ($Z \leq 15$) are described more fully in chapter 2 where it is indicated that, for such nuclei, measurements of ϵ/β^+ ratios cannot be used to derive K/β^+ ratios because of the large uncertainties in the exchange-overlap corrections. At higher values of Z, however, this restriction does not apply.

Experimental Techniques for Measuring K/β^+ and ϵ/β^+ Ratios

1 Direct measurements

(a) Internal source proportional counter

This technique is described in detail in chapter 2 in connection with the measurement of the K/β^+ ratio for ^{30}P. If the half life of the decay is short, the radioactive source can be flowed through the counter along with the normal counter filling gas. However, if the half life is sufficiently long, the gases may be static. The events due to K-electron capture (i.e. K x-rays and Auger electrons) are detected as a peak superimposed on the positron continuum. Since the K x-rays must be absorbed completely within the proportional counter, this technique is particularly suitable for low Z isotopes. The K/β^+ ratios for ^{11}C, ^{13}N, ^{15}O, ^{18}F, ^{19}Ne and ^{30}P have been determined using this technique.

(b) Internal source scintillation counter

In this technique the radioactive source is incorporated into a sodium iodide crystal by introducing it into the melt from which the crystal is grown. As with method (a), the K-capture events produce a well-defined peak on the continuous spectrum produced by the positrons. For obvious reasons this technique is not suitable for short-lived isotopes. This method has been used to determine the K/β^+ ratios of ^{22}Na (McCann and Smith, 1969) and ^{58}Co (Joshi and Lewis, 1961).

(c) Magnetic spectrometer

This technique differs from (a) and (b) in that, of the K-capture events, only the Auger electrons are detected. A knowledge of the fluorescence yield, ω_K, is therefore required. In this type of measurement the Auger electrons are observed as a peak in the spectrometer and this is compared with the continuous spectrum produced by the positrons. The K/β^+ ratio for ^{65}Zn (Perkins and Haynes, 1953) was determined by this method. Uncertainties in the values of ω_K have, in the past, limited the accuracy of this technique. However, an extensive review of fluorescence yields, including values obtained by a least squares fit to selected "reliable" data, has recently been published by Bambynek et al. (1972) which reduces this disadvantage.

(d) Other methods

The other techniques normally entail using sources external to the detectors, sometimes with the K-capture events and positrons being registered in different types of detector. Usually only the K x-rays are detected, the Auger electrons being absorbed before entering the detector and so, again, fluorescence yields may limit the accuracy.

Isotope	Maximum β^+ kinetic energy (keV)	Mean of experimental results		K/β^+ derived from ϵ/β^+	Theoretical K/β^+
		K/β^+	ϵ/β^+		
^{48}V	698.0 ± 2.8	-	0.744 ± 0.013	0.669 ± 0.012	0.706 ± 0.012
^{52}Mn	575.5 ± 3.5	-	1.93 ± 0.11	1.73 ± 0.10	1.89 ± 0.05
^{58}Co	475.5 ± 2.5	-	5.71 ± 0.05	5.10 ± 0.04	5.05 ± 0.11
		4.94 ± 0.07	-	-	5.05 ± 0.11
^{57}Ni (i)	851.0 ± 7.0	-	0.83 ± 0.07	0.74 ± 0.06	0.797 ± 0.028
(ii)	731.0 ± 7.0	-	1.46 ± 0.05	1.30 ± 0.04	1.325 ± 0.055
^{64}Cu	655.5 ± 1.8	1.99 ± 0.22	-	-	2.21 ± 0.03
^{65}Zn	328.7 ± 1.1	-	27.6 ± 2.4	24.5 ± 2.1	30.8 ± 0.4
		27.8 ± 1.2	-	-	30.8 ± 0.4
^{68}Ga	819.4 ± 3.9	1.28 ± 0.12	-	-	1.38 ± 0.03
^{89}Zr	904.1 ± 3.0	-	3.45 ± 0.08	3.03 ± 0.07	2.99 ± 0.04
^{89m}Zr	894.1 ± 3.0	-	3.76 ± 0.19	3.30 ± 0.17	3.10 ± 0.05
^{111}Sn	1486.0 ± 26.0	-	2.20 ± 0.15	1.90 ± 0.13	1.63 ± 0.14
^{118m}Sb	291 ± 6	-	620 ± 40	540 ± 25	693 ± 69
^{134}La	2688.0 ± 25.0	0.40 ± 0.04	-	-	0.487 ± 0.022

TABLE 3.1

2 Indirect measurements

These methods measure total capture to positron emission ratios (ϵ/β^+) for decays which lead to an excited state of the daughter nucleus. They consist of measurements of the number of positrons leading to a given level in the daughter nucleus and the number of gamma rays or conversion electrons leaving that level in a given time interval.

Indirect measurements can be divided into two distinct types.

(a) Positrons and gamma rays (or conversion electrons) detected in the same apparatus

In this method the positron annihilation quanta and the gamma rays may both be detected in scintillation counters or semiconductor detectors. For those cases where the gamma ray is highly internally converted, the conversion electrons and the positrons may be detected using a magnetic spectrometer.

(b) Positrons and gamma rays detected in different apparatus

A variety of detectors have been used to detect the positrons and their annihilation radiation including scintillation counters, proportional counters, semiconductor detectors and magnetic spectrometers, while the gamma rays have been detected in scintillation counters and semiconductor detectors. Coincidence techniques using two or three detectors measuring coincidences of gamma rays and positrons or triple coincidences of gamma rays and the two positron annihilation quanta have often been employed.

Review of Experimental Results

Table 3.1 lists the experimental values of K/β^+ and ϵ/β^+ ratios for allowed transitions with $Z > 15$. For those decays for which there

Isotope	Maximum β^+ kinetic energy (keV)	Mean of experimental results		K/β^+ derived from ϵ/β^+	Theoretical K/β^+
		K/β^+	ϵ/β^+		
^{140}Pr	2366.0 ± 6.0	0.74 ± 0.03	-	-	0.856 ± 0.026
^{141}Nd	782.0 ± 15.0	28 ± 1	-	-	35.8 ± 3.2
^{143}Sm	2457.0 ± 28.0	0.92 ± 0.09	-	-	0.984 ± 0.053

TABLE 3.1 (continued)

has been more than one measurement the result given here is the weighted mean of all the results. Details of the individual measurements and their references are given in appendix 2.

Derivation of K/β^+ Ratios from Measured ϵ/β^+ Ratios

The ratio of total electron capture to positron emission can be written as

$$\frac{\epsilon}{\beta^+} = \frac{K}{\beta^+}\left[1 + \frac{L}{K}\left(1 + \frac{M + N + \ldots}{L}\right)\right]$$

Thus a K/β^+ ratio may be derived from a measurement of the ϵ/β^+ ratio if the electron capture ratios L/K, M/L, etc are known. Experimental values of these electron capture ratios have been obtained for a limited number of cases and, therefore, only theoretical values have been employed in this analysis.

(i) Theoretical L/K ratios

L-electron capture can be written as the sum of L_I and L_{II} subshell captures, L_{III} capture being negligible for allowed decays. Thus

$$\frac{L}{K} = \frac{L_I + L_{II}}{K}$$

According to Bahcall (1963a), exchange-overlap corrections to L_I and K capture must be taken into account and, therefore, the ratio L_I/K is written as

$$\frac{L_I}{K} = X^{L/K}\left(\frac{L_I}{K}\right)^0$$

where $X^{L/K}$ is an exchange-overlap correction. $(L_I/K)^0$, the uncorrected theoretical ratio is given by

Isotope	$X^{L/K}$ (Vatai, 1970)	$\frac{L_{II}}{LI}$	$\left(\frac{L_I}{K}\right)^0$	$\frac{L}{K}$	$\frac{M+N+\ldots}{L}$ (Wapstra et al., 1959)
^{48}V	1.139	0.0044	0.0917	0.105	0.072
^{52}Mn	1.127	0.0053	0.0949	0.108	0.086
^{58}Co	1.117	0.0062	0.0978	0.110	0.098
^{57}Ni (i)	1.112	0.0068	0.0991	0.111	0.103
(ii)	1.112	0.0068	0.0991	0.111	0.103
^{65}Zn	1.104	0.0079	0.101	0.112	0.113
^{89}Zr	1.076*	0.0149	0.111	0.121	0.157
^{89m}Zr	1.076*	0.0149	0.111	0.121	0.157
^{111}Sn	1.059*	0.0247	0.121	0.131	0.193
^{118m}Sb	1.057*	0.0258	0.124	0.134	0.196

*Extrapolated using formula given by Vatai (1970)

TABLE 3.2

$$\left(\frac{L_I}{K}\right)^0 = \left[\frac{q_{L_I}\ g_{L_I}}{q_K\ \ g_K}\right]^2$$

where q_{L_I} and q_K are the neutrino energies for L_I and K capture, respectively, and g_{L_I} and g_K are the values of the electron radial wavefunctions at the nuclear surface.

The correction factor, $X^{L/K}$, has been calculated by several authors (Bahcall, 1963 c, Faessler et al., 1970, Martin and Blichert-Toft, 1970, Suslov, 1970 and Vatai, 1970). The results given by Vatai have been used in the present calculations.

The ratios $(L_I/K)^0$ and L_{II}/L_I were calculated using the expressions

$$\left(\frac{L_I}{K}\right)^0 = \left[\frac{q_{L_I}\beta_{L_I}}{q_K\ \beta_K}\right]^2$$

and

$$\frac{L_{II}}{L_I} = \left[\frac{\beta_{L_{II}}}{\beta_{L_I}}\right]^2$$

where the functions β_K, β_{L_I} and $\beta_{L_{II}}$ are the values of the electron radial wavefunctions given by Behrens and Jänecke (1969). In the formula for the L_{II}/L_I ratio the difference in the L_I and L_{II} binding energies has been neglected. The values obtained for these ratios are shown in table 3.2. Also shown are the values of the L/K ratio obtained using the expression

$$\frac{L}{K} = \left(\frac{L_I}{K}\right)^0 \left[X^{L/K} + \frac{L_{II}}{L_I}\right]$$

In this expression exchange-overlap corrections to the ratio L_{II}/L_I have been neglected. Such a correction factor (X^{L_{II}/L_I}) has been calculated by Martin and Blichert-Toft (1970) and it ranges in value from 0.777 at Z = 14 to

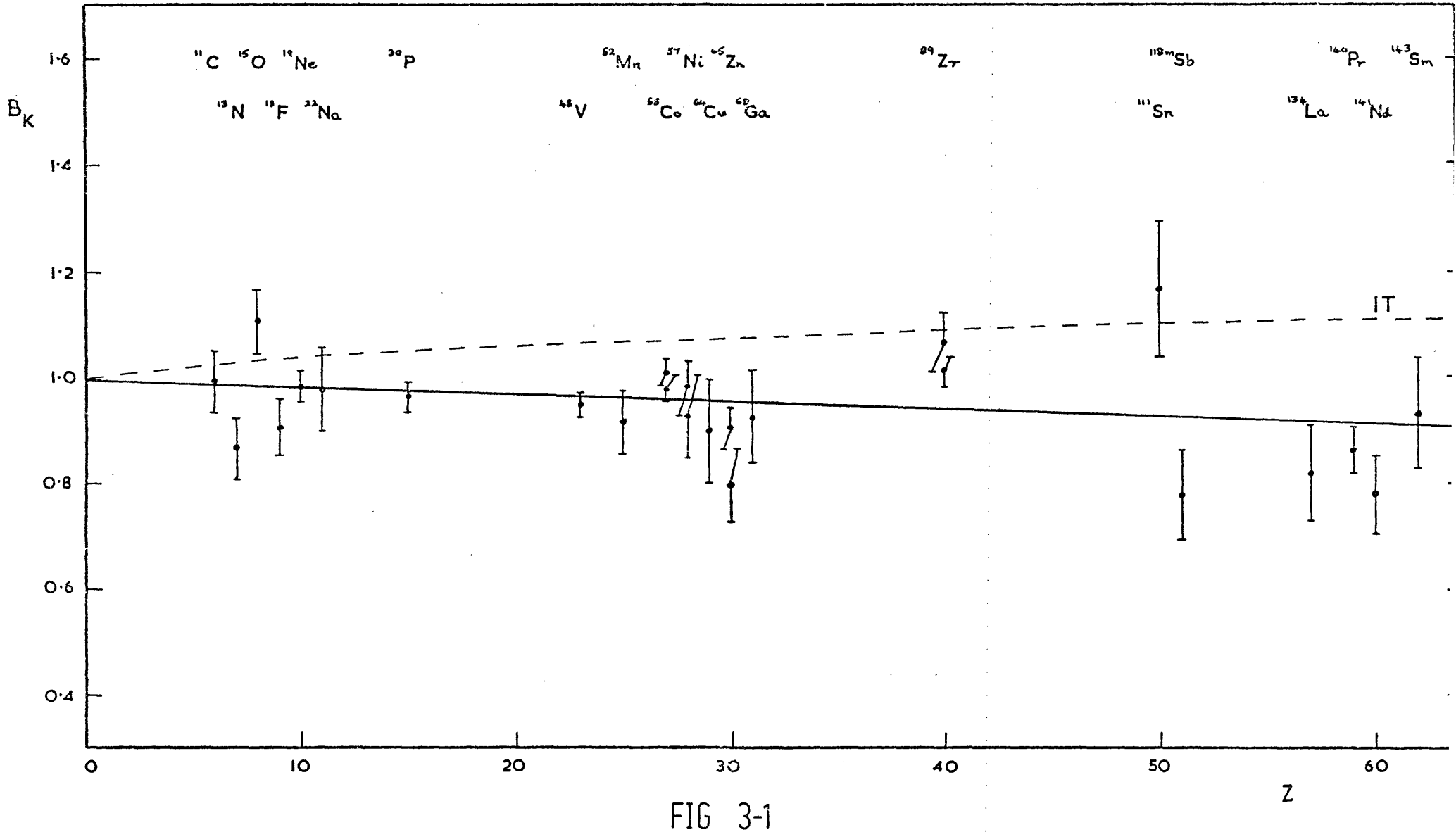
B_K
1·6
1·4
1·2
1·0
0·8
0·6
0·4
^{11}C ^{15}O ^{19}Ne ^{30}P
^{13}N ^{18}F ^{22}Na
^{48}V
^{52}Mn ^{57}Ni ^{65}Zn
^{55}Co ^{64}Cu ^{69}Ga
^{89}Zr
^{111}Sn
^{118m}Sb
^{134}La
^{140}Pr
^{141}Nd
^{143}Sm
IT
0
10
20
30
40
50
60
Z

FIG 3-1

0.962 at Z = 90. However, the uncorrected L_{II}/L_I ratios are themselves so small (see table 3.2) that omission of the exchange-overlap corrections to these ratios has a negligible effect on the theoretical L/K ratios.

(ii) Theoretical (M + N + ...)/L ratios

The values of these ratios were taken from tables given by Wapstra et al. (1959) and are shown in table 3.2. Values of these ratios could also have been calculated using the electron wavefunctions given by Behrens and Jänecke (1969), as for the L_I/K and L_{II}/L_I ratios described above but the difference which this would produce in the factor

$$1 + \frac{L}{K}\left(1 + \frac{M + N + \ldots}{L}\right)$$

is negligible.

Comparison of Experimental and Theoretical K/β^+ Ratios

The values of the K/β^+ ratios derived from ϵ/β^+ measurements using the method described above are shown in table 3.1.

The theoretical K/β^+ ratios also shown in this table were calculated by the method described in chapter 2 using Behrens and Jänecke's tables of Fermi functions, electron wavefunctions and K shell binding energies. The maximum positron kinetic energies were taken from the tables of Wapstra and Gove (1971).

Figure 3.1 shows the values of $(B_K)_{expt}$, defined by

$$(B_K)_{expt} = \frac{(K/\beta^+)_{expt}}{(K/\beta^+)_{theor}}$$

for all the decays listed in tables 3.1 and 2.2. For those isotopes for

which there are two values of $(K/\beta^+)_{expt}$ (i.e. one K/β^+ measurement and another K/β^+ ratio derived from an ϵ/β^+ measurement) the two values of $(B_K)_{expt}$ are shown separately on this graph. The results for the low Z isotopes described in chapter 2 are also included.

A linear least squares fit to the data (solid line on figure 3.1) is seen to be systematically below the value $B_K = 1$, the discrepancy increasing from about 0.3 per cent at Z = 0 to about 8 per cent at Z = 60.

Vatai (1971) has considered the effect on K/β^+ ratios of the induced tensor interaction. The induced interactions arise from alterations in the V - A weak interactions produced by the strong interaction. In the absence of strong interactions the beta decay interaction density can be written as

$$H = g\, \psi_p^*\, \gamma_\mu(1 + \gamma_5)\, \psi_n\, L_\mu$$

where $L_\mu = \psi_e^*\, \gamma_\mu(1 + \gamma_5)\, \psi_\nu$

Induced effects are included (Huffaker and Greuling, 1963) by writing H as

$$H = g\, \psi_p^* \Big[\gamma_\mu(1 + \lambda\gamma_5) + i\sigma_{\mu\nu}(F_{WM} + F_{IT}\gamma_5)\frac{\partial}{\partial x_\nu} + (F_{IS} + F_{IP}\gamma_5)\frac{\partial}{\partial x_\mu}\Big]\psi_n L_\mu$$

The first term in the square brackets represents the vector and axial vector interactions, with the renormalization of the A term being given by λ. The other terms are the induced terms and are momentum dependent. F_{WM} is the weak magnetism term (Gell-Mann, 1958) and bears the same relation to the vector interaction as magnetism bears to static electricity. The subscripts IT, IS and IP refer to the induced tensor,

scalar and pseudoscalar interactions, respectively.

These terms of H can be separated into two classes according to their properties under the transformation G, the product of charge symmetry and charge conjugation (Weinberg, 1958). Terms V, A, IP and WM belong to one class and terms IS and IT belong to the other.

Strong interactions are invariant under G and if the same invariance holds for weak interactions only one G class of interactions can exist. Since V and A do exist G invariance would imply $F_{IS} = F_{IT} = 0$.

The conserved vector current (CVC) theory implies G invariance for the V interaction and the induced terms associated with it, i.e. F_{WM} and F_{IS}. The G class separation then implies $F_{IS} = 0$.

There is no evidence that G invariance holds for the A interaction and its associated terms IT and IP. As the IP term belongs to the same G class as A it might exist without violating G invariance. However, existence of the induced tensor interaction, IT, would imply that G invariance does not hold for the weak interaction.

The effect of a finite value for the induced tensor coupling constant, g_{IT}, on the ft values of mirror beta decays has been considered by Wilkinson (1970). He estimated the magnitude of g_{IT} from the expression

$$\frac{(ft)^+}{(ft)^-} - 1 = \frac{4}{3}\left|\frac{g_V}{g_A}\right| g_{IT}\,(W_o^{+} + W_o^{-}) = \delta$$

where W_o^{+} and W_o^{-} are the end point energies for β^+ and β^- emission, respectively. If both nuclei are positron emitters, $(W_o^{+} + W_o^{-})$ is replaced by the difference in the end point energies. This expression is derived from Huffaker and Greuling (1963) and is valid for Gamow-Teller

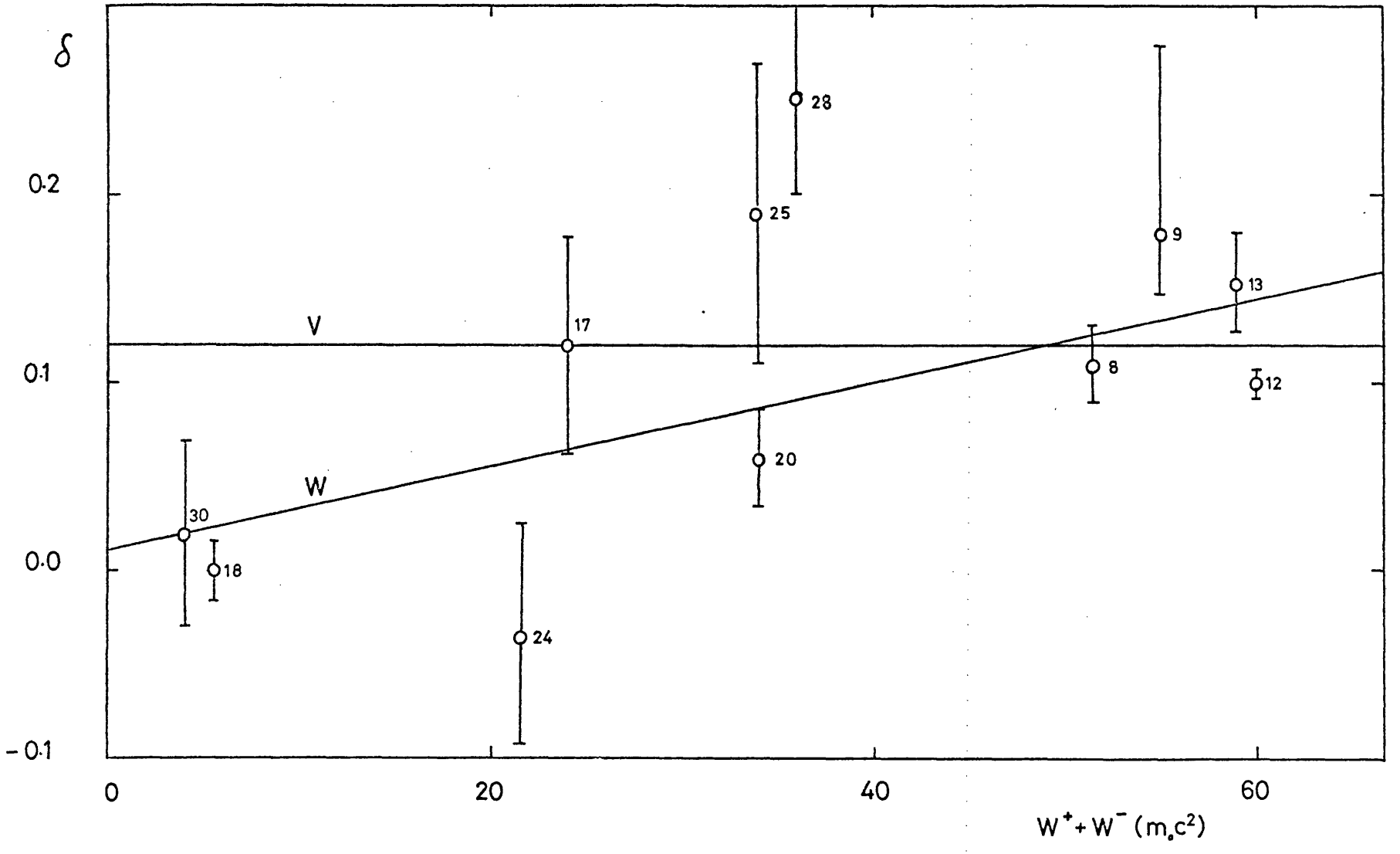

FIG 3-2

transitions in light nuclei and for $W_o >> 1$ (units of $m_o c^2$). Figure 3.2 shows the experimental values of δ as a function of $(W_o^+ + W_o^-)$, according to Wilkinson (1970). The line W is a least squares fit to the data from which Wilkinson estimated $g_{IT} \approx 2 \times 10^{-3}$. The numbers beside the points on figure 3.2 are the atomic mass numbers.

According to Vatai (1971), the results of the β^+ decaying pairs, i.e. at A = 18 and A = 30, should not be taken into account because the difference in energies for these pairs is small. If these points are omitted a better fit to the data is obtained with an energy independent term (line V, figure 3.2).

Vatai (1971) has also indicated that a finite value for g_{IT} should affect K/β^+ ratios. On figure 3.1, the curve IT represents the quantity $(B_K)_{theory}$ defined to be

$$\frac{(K/\beta^+)_{theory\ IT}}{(K/\beta^+)_{theory}}$$

where $(K/\beta^+)_{theory}$ is the usual, uncorrected theoretical ratio and $(K/\beta^+)_{theory\ IT}$ is the theoretical ratio including the effect of the induced tensor interaction. In calculating $(B_K)_{theory}$, Vatai used the value $g_{IT} = 2 \times 10^{-3}$. It is clear that most of the experimental points lie below the curve IT and also the general trend of the data with increasing Z is opposite in sign to that expected from an induced tensor interaction. It should be mentioned that Vatai's calculation of the effect of the IT interaction on K/β^+ ratios is valid only for pure Gamow-Teller decays or decays in which the Fermi admixture is small. This is not the case for all the decays shown in figure 3.1 (e.g. ^{11}C, Scobie and Lewis, 1957 and ^{13}N, Ledingham et al., 1963) but this

does not affect the conclusion that the induced tensor interaction does not account for the discrepancy between experimental and theoretical K/β^+ ratios.

In a recent examination of the beta decay of ^8Li and ^8Be, Wilkinson and Alburger (1971) found no evidence for an induced tensor interaction, concluding that $|g_{IT}| < 7 \times 10^{-4}$. This implies that Vatai's correction to K/β^+ ratios should be smaller by at least a factor of three, i.e. the curve IT should lie much closer to $B_K = 1$ on figure 3.1. However, this would still be considerably different from the linear least squares fit to the experimental points.

From figure 3.1 it is clear that the negative gradient to the linear least squares fit depends strongly on the group of four points at around $Z = 60$. The K/β^+ ratios for these isotopes (^{134}La, ^{140}Pr, ^{141}Nd and ^{143}Sm) were all measured using the same technique, by a single group (Biryukov and Shimanskaya, 1970) and, if a systematic error were present in these measurements, the gradient of the fit to the other points would be considerably altered.

It is interesting to note that Biryukov and Shimanskaya (1970) attribute the difference between the experimental and theoretical K/β^+ ratios for these four isotopes to a finite value of the Fierz interference term. They find $b = -0.020 \pm 0.009$. However, in the two component neutrino theory the interference terms between S and V, expressed as $C_S C_V + C_S' C_V'$, and between A and T, expressed as $C_T C_A + C_T' C_A'$, vanish because the neutrinos or antineutrinos associated with S and T or V and A have opposite helicity.

More experimental work on K/β^+ ratios in the region above $Z = 30$ is

clearly required to establish whether a departure from theory has been detected. The most suitable isotopes for study should, preferably, have reasonable half lives and fairly simple, well-known decay schemes.

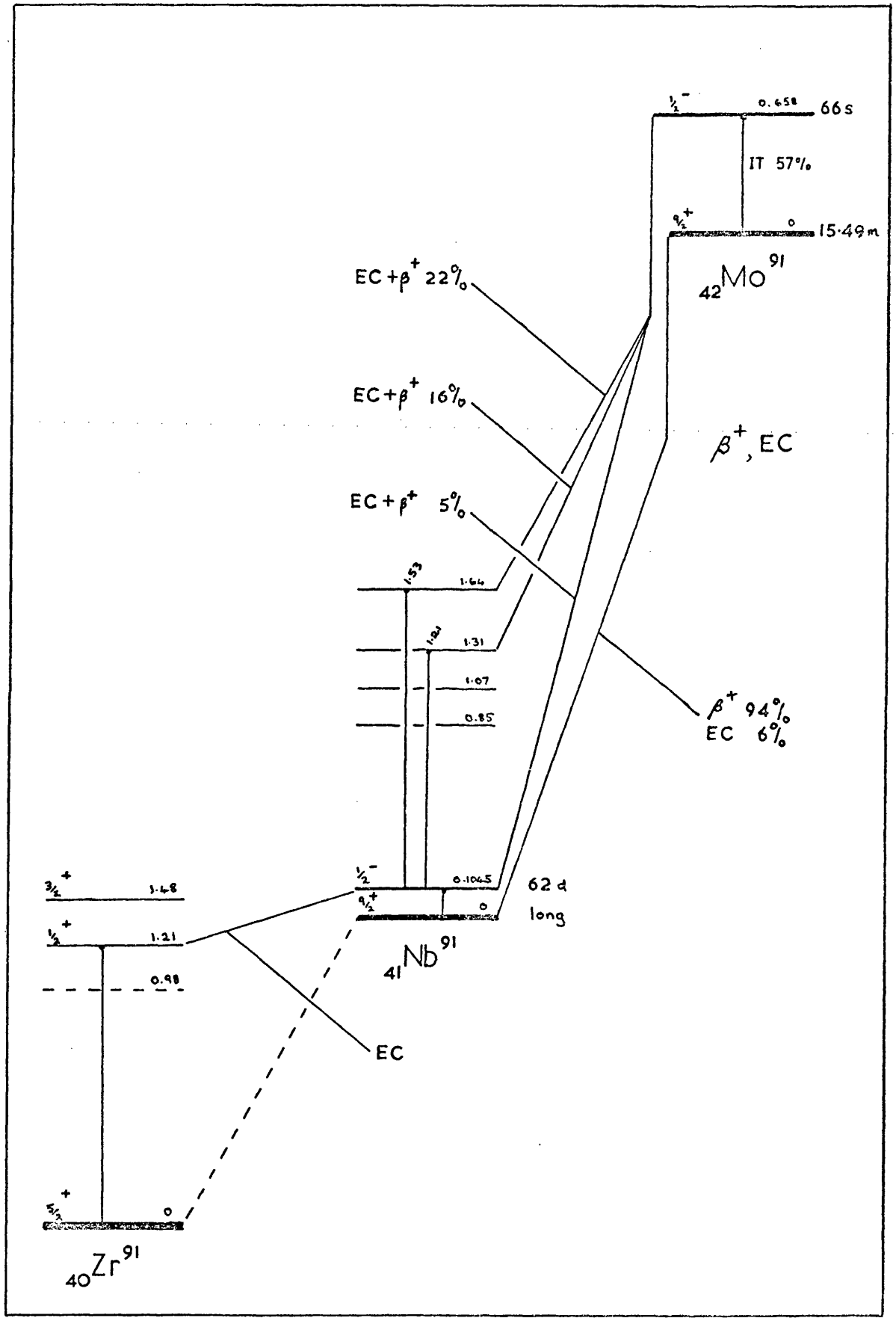
1/2⁻ 0.658 66s
IT 57%
9/2⁺ 0 15·49m
42Mo91
EC+β⁺ 22%
EC+β⁺ 16%
EC+β⁺ 5%
β⁺, EC
1.53
1.64
1.31
1.07
0.85
β⁺ 94%
EC 6%
1/2⁻ 0.1045
9/2⁺ 0
62 d
long
41Nb91
3/2⁺ 1.48
1/2⁺ 1.21
0.98
EC
5/2⁺ 0
40Zr91

FIG 4-1

CHAPTER 4

MEASUREMENT OF THE RATIO OF K-ELECTRON CAPTURE TO POSITRON EMISSION IN THE DECAY OF ^{91}Mo

This chapter describes the measurement of the K/β^+ ratio for the decay of the ground state of ^{91}Mo to the ground state of ^{91}Nb. Molybdenum (Z = 42) lies in a region where the discrepancy between experimental and theoretical K/β^+ ratios discussed in the previous chapter is fairly large. ^{91}Mo is a suitable isotope for a K/β^+ measurement because of its 15.49 ± 0.01 min half life (Ebrey and Gray, 1965) and because the decay is predominantly between ground states (Lederer et al., 1967) (figure 4.1). Also, it can be readily produced by the reaction

$$^{92}\text{Mo}(\gamma, n)^{91}\text{Mo}$$

using the stable isotope ^{92}Mo.

The maximum positron kinetic energy is 3.421 ± 0.028 MeV (Wapstra and Gove, 1971) and the theoretical K/β^+ ratio calculated in the manner described in chapter 2 is

$$0.0559 \pm 0.0022.$$

The ground state and isomeric state of ^{91}Mo are known to decay by positron emission with half lives of about 15.5 min and 66 sec, respectively (Smith et al., 1956). These authors also observed x-rays which they attributed to orbital electron capture and internal conversion in ^{91}Mo. The ratio of K-electron capture to positron emission for the decay of the ground state of ^{91}Mo has not previously been measured.

Recent measurements of the decay scheme of ^{91}Mo (Hesse and Finckh, 1970, and De Barros et al., 1970) indicate that the ground state of

^{91}Mo also decays to several excited states in ^{91}Nb. However, the intensity of these transitions is very low (less than 1 per cent of all decays) and the decay is assumed in this chapter to be simply a ground state-ground state transition. Further details about these weak transitions are presented in chapter 5.

Production of ^{91}Mo

The photoneutron cross-section of ^{92}Mo has been measured as a function of photon energy by several authors. Both the ground state and the isomeric state of ^{91}Mo can be produced by the reaction

$$^{92}\text{Mo}(\gamma, n)$$

and the probabilities of forming these two states are of interest.

Katz et al. (1953) found the energy for the maximum cross-section to be 18.7 MeV and they also measured the ratio of the cross-sections for the production of the ground state and the isomeric state. The decay scheme which they assumed, however, is now considered to be wrong. They associated the 15.5 min activity with the decay of the $\frac{1}{2}^-$ isomeric state and the 66 sec activity with the $9/2^+$ ground state and they assumed no isomeric transitions from the excited state to the ground state.

The (γ, n) threshold energy was measured by Mutsuro et al. (1959) to be 13.4 ± 0.1 MeV. They found the maximum cross-section to be 190 mb at an energy of 16.5 MeV.

Del Bianco and Stephens (1962) measured the (γ, n) cross-section at a photon energy of 20.5 MeV and found a value of 35.4 ± 2.3 mb for the production of the ^{91}Mo ground state.

The relative probability of forming the ground state and isomeric state of ^{91}Mo by the (γ, n) reaction has been measured by Costa et al. (1965) and Haustein and Voigt (1971) for photon energies from threshold up to 70 MeV. The isomeric ratio R is defined as

$$R = \frac{\int \sigma_{\frac{1}{2}^-}(E)\, dE}{\int \sigma_{\frac{9}{2}^+}(E)\, dE}$$

where $\sigma_{\frac{1}{2}^-}$ is the cross-section for the production of ^{91m}Mo (spin and parity = $\frac{1}{2}^-$) and $\sigma_{\frac{9}{2}^+}$ is the cross-section for the production of ^{91}Mo (spin and parity = $9/2^+$) and E is the photon energy. Costa et al. found R to be approximately 4.5 while Haustein and Voigt obtained a value of 1.92 ± 0.15.

Although agreement between the measured values of the isomeric ratio is poor, all results indicate that the low spin isomeric state is produced more readily than the high spin ground state. This is consistent with the idea that photon irradiation of even-even nuclei (e.g. ^{92}Mo, J = 0) is thought to occur by absorption of low multipolarity (l = 1) photons. The spin and parity of the compound nucleus is, therefore, 1^- (Levinger, 1960) and this compound nucleus is more likely to decay to the $\frac{1}{2}^-$ isomeric state than to the $9/2^+$ ground state.

Choice of Photon Bombardment Energy and Irradiation Time

In the present experiment ^{91}Mo was produced by the (γ, n) reaction on molybdenum foils enriched to 98.32 per cent in ^{92}Mo using bremsstrahlung radiation produced by the Glasgow electron linear accelerator. From the earlier discussion it is apparent that the greatest amount of ^{91}Mo is produced by photons with energies in the

range 16-19 MeV. However, it was found impracticable to irradiate at such low energies because of the low intensity of bremsstrahlung radiation which could be obtained. All irradiations were, therefore, carried out at a maximum bremsstrahlung energy of 50 MeV.

A disadvantage of irradiating at this higher energy is that the reaction

$$^{92}Mo(\gamma, 2n)^{90}Mo$$

which has a Q-value of 22.8 MeV (Wapstra and Gove, 1971), is also possible. Since ^{90}Mo (half life = 5.7 hr) and ^{91}Mo both decay by positron emission and electron capture the observed positron and K-capture events have to be corrected for the presence of ^{90}Mo.

In order to minimise the amount of ^{90}Mo produced, irradiation times were kept as short as production of reasonable amounts of ^{91}Mo would allow. Initially it was thought that irradiation times of 15-30 mins would be acceptable since they correspond to 1-2 half lives of ^{91}Mo and are short compared with the 5.7 hr half life of ^{90}Mo. However, it was then realised that irradiation times could be reduced to 1 or 2 mins taking advantage of the fact that ^{91m}Mo (half life = 66 secs) is produced more readily than the ground state and that 57 per cent of ^{91m}Mo decays lead to the ground state. It is apparent, therefore, that reducing the irradiation time does not seriously reduce the amount of ^{91}Mo formed but the amount of ^{90}Mo is reduced by a factor of about 15.

Foils of ^{92}Mo were, therefore, irradiated for 1 or 2 mins in a 50 MeV bremsstrahlung beam. The bremsstrahlung was produced by a 50 MeV electron beam striking a water-cooled aluminium target 5 cm thick. Molybdenum foils of thickness 5 mg/cm^2 ($\sim$5 μm) and areas

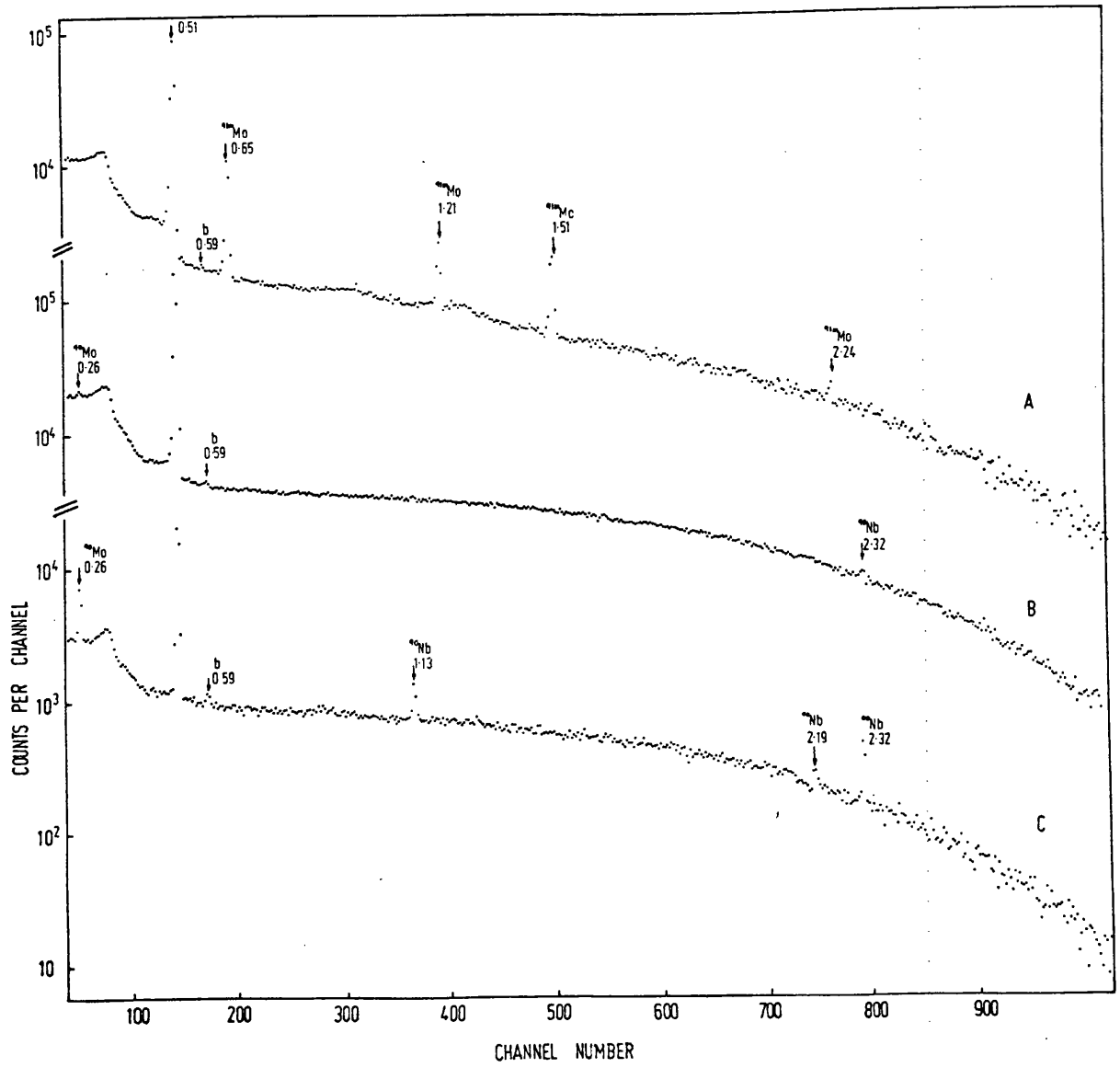
0·51
99mMo 0·65
b 0·59
99mMo 1·21
99mMc 1·51
99mMo 2·24
A
99Mo 0·26
b 0·59
99Nb 2·32
B
99Mo 0·26
b 0·59
99Nb 1·13
99Nb 2·19
99Nb 2·32
C
COUNTS PER CHANNEL
CHANNEL NUMBER
10⁵
10⁴
10³
10²
10
100
200
300
400
500
600
700
800
900

FIG 4-2

from 5 mm x 5 mm to 2 mm x 2 mm were used. For the gamma ray measurements thicker samples (52μm) were used. The molybdenum samples were irradiated inside aluminium containers which were transported from the irradiation position by a fast pneumatic transfer system.

Gamma Ray Measurements - Source Purity

The gamma rays emitted by irradiated foils of ^{92}Mo were examined with a 52 cc Ge(Li) detector. A series of gamma ray spectra were taken and are shown in figures 4.2 and 4.3.

Spectrum A in figure 4.2 shows the gamma rays detected in a 2 min. period starting 1 min. after the end of the irradiation. This spectrum represents the sum of data from four samples. B represents a 30 min. count taken 10 mins after the end of A. C is another 30 min. count taken 30 mins after the end of B. After spectrum C was taken the amplifier gain was increased by a factor of 4 to look at the low energy spectrum (figure 4.3).

In spectrum A the peaks at 0.65, 1.21, 1.51 and 2.24 MeV have the same energy as those assigned to the decay of ^{91m}Mo (66 secs) by Hesse and Finckh (1970). This interpretation is supported by the fact that these gamma rays are not seen in later spectra and, therefore, must have a short half life. The peak at 0.51 MeV is due to the annihilation of positrons. A background measurement showed the 0.59 MeV peak to be of the same intensity as in these spectra and it is, therefore, not associated with any activity in the molybdenum sample. All the other gamma rays seen in these spectra agree in energy with those from either ^{90}Mo or ^{90}Nb (Lederer et al., 1967) apart from the lead x-rays seen in figure 4.3 which are produced by fluorescence in the

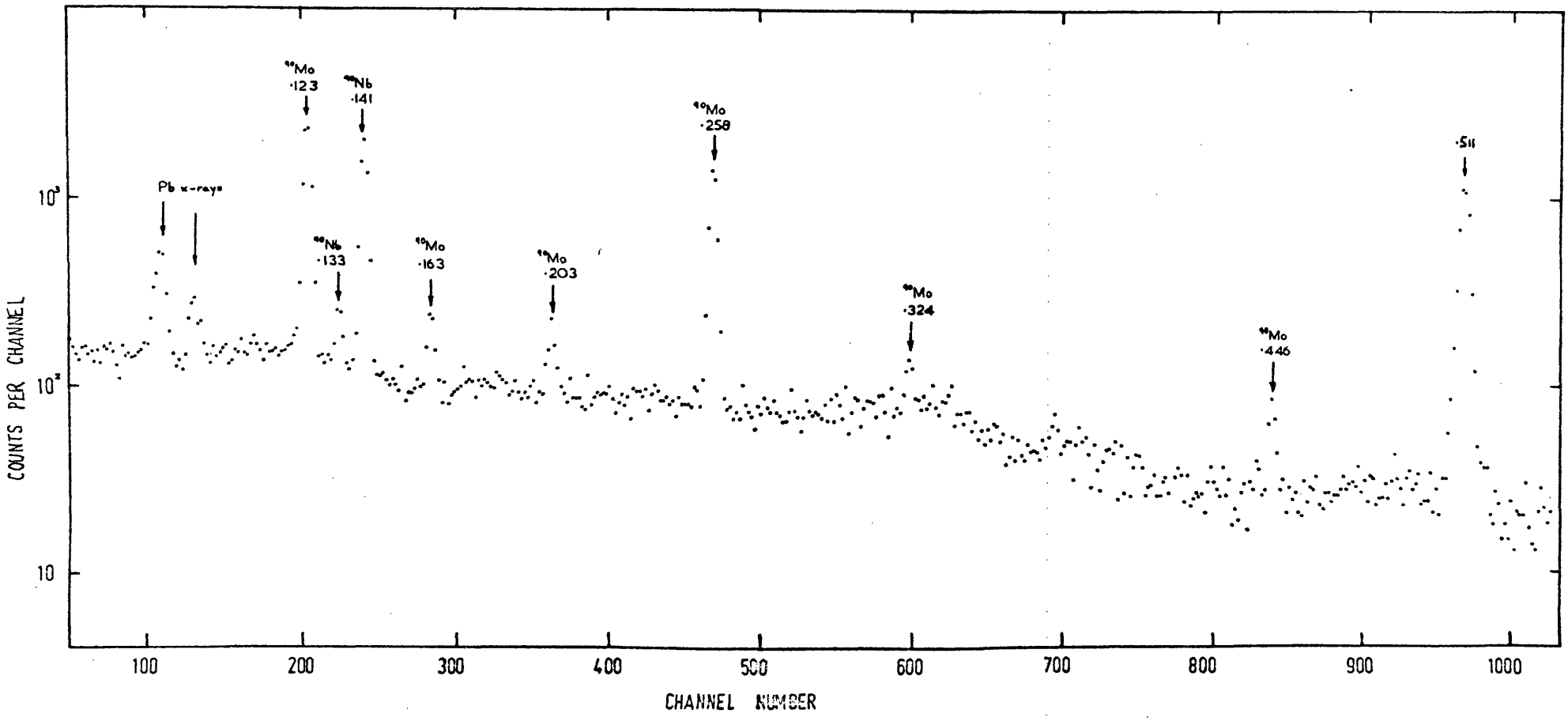
^{99}Mo
·123
^{99}Nb
·141
^{99}Mo
·258
·511
Pb x-rays
^{99}Nb
·133
^{99}Mo
·163
^{99}Mo
·203
^{99}Mo
·324
^{99}Mo
·446
10^3
10^2
10
COUNTS PER CHANNEL
100
200
300
400
500
600
700
800
900
1000
CHANNEL NUMBER

FIG 4-3

lead shielding around the detector. ^{90}Nb could be produced either directly during the irradiation by the reaction

$$^{92}\text{Mo}(\gamma, d)^{90}\text{Nb}$$

which has a Q-value of 17.3 MeV or by the decay of ^{90}Mo.

It is clear from these graphs that the only gamma ray emitting activities produced in measurable amounts are ^{91m}Mo, ^{90}Mo and ^{90}Nb. In fact, ^{91m}Mo decays partially to ^{91}Mo but the gamma rays emitted by ^{91}Mo are too weak to be detected here.

In order to estimate the relative amounts of positron-emitting activities produced, a half life measurement of the 0.511 MeV positron annihilation gamma rays was made. For this measurement a ^{92}Mo sample was irradiated as before. The sample was then sandwiched between two copper discs to stop all the positrons from the sample and placed in front of the Ge(Li) detector. The thickness of each copper disc (0.23 cm) was sufficient to stop the highest energy positrons expected from the sample (i.e. 3.421 MeV from ^{91}Mo). The maximum positron kinetic energies for ^{90}Mo and ^{90}Nb are 1.085 and 0.499 MeV, respectively.

After waiting 10 mins from the end of the irradiation to allow the ^{91m}Mo 66 sec activity to decay to a negligible amount, a series of 15 min. gamma ray spectra was taken.

The areas of the gamma ray peaks were estimated using the computer program SAMPO described below. Figure 4.4 shows the intensity of the 0.511 MeV positron annihilation peak as a function of time. Also shown is a least squares fit to the data of the expression

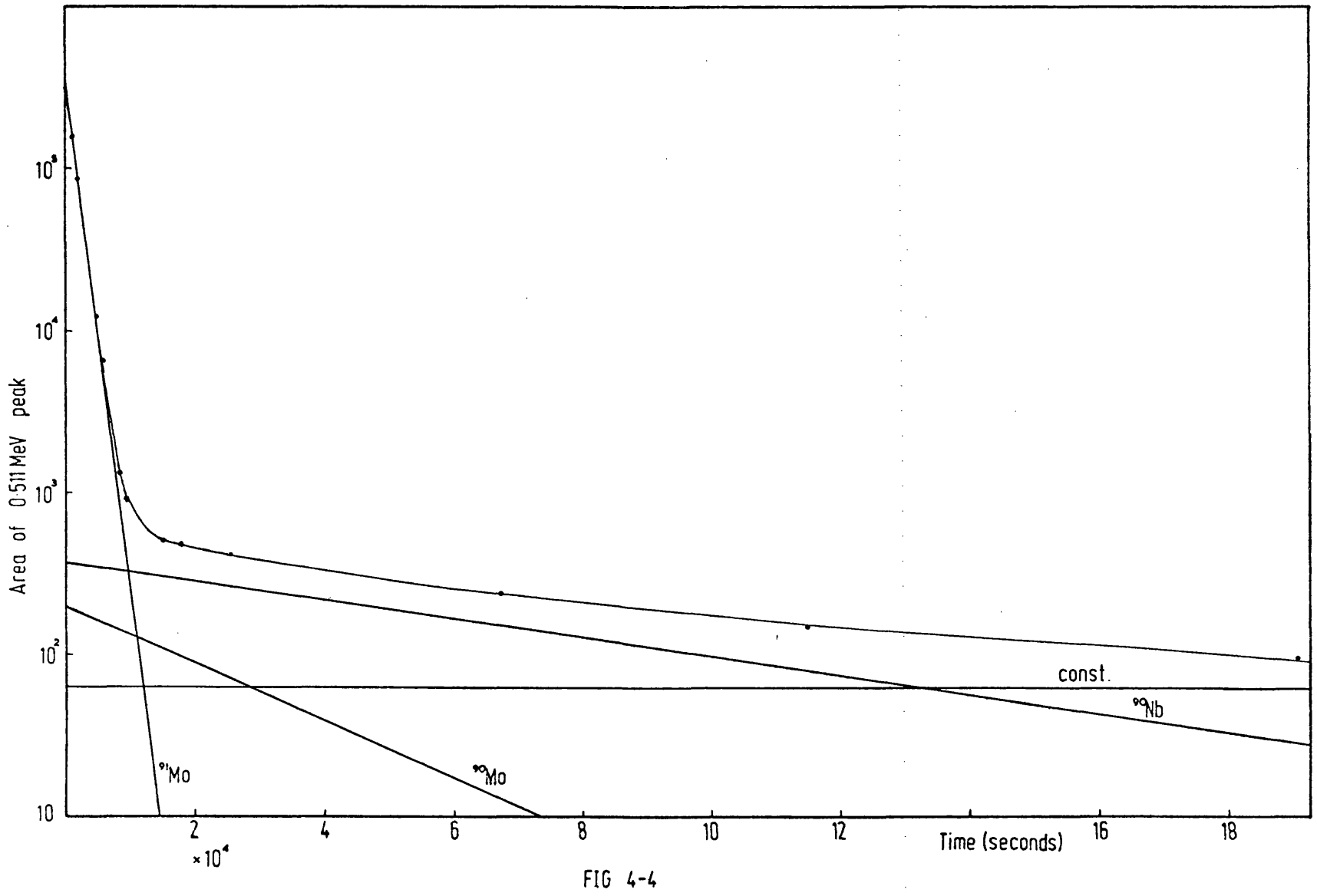
Area of 0.511 MeV peak
10⁵
10⁴
10³
10²
10
const.
⁹⁹Nb
⁹¹Mo
⁹⁹Mo
2
4
6
8
10
12
16
18
×10⁴
Time (seconds)

FIG 4-4

$$Ae^{-\lambda_1 t} + Be^{-\lambda_2 t} + Ce^{-\lambda_3 t} + D$$

where λ_1, λ_2 and λ_3 are the decay constants of ^{91}Mo, ^{90}Mo and ^{90}Nb, respectively. The computer program, VA04A (Powell, 1964) was used to vary the parameters A, B, C and D to obtain the best fit to the data. The errors in these parameters were estimated by the method described by Bevington (1969). The optimum values of A, B, C and D are chosen to minimise χ^2. To find the error in A, the value of A is increased to A + dA and all the other parameters (B, C and D) are optimised for minimum χ^2. The value of dA which causes χ^2 to increase by 1 is taken as the error in A. The errors in the other parameters are calculated in the same way. The optimum values of the parameters were

$$A = 384800 \pm 1300$$

$$B = 196 \pm 40$$

$$C = 373 \pm 28$$

$$D = 63 \pm 5.$$

From the values of these parameters the numbers of positrons from the different activities during any time interval can be calculated.

The measurement of the K/β^+ ratio described later in this chapter was made during a 30 min. period starting 10 mins after the end of a 1 min. irradiation. The above values of A, B, C and D imply that, during this 30 min period, the ratio of ^{91}Mo positrons to the total number of positrons detected is (99.3 ± 0.5) per cent and the ratio of ^{90}Mo to ^{91}Mo positrons is 0.0012 ± 0.0003.

Si(Li) DETECTOR

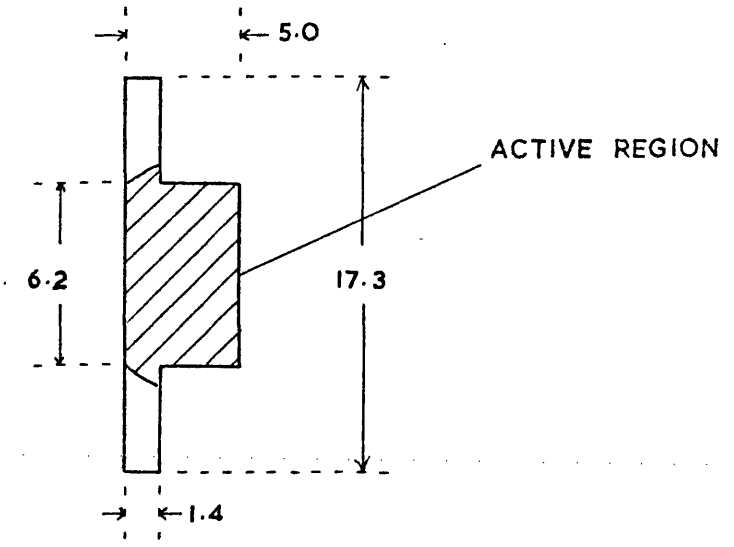

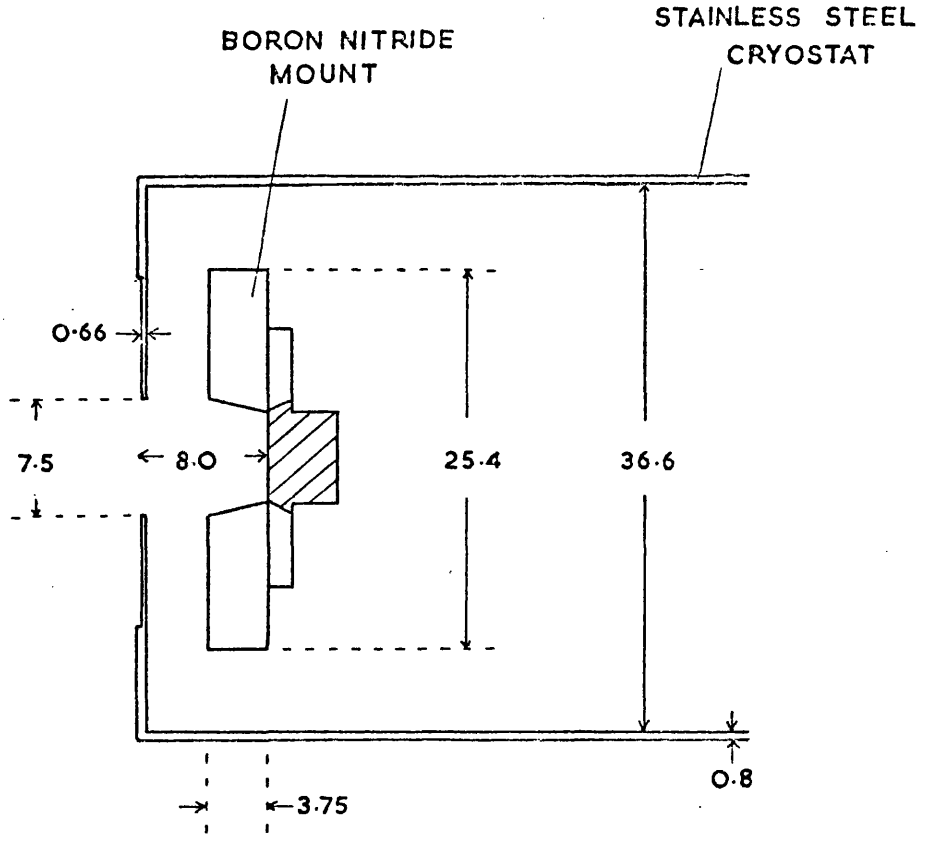

ALL DIMENSIONS IN mm

FIG 4-5

Analysis of Gamma Ray Spectra using the SAMPO Program

The intensities of photopeaks in the gamma ray spectra were calculated using a computer program, SAMPO (Routti and Prussin, 1969). In this program the central part of each peak is fitted with a Gaussian expression and the tails on either side of the peak are fitted with exponential functions which join the Gaussian so that the function and its derivative are continuous. Peak shapes are determined by three parameters, namely, the width of the Gaussian and the distances from the centroid to the junctions with the exponentials. These shape parameters are smoothly varying functions of energy. The SAMPO program calculates shape parameters for intense, well-isolated calibration peaks by fitting the Gaussian-plus-two-exponential expression to the calibration peaks and a straight line to the background by a least squares method. The values of the shape parameters for any peak are then found by interpolation between the calibration shape parameters. Once the shape parameters for a peak have been found a least squares fit to the data, using these parameters for the peak and a polynomial expression for the background, gives the area of the peak. The uncertainties in the parameters are estimated from the final value of χ^2 and the diagonal elements of the error matrix.

The measurement of the intensity of the 0.511 MeV positron annihilation gamma ray peak is a special case since the parameters describing the shape of this peak cannot be found by interpolation between the shape parameters of neighbouring gamma ray peaks, the positron annihilation peak being wider than a normal gamma ray peak of the same energy. In the present analysis the shape parameters for the 0.511 MeV peak were found from the peak itself and then used to find the area of the peak.

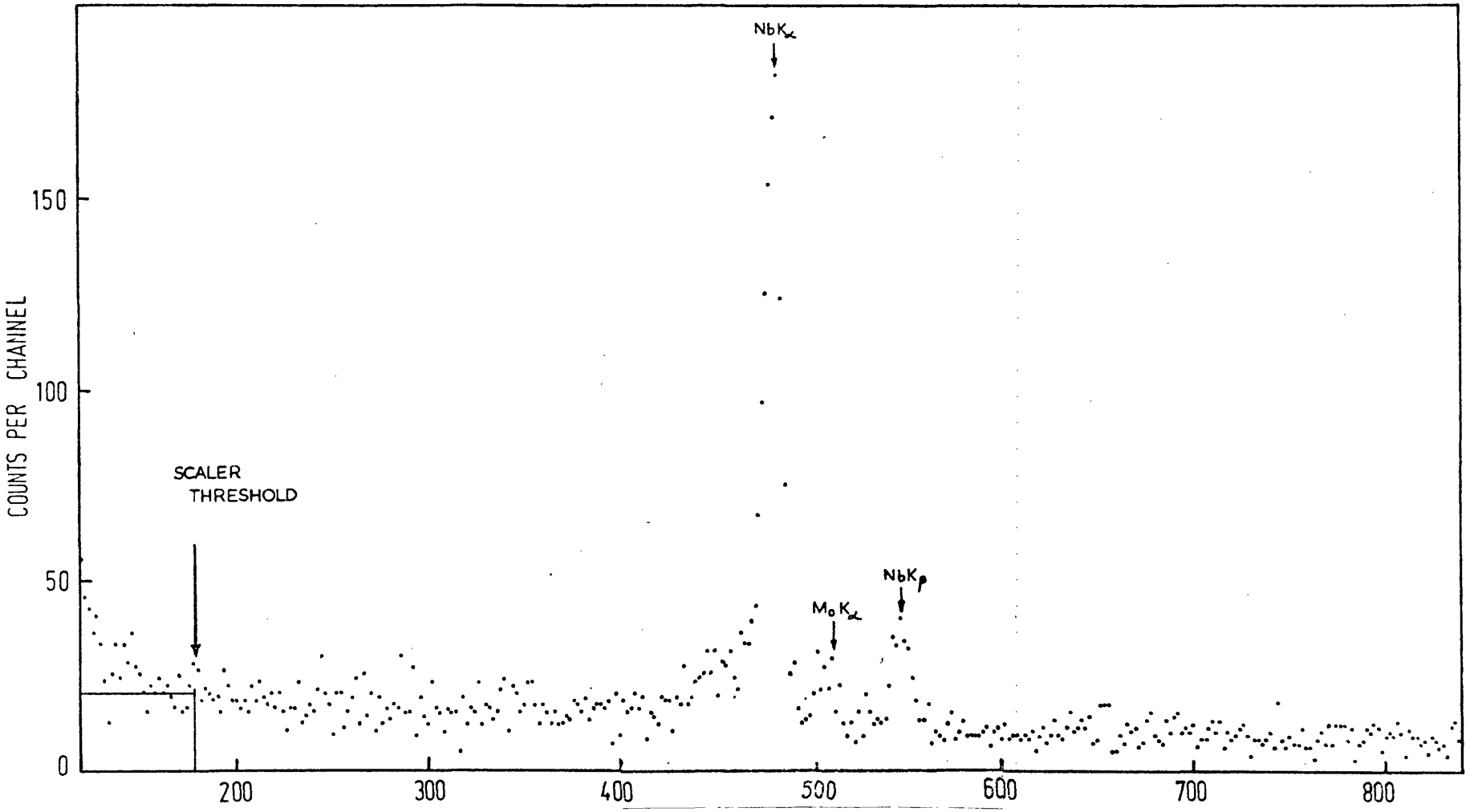
NbKα
SCALER
THRESHOLD
MoKα
NbKβ
COUNTS PER CHANNEL
0
50
100
150
200
300
400
500
600
700
800
CHANNEL NUMBER

FIG 4-6

Preliminary Measurements of the K/β^+ Ratio for ^{91}Mo using a Si(Li) Detector

The first attempts to measure the K/β^+ ratio for ^{91}Mo were undertaken using a cooled Si(Li) detector. This detector, which was supplied by Nuclear Semiconductor, had a surface area of 30 mm^2 and a thickness of 5 mm. The resolution of the detector was 184 eV fwhm at 5.9 keV. This was achieved using a pulsed optical feedback preamplifier. This preamplifier is described later in this chapter in connection with the dead time of the Si(Li) detector system. The resolution of the detector was more than adequate to resolve the K x-rays from adjacent atoms in the region of interest (i.e. around $Z = 41$) and it was, therefore, suitable for the measurement of the intensity of the Nb K_α and K_β x-rays produced by the K-capture decay of ^{91}Mo. The K-Auger electrons produced have insufficient energy to penetrate the 0.0025 cm thick beryllium window of the detector and be detected in the K peak.

Figure 4.5 shows details of the detector shape and the arrangement inside the cryostat. Not shown in this diagram is an aluminium frame which supports the detector and boron nitride mount. Between the detector and boron nitride mount there is a thin aluminium foil for electrical contact.

A typical x-ray spectrum obtained from a 5 mg/cm^2 thick foil of ^{92}Mo irradiated for 1 min. in a 50 MeV bremsstrahlung beam is shown in figure 4.6. The energies of the x-rays were found by calibrating the system with the Np L x-rays from ^{241}Am and also with the fluorescent x-rays from foils of Zr, Nb and Mo irradiated with 22 keV x-rays from ^{109}Cd.

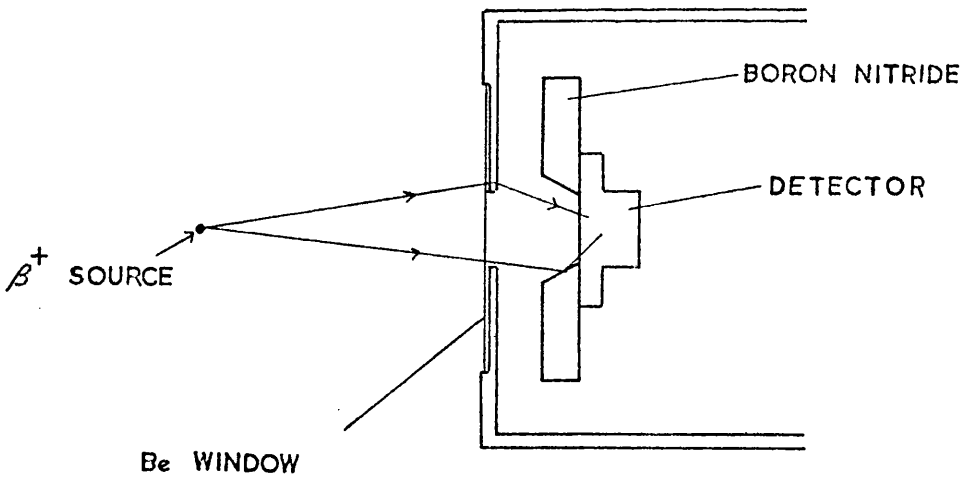

(b) WITH COPPER COLLIMATOR

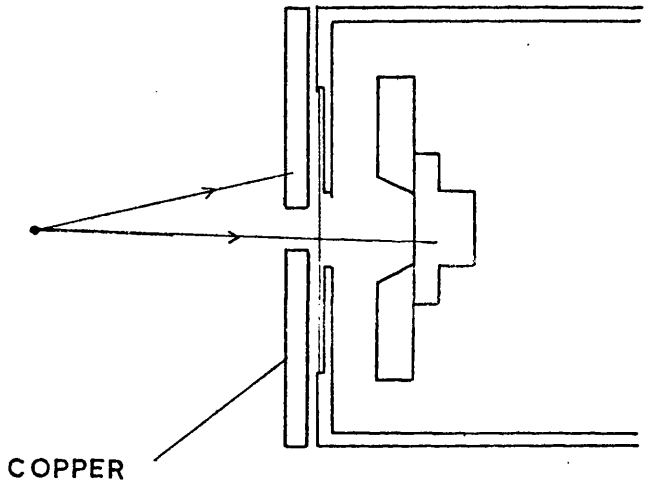

(c) SOURCE HOLDER (i)

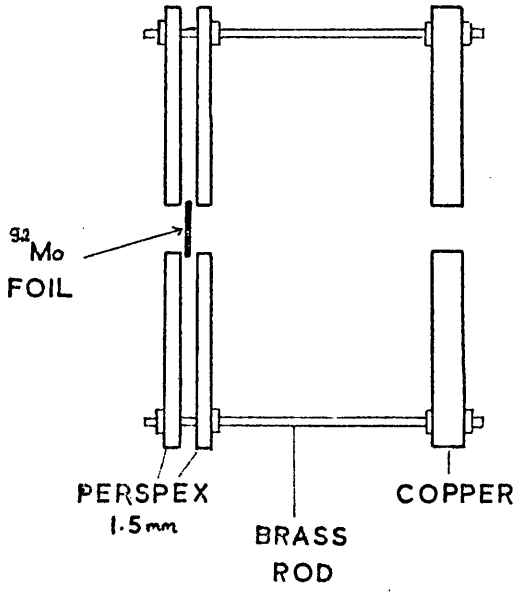

(d) SOURCE HOLDER (ii)

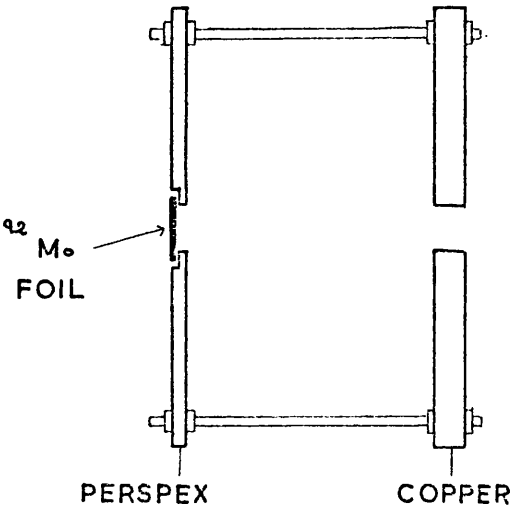

FIG 4-7

Since all positrons entering the detector will deposit some energy the K/β^+ measurement consists of measuring the ratio of the number of counts in the Nb K_α and K_β peaks to the number of events in the continuous positron background. (The presence of the Mo K x-rays seen in figure 4.6 is discussed later in this chapter.) To find the K/β^+ ratio this measurement must then be corrected using the fluorescence yield, ω_K, which is the ratio of the number of K shell vacancies which lead to the emission of K x-rays to the total number of K shell vacancies.

The value of ω_K for Nb is 0.748 ± 0.032. This is taken from a recent review of fluorescence yields by Bambynek et al. (1972). These authors examined all published measurements of ω_K and calculated semiempirical values of ω_K for $4 \leq Z \leq 80$, $Z = 82$ and $Z = 93$ by fitting selected 'most reliable' measured values to an analytical expression.

It can be seen from figure 4.7(a) that it is possible for positrons from the source to be scattered into the detector from, for example, the walls of the cryostat and the boron nitride support thus reducing the measured K/β^+ ratio below the true value by increasing the number of positrons detected. In an attempt to rectify this situation a copper disc, of sufficient thickness (0.23 cm) to stop all the positrons from ^{91}Mo, with a small central opening, was placed in front of the detector window. The diameter of the opening and the distance between the source and the copper disc were chosen so that only those positrons travelling directly from the sample to the detector could be detected (figure 4.7(b)). However, the situation was still not ideal as positrons could still be scattered into the detector but in this arrangement most of the scattering took place at the edges of the copper opening.

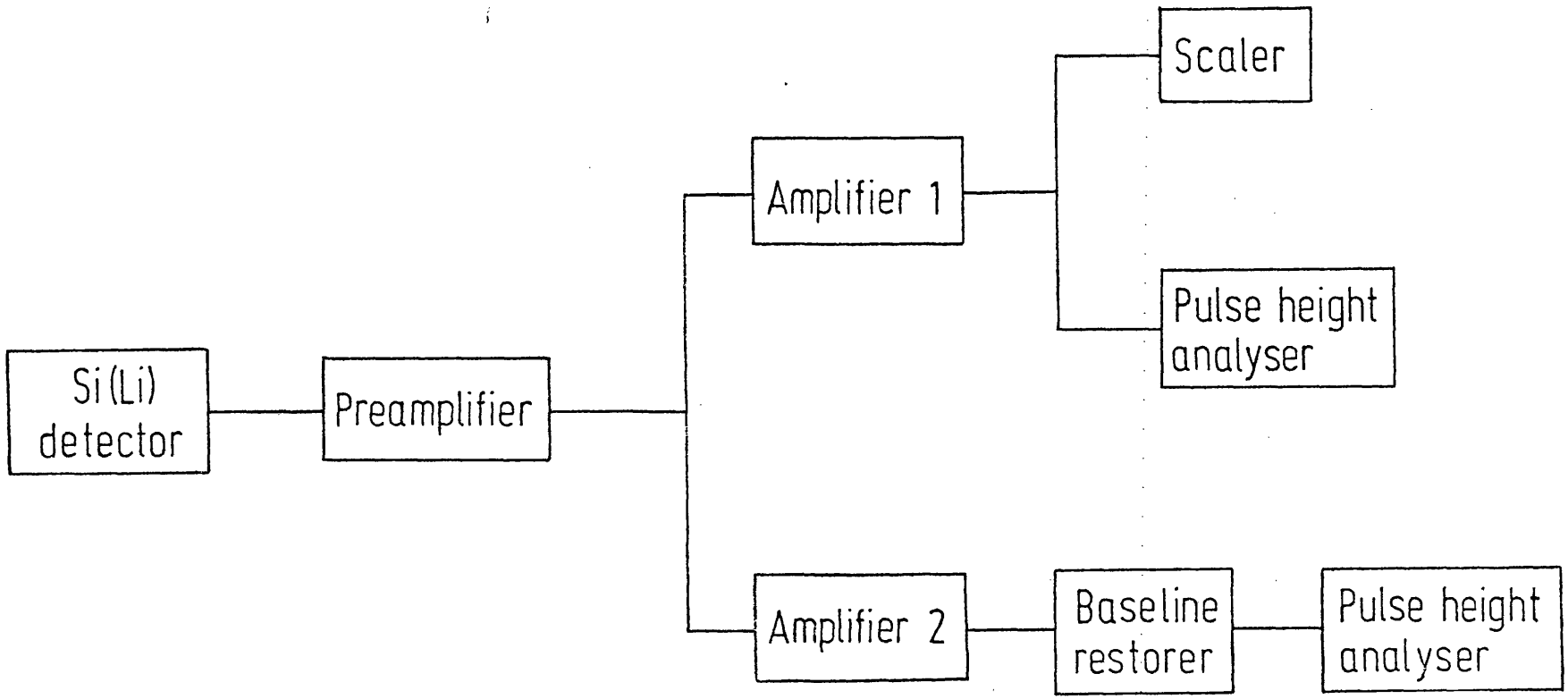
Si(Li) detector
Preamplifier
Amplifier 1
Amplifier 2
Scaler
Pulse height analyser
Baseline restorer
Pulse height analyser

FIG 4-8

Several types of sample holder were employed. In the design of all of them the main consideration was the reduction of the amount of material around the sample to keep to a minimum the amount of scattering of positrons in the sample holder. In one arrangement (figure 4.7(c)) the molybdenum foil was sandwiched between two thin perspex discs each with a central opening only slightly smaller than the sample itself. In another arrangement (figure 4.7(d)) only one perspex disc was used and the molybdenum sample was fitted into a groove in the perspex. The distance of the sample from the detector was 1.6 cm.

Figure 4.8 shows the electronic arrangement used to observe the K x-rays and positrons from the decay of ^{91}Mo. The output from the preamplifier was split so that amplifiers with different gains could be used to look at both the x-rays ($\sim$17 keV) and the positrons (0 - 3.5 MeV). The x-ray spectra were recorded using a Nuclear Semiconductor 511 amplifier (amplifier 1) and a 1024 channel Hewlett-Packard pulse height analyser. The total number of events was recorded on an Ortec scaler connected to the 511 Nuclear Semiconductor amplifier. The positron spectra were recorded using an Ortec 440A amplifier (amplifier 2), a baseline restorer and a 512 channel Northern Scientific pulse height analyser. The baseline restorer was used with the Ortec 440A amplifier because of the rapid change in the output voltage from the preamplifier when the optical feedback was switched on. The 511 Nuclear Semiconductor amplifier, which was designed to be used with a pulsed optical feedback preamplifier, was switched off whenever the optical feedback was switched on. This was the main cause of dead time in the Si(Li) system and is discussed later in this

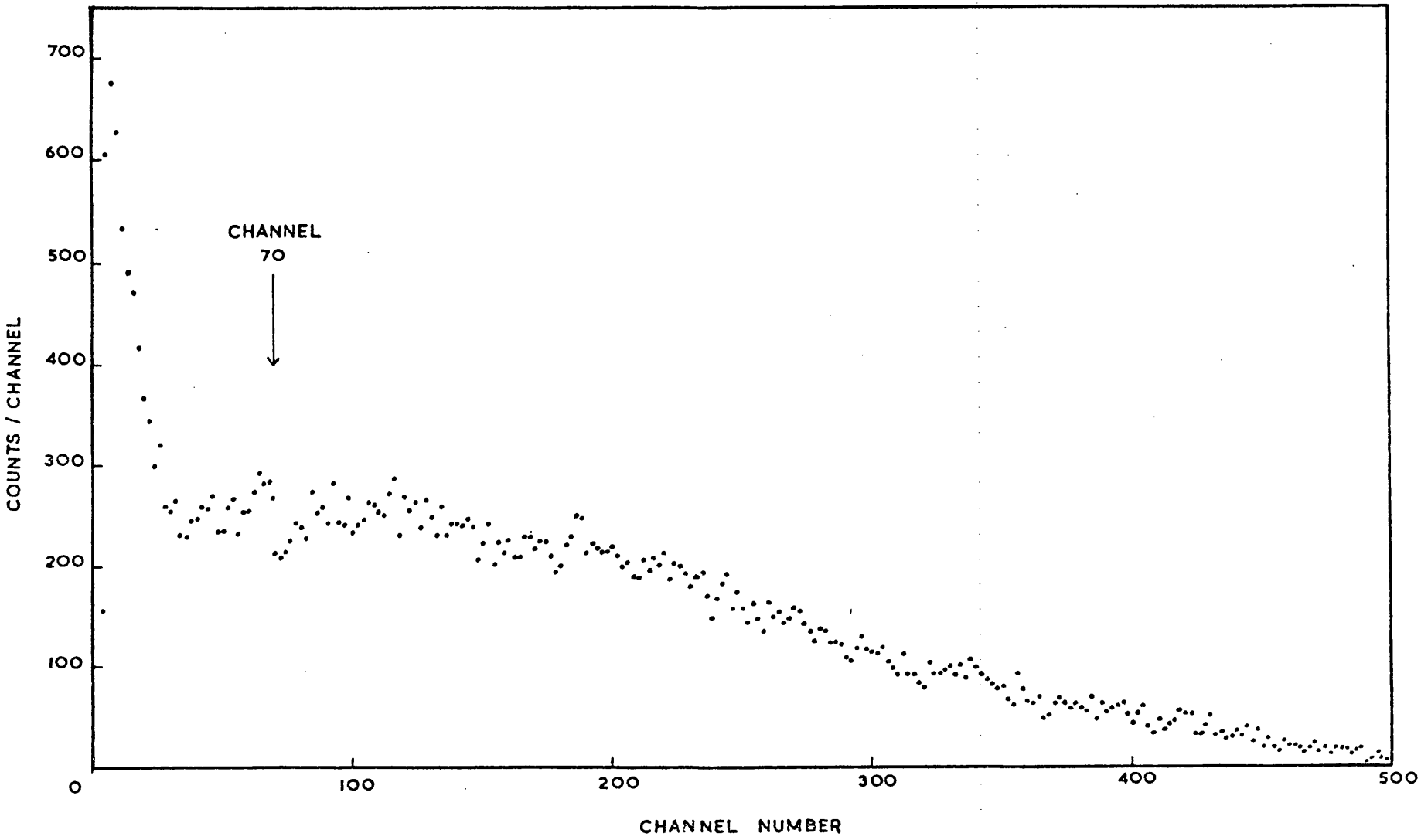
700
600
500
400
300
200
100
0
COUNTS / CHANNEL
CHANNEL
70
100
200
300
400
500
CHANNEL NUMBER

FIG 4-9

chapter. In the K/β^+ measurements all results were taken from the 511 amplifier data (i.e. the x-ray spectra and the scaler readings) and the data from the 440A amplifier was used only to indicate the shape of the positron spectrum so that differences in the dead times of the two amplifiers were unimportant. The scaler threshold was set below the K x-ray peaks and the threshold voltage was determined by connecting a pulse generator to the input of the 511 amplifier and reducing the pulse amplitude until it was just below the scaler threshold. The position of the pulser peak on the Hewlett-Packard analyser then indicated the pulse height below which events would not be registered on the scaler.

Figure 4.6 (a typical x-ray spectrum) shows the position of the scaler threshold. The correction which has to be made to the scaler reading to allow for the events which fall below the threshold is discussed later.

A typical positron spectrum is shown in figure 4.9. This spectrum was taken with the copper collimator in position in front of the detector. A striking feature of this graph is the sharp discontinuity in the spectrum around channel 70. In earlier measurements made without the copper this discontinuity was not so apparent. Since the copper is sufficiently thick to stop all the positrons from ^{91}Mo it is, effectively, a source of 0.511 MeV positron annihilation gamma rays. It was thought that the discontinuity around channel 70 could be the Compton edge from these 0.511 MeV gamma rays. Since the photopeak efficiency of the Si(Li) detector at 0.511 MeV is extremely low it is very unlikely that a photopeak of this energy would be seen.

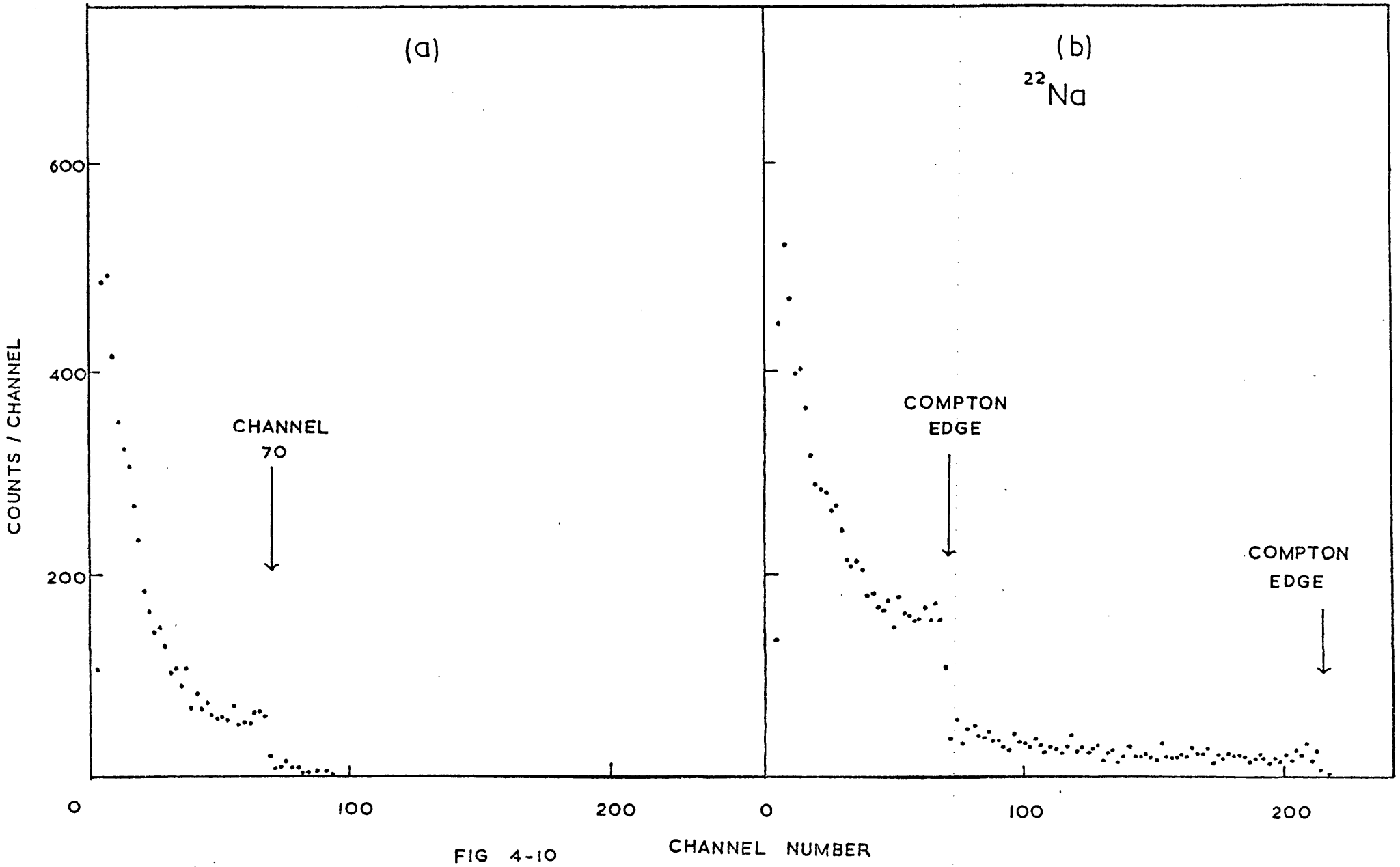
(a)
(b)
^{22}Na
600
400
200
COUNTS / CHANNEL
CHANNEL
70
COMPTON
EDGE
COMPTON
EDGE
0
100
200
0
100
200
CHANNEL NUMBER

FIG 4-10

This interpretation is confirmed by figure 4.10. Spectrum (a) was obtained by completely blocking the opening in the copper collimator with a copper plug. In this arrangement no positrons from the source could enter the detector. For comparison, graph (b) shows the spectrum from ^{22}Na which was enclosed in lead to stop all the positrons. The Compton distributions from the 0.511 and 1.27 MeV gamma rays can be clearly seen. There is very good agreement between the shape and position of the Compton edge produced by the ^{22}Na 0.511 MeV gamma rays (figure 4.10(b)) and the discontinuity in the ^{91}Mo spectrum (figures 4.9 and 4.10(a)). It is, therefore, clear that the increase in the number of low energy events associated with the introduction of the copper collimator is due to the Compton scattering of electrons in the detector by the 0.511 MeV annihilation gamma rays produced in the copper. In the measurements made without the copper collimator it was, of course, possible for some positrons to be stopped in the walls of the cryostat and in the material around the detector but the introduction of the copper greatly increased the number of positron annihilation gamma rays entering the detector.

Measurement of the Effect of Positron Annihilation

Two measurements were required to estimate the correction to the total number of observed events caused by the Compton electrons from the 0.511 MeV annihilation gamma rays. The first, without the plug in the collimator, registered the total number of events, i.e. x-rays, positrons and Compton electrons. The second, with the plug in the collimator and with a ^{91}Mo source prepared under the same conditions as for the first measurement, registered only the Compton electrons since neither the x-rays nor the positrons could penetrate the copper.

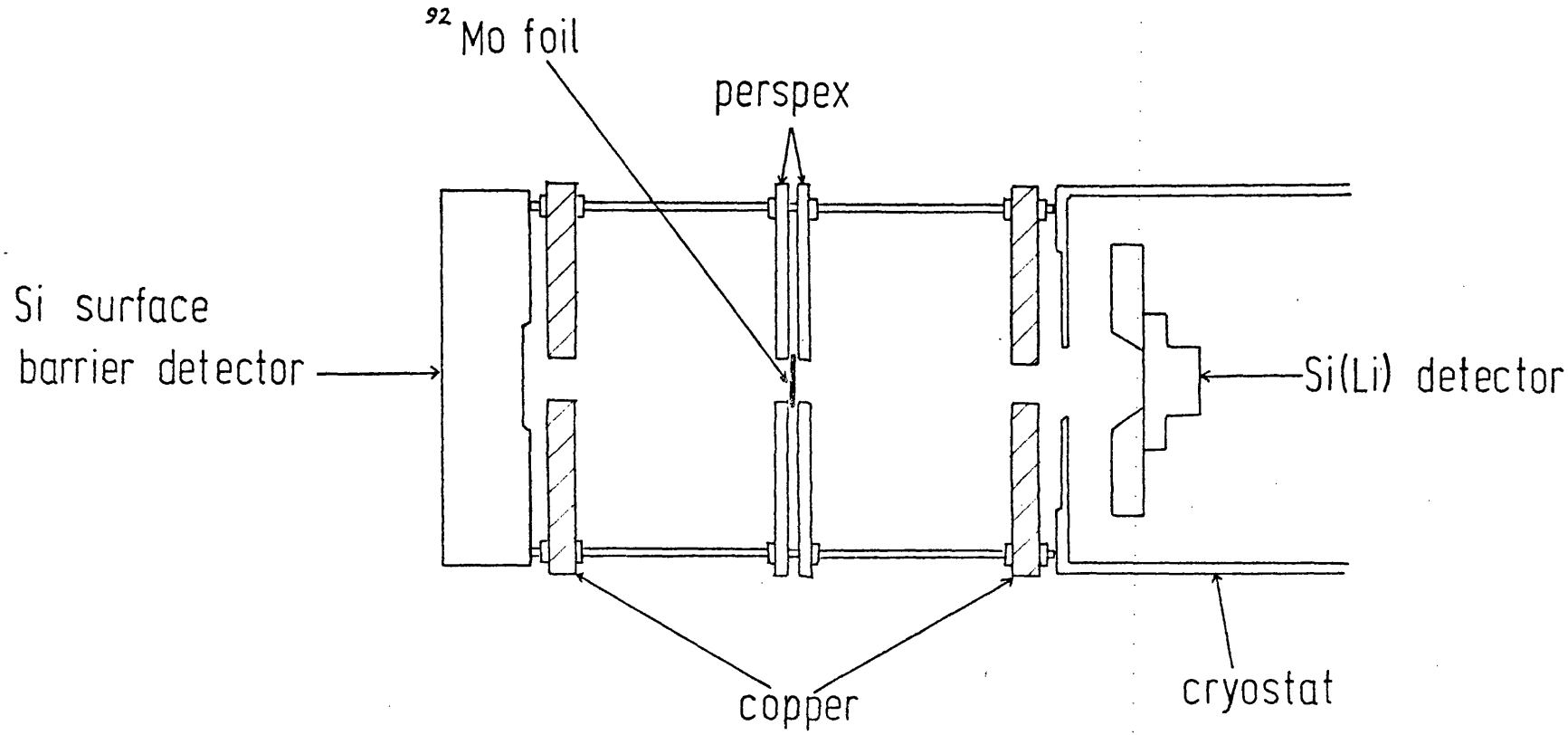
92 Mo foil
perspex
Si surface
barrier detector
Si(Li) detector
copper
cryostat

FIG 4-11

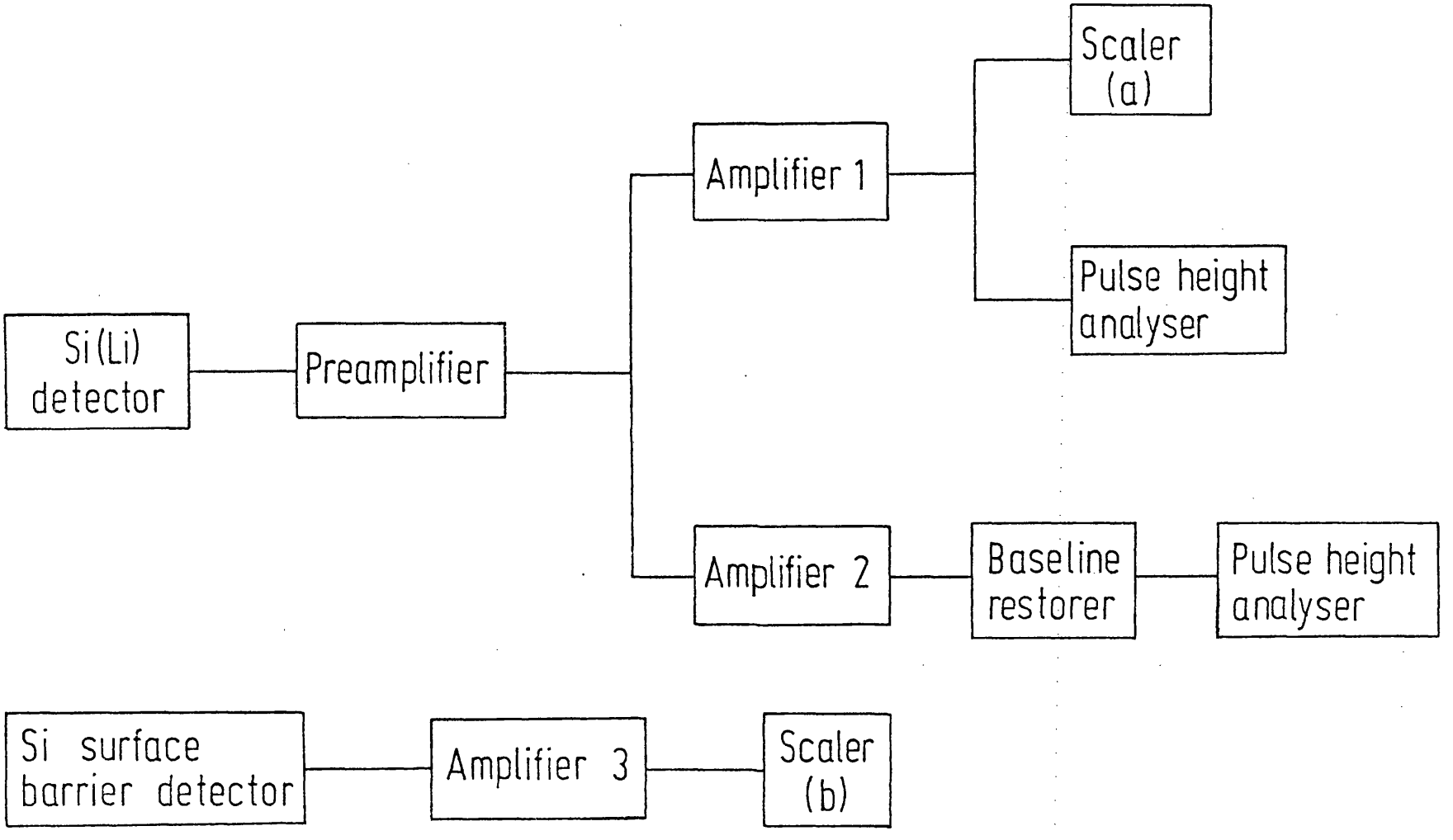
Scaler
(a)
Amplifier 1
Pulse height
analyser
Si(Li)
detector
Preamplifier
Amplifier 2
Baseline
restorer
Pulse height
analyser
Si surface
barrier detector
Amplifier 3
Scaler
(b)

FIG 4-12

After appropriate normalisation the difference between these two measurements eliminated the effect of the Compton electrons.

In order to ensure that the measurements made with and without the plug in the collimator were correctly normalised before subtraction a silicon surface barrier detector was placed on the opposite side of the source from the Si(Li) detector (figure 4.11) and was used to monitor the activity. The pulses from the surface barrier detector were amplified and counted on scaler (b) (figure 4.12). The threshold of this scaler was set above the noise level from the amplifier and counted positrons from the source. The readings from scaler (b) were used to normalise the measurements made with and without the plug in the collimator.

Measurement of the K/β^+ Ratio for ^{91}Mo using the Si(Li) Detector

A piece of molybdenum foil, enriched to 98.32 per cent in ^{92}Mo, 5 mg/cm^2 thick and of area 5 mm x 5 mm was irradiated for 60 secs in a 50 MeV bremsstrahlung beam. The sample was then removed from the irradiation area by a pneumatic transfer system and positioned (see figure 4.7(c) or (d)) 1.6 cm from the copper collimator. After a 10 min. wait to allow the 66 sec ^{91m}Mo activity to decay to a negligible amount a 30 min. count was taken. The x-ray spectrum, the total number of counts on scaler (a) and the positron spectrum in this 30 min. period were registered. In addition, the number of positrons detected in the surface barrier detector was indicated on scaler (b).

The molybdenum sample was then removed and the copper plug inserted in the collimator. Another piece of ^{92}Mo foil was irradiated and the procedure described above was repeated. Counting was continued

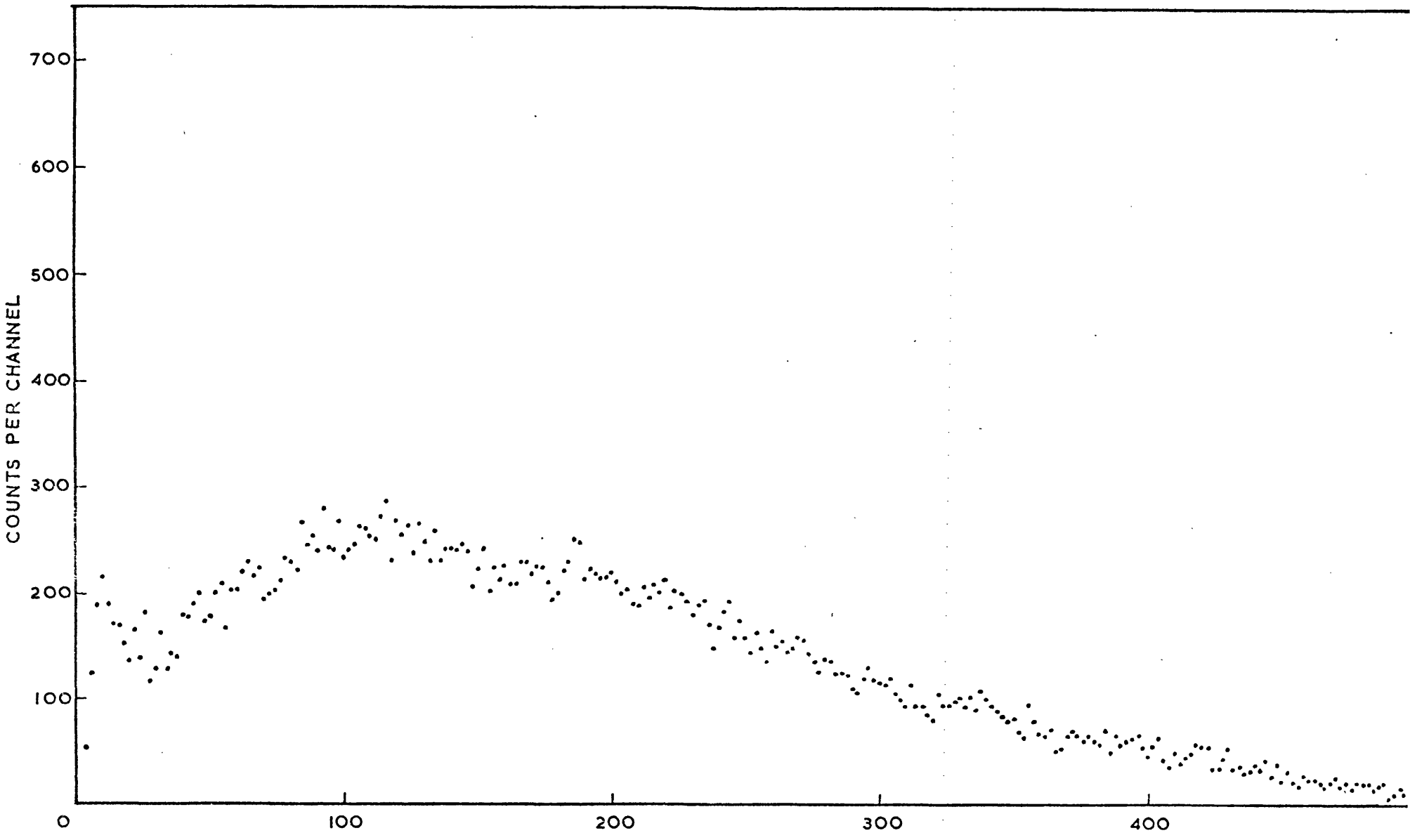
700
600
500
400
300
200
100
0
100
200
300
400
COUNTS PER CHANNEL
CHANNEL NUMBER

FIG 4-13

until the number of events recorded on scaler (b) was the same as before. The corresponding spectra and scaler readings from the two sets of data were subtracted thus eliminating the effects of the 0.511 MeV positron annihilation gamma rays. The resulting positron spectrum is shown in figure 4.13.

Results

	Scaler (a)	Scaler (b)
No plug in collimator	76112	7247
Plug in collimator	13444	7247

$\therefore$ Number of β^+ + x-rays above scaler threshold = 62668 ± 392

Number of counts in Nb K_α peak = 1402 ± 51

Number of counts in Nb K_β peak = 271 ± 29

$\therefore$ Number of β^+ above scaler threshold = 62668 - (1402 + 271)

= 60995 ± 472.

The areas of the Nb K_α and K_β peaks were determined using the SAMPO program and by graphical analysis. The ratio of Nb K x-rays to positrons is, therefore,

$$0.027 \pm 0.001.$$

Adopting a value of

$$\omega_K = 0.748 \pm 0.032 \qquad \text{(Bambynek et al., 1972)}$$

for the fluorescence yield, the K/β^+ ratio for ^{91}Mo was found to be

$$K/\beta^+ = 0.037 \pm 0.002.$$

The main corrections which have to be applied to this result are

now discussed briefly.

Corrections

(1) Events below the scaler threshold

The effect of taking this correction into account is to increase the number of positrons over those actually observed and, as a result, the value obtained for the K/β^+ ratio is reduced. In the present case it was estimated that about 1800 events (~ 3 per cent of the positrons) fell below the scaler threshold. This figure was obtained by extrapolating the x-ray spectrum below the scaler threshold as shown in figure 4.6.

(2) Correction for impurities

According to the gamma ray data the only impurities present in measurable quantities are ^{90}Nb and ^{90}Mo. Both of these isotopes decay by electron capture and positron emission. In the case of ^{90}Nb, positrons and zirconium x-rays are produced, both being counted on scaler (a). The effect of ^{90}Mo is particularly important since it contributes to the intensity of the observed Nb K x-ray peaks as well as to that of the positrons. The ϵ/β^+ ratio of ^{90}Mo has been measured by Cooper et al. (1965) to be 3.0 ± 0.5 suggesting that the K/β^+ ratio is approximately 2.7. This must be compared with the much smaller K/β^+ ratio for ^{91}Mo (theoretical K/β^+ (^{91}Mo) = 0.056). It is clear that even if only a small amount of the total activity is due to ^{90}Mo, the effect on the Nb K x-rays may be fairly large. Later in this chapter results are presented which show that impurities contribute less than 1 per cent to the total activity and about 13 per cent to the Nb K x-ray activity.

(3) Corrections for absorption of x-rays

Absorption of the K x-rays in the molybdenum sample itself, in the air and in the detector window can be calculated from published tables of mass absorption coefficients (Dewey et al., 1969). This correction is described later in this chapter where it is shown that the effect on the Nb K x-rays is of the order of 4-5 per cent.

(4) Scattering of positrons into the detector

The amount of material around the sample was kept to a minimum to reduce scattering of the positrons. The purpose of the copper collimator was to prevent positrons being scattered into the detector from the walls of the cryostat and any material inside the cryostat. The presence of the copper, however, introduces the possibility of scattering from the edge of the opening in the collimator into the detector and the magnitude of this effect is difficult to determine.

Corrections (1) to (3) have the effect of reducing the observed K/β^+ ratio by about 10 per cent. These effects can be determined much more accurately than correction (4). The increase in the observed K/β^+ ratio produced by this correction is considerably more difficult to estimate. The fact that the observed ratio is very much lower than the theoretical value ($B_K \sim 0.6$) suggests that the effect of positron scattering may be rather large. This value of B_K is considerably smaller than the majority of the results described in chapter 3. The difficulty of reliably estimating the effect of scattering led to the rejection of the use of the Si(Li) detector for measuring the ^{91}Mo K/β^+ ratio.

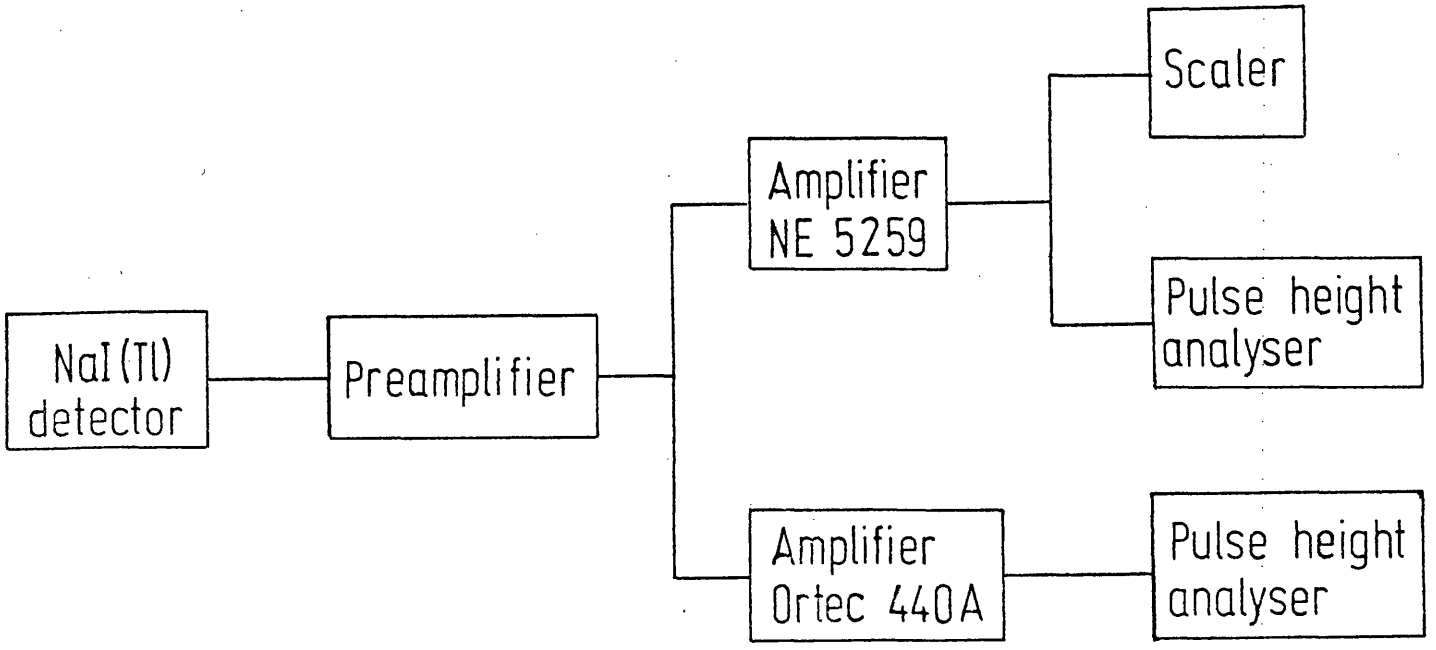
NaI(Tl)
detector
Preamplifier
Amplifier
NE 5259
Scaler
Pulse height
analyser
Amplifier
Ortec 440A
Pulse height
analyser

FIG 4-14

It was decided to employ a different type of detector to measure the K/β^+ ratio. The anti-coincidence proportional counter technique described in chapter 2 for ^{30}P was not suitable for ^{91}Mo for several reasons. The higher energy of the K-capture events from ^{91}Mo means that the x-rays would not be completely absorbed within the central counter. Also, there is the difficulty of obtaining a suitable gaseous compound of ^{92}Mo.

In view of the much larger surface areas available in NaI(Tl) detectors compared with the Si(Li) detector it was felt that the problem of positron scattering by material around the edge of the NaI(Tl) detector would be less important. It was decided to employ a 5.1 cm diameter, 0.64 cm thick NaI(Tl) detector. This thickness of sodium iodide is sufficient to stop all the positrons from ^{91}Mo. The window of the detector was 0.0025 cm thick aluminium. The material surrounding the detector window was also aluminium which, having a lower Z value than the material around the Si(Li) detector window (i.e. the stainless steel cryostat or the copper collimator), caused considerably less positron scattering. Nuclear Enterprises Ltd. supplied the NaI(Tl) detector mounted on a 7.6 cm photomultiplier (9708L) and also a charge sensitive preamplifier (NE 5289). The 7.6 cm photomultiplier was used in conjunction with the 5.1 cm crystal to improve the resolution of the system.

The resolution of this detector was considerably poorer than that of the Si(Li) detector. The Nb and Mo K_α and K_β peaks seen using the Si(Li) detector were not resolved using the NaI(Tl) detector. It was, therefore, necessary to use the relative intensities of these peaks obtained with the Si(Li) detector.

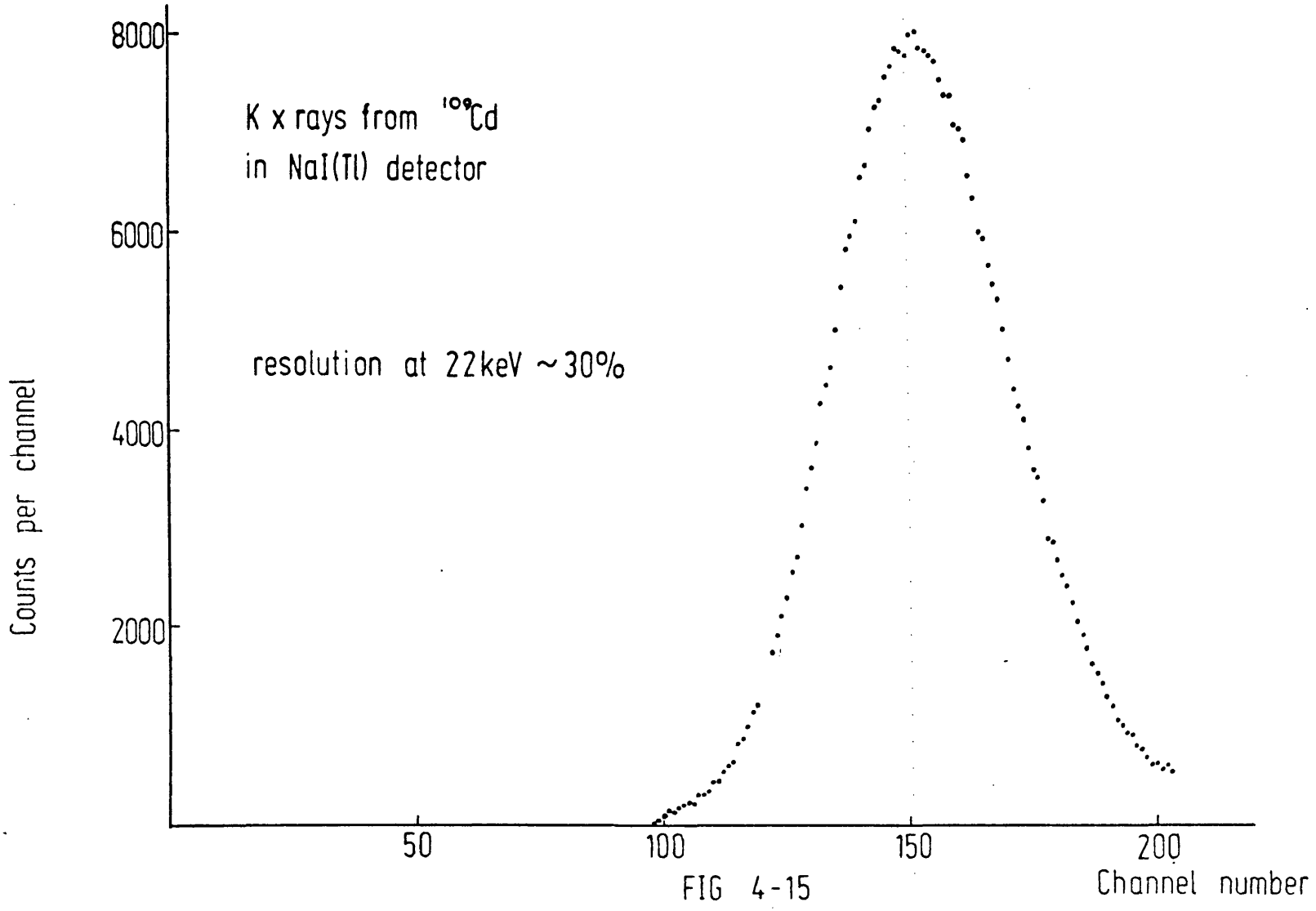
8000
6000
4000
2000
K x rays from ^{109}Cd
in NaI(Tl) detector
resolution at 22keV ~30%
Counts per channel
50
100
150
200
Channel number

FIG 4-15

Measurement of the K/β^+ Ratio for ^{91}Mo using the NaI(Tl) Detector

The electronic arrangement used to detect the positrons and K x-rays from ^{91}Mo is shown in figure 4.14. This arrangement is very similar to that used with the Si(Li) detector except that, in the charge sensitive preamplifier employed (NE 5289), resistive feedback rather than pulsed optical feedback was used. As before, the positron spectrum was obtained with an Ortec 440A amplifier and a Northern Scientific multichannel analyser. The x-ray spectrum was obtained using a Nuclear Enterprises amplifier (NE 5259) and a Hewlett-Packard multichannel analyser. The total number of events was registered on the scaler, whose threshold was set below the K x-ray peak.

The spectrum of x-rays from a calibration source of ^{109}Cd is shown in figure 4.15. This spectrum was accumulated on the 1024 channel Hewlett-Packard analyser and the channels were then added in groups of five. This was done to allow the use of the SAMPO program to find the areas of the x-ray peaks. This program can fit peaks only if they extend over less than 150 channels. Since the resolution of the NaI(Tl) detector is much poorer than that of the Si(Li) detector the x-ray peak is so wide that this grouping of the channels does not degrade the resolution.

The irradiation procedure was exactly as for the measurements with the Si(Li) detector, i.e. samples of ^{92}Mo were irradiated for 60 sec. in a 50 MeV bremsstrahlung beam. As before, data was accumulated in a 30 min. period starting 10 mins after the end of the irradiation.

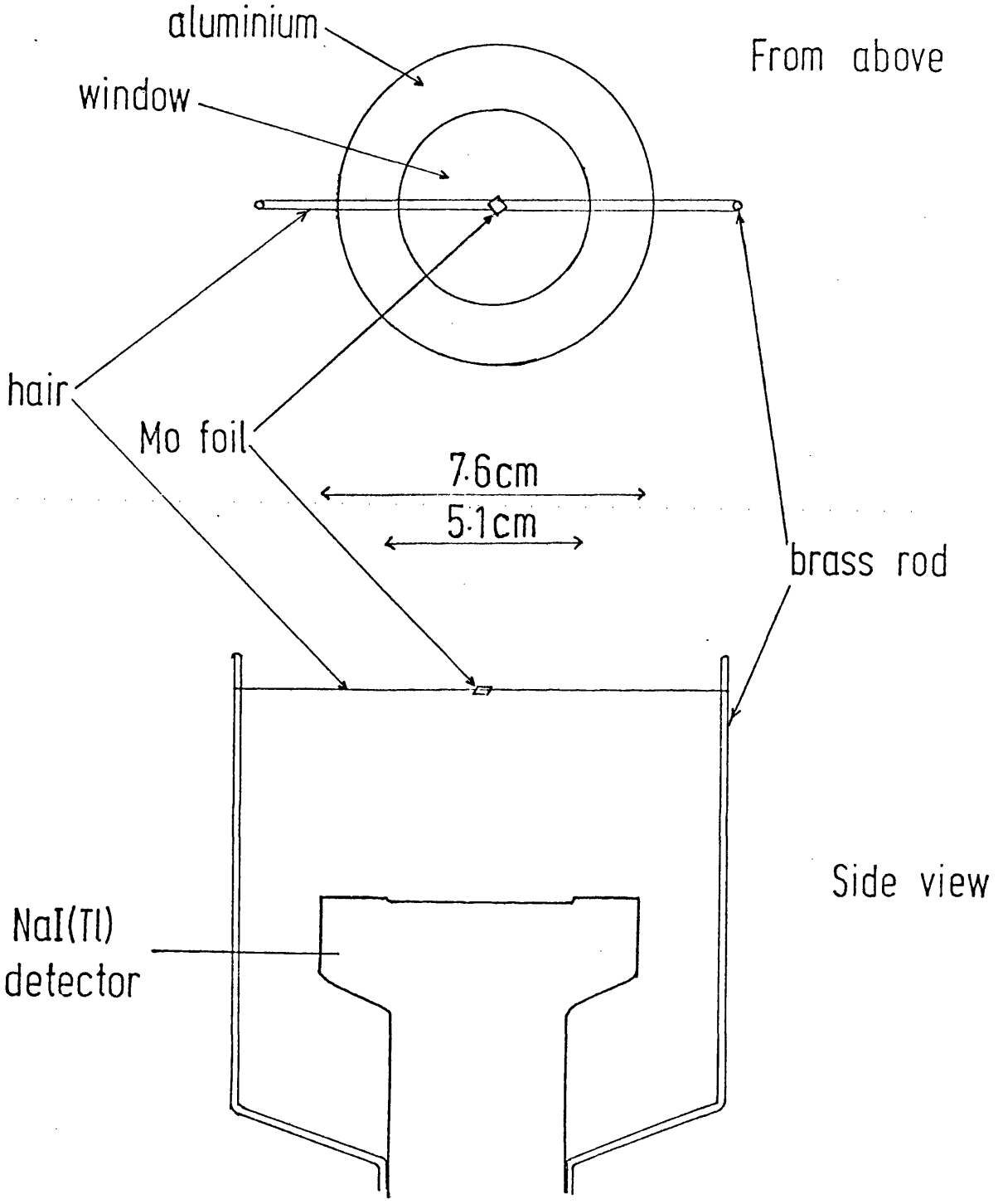
aluminium
window
From above
hair
Mo foil
7·6cm
5·1cm
brass rod
Side view
NaI(Tl)
detector

FIG 4-16

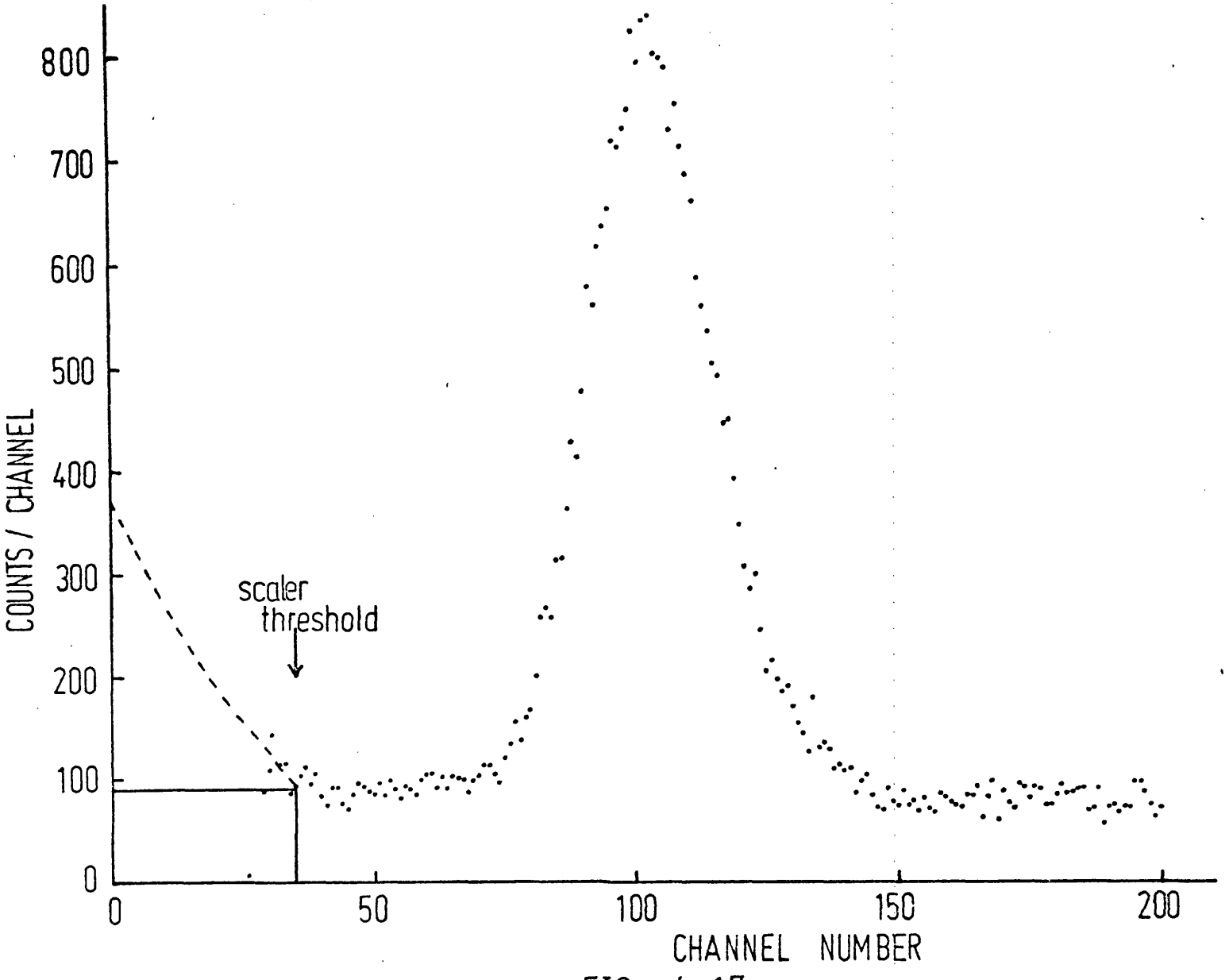
800
700
600
500
400
300
200
100
0
COUNTS / CHANNEL
scaler
threshold
0
50
100
150
200
CHANNEL NUMBER

FIG 4-17

The samples of ^{92}Mo which had been irradiated during the Si(Li) measurements were used again in this part of the experiment. The minimum time between the earlier irradiations and the beginning of the NaI(Tl) measurements was three weeks but for most of the samples the interval was longer. The residual activity in the samples before the NaI(Tl) measurements was found to be extremely small and has been neglected.

The NaI(Tl) detector was clamped in a vertical position and the ^{92}Mo sample was balanced directly above the centre of the detector on two hairs stretched between two vertical brass rods (figure 4.16). This arrangement was designed to have as little material as possible near the source to minimise scattering of the positrons. The brass rods were well separated and hair was used to support the foils in preference to, for example, wire because of its lower Z value. Measurements were made at source-detector distances of 1.5, 2.5 and 5.0 cm. The measurement at 1.5 cm was repeated with a copper collimator, 0.23 cm thick and with a 2.5 cm diameter opening placed over the detector window. The size of the ^{92}Mo foils used was 2 mm x 2 mm.

Figure 4.17 shows the x-ray spectrum obtained during a 30 min. period from an irradiated ^{92}Mo foil positioned 2.5 cm above the NaI(Tl) detector. The scaler threshold was determined as described for the Si(Li) detector measurements and is shown on this graph.

The positron spectrum obtained during the same period is shown in figure 4.18. The peak at 0.511 MeV from positrons which annihilate outside the detector can be clearly seen. (For comparison figure 4.19 shows the spectrum from a calibration source of ^{22}Na.) This in

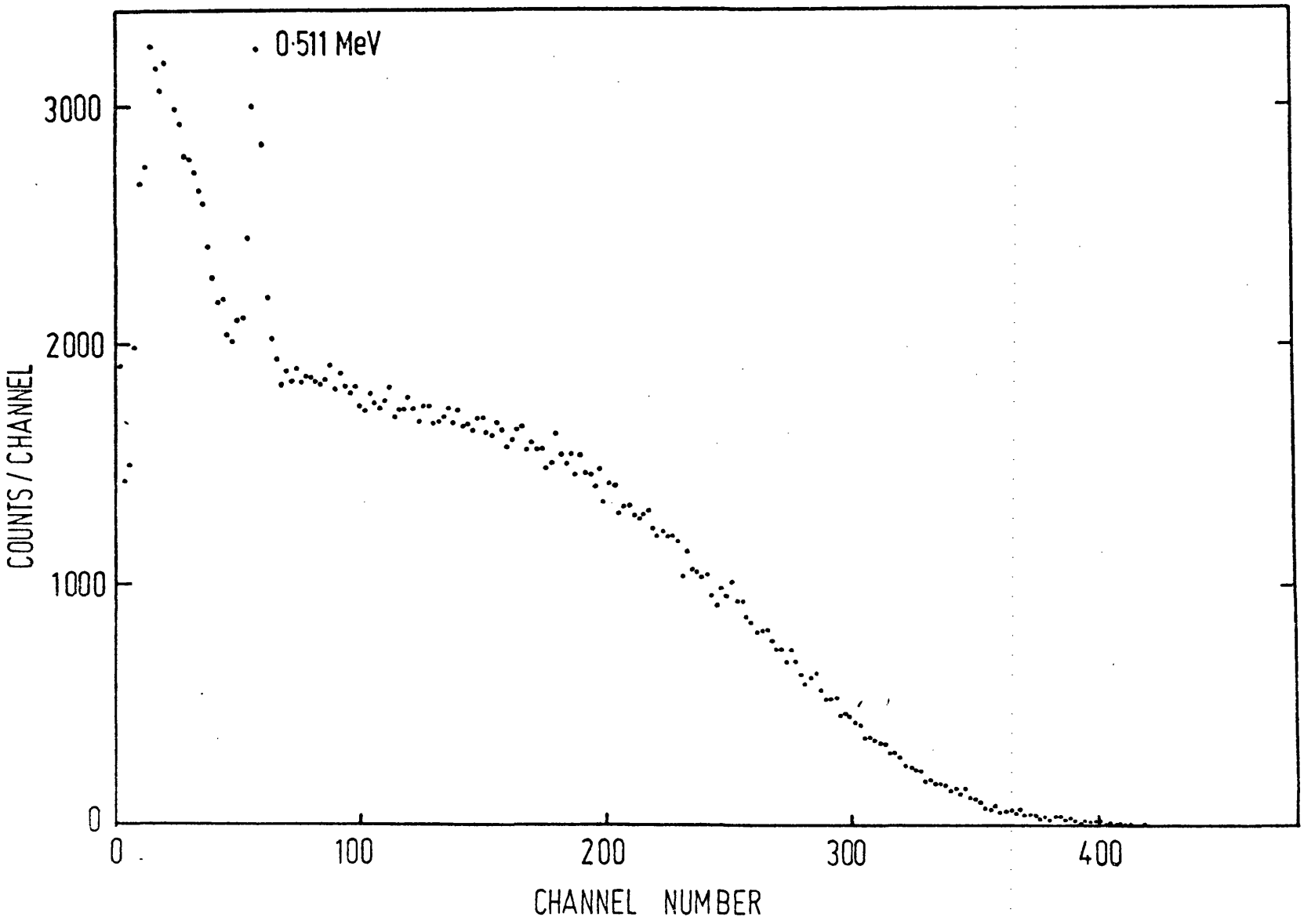
0·511 MeV
3000
2000
1000
0
COUNTS / CHANNEL
0
100
200
300
400
CHANNEL NUMBER

FIG 4-18

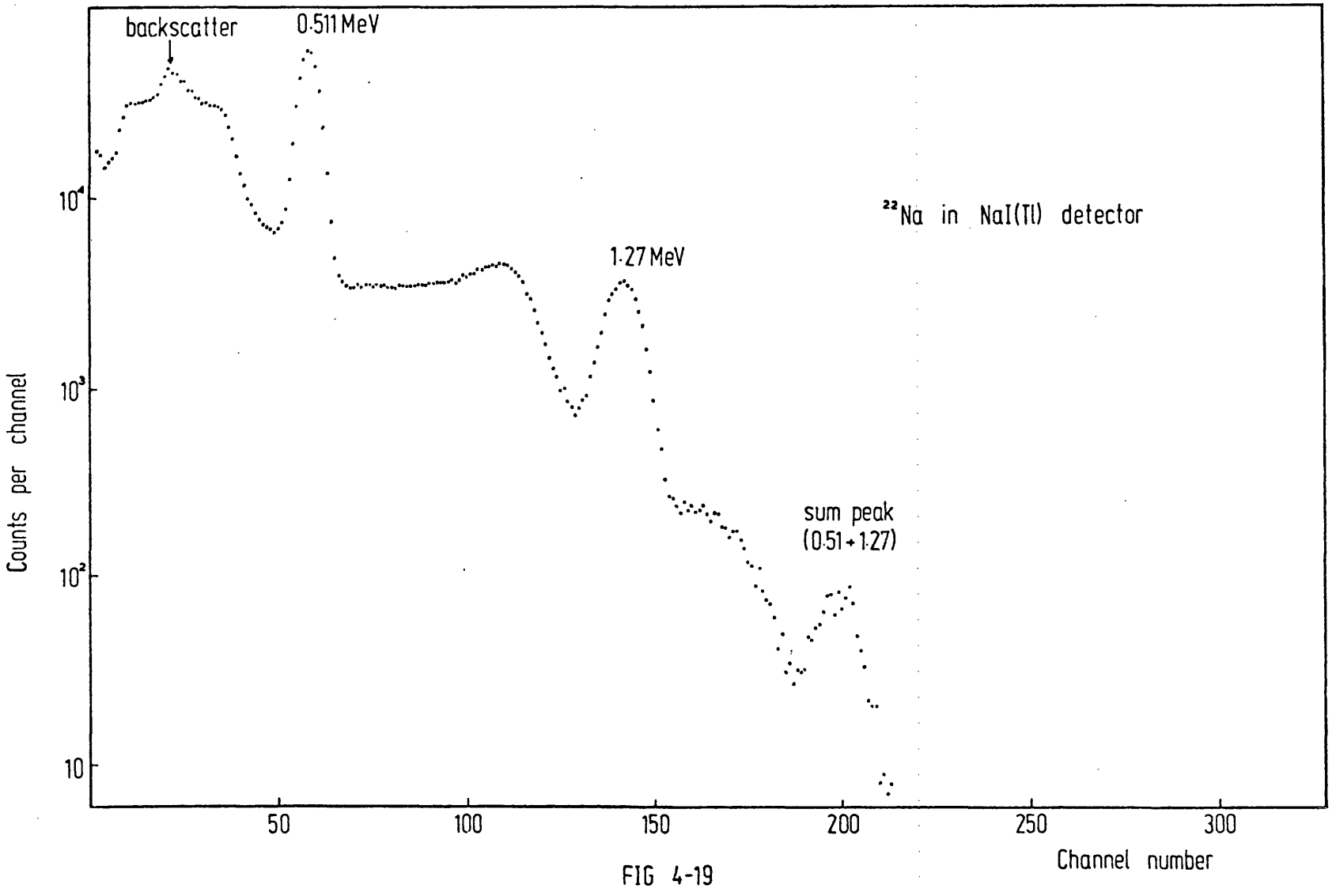
backscatter
0·511 MeV
1·27 MeV
sum peak
(0·51 + 1·27)
^{22}Na in NaI(Tl) detector
Counts per channel
Channel number
10
10^2
10^3
10^4
50
100
150
200
250
300

FIG 4-19

contrast with the Si(Li) detector results where only the Compton distribution from these annihilation gamma rays could be seen because of the lower photopeak efficiency.

Identical measurements of the x-rays, number of counts on the scaler and the β^+ spectrum were made without a molybdenum sample to determine the background. This background consists of noise from the detector and electronics and cosmic ray background. It was not thought advisable to reduce the detection of the background activity by shielding the detector because of the difficulties which would arise from positrons being scattered by the shielding. The background was subtracted from the x-ray and positron spectra and scaler readings.

These measurements were repeated at source-detector distances of 1.5 and 5.0 cm. The measurement at 1.5 cm was repeated with the copper collimator over the detector. The data obtained at each distance represents the sum of data from several samples. The measurements were made at these various source-detector distances to investigate the effect of positron scattering from the edge of the detector window or the collimator.

Corrections to the NaI(Tl) Detector Measurements

(1) Events below the scaler threshold

In figure 4.17, which shows a typical x-ray spectrum, the data has been extrapolated linearly (solid line) into the region below the scaler threshold. The area below this extrapolated line represents the correction to be made to the number of events registered on the scaler. This extrapolation of the x-ray spectrum was carried out for the measurements at each source-detector distance. The magnitude of

Run number	Source-detector distance (cm)	Corrected scaler reading	Intensity of 511 keV peak	Total number of events due to 511 keV gamma rays	Number of positrons + K x-rays
1	5.0	$(3.124 \pm 0.034) \times 10^5$	6109 ± 91	$(4.331 \pm 0.554) \times 10^4$	$(2.691 \pm 0.065) \times 10^5$
2	2.5	$(3.509 \pm 0.039) \times 10^5$	4588 ± 78	$(3.253 \pm 0.416) \times 10^4$	$(3.184 \pm 0.057) \times 10^5$
3	2.5	$(5.705 \pm 0.058) \times 10^5$	8422 ± 107	$(5.971 \pm 0.764) \times 10^4$	$(5.108 \pm 0.096) \times 10^5$
4	1.5	$(2.486 \pm 0.026) \times 10^5$	3072 ± 84	$(2.178 \pm 0.283) \times 10^4$	$(2.269 \pm 0.039) \times 10^5$
5	1.5*	$(1.882 \pm 0.021) \times 10^5$	8345 ± 150	$(5.917 \pm 0.757) \times 10^4$	$(1.290 \pm 0.079) \times 10^5$

*with copper collimator

TABLE 4.1

the correction was found to vary from 0.5 to 0.8 per cent of the total number of events. It was felt, therefore, that this extrapolation would not introduce any large errors. To allow for a possible systematic error in the extrapolation a more extreme form for the extrapolated spectrum was taken (dotted line in figure 4.17). This extrapolation was considered to represent the maximum possible correction for events below the threshold. In figure 4.17 this maximum correction amounts to 0.92 per cent of the total events. An error of 1 per cent has, therefore, been included to allow for a possible systematic error in the extrapolation. Table 4.1 shows the corrected number of scaler events obtained at each source-detector distance. The errors shown represent the statistical errors added in quadrature with a 1 per cent systematic error.

(2) Annihilation of positrons

Positrons which are stopped in the material around the detector produce 0.511 MeV annihilation gamma rays which may enter the detector and be recorded either in a 0.511 MeV photopeak or in the accompanying Compton distribution. Since the area of the photopeak can be readily estimated, the total contribution of the annihilation gamma rays to the observed number of events can be determined if the ratio of the intensities of the 0.511 MeV photopeak and its Compton distribution is known.

However, it is probable that this ratio depends on the angle at which the annihilation gamma rays enter the detector. Since the half life of ^{91}Mo is fairly short, it was decided to employ a longer lived positron source to investigate the effect of 0.511 MeV gamma rays entering the detector at different positions. However, no suitable

(a)

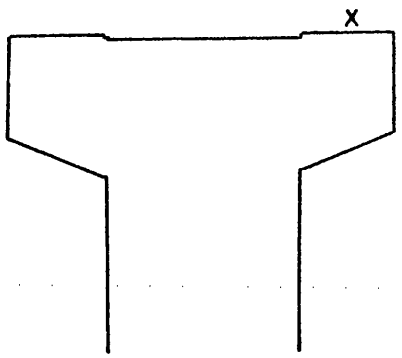

(b)

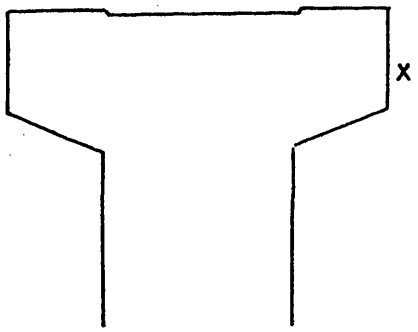

(c)

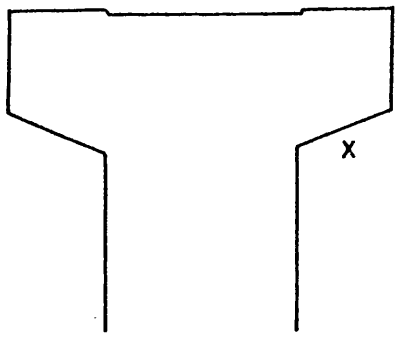

x – position of source (^{137}Cs or ^{203}Hg)

FIG 4-20

positron sources without gamma rays could be obtained and, instead, sources emitting single gamma rays with energies on either side of 511 keV were used. The sources employed were ^{203}Hg and ^{137}Cs. Both are β^- emitters. ^{203}Hg emits electrons with a maximum energy of 0.2 MeV and a gamma ray of energy 279.1 keV while ^{137}Cs emits electrons with a maximum energy of 1.18 MeV and a gamma ray of energy 661.6 keV. Therefore, provided there is sufficient material in front of the source to prevent the β^- particles reaching the detector, the observed spectra can be used to determine the total/photopeak ratios for 279.1 and 661.6 KeV gamma rays. According to Davisson (1965), the ratio of the total cross section to the photoelectric cross section for gamma rays in sodium iodide is approximately a linear function of energy in the region 250 - 700 keV. Therefore, the total/photopeak ratio for 511 keV gamma rays can be found by a linear interpolation of the results obtained for the 279.1 and 661.6 keV gamma rays.

The total/photopeak ratio for each of the gamma rays was determined as a function of source position using the configurations shown in figure 4.20 (a), (b) and (c). These three arrangements correspond roughly to the probable positions of positron annihilation during the K/β^+ measurements. The values of the total/photopeak ratio obtained in each of these positions are 6.40, 7.85 and 8.48 for the 661.6 keV gamma ray and 2.57, 3.38 and 3.54 for the 279.1 keV gamma ray. By linear interpolation the total/photopeaks ratio for 511 keV gamma rays in configurations (a), (b) and (c) are 6.14, 7.18 and 7.94, respectively. The mean of these results has been adopted as the true total/photopeak ratio for the annihilation gamma rays and the spread of these three values is taken to represent a possible systematic error in the ratio.

The total/photopeak ratio for the 0.511 MeV gamma rays is, therefore

$$7.09 \pm 0.90.$$

Another estimate of the total/photopeak ratio for annihilation gamma rays was made using a source of ^{22}Na. This isotope emits positrons and 1.27 MeV gamma rays. The presence of the Compton distribution from the 1.27 MeV gamma ray meant that only a rough estimate of the total/photopeak ratio for the positron annihilation gamma rays could be made. The results, however, were in agreement with the interpolated ratio given above.

Table 4.1 shows the areas of the 0.511 MeV photopeaks in the spectra obtained during the K/β^+ measurements. These areas were estimated using the SAMPO program. Also shown in this table are the total number of events due to the annihilation gamma rays calculated using the photopeak areas and the above total/photopeak ratio. The number of positrons plus K x-rays was obtained by subtracting the total number of events due to the 511 keV positron annihilation gamma rays from the corrected scaler reading.

(3) Correction for the presence of impurities

From the gamma ray evidence the only activities produced other than ^{91m}Mo and ^{91}Mo are ^{90}Mo ($\tau_{1/2}$ = 5.7 h) and ^{90}Nb ($\tau_{1/2}$ = 14.6 h). The large value of the K/β^+ ratio for ^{90}Mo and the important contribution made by this isotope to the intensity of the Nb K x-rays has already been mentioned.

In order to estimate the amount of these contaminant activities a half life measurement of the activity was made. The x-ray spectra from the Si(Li) detector showed both Nb and Mo K x-rays but these

(a) RESISTIVE FEEDBACK

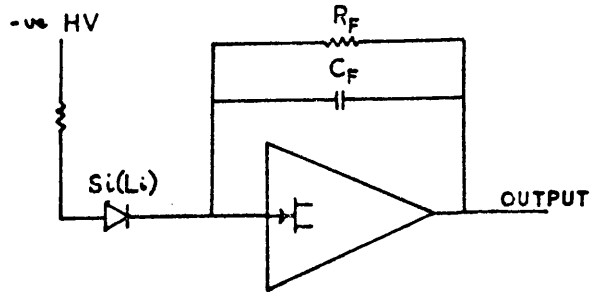

(b) OPTICAL FEEDBACK

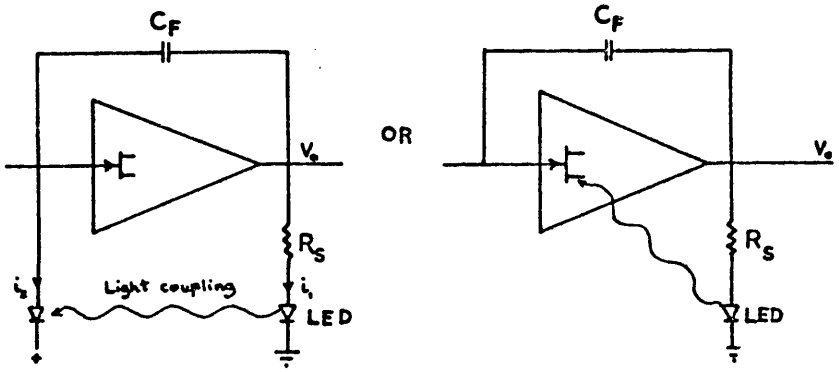

(c) PULSED OPTICAL FEEDBACK

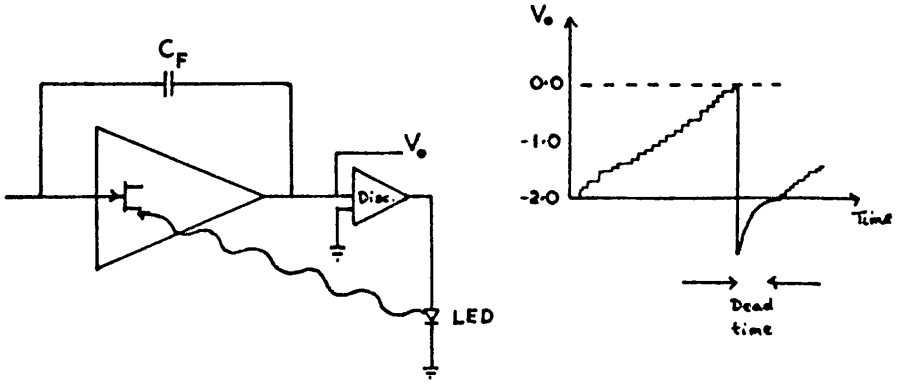

FIG 4-21

x-rays could not be resolved in the NaI(Tl) detector because of its much poorer resolution. The half life measurement was, therefore, made using the Si(Li) detector so that the half lives of the Nb and Mo K x-rays could be measured separately.

For the half life measurement, a thick sample (52 μm) of ^{92}Mo was irradiated for 60 secs in a 50 MeV bremsstrahlung beam and then positioned in front of the Si(Li) detector. Starting 10 mins after the end of the irradiation to allow the 66 sec activity of ^{91m}Mo to decay to a negligible amount, a series of x-ray spectra and corresponding scaler readings, of 3 mins duration, was taken over a period of about 26 hours. The number of counts in the Nb K_α and K_β and the Mo K_α peaks were determined but before half life measurements could be made the data had to be corrected for the dead time of the Si(Li) detector system.

The causes of the dead time and the measurement of its magnitude as a function of counting rate are now described.

Dead Time of a Pulsed Optical Feedback Preamplifier

The high resolution (184 eV fwhm at 5.9 keV) of the Si(Li) detector system was achieved using a pulsed optical feedback preamplifier and main amplifier supplied by Nuclear Semiconductor Inc. It is instructive at this stage to consider the advantages and disadvantages of this system compared with a more conventional resistive feedback preamplifier.

In earlier x-ray detectors the best resolution (~700 eV fwhm) was obtained using a cooled FET stage with a large feedback resistor, R_f, in the preamplifier (figure 4.21 (a)). However, the presence of this

resistor contributes thermal noise to the system and in order to reduce this noise a very large value of R_f must be used. In practice, the effective value of R_f cannot be increased indefinitely since the optimum frequency band for the best signal to noise ratio in the preamplifier is about 100 kHz and high valued resistors show a decrease in their resistive component if the frequency exceeds a few kHz (Goulding et al., 1969). The presence of R_f also increases the stray capacity to ground at the FET input. Both these effects limit the energy resolution which can be obtained.

The replacement of R_f by optical coupling as the d.c. feedback between the output and input of the preamplifier (figure 4.21 (b)) allows much better energy resolution to be obtained (Landis et al., 1972). The intensity of the light given out by the light-emitting diode (LED) is proportional to the current flowing through it and the current produced in the photodiode is proportional to the intensity of the light which illuminates it. Thus

$$i_2 = \phi i_1 = \phi \frac{V_o}{R_s} = \frac{V_o}{R_f'}$$

where ϕ represents the coupling involved in the production and detection of the light. R_f' is the effective feedback resistance. The magnitude of ϕ can be varied by changing the relative positions of the LED and the photodiode or by the use of absorbers. Typical values of ϕ range from 10^{-6} to 10^{-10}. For $R_s = 100\Omega$, R_f' ranges typically from 10^8 to $10^{12}\Omega$. Since the light coupling is almost instantaneous the value of R_f' is independent of frequency, at least up to several MHz. This arrangement still has the disadvantage of the stray capacity of the photodiode at the FET input but, in practice, the FET has its protective

cover removed and the drain-gate junction may be used as the photodiode.

A further development of this system leads to the pulsed optical feedback preamplifier employed in the present experiment. It had been observed (Landis et al., 1971) that non-linearity in the LED current-light relationship led to inferior resolution at high counting rates. However in the pulsed optical feedback preamplifier the LED is normally switched off. A discriminator compares the preamplifier output voltage with two reference voltages and the LED is pulsed on to maintain the output voltage within its normal operating range (figure 4.21 (c)). In the preamplifier employed in the ^{91}Mo experiment the charge on C_F builds up until the output voltage V_o rises to 0.0 volts. At this point, the discriminator switches on the LED to restore the output to a negative level and the LED is then switched off. The cycle is then repeated as the detector leakage current charges up the feedback capacitance and the output voltage rises. When the LED is pulsed on, a reject signal is fed to the main amplifier which then rejects all signals for a fixed period (in this case 700 μsec) until the output voltage is again within its operating range. This period when the main amplifier is gated off is the main cause of dead time in the system. The length of the period for which the amplifier is gated off after an optical feedback pulse is chosen to allow the output voltage to rise to its operating level before the amplifier again accepts pulses. However, at very low counting rates the detector leakage current is so low that the output voltage may not rise to its operating range within the 700 μsec period. In this case the dead time of the system may be very much longer than 700 μsec per feedback pulse.

The high resolution obtained with this system makes it well suited for x-ray fluorescence measurements since the K x-rays from neighbouring elements can be resolved for all but the very light elements.

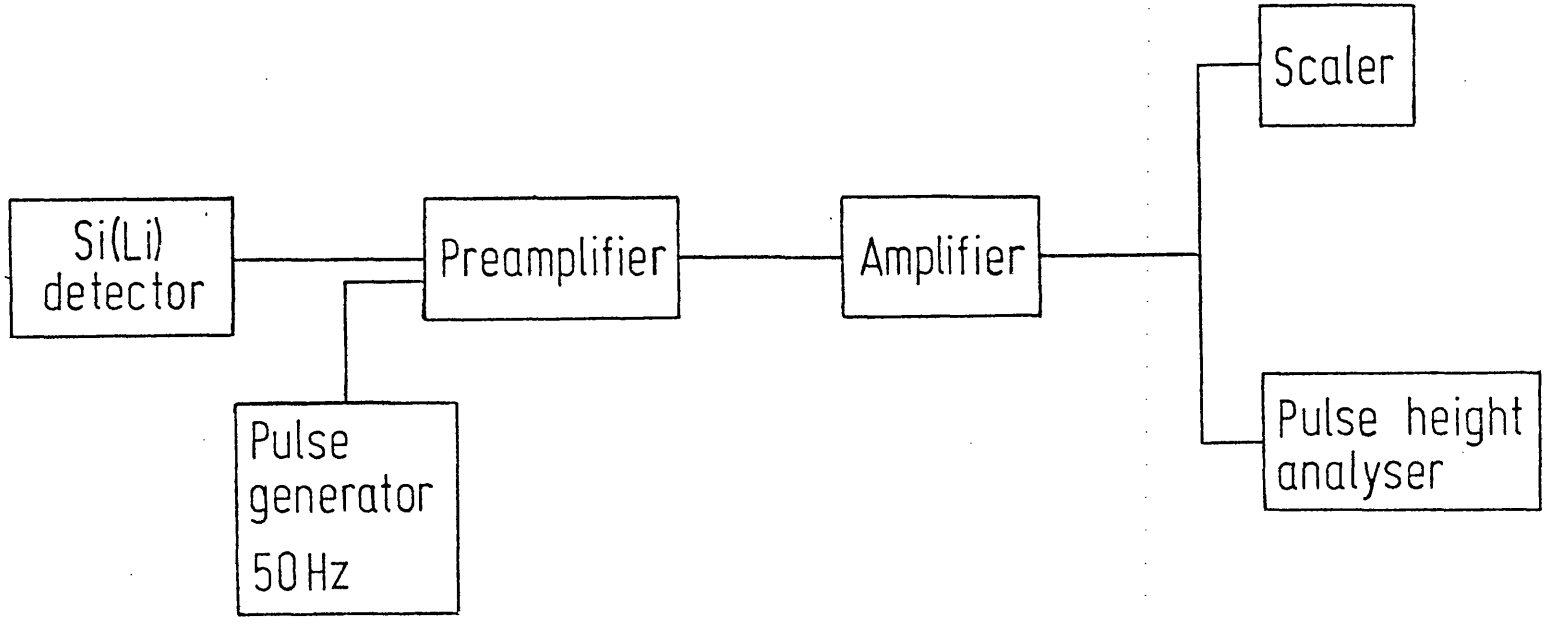
Si(Li)
detector
Preamplifier
Amplifier
Scaler
Pulse height
analyser
Pulse
generator
50 Hz

FIG 4-22

However measurements of the half lives of x-rays are difficult because of the large uncertainties in the dead time corrections at low counting rates.

Measurement of the Dead Time of Si(Li) Detector System

A block diagram of the electronics used to measure the dead time is shown in figure 4.22. The arrangement is identical to that used for the half life measurements described earlier except for the insertion of the output signal from a 50 Hz pulse generator into the test input of the preamplifier. In order to ensure that the dead time was being generated in the same way as for the half life measurements, a sample of ^{92}Mo, irradiated for 1 min. at 50 MeV, was used to produce dead time in the system. (This is discussed in more detail below in connection with dead time measurements made with a source of ^{106}Ru,) The amplitude of the pulse generator output was adjusted to be slightly greater than the K x-ray pulses and the resulting spectrum of x-ray and pulse generator peaks taken on the Hewlett-Packard 1024 channel analyser. The spectrum and the corresponding number of scaler counts in 3 min. counting periods were taken at different counting rates.

The frequency of the pulse generator was 50 Hz and, therefore, in 3 mins, 9000 pulses were produced. The actual number of pulses recorded in the pulse generator peak in the spectrum thus enabled the open time, and hence the dead time, of the system to be calculated. The areas of the peaks were estimated using the program SAMPO and the graph of dead time as a function of counting rate is shown in figure 4.23. The number of counts/min. on the x-axis is the number of scaler counts minus the number of counts in the pulser peak. This assumes that

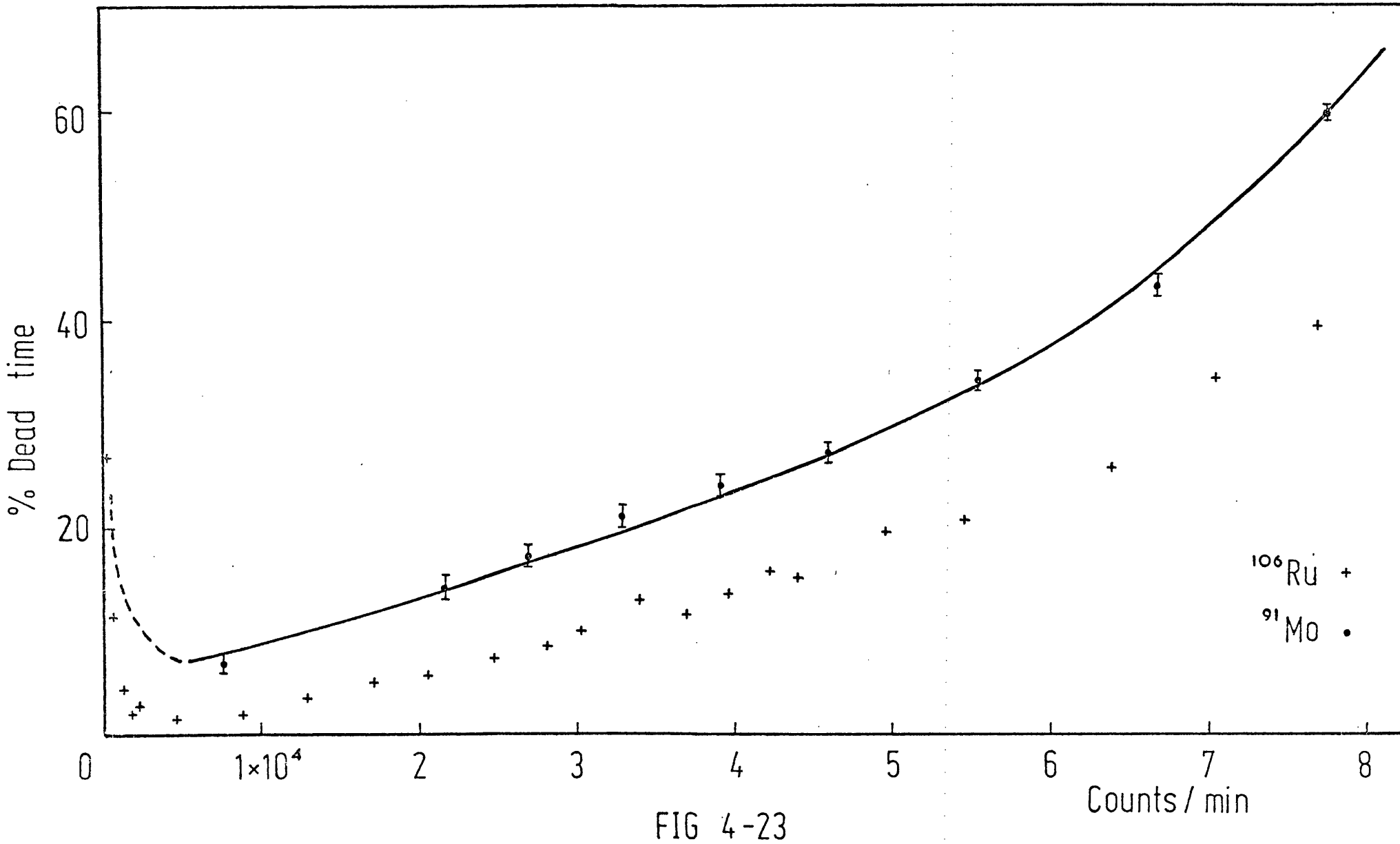

FIG 4-23

the pulser events do not contribute significantly to the dead time, which is a reasonable assumption at high counting rates. The justification of this assumption at lower counting rates is discussed below.

In order to obtain more information about the shape of the dead time correction curve, measurements similar to those described above were made with the ^{92}Mo sample replaced by a source of ^{106}Ru. The longer half life of this source (367 days) enabled a greater range of counting rates to be investigated. ^{106}Ru decays to ^{106}Rh which emits β^- particles with a maximum energy of $\sim$3.5 MeV (i.e. similar to the ^{91}Mo β^+ end point energy) but there are also other β^- branches with lower end points. The results obtained from ^{106}Ru are also shown on figure 4.23. For counting rates greater than 5000/min. it is clear that the dead time produced by ^{106}Ru is much less than that produced by the ^{91}Mo source. This is consistent with the view that most of the dead time arises from the detection of high energy β particles. Although the maximum β energy is approximately the same for ^{91}Mo and ^{106}Ru there are relatively fewer high energy β particles associated with ^{106}Ru than with ^{91}Mo. This association of dead time with the detection of high energy events also justifies the assumption that the dead time associated with pulse generator events is small.

The dead time measurements with ^{106}Ru at low counting rates exhibit a very sudden rise in dead time as the counting rate decreases. As mentioned earlier this rise in dead time is due to the very low detector leakage current. It was not possible to make reliable estimates of the dead time of the system at these very low counting rates with the ^{91}Mo source because of the short half life of this source. It was merely possible to observe that, at low counting rates

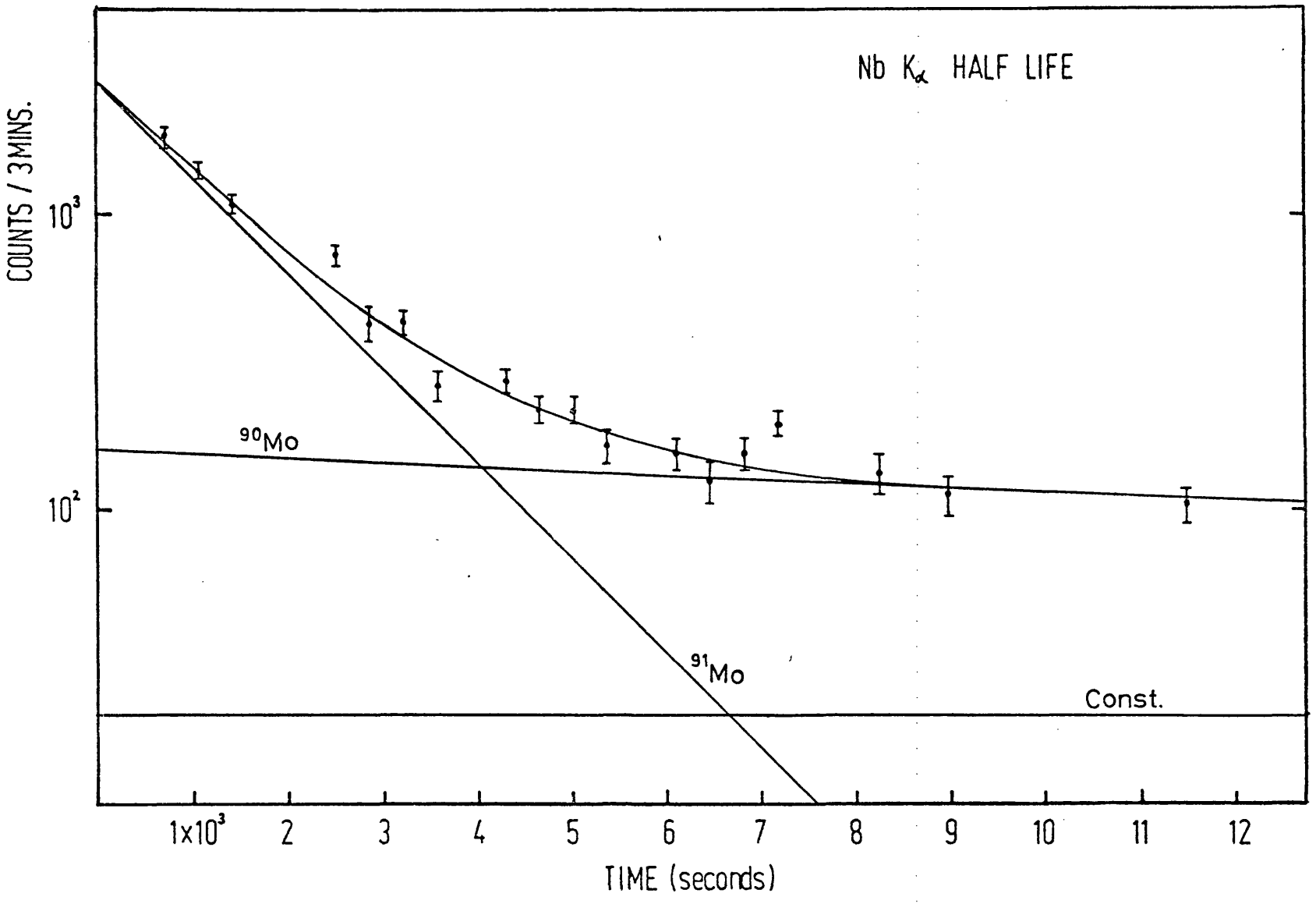
Nb K_α HALF LIFE
COUNTS / 3 MINS.
10^3
10^2
^{90}Mo
^{91}Mo
Const.
1x10^3
2
3
4
5
6
7
8
9
10
11
12
TIME (seconds)

FIG 4-24

with ^{91}Mo, the dead time was high and has been assumed to follow the general shape shown by ^{106}Ru below counting rates of 5000/min. (dotted curve in figure 4.23). It must be emphasised that the dead times measured with the ^{106}Ru source were not used to correct the half life data but were used only to indicate the lowest counting rate to which the ^{91}Mo dead time measurements could be applied.

A least squares fit to the dead time data from ^{91}Mo was performed using the minimization program VA04A. It was found that an expression of the form

$$y = Ae^{Bx} + Ce^{Dx} + E$$

where y = dead time

x = counts/min.

gave a good fit to the data. The parameters A, B, C, D and E were varied by the program to obtain the optimum fit which is shown as the solid curve on figure 4.23. This expression was used to correct all half life data for counting rates greater than 5000/min. For lower counting rates the dead time correction could not be reliably estimated and such data had to be neglected. This meant that information about long-lived activities in the half life measurements was greatly restricted.

Results from Half Life Measurements

Half life data for the Nb K_α activity and the scaler readings were corrected for dead time as described above. The resulting graphs of activity against time are shown in figures 4.24 and 4.25. The Nb K_β and Mo K_α peaks were not sufficiently intense to allow accurate half life determinations although a rough estimate of the Mo K_α half life is described later in connection with the origin of these molybdenum K x-rays.

(a) Nb K_α activity

(i) The experimental points were fitted using the VA04A program to the expression

$$y = A_1 e^{-\lambda_1 t} + A_2 e^{-\lambda_2 t} + A_3$$

where λ_1 and λ_2 are the decay constants of ^{91}Mo and ^{90}Mo, respectively. An expression of this form was chosen since it was known that, of all the activities observed in the gamma ray measurements, only ^{91}Mo and ^{90}Mo could produce Nb x-rays. The constant term A_3 was included to allow for the very long-lived activity (62 days) due to internally converted gamma rays from the 0.1045 MeV isomeric state in ^{91}Nb. Since this activity is extremely long-lived compared with the ^{91}Mo and ^{90}Mo activities, it was thought reasonable to represent it by a constant term. The values obtained for the parameters A_1, A_2 and A_3 are

$$A_1 = 2838 \pm 112$$

$$A_2 = 133 \pm 19$$

$$A_3 = 22 \pm 13.$$

This fit is shown in figure 4.24.

(ii) Since the value of A_3 obtained above is very small, the experimental points were also fitted to the expression

$$y = B_1 e^{-\lambda_1 t} + B_2 e^{-\lambda_2 t}$$

with λ_1 and λ_2 as before. The values obtained for B_1 and B_2 are

$$B_1 = 2812 \pm 110$$

$$B_2 = 161 \pm 8.$$

The inability of the minimization program to distinguish between the 5.7 hr ^{90}Mo activity and the same activity plus a constant, occurs

here because insufficient information about long-lived activities was available. This is a consequence of the uncertainty in the dead time corrections at low counting rates. Although measurements of the Nb K_α x-ray activity were taken for about 26 hours only the data for the first 3 hours could be corrected reliably for dead time.

The measurements of the K/β^+ ratio were made during the time from 10 to 40 mins after the end of the irradiation and, using the known ^{91}Mo and ^{90}Mo half lives and the above results, the various contributions to the Nb K_α activity in this time interval can be calculated. The percentage of the total Nb K_α activity associated with the 15.49 ^{91}Mo activity in this 30 min. period is found to be

(i) $(87.6 \pm 2.3)\%$

and (ii) $(87.1 \pm 0.7)\%$.

It is clear from this that the estimation of the percentage of Nb K x-rays due to ^{91}Mo is little affected by the exact nature of the longer-lived components. However, the value obtained from (i) has been adopted since this is derived from the more realistic representation of the activities contributing to the Nb K x-rays.

(b) Scaler readings

The scaler readings, after correction for dead time, were fitted to several expressions using the program VA04A.

(i) The experimental points were fitted to the expression

$$y = C_1 e^{-\lambda_1 t} + C_2 e^{-\lambda_2 t} + C_3 e^{-\lambda_3 t}$$

where λ_1, λ_2 and λ_3 are the decay constants of ^{91}Mo, ^{90}Mo and ^{90}Nb, respectively. These are all the activities known to be present from

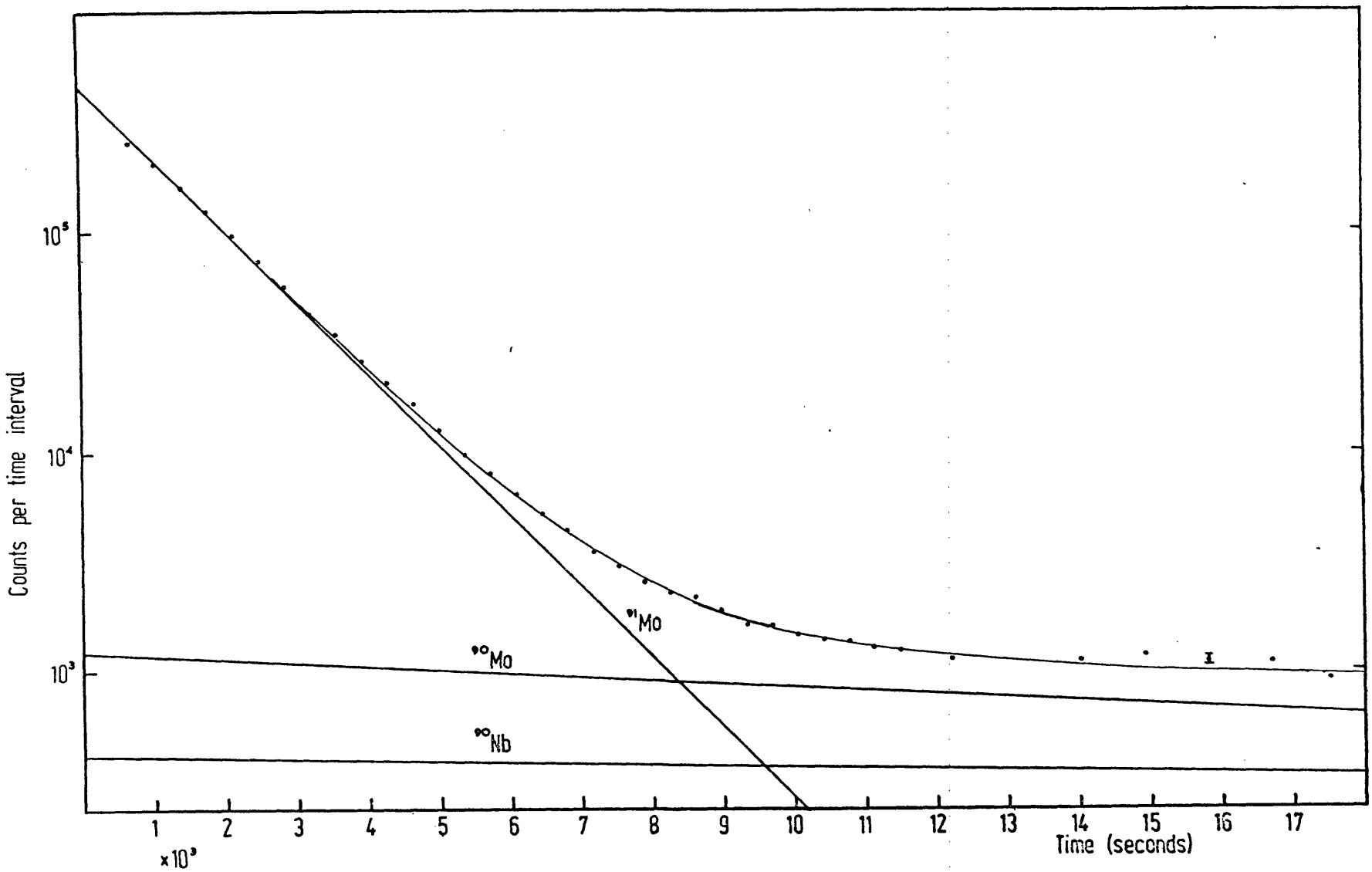
Counts per time interval
10^5
10^4
10^3
^{91}Mo
^{90}Mo
^{90}Nb
1
2
3
4
5
6
7
8
9
10
11
12
13
14
15
16
17
×10³
Time (seconds)

FIG 4-25

gamma ray studies. The values obtained for the parameters C_1, C_2 and C_3 are

$$C_1 = 461410 \pm 2600$$

$$C_2 = 1133 \pm 320$$

$$C_3 = 458 \pm 260.$$

This fit is shown in figure 4.25.

(ii) As with the x-ray half life data, the actual half lives of the long-lived components did not significantly affect the fit. The expression

$$y = D_1 e^{-\lambda_1 t} + D_2 e^{-\lambda_1 t} + D_3$$

also gave a good representation of the data with

$$D_1 = 461410 \pm 2400$$

$$D_2 = 1360 \pm 190$$

$$D_3 = 239 \pm 130.$$

From these results the contribution of ^{91}Mo to the total activity is found to be

(i) $(99.16 \pm 0.29)\%$

and (ii) $(99.10 \pm 0.18)\%$.

Thus only a very small amount of the total activity is associated with impurities. However, even a very small amount of the ^{90}Mo contaminant activity produces a large contribution to the Nb K x-ray activity due to the relatively high K/β^+ ratio for this isotope.

(4) Correction for the presence of Molybdenum K x-rays

It can be seen from the x-ray spectra taken with the Si(Li) detector (figure 4.6) that Mo K x-rays are present together with the expected Nb K x-rays from the K-capture decay of ^{91}Mo. An accurate

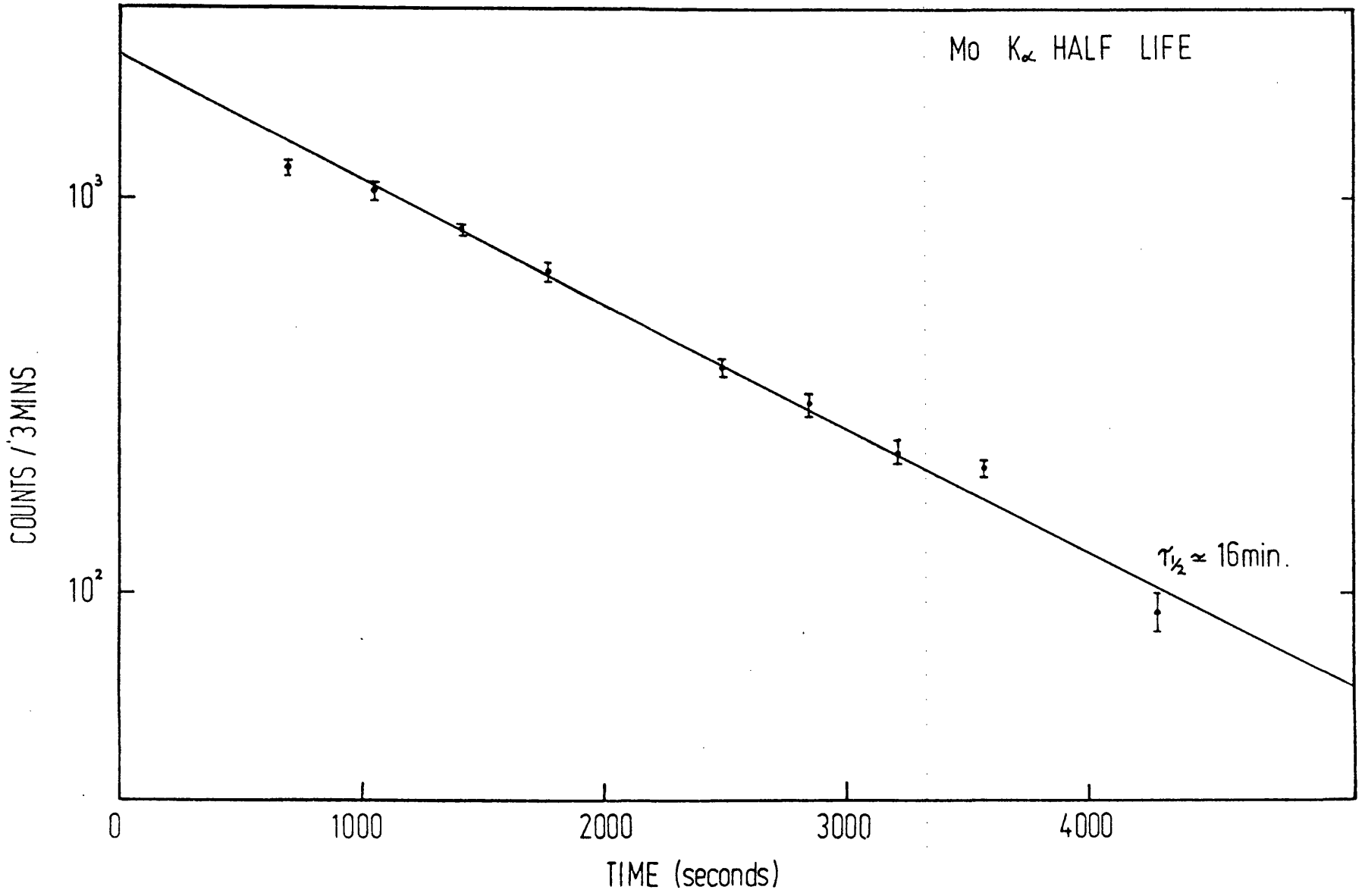
Mo Kα HALF LIFE
10^3
10^2
COUNTS / 3 MINS
$\tau_{1/2} \simeq$ 16min.
0
1000
2000
3000
4000
TIME (seconds)

FIG 4-26

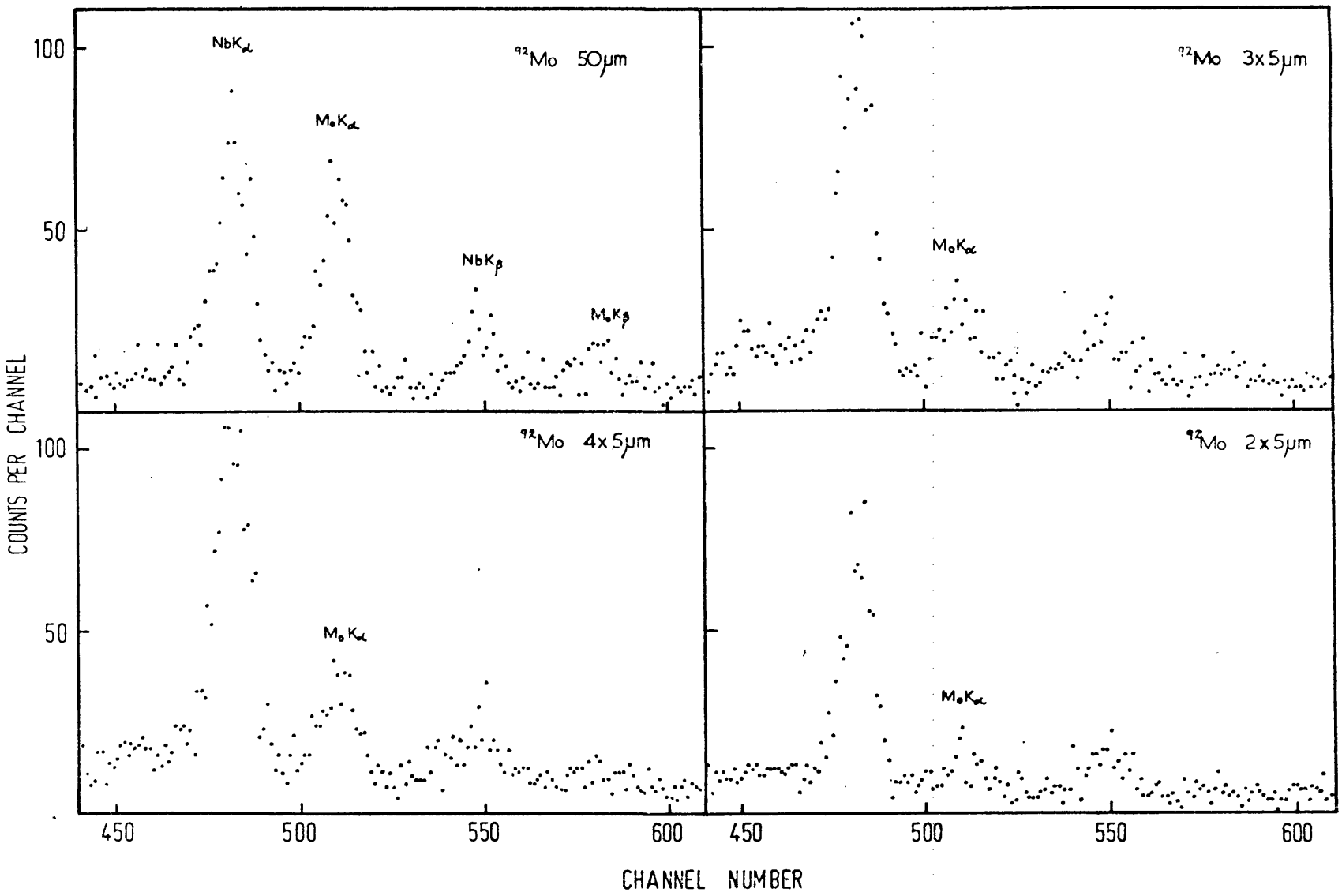
^{92}Mo 50μm
^{92}Mo 3x5μm
^{92}Mo 4x5μm
^{92}Mo 2x5μm
NbKα
MoKα
NbKβ
MoKβ
100
50
COUNTS PER CHANNEL
450
500
550
600
CHANNEL NUMBER

FIG 4-27

determination of the half life of the Mo K_α x-rays was not possible because of the low intensity of these x-rays ($\sim$10 per cent of the Nb K_α intensity). Figure 4.26 shows all the data which could be obtained on the decay of this x-ray. The points shown have been corrected for dead time. From this graph the half life of the Mo K_α x-rays is estimated to be approximately 16 mins. If a long-lived component of Mo K_α x-rays is also present this estimate must be reduced.

Molybdenum K x-rays could arise from K-electron capture in a technetium isotope or from internal conversion in a molybdenum isotope. However, no such isotope, with a suitable half life, is known to exist.

Another possibility is the production of molybdenum K x-rays by fluorescence in the molybdenum foil caused by positrons from the decay of ^{91}Mo. If this interpretation is correct it explains the fact that the half life of the Mo K_α x-rays is approximately the same as that of ^{91}Mo. There should also be components with half lives of 5.7 hrs and 14.6 hrs corresponding to excitation of the sample by positrons from ^{90}Mo and ^{90}Nb but the intensities of these activities are so small that their effect on the Mo K_α half life would be almost negligible.

Figure 4.27 shows the x-ray spectra from molybdenum samples of different thicknesses. Samples consisting of two, three and four thicknesses of the 5 μm ^{92}Mo foil as well as one thick piece of ^{92}Mo (52 μm) were studied. These samples were each irradiated for 60 secs and, after a period of 10 mins, a 30 min. x-ray spectrum was accumulated. The areas of the Nb and Mo K_α peaks were determined and, after correction for absorption of the x-rays in the molybdenum sample, in the air

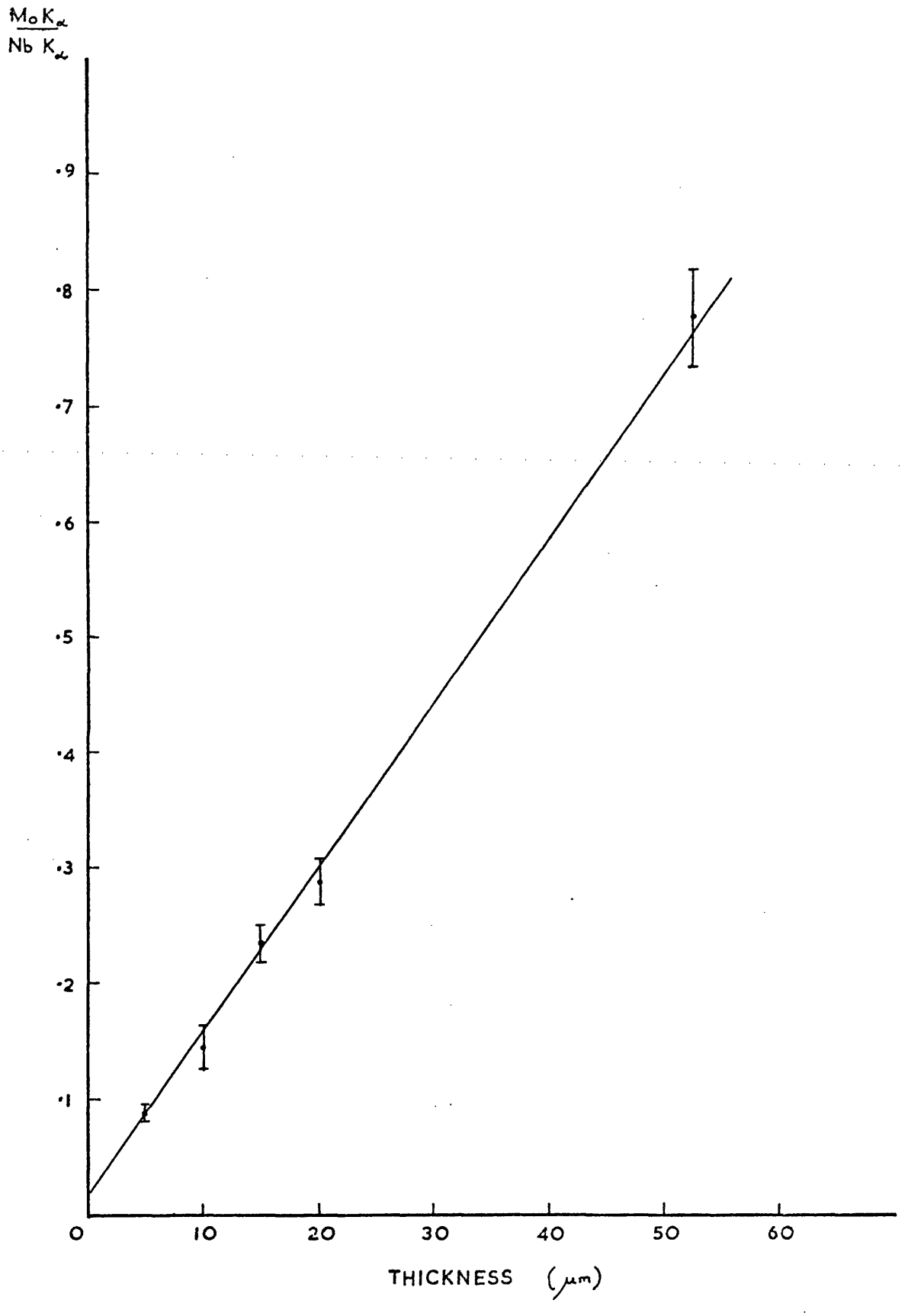

FIG 4-28

between the sample and the detector and in the beryllium window of the detector, the ratio of the intensities of these x-rays was calculated. A description of the absorption corrections appears in a later section of this chapter. Figure 4.28 shows the ratio of the intensities of the Mo and Nb K_α x-rays as a function of sample thickness. The point at 5 μm is the weighted mean of four measurements and the other points are taken from the single measurements shown in figure 4.27. It appears from this graph that the number of Mo K_α x-rays per Nb K_α x-ray (and, therefore, per positron) is directly proportional to the thickness of the molybdenum sample. This is consistent with the above hypothesis that the Mo K x-rays are produced by excitation of the molybdenum foil by positrons from the decay of ^{91}Mo.

(5) Absorption of x-rays

(i) Absorption in air and detector window

For x-rays travelling at an angle θ from a point source on the detector axis, the fraction of the emitted x-rays which is transmitted through the air and the window to the detector is

$$e^{-\mu_a X/\cos\theta} \qquad e^{-\mu_w T/\cos\theta}$$

where X is the distance between the sample and the window, T is the thickness of the window (see figure 4.29 (a)) and μ_a and μ_w are the linear absorption coefficients of the air and window, respectively, for the particular x-ray energy being considered. The solid angle between the cones with semi-angle θ and θ + dθ is

$$d\omega = 2\pi \sin\theta \, d\theta$$

and the fraction of x-rays emitted from the sample into this solid

(a)

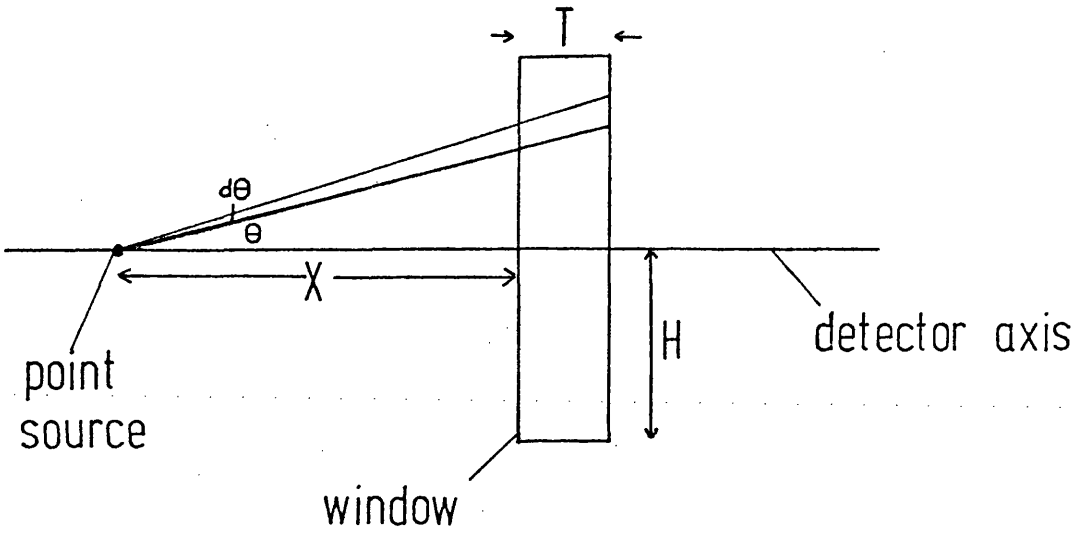
T
dθ
θ
X
H
detector axis
point
source
window

(b)

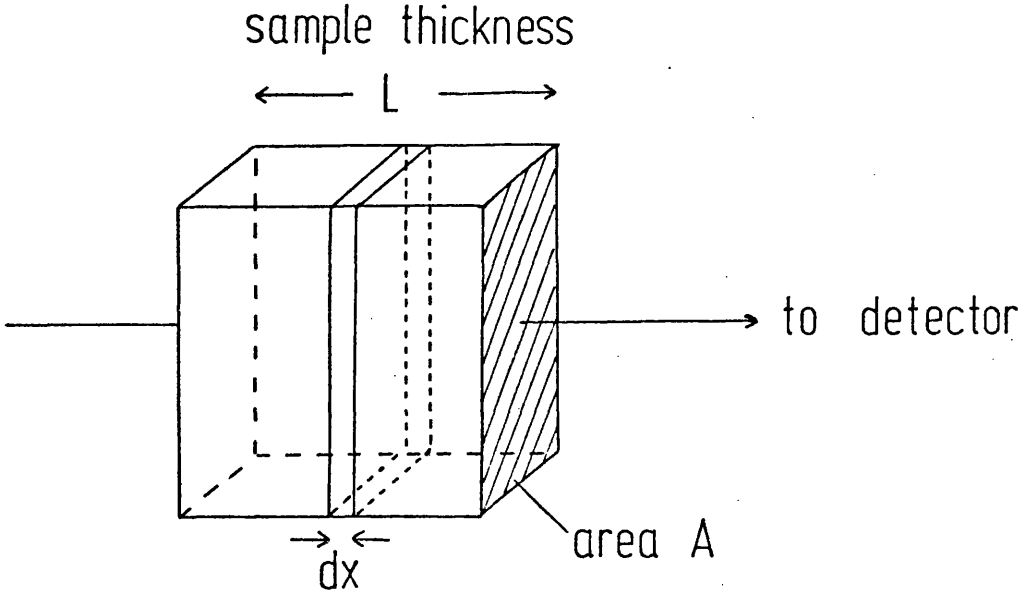
sample thickness
L
to detector
area A
dx

FIG 4-29

angle is proportional to

$$I_\theta \, 2\pi \sin\theta \, d\theta$$

where I_θ is the fraction of x-rays emitted from the sample, per unit solid angle, at angle θ. An expression for I_θ is given below.

(ii) Absorption in the molybdenum sample

If the activity is assumed to be uniformly distributed throughout the sample and, if N_o is the total number of x-rays emitted parallel to the detector axis then, in the volume Adx (figure 4.29 (b)), the number of x-rays emitted parallel to the detector axis is

$$\frac{N_o \, Adx}{AL}$$

where A is the cross-sectional area of the sample and L is the sample thickness. The number which reach the surface of the sample is

$$\frac{N_o}{L} e^{-\mu_s x} \, dx$$

where μ_s is the linear absorption coefficient of molybdenum. Therefore, the number of x-rays from the whole sample, which reach the surface, is

$$\int_0^L \frac{N_o}{L} e^{-\mu_s x} \, dx = \frac{N_o}{\mu_s L}\left(1 - e^{-\mu_s L}\right)$$

Therefore, $I_o = \frac{1}{\mu_s L}\left(1 - e^{-\mu_s L}\right)$.

For transmission through the sample at angle θ, the maximum distance travelled by the x-rays is $L/\cos\theta$ and, therefore

$$I_\theta = \frac{\cos\theta}{\mu_s L}\left(1 - e^{-\mu_s L/\cos\theta}\right)$$

Hence, the fraction of x-rays from the sample which reaches the detector, is given by

$$\frac{\int_0^{\tan^{-1}\frac{H}{X}} I_\theta \, e^{-\mu_a X/\cos\theta} \, e^{-\mu_w T/\cos\theta} \, 2\pi \sin\theta \, d\theta}{\int_0^{\tan^{-1}\frac{H}{X}} 2\pi \sin\theta \, d\theta}$$

x-ray	Fraction transmitted - Si(Li) detector -
Nb K_{α}	0.944 ± 0.007
Mo K_{α}	0.952 ± 0.007
Nb K_{β}	0.960 ± 0.006
Mo K_{β}	0.965 ± 0.006

TABLE 4.2

By numerical integration of the numerator of this equation using Simpson's rule the fractions of Nb and Mo K_α and K_β x-rays transmitted to the detector were calculated for various values of X (source-detector distance) and H (radius of detector window). The values of the linear absorption coefficients μ_s and μ_w were taken from tables given by Deway et al. (1969) who give values of mass absorption coefficients (μ/ρ) as a function of photon energy for absorption in various materials. A linear interpolation between the tabulated values was used to determine the absorption coefficients of niobium and molybdenum K_α and K_β x-rays in molybdenum, beryllium (Si(Li) detector window) and aluminium (NaI(Tl) detector window). The energies of these x-rays were taken from Bearden (1967). The mass absorption coefficient of air was calculated from the expression

$$\left(\frac{\mu}{\rho}\right)_{air} = \sum_{i=1}^{N} \left(\frac{\mu}{\rho}\right)_i a_i$$

where a_i is the fractional amount by weight of the i^{th} component (Davisson, 1965). According to Davisson, the constituents of air are nitrogen (a = 0.755), oxygen (a = 0.232) and argon (a = 0.013). The values of the mass absorption coefficients for nitrogen, oxygen and argon were taken, by linear interpolation, from the tables of Deway et al. (1969).

Since the Nb and Mo K_α and K_β x-rays are not resolved by the NaI(Tl) detector the relative intensities of these x-rays observed in the Si(Li) detector system must be used to determine the relative magnitudes of the components of the K x-ray peak observed in the NaI(Tl) detector.

Table 4.2 shows the calculated values of the transmission of the

Nb and Mo K_α and K_β x-rays through the sample, air and window in the Si(Li) detector system. The errors shown were obtained by consideration of the following points.

The effect of the finite area of the sample has not been taken into account in these absorption calculations. Approximate calculations of the type described earlier for a point source on the detector axis have also been carried out for point sources a few millimetres off the axis to allow for finite sample size. The maximum effect has been estimated to be about 0.5 per cent for the transmission of Nb K_α x-rays and less for the higher energy x-rays.

The effects of uncertainties in the source-detector distance, in the window thickness and in the sample thickness have also been included.

A change of 0.1 cm in the source-detector distance introduces a 0.02 per cent change in the transmission of Nb K_α x-rays decreasing to a 0.01 per cent change for Mo K_β x-rays. A 10 per cent uncertainty in the thickness of the detector window also introduces uncertainties of about 0.02 per cent in the transmission of Nb K_α x-rays and 0.01 per cent for the transmission of Mo K_β x-rays. The actual uncertainty in the window thickness is not known but 10 per cent has been chosen as a reasonable estimate. The molybdenum foil thickness is known with an accuracy of about 10 per cent and this leads to uncertainties in the transmission ranging from 0.53 per cent for the Nb K_α x-rays to 0.33 per cent for the Mo K_β x-rays.

The errors shown in table 4.2 have been obtained by adding in quadrature the uncertainties described above.

The ratio of Mo to Nb K_α x-rays observed in the silicon detector

Distance (cm)	Fraction transmitted - NaI(Tl) detector -			
	Nb K_α	Mo K_α	Nb K_β	Mo K_β
1.5	0.878 ± 0.008	0.893 ± 0.007	0.911 ± 0.006	0.922 ± 0.005
2.5	0.892 ± 0.008	0.905 ± 0.007	0.921 ± 0.006	0.931 ± 0.005
5.0	0.899 ± 0.008	0.912 ± 0.007	0.926 ± 0.006	0.936 ± 0.005
1.5*	0.897 ± 0.008	0.910 ± 0.007	0.925 ± 0.006	0.935 ± 0.005

*with copper collimator (2.5 cm diameter opening)

TABLE 4.3

is 0.088 ± 0.007. After correction for absorption in the Si(Li) detector system using the results shown in table 4.2 the ratio becomes

$$\frac{\text{Mo } K_\alpha}{\text{Nb } K_\alpha} = 0.087 \pm 0.007.$$

The ratio K_β/K_α for the Nb x-rays was observed in the silicon detector to be 0.193 ± 0.009. This is a weighted mean of five measurements. After correction for absorption in the molybdenum, air and beryllium the ratio becomes

$$\left(\frac{K_\beta}{K_\alpha}\right)_{Nb} = 0.190 \pm 0.009.$$

This is in agreement with a value of 0.193 ± 0.004 obtained by Salem et al. (1972) using a proportional counter. The agreement indicates that any difference in the detection efficiency of the Si(Li) detector at the Nb K_α and K_β x-ray energies is negligible.

It was not possible to measure the K_β/K_α ratio for the molybdenum x-rays in the Si(Li) detector because of the low intensities of the x-rays involved. The ratio has, however, been measured by Slivinsky and Ebert (1969) to be 0.197 ± 0.006 and this value has been adopted here.

The calculated values of the transmission of the Nb and Mo K x-rays through the sample, air and aluminium window for the NaI(Tl) detector system are shown in table 4.3 for various source-detector distances. The errors shown were obtained in a similar manner to that described for the Si(Li) detector. In this case, however, no account was taken of the finite area of the source since it is very much smaller than the area of the detector window. These values of x-ray transmission have been used to calculate the ratios Mo K_α/Nb K_α, $(K_\beta/K_\alpha)_{Nb}$ and $(K_\beta/K_\alpha)_{Mo}$ which would be observed (if resolved) in the NaI(Tl) detector. These ratios are

Ratio	Observed in Si(Li) detector	Corrected for absorption	'Observed' in NaI(Tl) detector at different source-detector distances			
			1.5 cm	2.5 cm	5.0 cm	1.5 cm*
$\frac{\text{Mo } K_\alpha}{\text{Nb } K_\alpha}$	0.088 ± 0.007	0.087 ± 0.007	0.089 ± 0.007	0.088	0.088	0.088
$\left(\frac{K_\beta}{K_\alpha}\right)_{\text{Nb}}$	0.193 ± 0.009	0.190 ± 0.009	0.197 ± 0.009	0.196	0.196	0.196
$\left(\frac{K_\beta}{K_\alpha}\right)_{\text{Mo}}$	-	0.197 ± 0.006[‡]	0.204 ± 0.006	0.203	0.202	0.203

[‡]From Slivinsky and Ebert (1969)

*With copper collimator

TABLE 4.4

RELATIVE INTENSITIES OF X-RAYS IN THE Si(Li) AND THE NaI(Tl) DETECTORS

shown in table 4.4.

(6) Detector efficiency

(i) Si(Li) detector

The only results from the Si(Li) detector measurements employed in the calculation of the K/β^+ ratio are ratios of x-ray intensities (e.g. Mo K_α/Nb K_α). Therefore, it is sufficient to know the relative efficiencies at the various x-ray energies. The variation in photopeak efficiency in this region (16 - 20 keV) is extremely small and has been neglected. This is supported by the agreement between the values of the ratio $(K_\beta/K_\alpha)_{Nb}$ as observed in the Si(Li) detector, without efficiency corrections, and by Salem et al. (1972) using a proportional counter.

(ii) NaI(Tl) detector

For the x-ray measurements made with this detector, the absolute photopeak efficiency for each of the x-ray energies must be known. At these low energies, the photoelectric effect dominates and for a thickness of 0.64 cm of NaI(Tl) the photopeak efficiency is 100 per cent for the Nb and Mo K_α and K_β x-rays (Davisson, 1965).

(7) Corrections to the number of positrons

(i) Positrons stopped before reaching the detector

The energy loss expected for positrons travelling through the molybdenum sample (thickness 5 mg/cm^2) and the detector window (6.9 mg/cm^2 aluminium) is approximately 100 keV (Evans, 1955, Berger and Seltzer, 1964). The number of positrons from ^{91}Mo (maximum positron energy = 3.421 MeV) with energies less than 100 keV is less than 0.1 per cent of the total positron intensity. This correction, therefore, can be neglected.

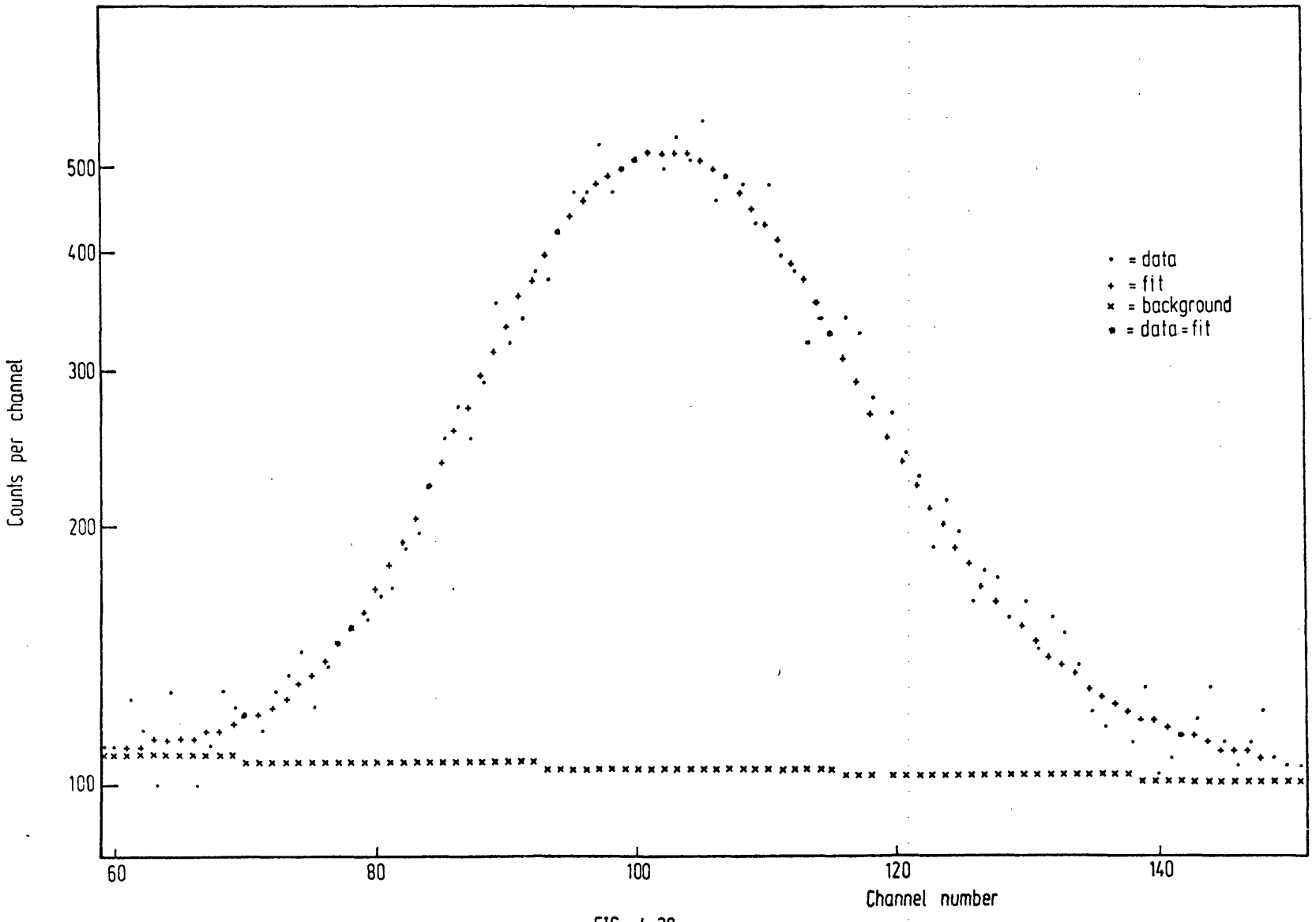
Counts per channel
500
400
300
200
100
60
80
100
120
140
Channel number
· = data
+ = fit
× = background
* = data = fit

FIG 4-30

(ii) Positrons scattered out of the detector

Because of the high effective atomic number of NaI(Tl), many positrons are expected to be scattered out of the detector before losing all their energy (Neiler and Bell, 1965). Since the actual shape of the positron spectrum in the NaI(Tl) detector is of no consequence in the present experiment, this effect is only important for those positrons which lose only a small amount of energy before being scattered out of the detector. From figure 4.17 it can be seen that the scaler threshold corresponds to an energy of about 6 keV. Therefore, to be detected, positrons must lose about 6 keV before being scattered out of the detector. The effect of positrons losing less than 6 keV in the detector can be represented by an extrapolation of the positron spectrum below the scaler threshold. Two forms for this extrapolation are shown in figure 4.17. The dotted curve has been adopted on purely subjective grounds, as the most extreme form of the extrapolation and the area under this curve represents the maximum value for the number of positrons depositing less than 6 keV of energy in the detector. It has already been stated that the difference between the two forms of the extrapolation (solid and dotted curves on figure 4.17) amounts to less than 1 per cent of the total number of events and an error of this magnitude has been included along with the statistical error.

RESULTS

(i) K x-rays

The areas of the K x-ray peaks observed in the NaI(Tl) detector were determined using the SAMPO program. The Gaussian-plus-exponential expression used in this program was found to be a good representation of the data despite the fact that the K-peak is actually composed of several

Run number	Number of events in K-peak	After absorption corrections		Number of Nb K x-rays associated with ^{91}Mo
		Number of Nb K_α x-rays	Number of NbK_β x-rays	
1	$(1.242 \pm 0.037) \times 10^4$	$(1.061 \pm 0.030) \times 10^4$	$(2.019 \pm 0.107) \times 10^3$	$(1.107 \pm 0.045) \times 10^4$
2	$(1.277 \pm 0.024) \times 10^4$	$(1.098 \pm 0.022) \times 10^4$	$(2.085 \pm 0.103) \times 10^3$	$(1.145 \pm 0.041) \times 10^4$
3	$(2.242 \pm 0.047) \times 10^4$	$(1.929 \pm 0.037) \times 10^4$	$(3.661 \pm 0.180) \times 10^3$	$(2.010 \pm 0.070) \times 10^4$
4	$(9.482 \pm 0.230) \times 10^3$	$(8.281 \pm 0.201) \times 10^3$	$(1.572 \pm 0.081) \times 10^3$	$(8.631 \pm 0.340) \times 10^3$
5	$(4.816 \pm 0.082) \times 10^3$	$(4.124 \pm 0.080) \times 10^3$	$(7.84 \pm 0.38) \times 10^2$	$(4.299 \pm 0.150) \times 10^3$

TABLE 4.5

different K x-rays. Figure 4.30 shows a K-peak together with the SAMPO fit to the peak and background. All the K-peaks were examined several times using the SAMPO program, each fit including different numbers of channels around the peak. The mean of the values obtained for each peak was adopted as the area and the range of the values was taken as a measure of the systematic error involved in determining the background under the peak. This error was added in quadrature with the statistical error in the peak area. The areas and corresponding errors are given in table 4.5.

The ratios of the relative intensities of the various components in the K-peak (table 4.4) were used to calculate the numbers of Nb K_α and K_β x-rays in the K-peaks observed in the NaI(Tl) detector. The absorption corrections from table 4.3 were then applied to find the actual numbers of Nb K_α and K_β x-rays produced (columns 3 and 4, table 4.5).

The half life data showed that (87.6 ± 2.3) per cent of the Nb K_α x-rays were associated with ^{91}Mo. Applying this result to both the Nb K_α and K_β x-rays, yielded the values shown in the last column of table 4.5.for the number of Nb K x-rays from the decay of ^{91}Mo.

(ii) Positrons

By subtracting the number of events in the K-peak from the number of positrons plus K-events (table 4.1), the number of positrons in each run was obtained. The results are shown in table 4.6.

From the half life measurements of the 0.511 MeV positron annihilation gamma rays observed in the Ge(Li) detector, it was found that (99.3 ± 0.5) per cent of the positrons were due to ^{91}Mo. This result was obtained from

Run number	Number of positrons	Number of positrons associated with ^{91}Mo	$\frac{\text{K x-rays}}{\beta+}$
1	$(2.566 \pm 0.068) \times 10^5$	$(2.548 \pm 0.069) \times 10^5$	$(4.342 \pm 0.213) \times 10^{-2}$
2	$(3.057 \pm 0.059) \times 10^5$	$(3.035 \pm 0.068) \times 10^5$	$(3.772 \pm 0.155) \times 10^{-2}$
3	$(4.884 \pm 0.099) \times 10^5$	$(4.850 \pm 0.098) \times 10^5$	$(4.145 \pm 0.166) \times 10^{-2}$
4	$(2.174 \pm 0.041) \times 10^5$	$(2.158 \pm 0.041) \times 10^5$	$(3.999 \pm 0.172) \times 10^{-2}$
5	$(1.242 \pm 0.079) \times 10^5$	$(1.233 \pm 0.079) \times 10^5$	$(3.486 \pm 0.254) \times 10^{-2}$

TABLE 4.6

a series of 15 min. gamma ray spectra but no allowance was made for the decay of ^{91}Mo within the 15 min. period. Allowing for this decay has only a very small effect on the calculation. This result is used in preference to that obtained from the half life measurements on the scaler readings from the Si(Li) detector. The reason is that these scaler readings include events caused by 0.511 MeV annihilation gamma rays and the intensity of these gamma rays relative to the positrons for each of the activities present (i.e. ^{91}Mo, ^{90}Mo and ^{90}Nb) is not known.

The values obtained for the ratio (K x-rays)/β^+ for ^{91}Mo are shown in table 4.6. The result obtained from the measurements with the copper collimator (run number 5) is considerably lower than the other results. This is thought to be due to positrons which were scattered into the detector from the edge of the opening in the collimator, thus reducing the observed K/β^+ ratio. This is consistent with the results obtained using the Si(Li) detector, although, in that case, the effect was even greater because the very small opening in the collimator meant that scattering from the edges was more important.

The results obtained at source distances of 1.5, 2.5 and 5.0 cm, with no collimator, are in good agreement. This implies that the scattering of positrons into the detector from material around the window was not an important effect since the value obtained for the K/β^+ ratio did not apparently depend on solid angle.

The mean of these four results was found by weighting each result in inverse proportion to the square of its error and the results were tested for internal and external consistency (Topping, 1962).

Two expressions exist for the standard error α of a weighted mean.

The first depends on the internal consistency of the separate observations (Birge, 1932) and is defined as

$$\alpha_i^2 = \frac{1}{\sum(\frac{1}{\alpha_s^2})}$$

where α_s is the standard error of the observation x_s. The other expression depends on the external consistency of the observations and is given by

$$\alpha_e^2 = \frac{\sum(x_s - \bar{x})^2/\alpha_s^2}{(n-1)\sum(\frac{1}{\alpha_s^2})}$$

where $\bar{x}$ is the weighted mean of the observations x_s. The ratio of the errors α_e and α_i is unity with standard error $1/\sqrt{(2n - 2)}$, where n is the number of observations, for samples taken from an infinite normal population. If, for a given series of results, the ratio α_e/α_i is found to be unity within the error, the larger of α_e and α_i is taken as the standard error of the weighted mean. If the ratio differs significantly from unity, however, it is probable that systematic errors are present and a different weighting of the observations is necessary.

In the present case, the weighted mean of the four measurements is 0.0403 and α_e and α_i are 0.00116 and 0.00086, respectively. Therefore,

$$\frac{\alpha_e}{\alpha_i} = 1.34.$$

Since $1/\sqrt{(2n - 2)} = 0.41$, the standard error α_e has been adopted as the error in the weighted mean. The result is, therefore,

$$\frac{\text{K x-rays}}{\beta^+} = 0.0403 \pm 0.0012.$$

Using the value of ω_K, the fluorescence yield, given by Rambynek

et al. (1972), i.e. $\omega_K = 0.748 \pm 0.032$, gives the result

$$K/\beta^+ = 0.0539 \pm 0.0028.$$

The error in the final result consists of the 3 per cent error in the measured (K x-ray/β^+) ratio and the 4.3 per cent error in the fluorescence yield added in quadrature.

The experimental errors in the individual measurements arise from the following

(a) statistical errors in the scaler readings and in the number of events in the K-peak

(b) the systematic error in determining the background under the K-peak

(c) the error in determining the contribution to the K-peak from Nb K_α and K_β x-rays. This arises from the errors in the ratios (Mo K_α /Nb K_α), $(K_\beta/K_\alpha)_{Nb}$ and $(K_\beta/K_\alpha)_{Mo}$

(d) errors in absorption corrections

(e) errors in determining the contribution of ^{90}Mo to the Nb K x-rays. This comes from the x-ray half life measurement in the Si(Li) detector

(f) the systematic error in the extrapolation below the scaler threshold

(g) the error in determining the photopeak/total ratio for the 0.511 MeV gamma rays

(h) the error from the half life measurement of the 0.511 MeV peaks in the Ge(Li) detector to determine the contribution made by impurities to the positron activity.

Of these, (e) and (g) make the largest contribution to the final

error. The magnitude of effect (e) could probably have been reduced if more information about long-lived components of the Nb K x-rays had been available. However, the uncertainties in the dead time of the Si(Li) detector system at low counting rates rendered this impossible.

The most awkward effect to determine was (g), i.e. the detection of 0.511 MeV annihilation gamma rays from positrons stopped in the material outside the detector. To investigate this effect, a fairly long-lived source emitting positrons and no gamma rays, would have been ideal. However, no such source was available and the method employed of using sources with single gamma ray with energies around 0.511 MeV and interpolating the results led to a fairly large, unavoidable uncertainty.

As stated at the beginning of this chapter, ^{91}Mo does not decay solely to the ground state of ^{91}Nb. Details of transitions to higher levels in ^{91}Nb and the K/β^+ ratio for the decay to the ground state are presented in the next chapter.

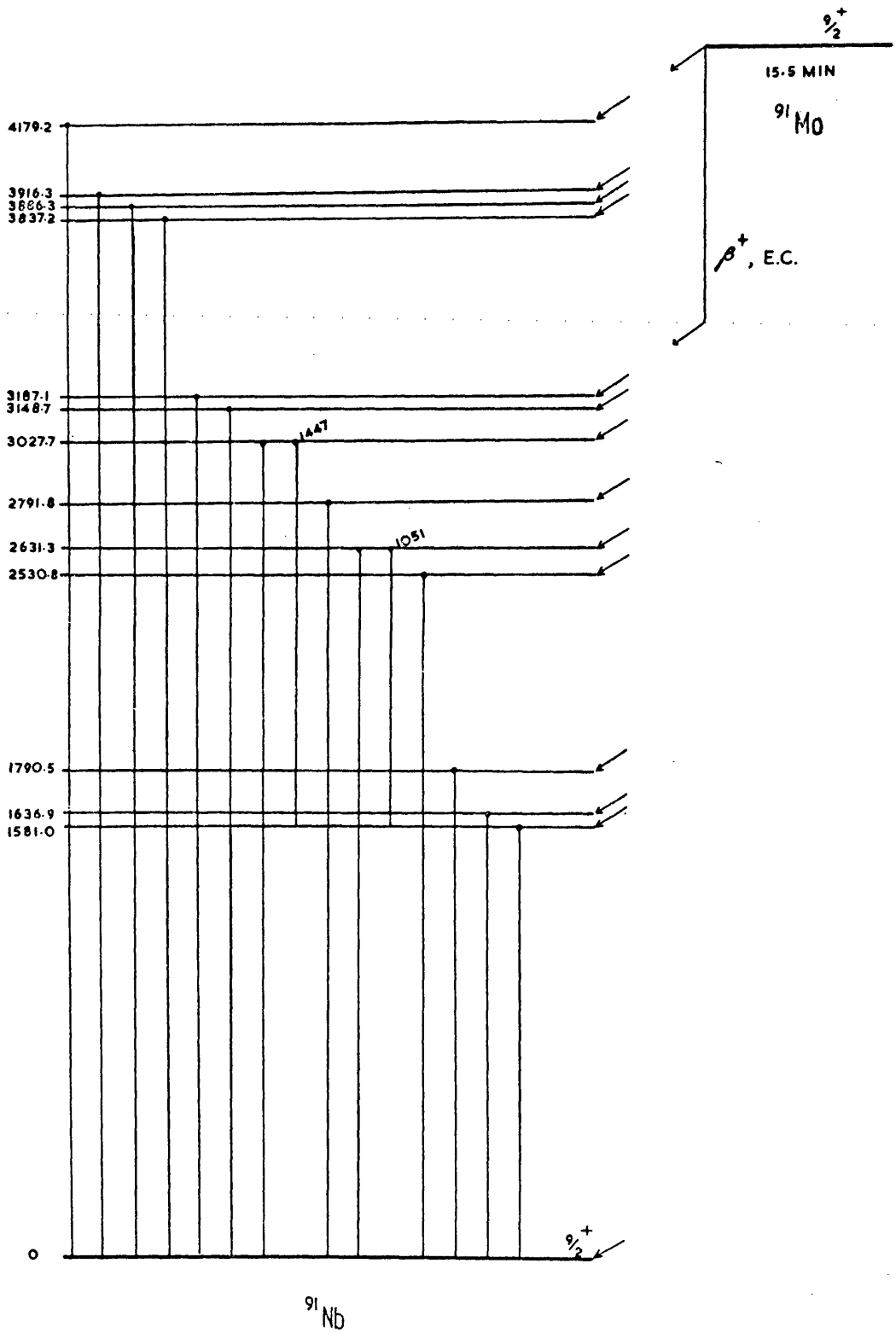
9/2+
15.5 MIN
91Mo
β+, E.C.
4179.2
3916.3
3886.3
3837.2
3187.1
3148.7
3027.7
1447
2791.8
2631.3
1051
2530.8
1790.5
1636.9
1581.0
0
9/2+
91Nb

FIG 5-1

CHAPTER 5

WEAK TRANSITIONS IN THE DECAY OF ^{91}Mo AND THE K/β^+ RATIO FOR THE TRANSITION TO THE GROUND STATE OF ^{91}Nb

It has been mentioned in the previous chapter that the decay of ^{91}Mo is not simply a ground state-ground state transition as shown in figure 4.1. Work by Cretzu et al. (1965), using natural molybdenum irradiated in a 25 MeV bremsstrahlung beam, showed gamma rays with a 15 min. half life at energies of 800, 1040 and 1600 keV. They assumed that these gamma rays were associated with the de-excitation of levels in ^{91}Nb fed by transitions from ^{91}Mo. Similar results were obtained by Das et al. (1969).

Both of these groups irradiated samples of natural molybdenum to produce ^{91}Mo by the reactions

$$^{92}\text{Mo}(\gamma, n)\ ^{91}\text{Mo} \text{ or } ^{92}\text{Mo}(n, 2n)\ ^{91}\text{Mo}$$

on the stable ^{92}Mo isotope, which has a natural abundance of approximately 16 per cent.

More recent studies (Hesse and Finckh, 1970, and De Barros et al., 1970) have employed samples enriched to 95 per cent in ^{92}Mo and have failed to confirm the gamma rays at 800 and 1040 keV. It seems likely that these gamma rays are associated with some other activity produced by irradiating natural molybdenum. The relative intensities of the ^{91}Mo gamma rays from these recent measurements are compared in table 5.1. The decay scheme according to Hesse and Finckh is shown in figure 5.1.

Neither of these groups measured the intensity of the gamma rays relative to the positrons from ^{91}Mo. However, Cretzu et al. (1965) measured the relative intensities of the 511 keV positron annihilation

De Barros et al. 1970		Hesse and Finckh 1970	
Energy of gamma ray (keV)	Relative intensity	Energy of gamma ray (keV)	Relative intensity
-	-	1050.7 ± 0.4	10.8 ± 2.0
-	-	1082.0 ± 0.4	5.8 ± 1.5
-	-	1195.1 ± 0.7	2.8 ± 1.0
-	-	1446.9 ± 0.5	3.7 ± 1.5
-	-	1460.5 ± 0.6	2.4 ± 1.0
1580.5 ± 0.4	70 ± 5	1581.0 ± 0.3	69 ± 7
1636.3 ± 0.4	100	1636.9 ± 0.3	100
-	-	1740.4 ± 0.4	4.9 ± 1.0
1789.1 ± 0.5	15 ± 3	1790.5 ± 0.4	8.6 ± 1.5
2119.2 ± 0.6	~8	-	-
-	-	2530.8 ± 0.4	1.7 ± 0.8
2630.8 ± 0.5	39 ± 6	2631.3 ± 0.4	36.5 ± 4.0
-	-	2791.8 ± 0.6	3.2 ± 1.0
3027.0 ± 0.5	29 ± 4	3027.7 ± 0.5	28.0 ± 0.3
3147.5 ± 0.6	16 ± 2	3148.7 ± 0.5	15.0 ± 2.0
-	-	3187.1 ± 1.0	1.4 ± 0.7
-	-	3837.2 ± 1.0*	-
-	-	3886.3 ± 1.0*	-
-	-	3916.3 ± 1.0*	-
-	-	4179.2 ± 1.0*	-

*Detected by double escape peak only

TABLE 5.1

GAMMA RAYS FROM THE DECAY OF ^{91}Mo

quanta and 1600 keV gamma rays. They found

$$I(511 \text{ keV}) : I(1600 \text{ keV}) = 300:1$$

If this 1600 keV gamma ray is assumed to correspond to the two most intense gamma rays in table 5.1 (i.e. 1580 and 1636 keV), it can be shown that the decay of ^{91}Mo is predominantly a ground state-ground state transition with only about 1 per cent of the decays leading to excited states in ^{91}Nb.

For the present experiment it is necessary to make an accurate determination of the intensity of the transitions to the excited states relative to the ground state transition in order to determine the K/β^+ ratio for this latter transition from the measured total K/β^+ ratio.

In the gamma ray spectra from irradiated ^{92}Mo foils presented in the previous chapter (figure 4.2) none of the gamma rays from ^{91}Mo could be seen because of their low intensity. The thickness of the foil used for these measurements was 5 μm. In order to see even the most intense ^{91}Mo gamma rays, a thicker foil (52 μm) had to be used.

Measurement of the Intensities of the 1.58 and 1.64 MeV Gammas relative to the Positrons from ^{91}Mo

For the measurement of the half life of the 0.511 MeV positron annihilation gamma rays described in chapter 4, a piece of ^{92}Mo (52 μm) thick was irradiated for 60 secs in a 50 MeV bremsstrahlung beam and, after a 10 min. wait, a series of gamma ray spectra, each of 15 mins duration, was accumulated. For these measurements the ^{92}Mo foil was sandwiched between two copper discs, 0.23 cm thick, to stop all the positrons close to the source. This ensured that the geometry

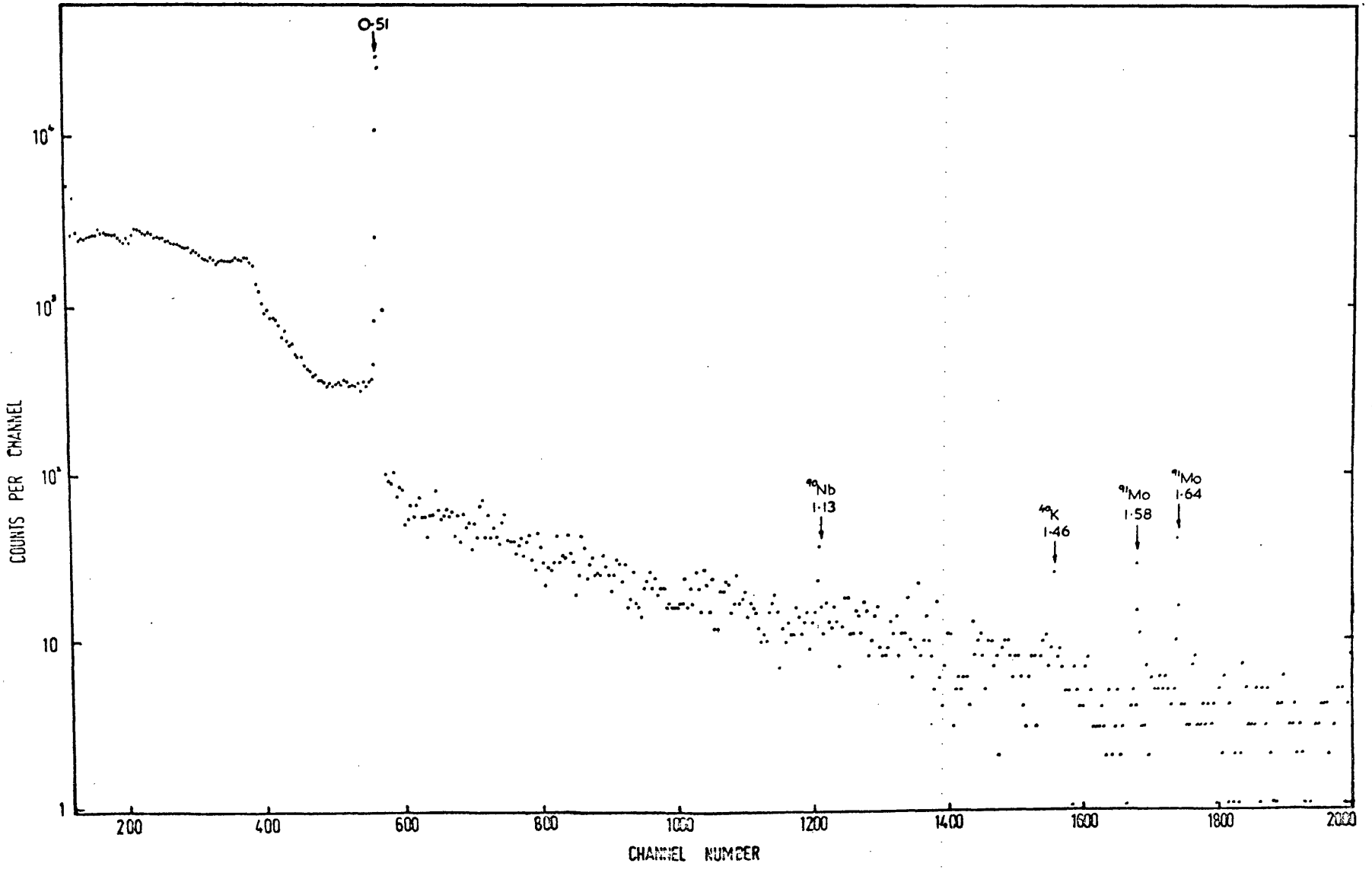
0·51
^{99}Nb
1·13
^{40}K
1·46
^{91}Mo
1·58
^{91}Mo
1·64
COUNTS PER CHANNEL
CHANNEL NUMBER
1
10
10^2
10^3
10^4
200
400
600
800
1000
1200
1400
1600
1800
2000

FIG 5-2

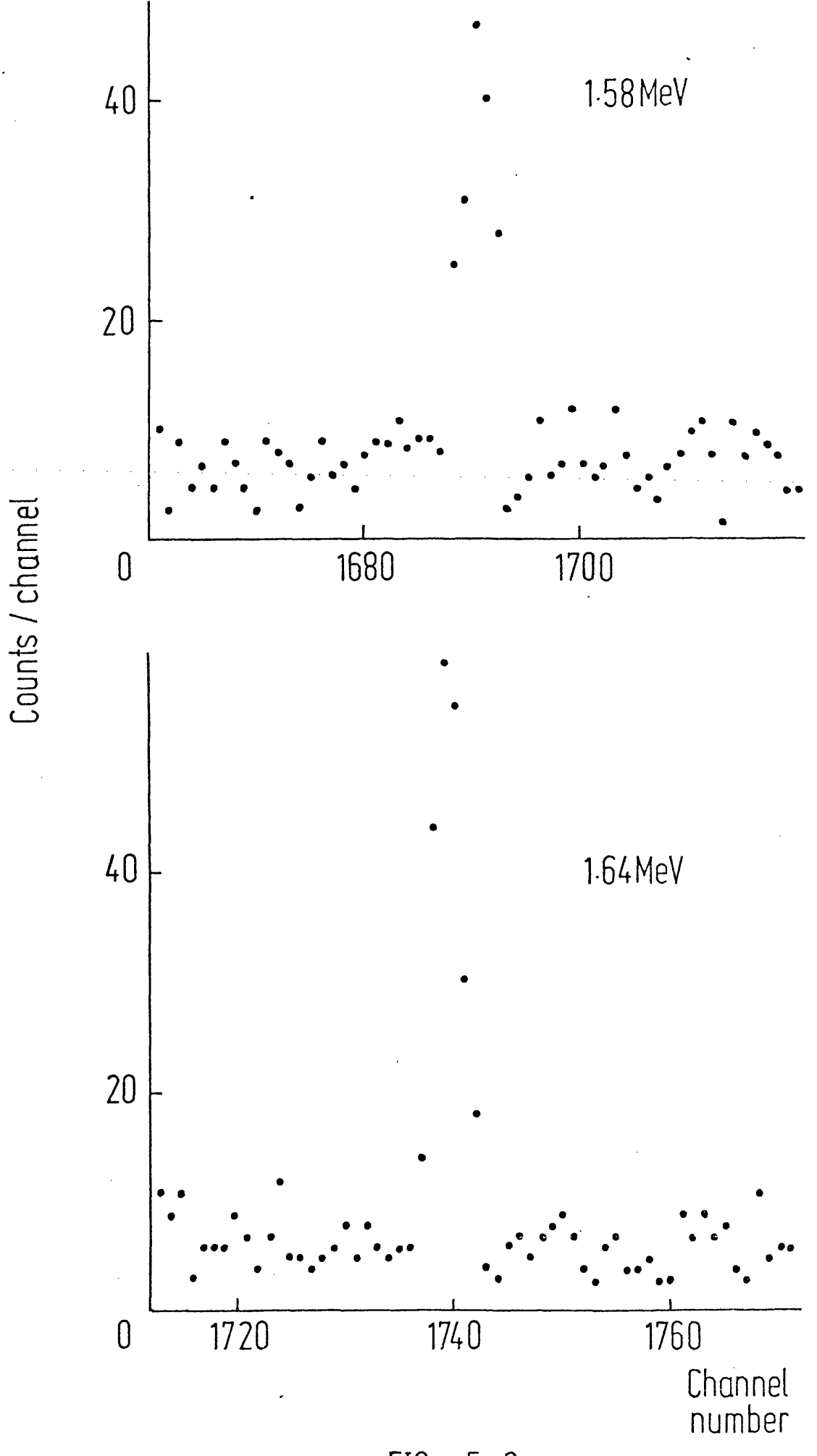
1·58 MeV
40
20
0
1680
1700
Counts / channel
1·64 MeV
40
20
0
1720
1740
1760
Channel number

FIG 5-3

was, as nearly as possible, the same for the 0.511 MeV positron annihilation quanta and the other gamma rays.

The gamma ray spectrum obtained during the first 15 min. period is shown in figure 5.2. In addition to the ^{90}Mo and ^{90}Nb gamma rays, peaks at energies of 1.58 and 1.64 MeV can be seen. These peaks were also seen in the second 15 min. spectrum but not in later spectra. These gamma rays correspond in energy to the most intense gamma rays from ^{91}Mo (table 5.1). The data from the first two spectra were added to improve the statistics and the regions around 1.58 and 1.64 MeV are shown in figure 5.3. The numbers of counts in these peaks were estimated to be

129 ± 25 for the 1.58 MeV photopeak

and 180 ± 26 for the 1.64 MeV photopeak.

The measurement of the half life of the 0.511 MeV peak has been described in chapter 4. The results obtained are necessary to determine the contribution of ^{91}Mo to the intensity of the 0.511 MeV peak. The numbers of 0.511 MeV gamma rays associated with ^{91}Mo were found to be 168300 ± 570 and 85980 ± 290 during the first and second counts, respectively. The total number of ^{91}Mo annihilation gamma rays in these two counts is, therefore,

254280 ± 650.

Relative Efficiency Calibration of the Ge(Li) Detector

Since the photopeak efficiency of a Ge(Li) detector depends on the gamma ray energy, it was necessary to calibrate the detector using sources emitting gamma rays of known energy and intensity in the region from 0.511 to 1.64 MeV.

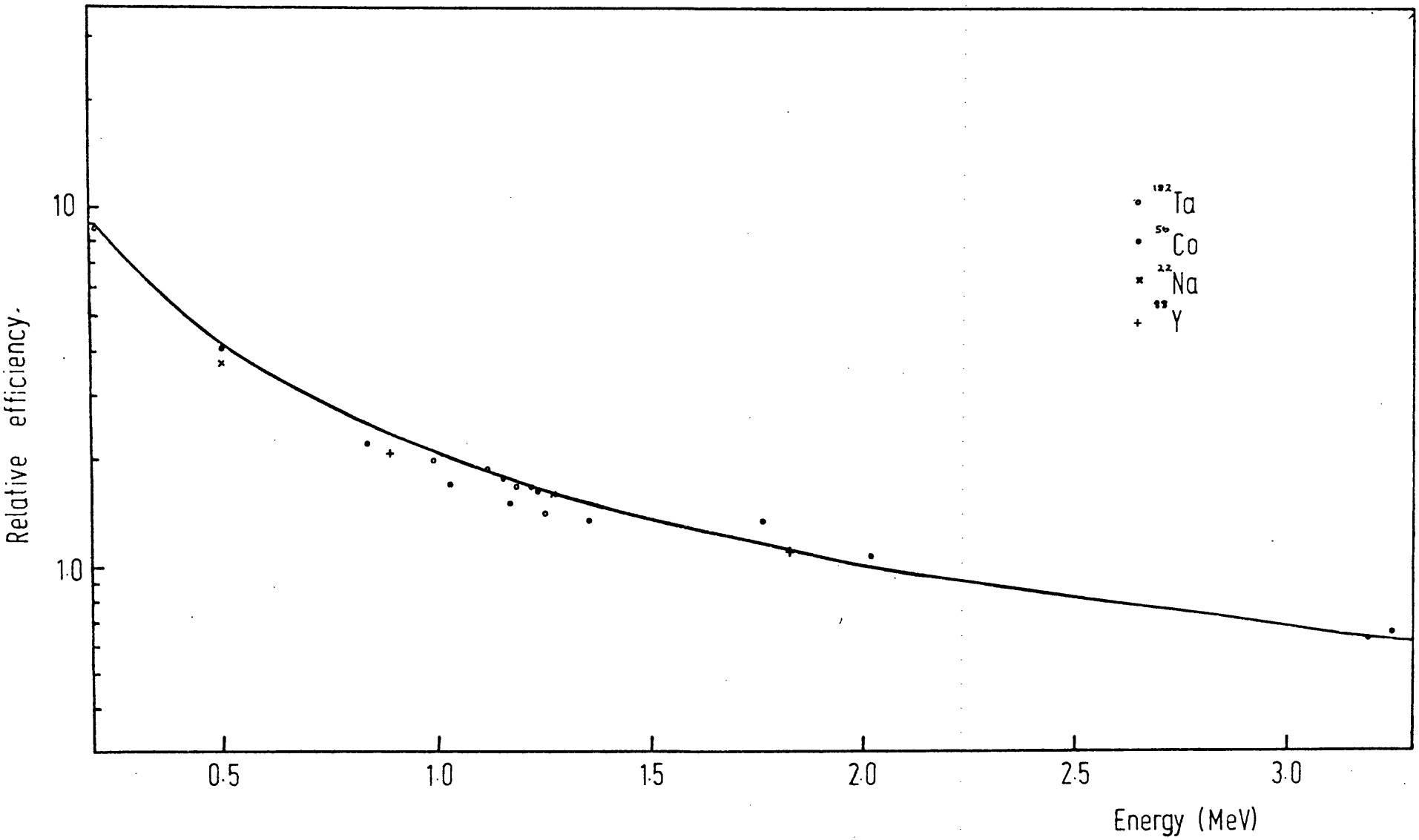
Relative efficiency
10
1·0
0·5
1·0
1·5
2·0
2·5
3·0
Energy (MeV)
^{182}Ta
^{56}Co
^{22}Na
^{88}Y

FIG 5-4

The measurements of relative efficiency were carried out by Mr M. Campbell. The sources employed were ^{22}Na, ^{88}Y, ^{56}Co and ^{182}Ta. These sources were each placed in the same position as the ^{92}Mo foil behind a 0.23 cm thick copper disc. The energies and relative intensities of the gamma rays from ^{56}Co and ^{182}Ta were taken from Camp and Meredith (1971) and Pagden et al. (1971), respectively. Similar data for ^{22}Na and ^{88}Y were taken from Lederer et al. (1967). The areas of the photopeaks were determined using the SAMPO program and a graph of relative efficiency against photopeak energy was drawn (figure 5.4).

The expression

$$\log e = \sum_{i=1}^{n} a_i (\log E)^i$$

where e and E are the relative efficiency and gamma ray energy, respectively, was fitted by a least squares method to the data from ^{56}Co. The above expression with n = 4 was chosen since a log-log plot of the data indicated that an S-shaped curve was necessary to give a good fit (Robinson et al., 1972). The same expression fitted to the ^{182}Ta data yielded similar values for the parameters a_1, a_2, a_3 and a_4. The solid curve in figure 5.4 is the fit of the above four-parameter expression to the data from ^{56}Co and ^{182}Ta.

From this fit to the data, the relative efficiencies at 0.511, 1.58 and 1.64 MeV were found to be 4.01, 1.28 and 1.23, respectively.

From these values and the 1.58 and 1.64 MeV photopeak areas, the ratio of the intensities of these gamma rays is

$$\frac{I_\gamma(1.58)}{I_\gamma(1.64)} = 0.69 \pm 0.18$$

Energy of excited state (keV)	Percentage of ^{91}Mo decays leading to given state	Maximum β^+ kinetic energy (keV)	log ft
1581.0	.237 ± .057	1840.0 ± 28	7.00 ± 0.11
1636.9	.435 ± .062	1785.1 ± 28	6.68 ± 0.07
1790.5	.037 ± .008	1630.5 ± 28	7.57 ± 0.10
2530.8	.0074 ± .0036	890.2 ± 28	7.13 ± 0.22
2631.3	.206 ± .039	789.7 ± 28	5.46 ± 0.11
2791.8	.014 ± .005	629.2 ± 28	6.21 ± 0.17
3027.7	.138 ± .021	393.3 ± 28	4.31 ± 0.16
3148.7	.065 ± .013	272.3 ± 28	3.91 ± 0.29
3187.1	.0061 ± .0031	233.9 ± 28	4.66 ± 0.35

TABLE 5.2

This is in agreement with the values of 0.69 ± 0.07 and 0.70 ± 0.05 obtained by Hesse and Finckh (1970) and De Barros et al. (1970), respectively.

The ratio of the intensities of the 1.64 and 0.511 MeV gamma rays is, from the present results

$$\frac{I_\gamma(1.64)}{I_\gamma(0.511)} = (2.31 \pm 0.33) \times 10^{-3}$$

Therefore, the number of 1.64 MeV gamma rays per positron is

$$\frac{I_\gamma(1.64)}{\beta^+} = (4.62 \pm 0.66) \times 10^{-3}$$

The value of the total ϵ/β^+ ratio for ^{91}Mo can be determined from the measured total K/β^+ obtained in the previous chapter and the ratio of total electron capture to K electron capture calculated as described in chapter 3. It can then be shown that the number of 1.64 MeV gamma rays per ^{91}Mo decay is

$$(4.35 \pm 0.62) \times 10^{-3}$$

The intensities of the transitions from ^{91}Mo to the excited states relative to the total number of decays have been calculated using this result and the relative gamma ray intensities given by Hesse and Finckh (1970) (table 5.2).

Log ft Values for the Weak Transitions in the Decay of ^{91}Mo

The maximum positron kinetic energies for the transitions to the excited states are given in table 5.2. The f-values were calculated by numerical integration using the Fermi functions of Behrens and Jänecke (1969) as described in chapter 2.

Energy of excited state in ^{91}Nb (keV)	*Spin and parity	ΔI, parity change	Type of transition
1581.0	$7/2^+$	1 (no)	Allowed
1636.9	$9/2^+$	0 (no)	Allowed
1790.5	$9/2^-$	0 (yes)	First forbidden
2530.8	$11/2^-$	1 (yes)	First forbidden
2631.3	$9/2^+$	0 (no)	Allowed
2791.8	$7/2^+$	1 (no)	Allowed

*From Matsuki et al. (1973)

TABLE 5.3

The partial half lives for the transitions were calculated using the half life of ^{91}Mo (15.49 ± 0.01 min) and the intensities of the transitions as determined above. The log ft values thus obtained are shown in table 5.2.

Spin and parity assignments for many of the excited states of ^{91}Nb have been made recently by Matsuki et al. (1973) from the ^{91}Zr (p, nγ) ^{91}Nb reaction and the assignments for the states of interest in this discussion are shown in table 5.3. These authors do not give spin-parity assignments for the ^{91}Nb levels at 3027.7, 3148.7 and 3187.1 keV. Since the spin and parity of the ^{91}Mo ground state is $9/2^+$ the transitions from this state to the levels given in table 5.3 should all be either allowed or first forbidden.

Figure 5.5 shows the distribution of log ft values for allowed and nonunique first forbidden transitions according to Wu and Moszkowski (1966). From this it appears that the log ft values for the transitions to the 1581.0, 1636.9, 2631.3 and 2791.8 keV levels are typical of those for allowed transitions. Also, the log ft values for the decays to the 1790.5 and 2530.8 keV levels are in the range expected for nonunique first forbidden transitions. These results are, therefore, not at variance with the spin-parity assignments of Matsuki et al.

The log ft values for the decays to the 3027.7, 3148.7 and 3187.1 keV levels are all rather low. In particular, the value of 3.91 ± 0.29 for the transition to the 3148.7 keV level is near the lower limit expected for the log ft value of an allowed transition. This slightly suggests that the intensity of this transition as given by Hesse and Finckh (1970) may be too high. If this level were also fed by gamma ray

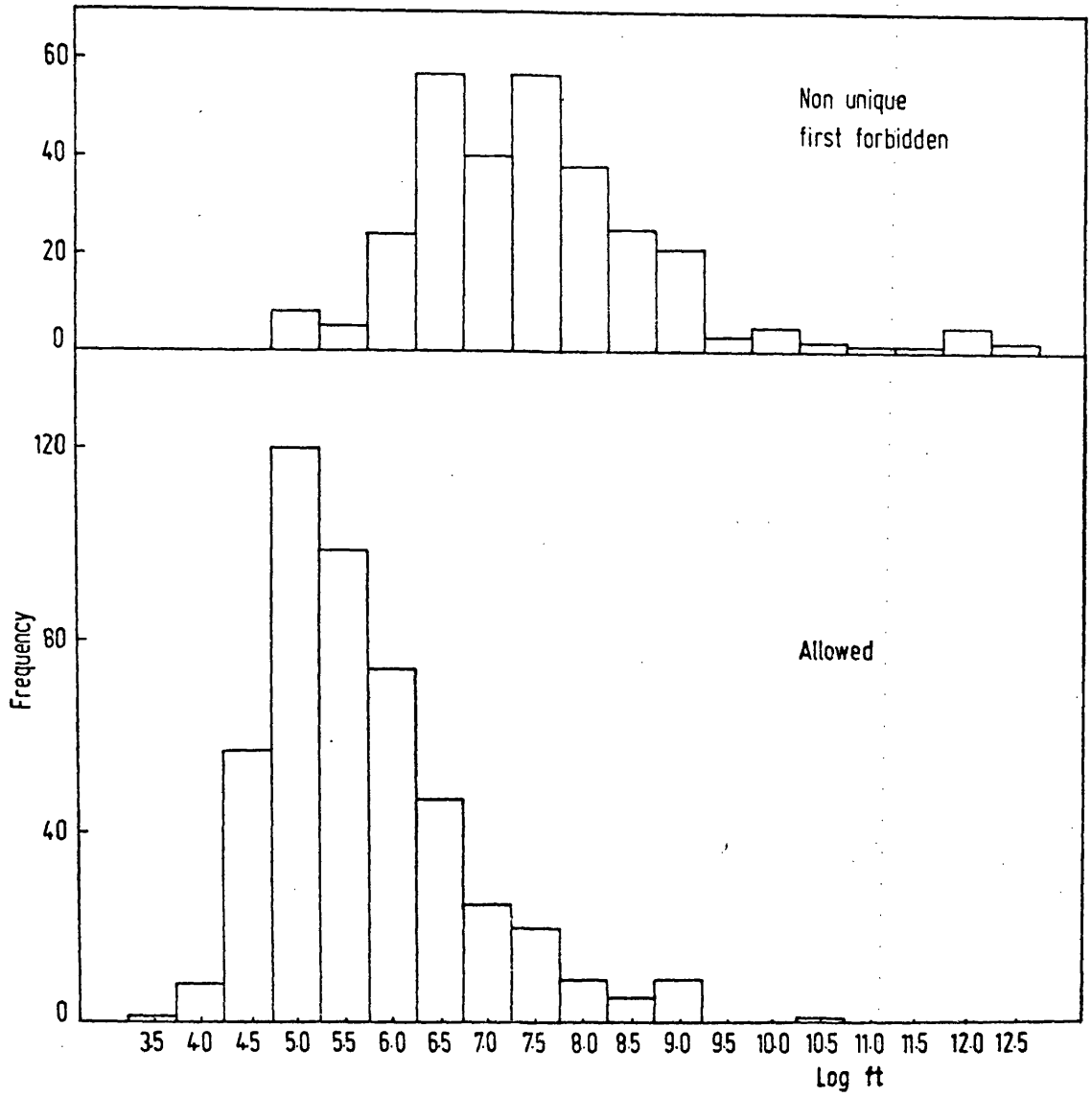
Non unique
first forbidden
Allowed
Frequency
60
40
20
0
120
80
40
0
3.5 4.0 4.5 5.0 5.5 6.0 6.5 7.0 7.5 8.0 8.5 9.0 9.5 10.0 10.5 11.0 11.5 12.0 12.5
Log ft

FIG 5-5

cascades from higher levels in ^{91}Nb the partial half life and, hence, the log ft value for this transition would be increased.

The K/β^+ Ratio for the Decay of ^{91}Mo to the Ground State of ^{91}Nb

The total K/β^+ ratio can be expressed as

$$(K/\beta^+)_{total} = \frac{K_o + K_1 + K_2 + \ldots}{\beta_o + \beta_1 + \beta_2 + \ldots}$$

where the suffixes 0, 1, 2, etc refer to the decay to the ground state, first excited state, second excited state, etc in ^{91}Nb. The ratio for the decay to the ground state, K_o/β_o, can be determined from the measured $(K/\beta^+)_{total}$ if the intensities of the decays to the excited states and the ratios K_1/β_1, K_2/β_2, etc are known.

Theoretical values of these K/β^+ ratios are given in table 5.4. The technique used for calculating these ratios and the ratio of total electron capture to K-capture are described in chapter 2. The ratios of total electron capture to positron emission shown in table 5.4 were calculated using

$$\frac{K + L + M + \ldots}{K} = 1 + \frac{L}{K} + \frac{M}{L} \cdot \frac{L}{K} + \ldots = 1.13$$

Since the intensity of the transition to any level is known it can be shown that, for example, for the decay to the third excited state (at 1790.5 keV),

intensity of the decay to the 1790.5 keV level

= .086 x (Intensity of the decay to the 1636.9 keV level)

i.e. $\epsilon_3 + \beta_3 = .086 \times (\epsilon_2 + \beta_2)$

$\therefore$ $1.611\,\beta_3 = .086 \times 1.460\,\beta_2$

Energy of excited state (keV)	Theoretical K/β^+	ϵ/β^+
1581.0	0.370 ± 0.026	0.418 ± 0.029
1636.9	0.407 ± 0.030	0.460 ± 0.034
1790.5	0.541 ± 0.043	0.611 ± 0.049
2530.8	4.01 ± 0.60	4.53 ± 0.68
2631.4	5.93 ± 0.96	6.70 ± 1.08
2791.8	13.3 ± 3.0	15.0 ± 3.4
3027.7	75.4 ± 26.0	85.2 ± 29.4
3148.7	339 ± 214	383 ± 242
3187.1	602 ± 369	680 ± 417

TABLE 5.4

In this way $\beta_1, \beta_3, \ldots, \beta_9$ can be expressed in terms of β_2. It can be shown that

$$\beta_1 + \beta_2 + \beta_3 + \ldots \beta_9 = (1.742 \pm 0.146)\beta_2$$

Also, from the theoretical K/β^+ ratios,

$$K_3 = 0.541\ \beta_3$$

and it can be shown that

$$K_1 + K_2 + \ldots + K_9 = (1.898 \pm 0.304)\beta_2$$

Therefore,

$$(K/\beta^+)_{total} = \frac{K_o + 1.898\ \beta_2}{\beta_o + 1.742\beta_2}$$

In order to determine K_o/β_o, an expression for β_2 in terms of β_o must be derived. This can be obtained from the measured ratio of the intensities of the 1.64 MeV gamma rays and the positrons. Thus

$$\frac{I_\gamma\ (1.64)}{\beta^+} = \frac{1.460\beta_2}{\beta_o + 1.742\beta_2} = (4.62 \pm 0.66) \times 10^{-3}$$

giving

$$\beta_2 = (3.18 \pm 0.46) \times 10^{-3}\ \beta_o$$

Therefore,

$$(K/\beta^+)_{total} = \frac{K_o + 0.00604\ \beta_o}{1.0055\ \beta_o}$$

The mean value of $(K/\beta^+)_{total}$ was shown in chapter 4 to be

$$(K/\beta^+)_{total} = 0.0539 \pm 0.0028$$

and, therefore, the K/β^+ ratio for the decay of ^{91}Mo to the ground state of ^{91}Nb is

$$\frac{K_o}{\beta_o} = 0.0482 \pm 0.0031.$$

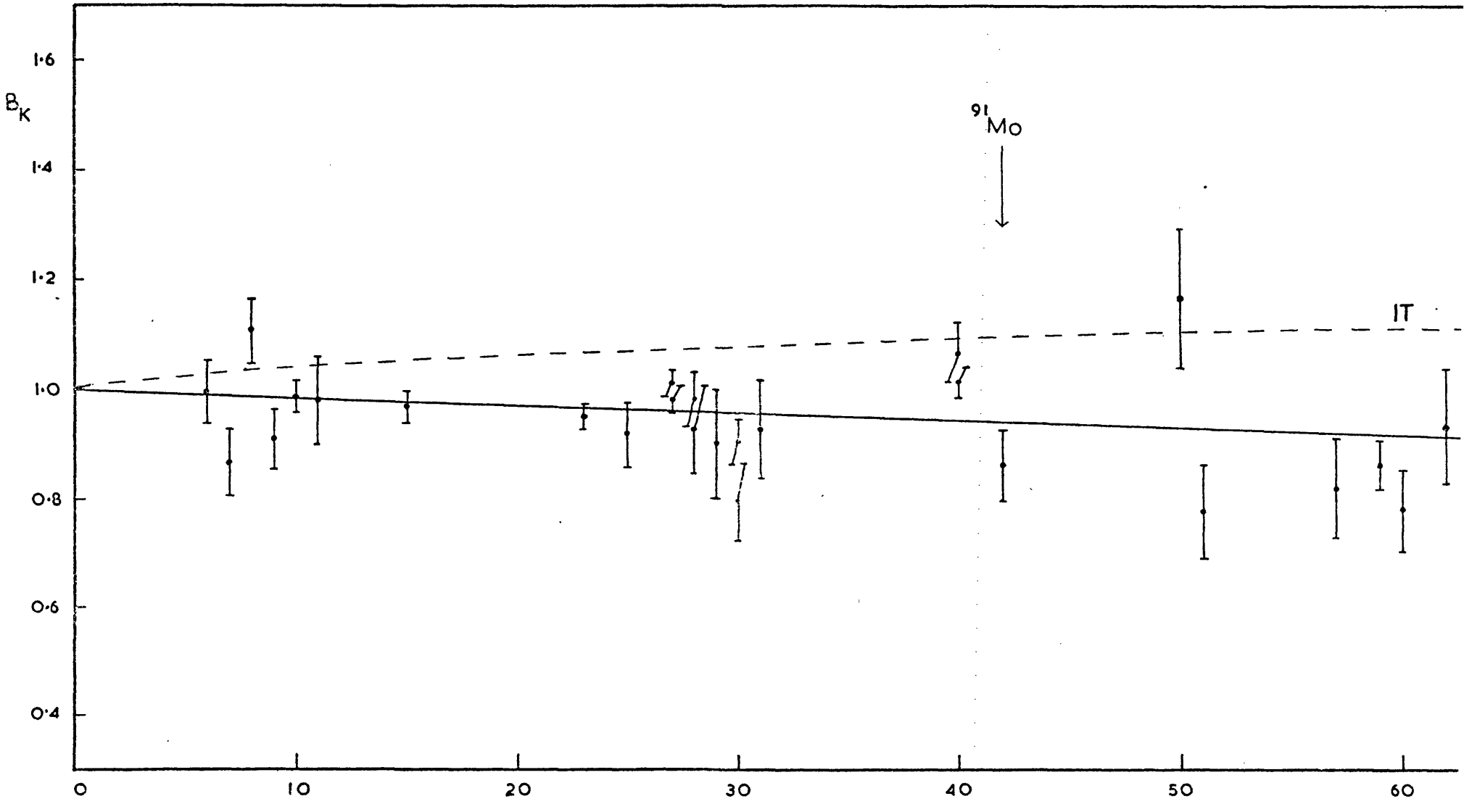

FIG 6-1

CHAPTER 6

RESULTS AND CONCLUSIONS

The experimental value of the K/β^+ ratio for the decay of ^{91}Mo to the ground state of ^{91}Nb was found to be 0.0482 ± 0.0031. The theoretical value of this ratio is 0.0559 ± 0.0022. This value was obtained using the Fermi functions, K electron wavefunction and K shell binding energy given by Behrens and Jänecke (1969). The method of calculation of the theoretical K/β^+ ratio is described in chapter 2. A value of 3421 ± 28 keV was adopted as the maximum positron kinetic energy (Wapstra and Gove, 1971). From these results the value of $(B_K)_{expt}$, defined as

$$(B_K)_{expt} = \frac{(K/\beta^+)_{expt}}{(K/\beta^+)_{theor}}$$

was found to be 0.862 ± 0.066.

Figure 6.1 shows all available values of $(B_K)_{expt}$ as a function of Z, including the present result. The straight line represents a linear least squares fit to the data, excluding the result for ^{91}Mo. It is clear that the value of $(B_K)_{expt}$ obtained for ^{91}Mo supports the tentative conclusion, reached in chapter 3, that the experimental K/β^+ ratios are smaller than the theoretical ratios, the discrepancy increasing as Z increases.

It is necessary to compare the experimental value of the K/β^+ ratio obtained for ^{91}Mo with theoretical ratios calculated by different authors to ensure that the discrepancy observed is not due merely to the orbital electron wavefunctions used in calculation of the theoretical ratio.

Theoretical K/β^+ ratios have been calculated by Zweifel (1957), Feenberg and Trigg (1950), Zyrianova and Suslov (1968, 1970). The calcula-

tions of Zweifel, and Feenberg and Trigg do not include the effect of finite nuclear size and, also, Feenberg and Trigg's results do not include screening corrections. The more recent calculations (Zyrianova and Suslov, 1968 and 1970) unfortunately do not extend above W_o = 2.6 MeV. The only other available theoretical K/β^+ ratios are those which can be obtained from tables given by Dzhelepov and Zyrianova (1956) and electron radial wavefunctions of Zyrianova (1963). These results lead to a value of 0.055 for the theoretical ratio which is in good agreement with the value derived from the tables of Behrens and Jänecke (1969). This, therefore, indicates that the difference between the experimental and theoretical K/β^+ ratios for ^{91}Mo is real and not merely dependent on the theoretical calculations. The problem of theoretical K/β^+ ratios being, in general, higher than experimental values is being considered by Professor H Behrens but at present no theoretical explanation has been found.

For most of the points shown in figure 6.1, B_K is less than unity but there are a few exceptions. In particular, for ^{89}Zr, the experimental evidence for a value of B_K greater than unity is very convincing. It has already been mentioned that the group of measurements around Z = 60 (i.e. ^{134}La, ^{140}Pr, ^{141}Nd and ^{143}Sm) were all carried out by a single group using the same technique (Biryukov and Shimanskaya, 1970). Since the gradient of the fit to the data depends strongly on these four points, the possibility that these results are systematically low must be considered. If these points are omitted and the present result for ^{91}Mo included, the linear least squares fit gives values of B_K ranging from 0.970 at Z = 0 to 0.966 at Z = 60.

It is, therefore, desirable to make a precise measurement of the

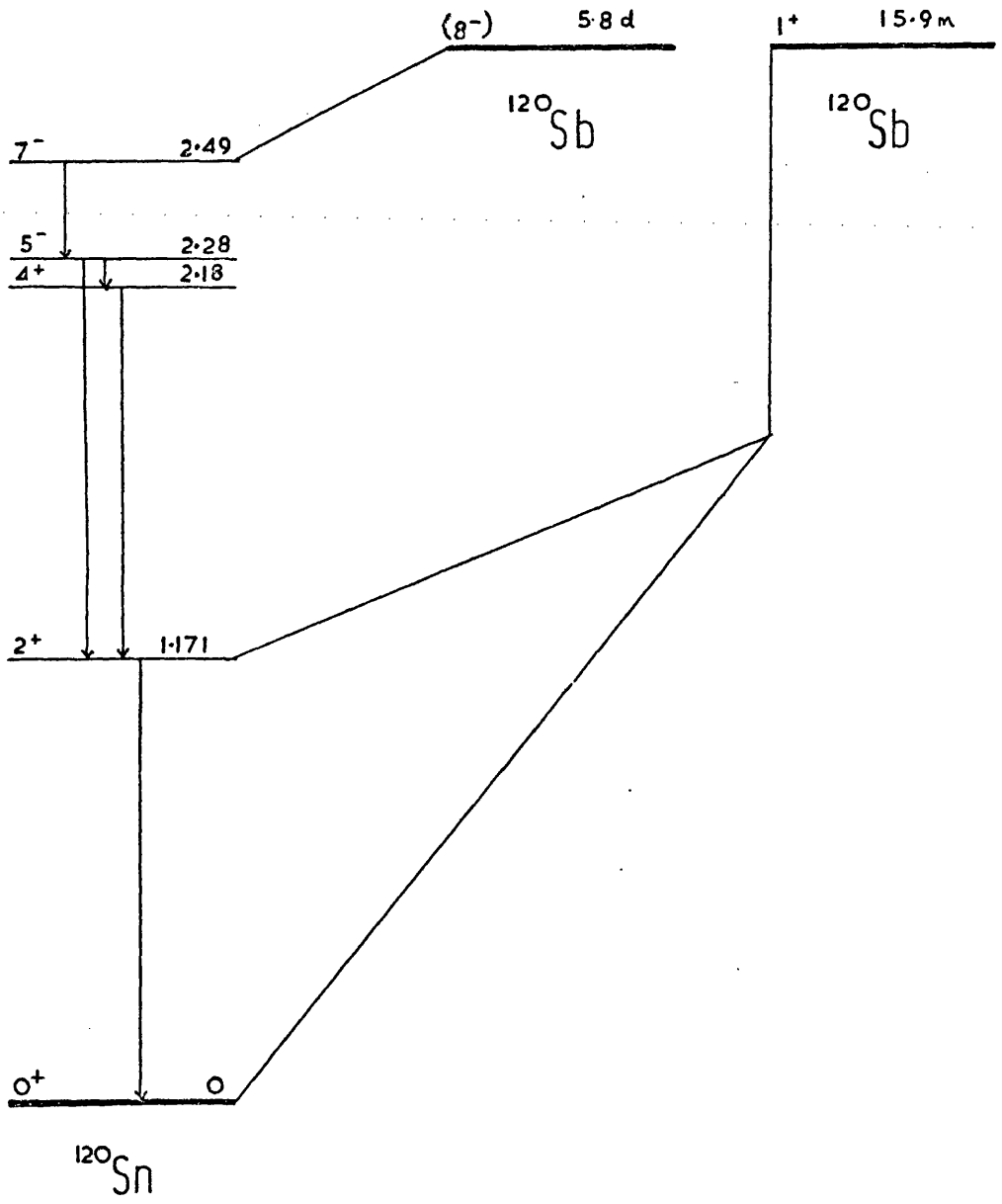

FIG 6-2

K/β^+ ratio for at least one isotope in the region above Z = 30. The experience gained from the ^{91}Mo measurement may be used to indicate the most suitable isotope for such a precision measurement. The major sources of error in the ^{91}Mo measurement must be examined to decide how they could best be overcome or reduced.

In the determination of the K x-ray intensity, the largest error was associated with the determination of the contribution from ^{90}Mo. Since ^{90}Mo was produced by the reaction ^{92}Mo (γ,2n), irradiation at an energy below the threshold for this reaction (22.8 MeV) would have ensured that no ^{90}Mo was produced. However, it is not possible with the present accelerator to obtain a sufficiently intense beam at such a low energy. This problem was particularly serious in the experiment using ^{91}Mo because the K-capture events form only a small fraction of the activity from this isotope while ^{90}Mo decays mainly by electron capture. Therefore, even if only a small fraction of the total activity is due to ^{90}Mo, the effect on the K x-rays is considerable.

Consideration of this point and of the desirability of an isotope with a fairly simple decay scheme and reasonable half life has led to the choice of ^{120}Sb. The decay scheme according to Lederer et al. (1967) is shown in figure 6.2. It is proposed to measure the K/β^+ ratio for the decay of the 1^+ ground state of ^{120}Sb to the ground state of the ^{120}Sn. The maximum positron kinetic energy is 1658 ± 7 keV (Wapstra and Gove, 1971) and the theoretical K/β^+ ratio is 1.26 ± 0.05. ^{120}Sb can be produced by the reaction.

$$^{121}\text{Sb}\ (\gamma,n)$$

using the stable isotope ^{121}Sb which has a natural abundance 57.25 per cent. The impurity produced in this case by the (γ,2n) reaction is

^{119}Sb, which decays solely by electron capture with a half life of 38 hours. The effect of this impurity is expected to be almost negligible compared with the effect of ^{90}Mo in the ^{91}Mo experiment since the K/β^+ ratio for ^{120}Sb is fairly large.

Another advantage of ^{120}Sb is the higher K x-ray energies compared with ^{91}Mo which means that absorption of the x-rays in the sample, air and detector window will be lower. Also, the fluorescence yield is higher and has a smaller error than for ^{91}Mo. The value of ω_K (Bambynek et al., 1972) for Sn is 0.859 ± 0.028 compared with a value of 0.748 ± 0.032 for Nb.

Preliminary measurements on ^{120}Sb are already in progress using the same techniques as for the ^{91}Mo experiment. A half life measurement on the K x-ray activity indicates that, as expected, the effect of ^{119}Sb is very small. Less than 1 per cent of the initial K x-ray activity is associated with ^{119}Sb. In the ^{91}Mo experiment, the amount of the corresponding impurity, ^{90}Mo, was about 13 per cent of the initial K x-ray activity.

Another important source of error in the ^{91}Mo experiment was the detection of 0.511 MeV gamma rays from positrons which annihilated outside the detector. A method of overcoming this difficulty which was considered for the ^{91}Mo experiment was a 4π NaI(Tl) detection system with the source between two detectors. In this arrangement all the positrons would be stopped within the detectors. The pulses from the two detectors must be summed otherwise a positron which entered one detector and was then scattered into the other would be counted more than once. This method was not, in fact, employed, mainly because of the

large absorption in the detector window of the x-rays entering the detector at large angles to the axis. However, if detectors without windows were employed, the 4π arrangement would have a considerable advantage over the single detector system. NaI(Tl) could not be used since it is hygroscopic and must be kept in a sealed container. However, both of the scintillators, CsI(Tl) and Ca F_2(Eu), are non-hygroscopic and the work of testing the performance of both these materials as windowless x-ray detectors has already commenced.

However, the use of scintillators has one important disadvantage compared with the Si(Li) detector system described in chapter 4, i.e. the much poorer energy resolution which means that, for isotopes in the region of interest, the K x-rays from adjacent atoms cannot be resolved. The good resolution of the Si(Li) detector enables the intensity of the fluorescent x-rays from the sample to be determined. For this reason, the determination of the K/β^+ ratio for ^{91}Mo involved measurements made with both types of detector. At the suggestion of Dr K. W. D. Ledingham, an improvement in the solid state detector system is being considered. It is proposed to replace the copper collimator by a thin sheet of plastic scintillator with a small hole in front of the detector window. Pulses from the detector would then be taken in anti-coincidence with those from the plastic scintillator. The scintillator could be made as thin as possible since, unlike the case with the copper collimator, there is no necessity to stop the positrons which enter the scintillator. Thus edge effects can probably be made negligible. A further refinement involves the use of two sheets of plastic scintillator to determine the direction from which positrons enter the scintillator, i.e. to distinguish between positrons which

enter the scintillator directly from the source and those which are scattered out of the detector and then enter the scintillator.

CONCLUSIONS

1 $Z \leq 15$

In this region it has been shown that the existing experimental data are not accurate enough to distinguish unambiguously between the theories of Bahcall and Vatai although the results slightly favour Vatai (i.e. exchange-overlap corrections are small). Present experimental techniques, however, are not sufficiently accurate to allow determination of the magnitudes of these corrections to the theoretical ratios.

2 $Z > 15$

The majority of the results indicate that experimental K/β^+ ratios are smaller than the theoretical ratios and that the difference increases as Z increases. However, the existence of some values of $B_K > 1$ and the possibility of systematic errors in the group of results around $Z = 60$ indicates the need for at least one precise K/β^+ measurement in the region above $Z = 30$. Experimental accuracy of the order of 1 - 2 per cent should be possible if a suitable isotope is chosen for study.

The author also intends to examine K/β^+ ratios for forbidden transitions. There are few experimental results for such transitions. The internal source scintillation counter technique (cf. McCann and Smith, 1969, and Joshi and Lewis, 1961) would be suitable for the determination of K/β^+ ratios for long-lived, forbidden transitions. The non-unique first forbidden transitions are expected to differ very little from allowed transitions (Wapstra et al., 1959) while the unique first for-

bidden transitions are expected to differ by a factor which depends on W_o alone.

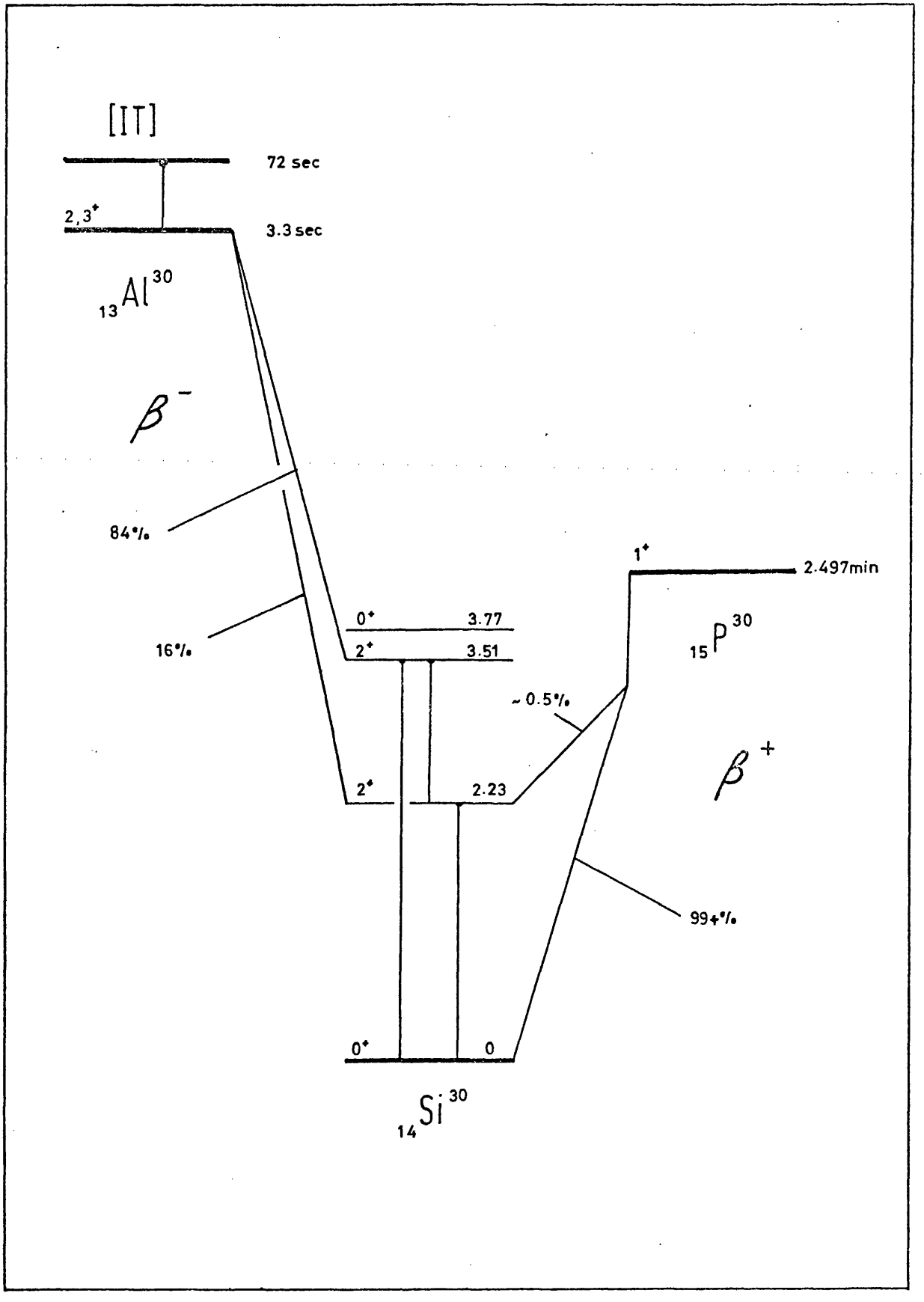
[IT]
72 sec
2,3+
3.3 sec
13Al30
β−
84%
16%
0+ 3.77
2+ 3.51
2+ 2.23
0+ 0
14Si30
1+
2.497min
15P30
~0.5%
β+
99+%

FIG A-1

APPENDIX 1

Decay of ^{30}P to the First Excited State of ^{30}Si

The decay scheme of ^{30}P is shown in figure A.1. ^{30}P can decay to both the ground state and the first excited state of ^{30}Si and, from the spins and parities of the states involved, both are allowed Gamow-Teller decays. The positron end point energy for the transition to the ground state of ^{30}Si is 3205.4 ± 2.6 keV (Wapstra and Gove, 1971) and the half life of ^{30}P is 2.497 ± 0.005 min. (McDonald et al., 1963).

If the nuclear matrix elements for the two transitions are assumed to be equal, the intensity of the transition to the first excited state is expected to be about 0.6 per cent of that to the ground state. This calculation used the positron end point energy and the ^{30}P half life given above and the Fermi functions calculated from the tables of Behrens and Jänecke (1969). The corresponding log ft value for each transition is 4.84.

Morinaga and Bleuler (1956) investigated the gamma rays following the decay of ^{30}P using a sodium iodide scintillation spectrometer. They detected a 2.24 MeV gamma ray and measured its intensity relative to the positron annihilation radiation. They estimated the branching to the first excited state of ^{30}Si to be 0.5 per cent. This intensity is in agreement with that given above, which was calculated on the assumption that the difference in intensity of the two transitions depends only on the difference of the end point energies.

However, during the measurement of the K/β^+ ratio for ^{30}P des-

Diagram of electronics used in detection of ^{30}P gamma ray

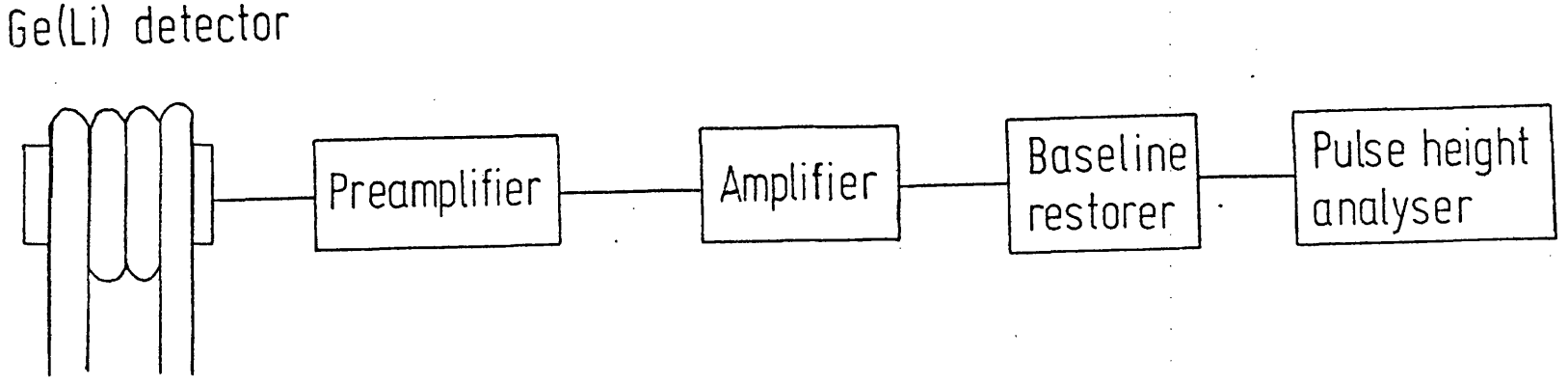

FIG A-3

cribed in chapter 2, examination of the gamma rays from the irradiated phosphine to determine what impurities were present showed that the 2.23 MeV gamma ray was much less intense than indicated above. Further measurements of the intensity of the 2.23 MeV gamma ray were undertaken using a Ge(Li) detector and are described below.

Experimental Technique

The phosphine was irradiated and mixed with argon-methane exactly as for the K/β^+ measurement described in chapter 2 but, instead of flowing into the anticoincidence proportional counter, the gas flowed through about 2 m of polythene tubing (internal diameter 0.7 cm, thickness 0.2 cm) wound round the aluminium can of a Ge(Li) detector. The source was thus concentrated in a volume of about 80 ml around the detector. The Ge(Li) detector had an active volume of about 28 ml and an energy resolution of about 4 keV for 1 MeV gamma rays. A diagram of the source-detector arrangement is shown in figure A.2. Polythene tubing was used in preference to metal tubing to reduce the bremsstrahlung produced by the positrons travelling through the tubing. This bremsstrahlung produces a continuous background up to the end point energy of the positrons (3.2 MeV) and could obscure any weak 2.23 MeV gamma ray. The detector was shielded on all sides by about 8 cm of lead to reduce background due to the accelerator and natural activities. A diagram of the electronic arrangement used is shown in figure A.3.

The phosphine and argon-methane flow rates were about 2 ml per min and 170 ml per min, respectively. These rates were chosen to ensure that the phosphine was irradiated for two or three half lives

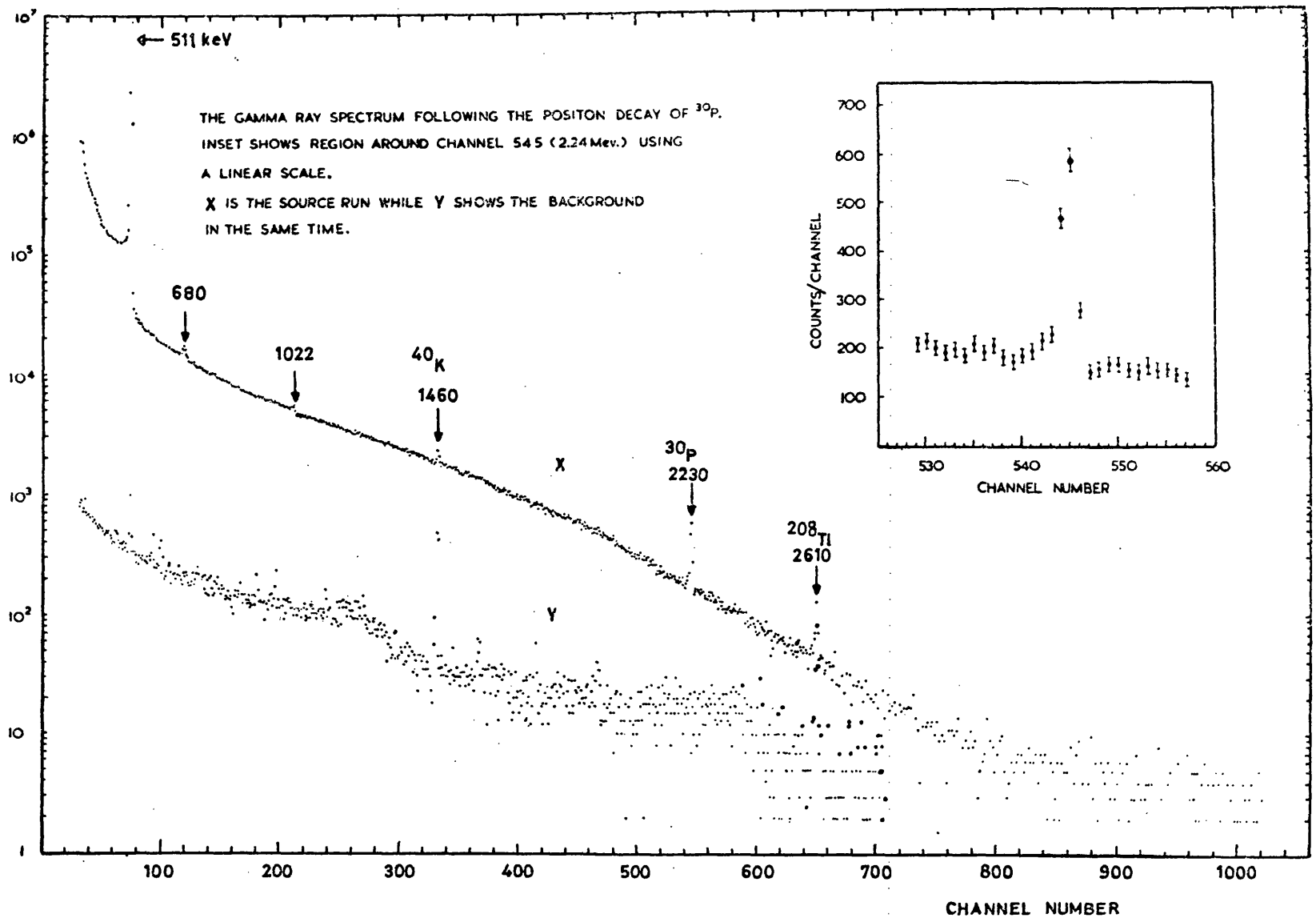
511 keV
THE GAMMA RAY SPECTRUM FOLLOWING THE POSITON DECAY OF ^{30}P.
INSET SHOWS REGION AROUND CHANNEL 545 (2.24 Mev.) USING
A LINEAR SCALE.
X IS THE SOURCE RUN WHILE Y SHOWS THE BACKGROUND
IN THE SAME TIME.
680
1022
^{40}K
1460
X
^{30}P
2230
^{208}Tl
2610
Y
COUNTS/CHANNEL
CHANNEL NUMBER
CHANNEL NUMBER

FIG A-4

of ^{30}P and that the decay of ^{30}P between the irradiation vessel and the detector was small. Ten runs, each of about one hour's duration, were made and counting rates of 20 000 to 30 000 per minute were obtained. The stability of the electronics was checked after each run by analysing the spectra obtained from calibration sources of ^{22}Na, ^{60}Co and ^{88}Y. The gain was found to be constant for each of the calibration runs and the ten spectra from phosphine were added giving the spectrum in figure A.4. Also shown in this figure is a background spectrum of the same duration (10 hours). For this background measurement the irradiation vessel was removed from the bremsstrahlung beam and the gas flow was stopped.

The peak at 1.02 MeV is due to the simultaneous detection of two positron annihilation quanta. The peaks at 1.46 and 2.61 MeV, also seen in the background with the same intensity, are due to ^{40}K and ^{208}Tl. The ^{40}K activity probably comes from concrete near the detector. ^{208}Tl is part of the ^{232}Th series which ends in the stable isotope ^{208}Pb. The other peaks are at 0.511, 0.680 ± 0.003 and 2.23 ± 0.003 MeV. The small peak at 0.511 MeV in the background may be due to positrons produced by cosmic rays. The peaks at 0.680 and 2.23 MeV are not seen in the background. The origin of the 680 keV peak could not initially be identified. Its intensity was too low to allow an accurate measurement of its half life although it was estimated roughly to be of the order of a few minutes. The region around 680 keV is shown in more detail in figure A.5.

It was noticed that ^{30}S decays by positron emission to the first excited state of ^{30}P which then decays with the emission of a 687 keV gamma ray. However, the 1.4 sec. half life of ^{30}S makes it

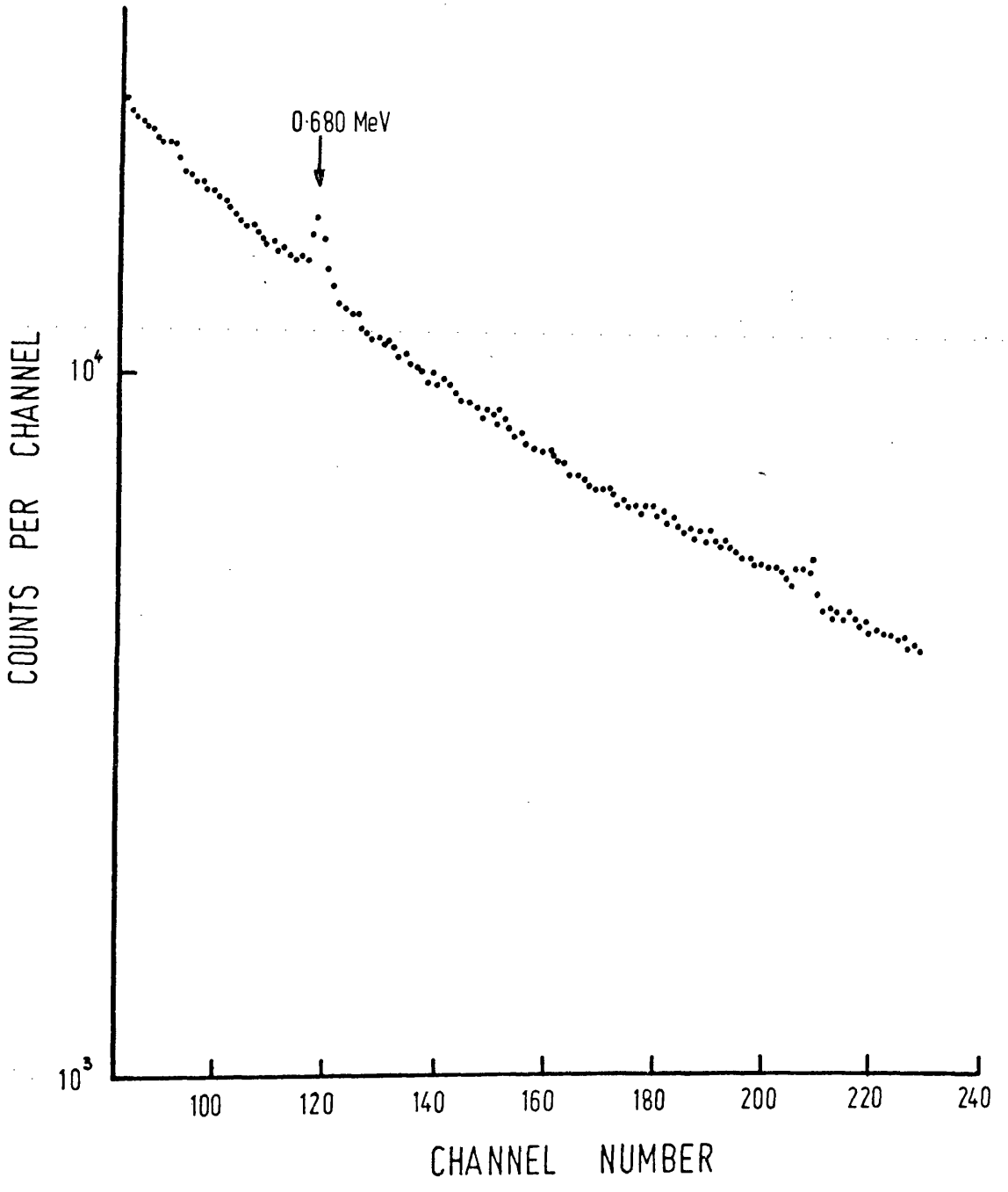
PHOSPHINE IRRADIATION
SUM OF 10 RUNS IN REGION OF 680 KeV.
0·680 MeV
COUNTS PER CHANNEL
10^4
10^3
100
120
140
160
180
200
220
240
CHANNEL NUMBER

FIG A-5

impossible for this activity to reach the detector and rules out this interpretation.

Another possibility which was considered was that the 680 keV line was due to the de-excitation of the first excited state of ^{72}Ge in the Ge(Li) detector. This isotope has a natural abundance of 27 per cent and a first excited state at 690 keV. It was thought that positrons from ^{30}P were exciting this 690 keV level. Since both the ground state and 690 keV state of ^{72}Ge have spin and parity 0^+, de-excitation of the 690 keV level occurs by emission of an electron of energy 679 keV (the energy difference between the levels minus the K shell binding energy of germanium). In order to test this hypothesis the ^{30}P source was replaced by a β^- source, ^{90}Sr. The maximum β^- energy from this source is 2.0 MeV and hence the 680 keV line should also be present in this case. However, no such line was found and this hypothesis was rejected.

The present author noticed that a peak at about 680 keV could be produced by the simultaneous detection of one 511 keV positron annihilation gamma ray and the backscattered gamma ray from a similar annihilation gamma ray ($E_{backscatter} \doteqdot 170$ keV). This effect has been observed in NaI(Tl) detectors (Girgis and Van Lieshout, 1959 and Van Lieshout, 1965). At large scattering angles (i.e. $\sim 180^{\circ}$) the energy of the backscattered gamma has only a weak dependence on the scattering angle and hence a peak is seen. The width of this peak in a Ge(Li) detector is greater than that produced by a 680 keV gamma ray but in the present experiment the intensity of the 680 keV peak was too low to permit reliable estimation of its width. This interpretation also explains the value of a few minutes for the half

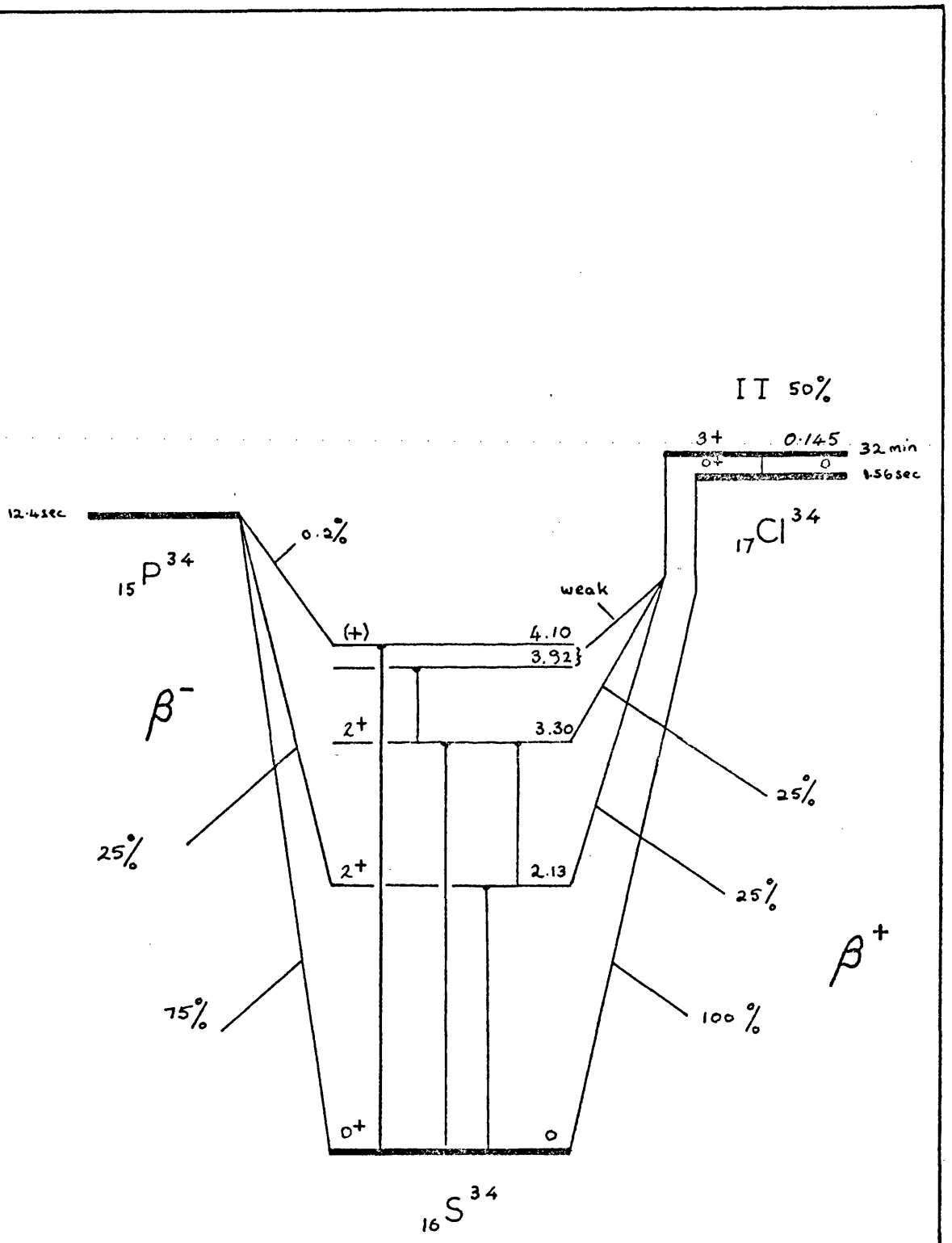
IT 50%
3+
0.145
32 min
0+
0
1.56 sec
12.4 sec
0.2%
$_{15}P^{34}$
$_{17}Cl^{34}$
weak
(+)
4.10
3.92
β^-
2+
3.30
25%
25%
2+
2.13
25%
β^+
75%
100 %
0+
0
$_{16}S^{34}$

FIG A-6

life of the 680 keV peak since it should decay with the same half life as the positrons.

The intensity of the 2.23 MeV gamma ray was also too small for a half life measurement to be feasible but since no other gamma rays were present it seems reasonable to assign it to the de-excitation of the first excited state of ^{30}Si. This level could also be reached by the β^- decay of ^{30}Al but, if this were the case, another gamma ray of almost equal intensity and of energy 1.27 MeV should also be present and this is clearly not the case. Therefore, the 2.23 MeV gamma ray seen in the phosphine spectrum was assumed to result from the decay of ^{30}P to the first excited state of ^{30}Si.

Relative Efficiency of the Ge(Li) Detector

Since the efficiency of a Ge(Li) detector varies with gamma ray energy the relative efficiency of the detector at 0.511 and 2.23 MeV must be measured before the intensity of the transition to the 2.23 MeV level can be calculated.

Suitable calibration sources should have gamma rays of known intensity at these energies (0.511 and 2.23 MeV). ^{38}K is a suitable source since it has a single gamma ray (2.16 MeV) of almost the same energy as the gamma ray of interest and positrons of almost the same end point energy as ^{30}P. This was the source used by Morinaga and Bleuler (1956) to find the relative efficiency of their sodium iodide detector. However, in the present measurement, it is desirable to use a gaseous calibration source which can flow through the system in place of phosphine and no suitable compound of potassium exists. Instead ^{34m}Cl, in the form of a gas, methyl chloride, was irradiated

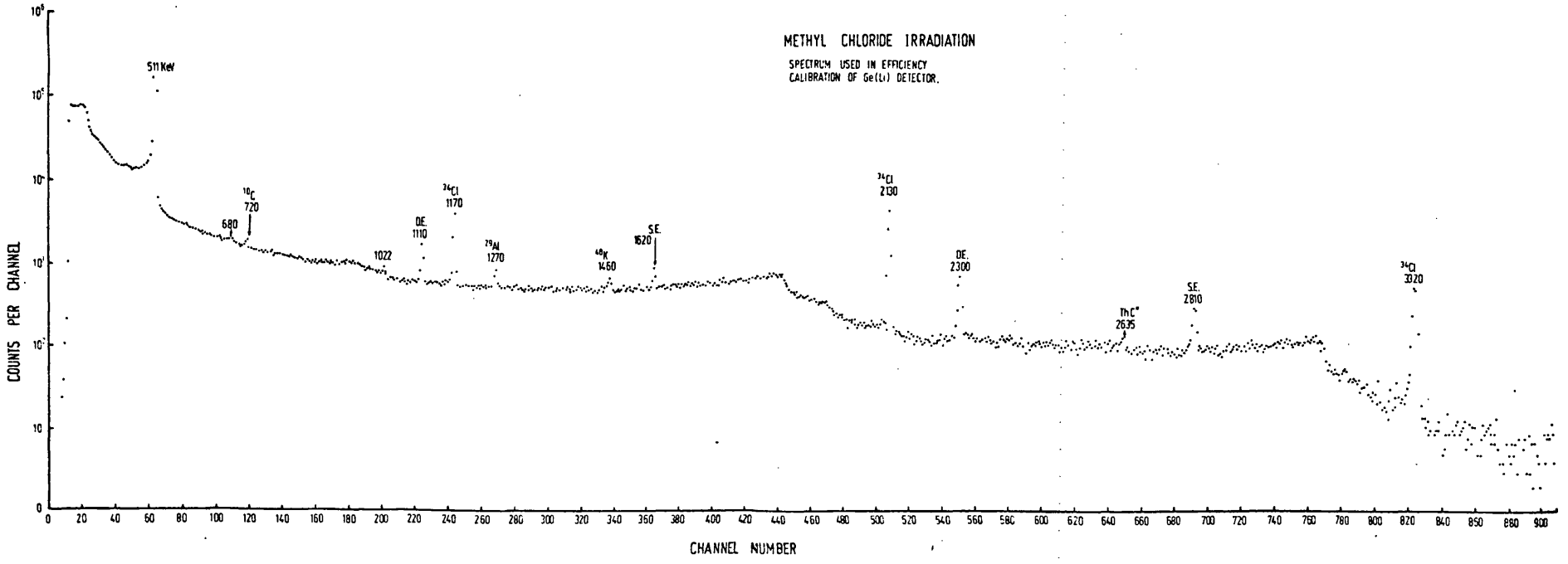
METHYL CHLORIDE IRRADIATION
SPECTRUM USED IN EFFICIENCY CALIBRATION OF Ge(Li) DETECTOR.
511 KeV
680
^{11}C 720
1022
DE. 1110
^{34}Cl 1170
^{29}Al 1270
^{40}K 1460
S.E. 1620
^{34}Cl 2130
DE. 2300
ThC'' 2615
S.E. 2810
^{34}Cl 3020
COUNTS PER CHANNEL
CHANNEL NUMBER

FIG A-7

and flowed through the system in place of phosphine. ^{34m}Cl emits several gamma rays of known energy and intensity (Endt and Van Der Leun, 1967) which could be used to measure the efficiency of the detector at several energies and the results interpolated to 2.23 MeV.

The decay scheme of ^{34}Cl is shown in figure A.6. ^{34}Cl exists as a mixture of two states. The first excited state decays by positron emission with a half life of 32 min to several excited states of ^{34}S which decay by gamma emission. The ground state of ^{34}Cl decays entirely to the ground state of ^{34}S with a half life of 1.56 sec. The first excited state of ^{34}Cl also decays to the ground state of ^{34}Cl by the emission of a 145 keV gamma ray.

^{34m}Cl was produced by the reaction

$$^{35}Cl(\gamma,n)$$

on the stable isotope ^{35}Cl in methyl chloride (CH_3 Cl). This reaction produces both the ground state and the isomeric state of ^{34}Cl. The methyl chloride flow rate was chosen so that the short-lived ground state of ^{34}Cl produced directly by the irradiation had decayed to a negligible amount before reaching the detector. This meant that knowledge of the relative production rates of the two states of ^{34}Cl was not required.

The gamma ray spectrum obtained from the methyl chloride irradiation is shown in figure A.7.

Since ^{11}C, a positron emitter with a 20 min half life, was also produced by the irradiation of the methyl chloride, a half life measurement of the irradiated gas was made in order to find the relative amounts of ^{34m}Cl and ^{11}C contributing to the 0.511 MeV peak.

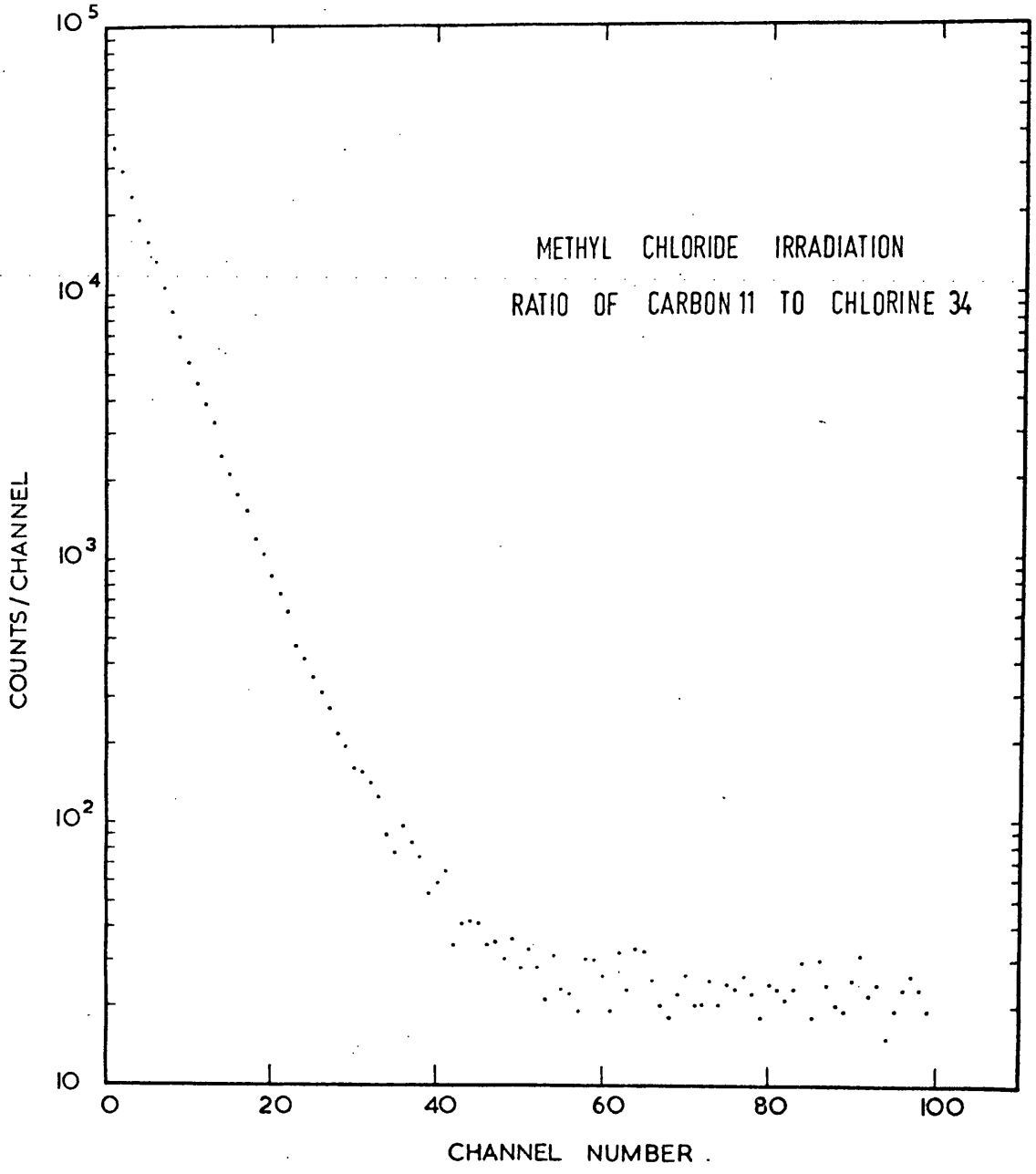
METHYL CHLORIDE IRRADIATION
RATIO OF CARBON 11 TO CHLORINE 34
COUNTS / CHANNEL
CHANNEL NUMBER
10^5
10^4
10^3
10^2
10
0
20
40
60
80
100

FIG A-8

This was done by building up a large activity in the target and then flowing the irradiated methyl chloride to the detector and closing valves on either end of the polythene tubing thus containing the gas in a region around the detector. After 2 min the activity of the gas was examined using the multiscale facility of a 100 channel analyser. Only events in the region of 0.511 MeV were analysed. The analyser counted for 100 secs in each channel with a waiting time of 300 secs between channels. The data obtained can be seen in figure A.8. These results were fitted by a least squares method to the sum of two exponentials using the VA04A program mentioned in chapter 4. The ratio of ^{34m}Cl to ^{11}C was found to be 0.223 ± 0.011. This analysis was performed by Dr J Y Gourlay.

A graph of the relative efficiency of the Ge(Li) detector was then drawn using the areas of the gamma ray peaks in the methyl chloride spectrum, the known intensities of ^{34m}Cl gamma rays and the above ratio of ^{34m}Cl to ^{11}C positrons (figure A.9). Also shown on this graph are the relative efficiencies obtained for point sources of ^{22}Na and ^{56}Co on the axis of the detector about 1 cm from the detector can. The data from the point sources was fitted by the expression

$$\log \epsilon = a + b \log E + c(\log E)^2$$

where ϵ and E are the relative efficiency and gamma ray energy, respectively. This expression is given by Barker and Connor (1967) who also give the relative intensities of the ^{56}Co gamma rays used in this calibration.

The data points due to ^{34m}Cl were normalised so that both

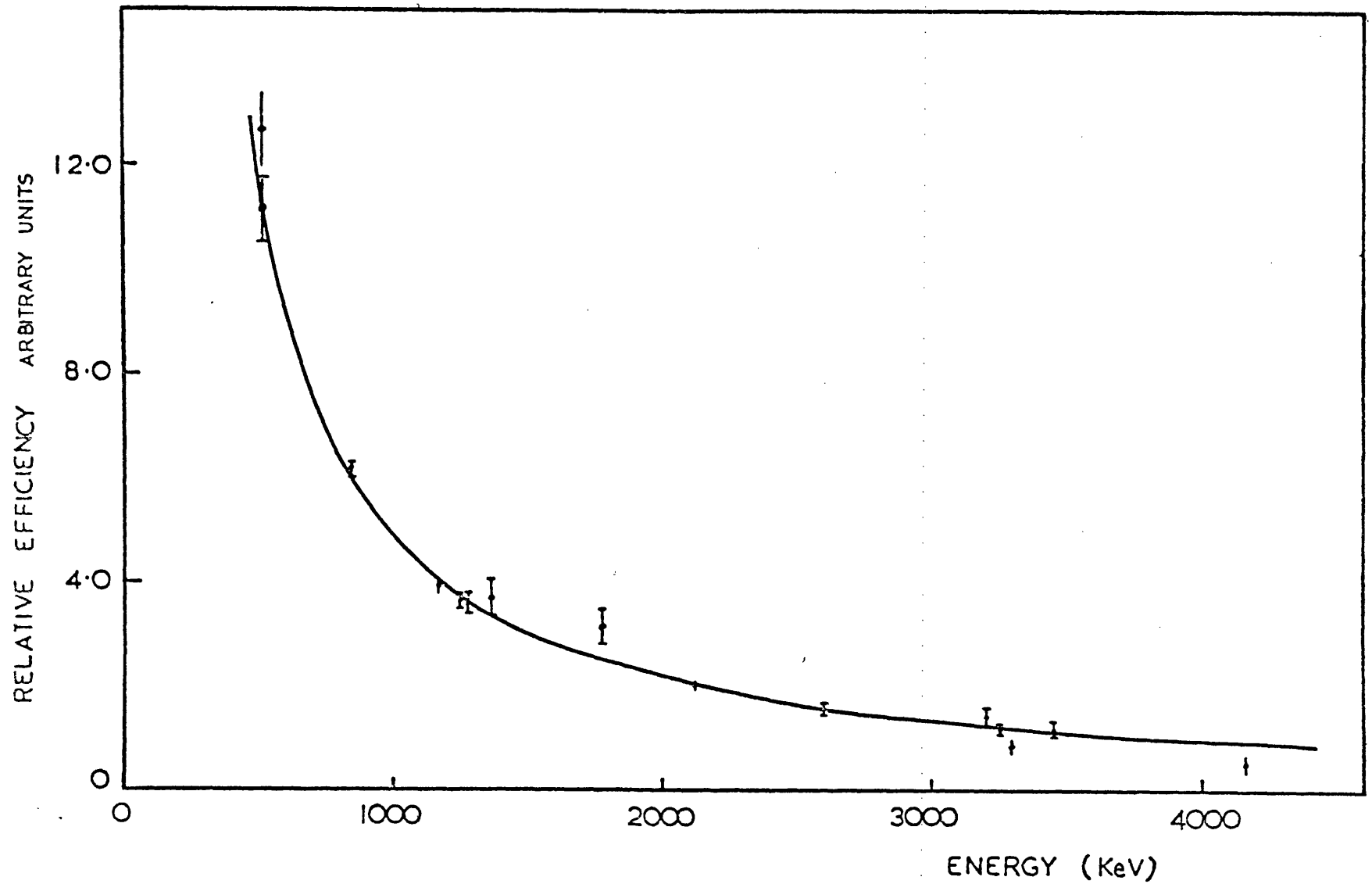
RELATIVE EFFICIENCY ARBITRARY UNITS
12·0
8·0
4·0
0
0
1000
2000
3000
4000
ENERGY (KeV)

FIG A-9

methods gave the same relative efficiency at 2.13 MeV. From the graph the ratio of the relative efficiencies at 0.511 and 2.23 MeV is 6.74 ± 0.47.

This result, however, is based on the measurement of the relative amounts of positrons from ^{34m}Cl and ^{11}C in the methyl chloride irradiation and assumes that the ^{11}C positron annihilation gamma rays are detected with the same efficiency as those from ^{34m}Cl. This may not be the case since their positron end point energies are different (0.96 MeV for ^{11}C and 4.5 MeV for ^{34m}Cl). Positrons from the source may penetrate the polythene tubing and annihilate at some distance from the detector. The ^{34m}Cl positrons would, therefore, tend to annihilate further from the detector than ^{11}C positrons and so reduce the number of ^{34m}Cl positrons detected. Hence the measured ratio of ^{34m}Cl to ^{11}C positron annihilation gamma rays would not be the true ratio of these activities in the source. This also implies that the geometry for the decay of ^{30}P would be different from that of either ^{11}C or ^{34m}Cl because of the different end point energy.

It was decided to check the effect of geometry by using solid phosphorus samples. A number of samples of red phosphorus, purity 99.999 per cent, and each weighing about 1 g were irradiated and then completely enclosed in a 1 cm thick aluminium container to stop all the positrons (i.e. all the positrons annihilated near the source). The aluminium container was placed on top of the Ge(Li) detector can. The resulting spectrum is shown in figure A.10.

The ratio of the intensities of the 2.23 and 0.511 MeV gamma

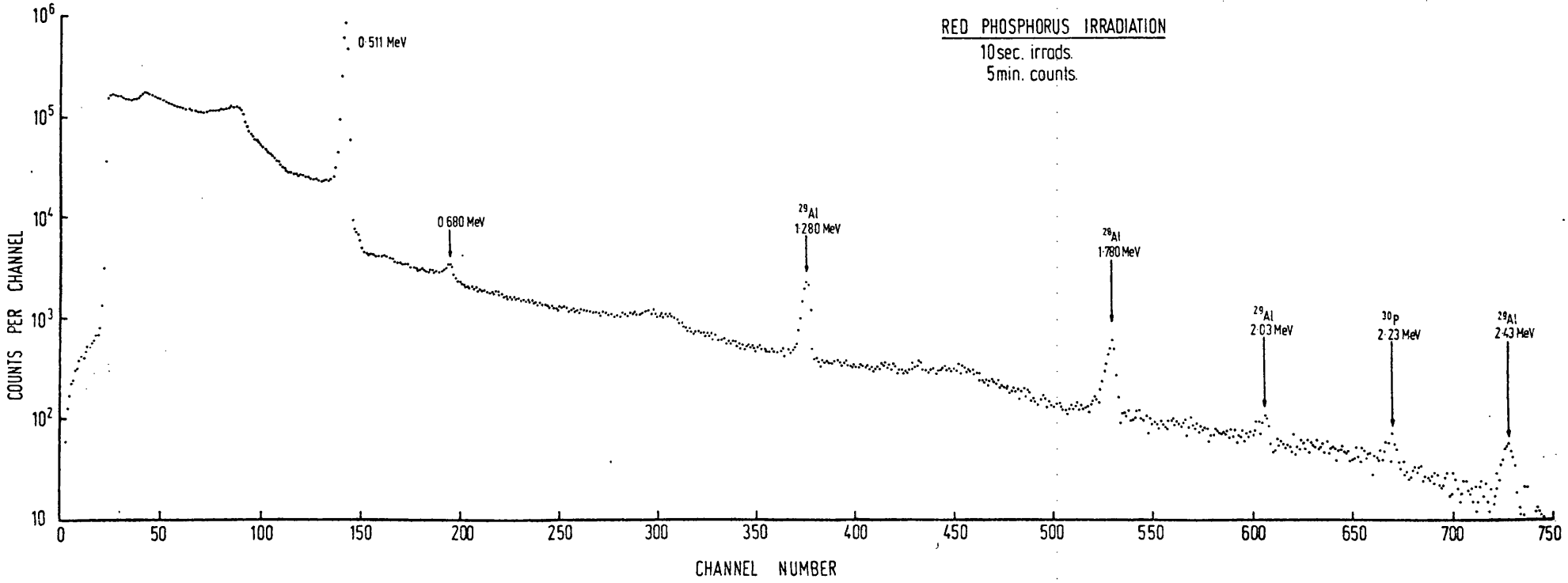
RED PHOSPHORUS IRRADIATION
10 sec. irrads.
5 min. counts.
0·511 MeV
0·680 MeV
29Al
1·280 MeV
29Al
1·780 MeV
29Al
2·03 MeV
30P
2·23 MeV
29Al
2·43 MeV
COUNTS PER CHANNEL
CHANNEL NUMBER
10⁶
10⁵
10⁴
10³
10²
10
0
50
100
150
200
250
300
350
400
450
500
550
600
650
700
750

FIG A-10

rays from this spectrum was found to be the same, within experimental errors, as from the phosphine irradiations implying that the effect of positrons annihilating far from the detector was negligible.

Results

The ratio of the number of 2.23 MeV gamma rays to positrons from the phosphine measurement described earlier is

$$(1.40 \pm 0.11) \times 10^{-4}$$

and from the red phosphorus measurement

$$(1.24 \pm 0.15) \times 10^{-4}.$$

A further phosphine measurement gave the result

$$(1.24 \pm 0.09) \times 10^{-4}.$$

The weighted mean of these results is

$$(1.29 \pm 0.06) \times 10^{-4}$$

and, together with the previously quoted relative efficiency at 0.511 and 2.23 MeV, gives the value of

$$(8.7 \pm 0.9) \times 10^{-4}$$

for the intensity of the transition to the 2.23 MeV level relative to the transition to the ground state. This result is a factor of about six less than that given by Morinaga and Bleuler.

The log ft value for the transition to the 2.23 MeV level in ^{30}P, from the present result, is 5.66 ± 0.04. The theoretical value calculated by Engelbertink and Brussaard (1966), using nuclear wave functions derived from shell-model calculations of Glaudemans et al. (1964), is 3.86.

The wave functions obtained for ^{30}P and ^{30}Si by Glaudemans et al.

were calculated assuming an inert core of fourteen protons and fourteen neutrons with the two remaining particles existing in combinations of the $2s_{1/2}$ and $1d_{3/2}$ shells. If this description is valid the present result can be used to obtain an estimate of the s and d shell amplitudes in the ^{30}P and ^{30}Si states involved.

The three relevant nuclear states (i.e. the ground state of ^{30}P and the ground and first excited states of ^{30}Si), can be written in terms of seven parameters representing the combinations of $2s_{1/2}$ and $1d_{3/2}$ wavefunctions. For example, the ^{30}P ground state can be represented by

$$A\left[s_{1/2}{}^2\right] + B\left[s_{1/2}\, d_{3/2}\right] + C\left[d_{3/2}{}^2\right]$$

where the two particles are coupled to give $J = 1^+$. A represents the probability that both nucleous will be found in the $2s_{1/2}$ shell. Similarly the ^{30}Si ground and excited states can be written as

$$D\left[s_{1/2}{}^2\right] + E\left[d_{3/2}{}^2\right] \quad \text{for } ^{30}Si,\ J = 0^+ \text{ ground state}$$

and $$F\left[s_{1/2}\, d_{3/2}\right] + G\left[d_{3/2}{}^2\right] \quad \text{for } ^{30}Si,\ J = 2^+ \text{ excited state.}$$

For each of the two β decay transitions from the ^{30}P (1^+), a relationship between the coefficients A, B, C, D, E, F and G can be established. These two relations, along with the normalization conditions

$$A^2 + B^2 + C^2 = 1$$

$$D^2 + E^2 = 1$$

and $$F^2 + G^2 = 1$$

give five constraints among the seven parameters. A further relationship was derived by Dr Watt (University of Glasgow) using the known electromagnetic transition rate from the 2^+ to the 0^+ state in ^{30}Si. It has been shown (Gourlay, 1971) that, although unique values for the

parameters cannot be obtained, the number of solutions is small. All the solutions point to the amount of $d_{3/2}$ mixing in each of the states being larger than that given by Glaudemans et al. (1964). In the case of the ground state of ^{30}P an increase by a factor of about six is obtained.

APPENDIX 2

REVIEW OF MEASUREMENTS OF ϵ/β^+ AND K/β^+ RATIOS FOR ALLOWED TRANSITIONS

The experimental values of K/β^+ ratios for light nuclei ($Z \leq 15$) are reviewed in chapter 2. This appendix contains a description of measurements of K/β^+ and ϵ/β^+ ratios for allowed transitions in nuclei with $Z > 15$. Because of the vast range of errors reported, only those results with an experimental error of 10 per cent or less have been included here. These were arbitrarily considered more reliable, although in some cases the quoted result has been corrected with more recent values of fluorescence yield (Bambynek et al., 1972). Many other measurements of K/β^+ ratios with errors greater than 10 per cent, with decay schemes which are known to be faulty, and with unknown fluorescence yields, have been rejected. Most of these measurements are reviewed elsewhere by Depommier et al. (1960), Bouchez and Depommier (1960) and Berenyi (1963, 1968). The derivation of K/β^+ ratios from ϵ/β^+ measurements is described in chapter 3 where the experimental results reviewed in this appendix are compared with theory.

^{22}Na

The measurement of the K/β^+ ratio for this isotope by McCann and Smith (1969) has already been described in chapter 2. For the reasons given in that chapter the measurements of the ϵ/β^+ ratio were not considered in reaching conclusions about exchange-overlap corrections. However, for completeness, the experimental ϵ/β^+ results for this isotope are included here.

The decay of ^{22}Na to the 1.274 MeV excited state of ^{22}Ne is a pure

Gamow-Teller decay with a positron end point energy of 545.7 ± 0.5 keV. There have been many measurements of the ϵ/β^+ ratio for ^{22}Na but the results seem to fall into two distinct groups. According to Leutz and Wenninger (1967), the weighted mean of all measurements made before 1960 is 0.1130 ± 0.0035 while the more recent results are in considerable disagreement with this value. Only these recent measurements are described here.

Reference	Technique	ϵ/β^+
Williams 1964	$4\pi\,\beta$-γ coincidence method using a 4π proportional counter for β^+ and NaI(Tl) crystals for gamma rays	0.1041 ± 0.0007
Leutz and Wenninger 1967	β^+ detected in NaI(Tl) crystal containing ^{22}Na; 1.27 MeV gammas detected in another NaI(Tl) crystal	0.1048 ± 0.0007
Vatai et al. 1968	(i) Coincidences between β^+ in 4π plastic scintillator and 1.27 MeV gammas in NaI(Tl) detector (ii) Coincidences between 0.511 and 1.27 MeV gammas in NaI(Tl) detectors	0.1042 ± 0.0010
MacMahon and Baerg 1970	$4\pi\,\beta$-γ coincidence method	0.1076 ± 0.0003.

Apart from the last measurement, these results are in good agreement. The weighted mean of the first three results is 0.1045 ± 0.0005. The most recent measurement, by MacMahon and Baerg, which is also the most precise, is in significant disagreement with the other results. A private communication with Dr MacMahon indicated that the result is $\epsilon/\beta^+ = 0.1077 \pm 0.0003$, the small change (from 0.1076 to 0.1077) being

due to the correction for the weak transition to the ^{22}Ne ground state. This work by MacMahon and Baerg has not yet been published and appears only as an abstract.

^{44}Sc

This isotope decays to the 1.156 MeV level in ^{44}Ca which decays to the ground state by emission of a gamma ray.

Reference	Technique	ϵ/β^+
Blue and Bleuler 1955	(i) Comparison of relative intensities of 0.511 MeV and nuclear gamma ray for ^{44}Sc and ^{22}Na using NaI(Tl) detector. (Assumed β^+/γ = 0.901 ± 0.005 for ^{22}Na.)	0.072 ± 0.017
	(ii) Coincidences between β^+ in magnetic spectrometer and 1.16 MeV gamma rays in NaI(Tl) detector	
Konijn et al. 1958/59	Coincidences between gamma rays in NaI(Tl) and β^+ in proportional counter	0.023 ± 0.019.

In view of the large errors and the considerable difference between these results they are not considered further and are neglected in the discussion in chapter 3.

^{48}V

There have been several measurements of the ϵ/β^+ ratio for the decay of ^{48}V to the 2.295 MeV level in ^{48}Ti. Most of the experiments involve measurement of the intensities of the positrons, or their annihilation gamma rays, and the 1.31 MeV gamma ray which follows the decay to the 2.295 MeV level. In the early measurements it was assumed

that this level was fed solely by the direct beta decay of ^{48}V. However, Ristinen et al. (1963) found a 0.94 MeV gamma ray forming a triple cascade with the previously known 0.98 and 1.31 MeV gamma rays. Konijn et al. (1967 a) confirmed that electron capture decays to higher levels in ^{48}Ti contribute to the intensity of the 1.31 MeV gamma rays. Consequently, some of the earlier results for the ϵ/β^+ ratio require correction. Many of these results have been reviewed by Konijn et al. (1967 b), who compared the values of P_{β^+} (percentage of positrons per disintegration) obtained by the various authors. The following list of results, with the exception of that of Biryukov et al. (1966) is taken from Konijn et al. (1967 b).

Reference	P_{β^+}
Good et al. 1946	58 ± 4
Sterk et al. 1953	60 ± 4
Casson et al. 1953	45 ± 4 *
Bock 1956	57 ± 3
Konijn et al. 1958/59	56.0 ± 0.6
Ristinen et al. 1963	61 ± 3
Biryukov et al. 1966	51.1 ± 0.7 *
Konijn et al. 1967 b	48.1 ± 1.6 * 50.1 ± 1.6 *

The weighted mean of all these results is $P_{\beta^+} = 53.4$. There are two methods of calculating the standard error of a weighted mean (Topping, 1962), the first (α_e) depending on the external consistency

of the measurements while the second (α_i) depends only on the internal consistency.

In this case

$$\alpha_e = 1.12 \text{ and } \alpha_i = 0.41.$$

According to Topping, the measurements may be regarded as consistent if the ratio α_e/α_i is unity with standard error $1/\sqrt{2n-2}$, (n = number of measurements). However, for the present results the ratio α_e/α_i is 2.73 which is very different from 1 ± 0.25 and it is likely, therefore, that systematic errors are present. This is not unexpected since, as Konijn et al. (1967 b) indicate, the results occur in two distinct groups, one around $P_{\beta^+} = 50$ and the other around $P_{\beta^+} = 59$. Since the recent, precise results are all in the former category only the results marked * in the table are retained.

The weighted mean of these four results is 50.4 with

$$\alpha_e = 0.8, \quad \alpha_i = 0.6, \qquad \alpha_e/\alpha_i = 1.3$$

and $1/\sqrt{2n-2} = 0.4$.

Therefore the results are consistent and the larger of the values α_e and α_i is adopted as the standard error of the weighted mean. Therefore,

$$P_{\beta^+} = 50.4 \pm 0.8.$$

This value together with the decay scheme of Konijn et al. (1967 b) gives

$$\epsilon/\beta^+ = 0.744 \pm 0.013.$$

^{52}Mn

All the measurements of the ϵ/β^+ ratio for the decay of ^{52}Mn to the 3.115 MeV level in ^{52}Cr have been summarized by Konijn et al. (1967 b).

As for ^{48}V, the early results for the ϵ/β^+ ratio require correction since it has been shown by Freedman et al. (1966) that the decay scheme is more complicated than previously assumed. The values of P_{β^+} obtained by Freedman et al. and Konijn et al. are shown below together with the results of earlier measurements.

Reference	P_{β^+}
Good et al. 1946	35 ± 2
Sehr 1954	33 ± 2
Konijn et al. 1958/59	33.8 ± 0.8
Wilson et al. 1962	29.2 ± 2.9 *
Freedman et al. 1966	27 ± 1 *
Konijn et al. 1967 b	26.2 ± 1.1 *
	29.2 ± 0.8 * .

These results fall into two groups, one with values of P_{β^+} around 34 and the other with values around 28. All the recent measurements belong to the latter group and only these results (marked *) have been used to determine the mean value of P_{β^+}.

The weighted mean of these four results is

$$P_{\beta^+} = 27.9 \pm 0.8$$

and, using the decay scheme given by Konijn et al. (1967 b) gives

$$\epsilon/\beta^+ = 1.93 \pm 0.11.$$

^{58}Co

There have been several measurements of both the K/β^+ and the ϵ/β^+

ratios for the decay of this isotope to the 810 keV level in ^{58}Fe.

The measurements of the K/β^+ ratio are described in the table below.

Reference	Technique	K/β^+
Joshi and Lewis 1961	Internal source scintillation counter	4.92 ± 0.09
Kramer et al. 1962	4π proportional counter	4.83 ±0.10
Bambynek et al. 1968	K x-ray emission rate determined using a proportional counter. β^+ emission rate measured by a variety of techniques including 4π pressure counter, Ge(Li) detector and triple coincidence methods	5.05 ± 0.09.

The weighted mean of these results is

$$K/\beta^+ = 4.94 \pm 0.07.$$

The various measurements of the ϵ/β^+ ratio for ^{58}Co are summarized in the following table.

Reference	Technique	ϵ/β^+
Good et al. 1946	Coincidences between gamma rays and 0.511 MeV β^+ annihilation radiation	5.90 ± 0.20
Cook and Tommovec 1956	Comparison of intensities of 810 and 511 keV gamma rays in NaI(Tl) detector	5.9 ± 0.2
Grace et al. 1956	Measurement of P_{β^+} using scintillation counter	6.6 ± 0.8 *

Reference	Technique	ϵ/β^+
Konijn et al. 1958/59	β-gamma coincidences using proportional and scintillation counters	5.67 ± 0.16
Ramaswamy 1961	Coincidences between 810 and 511 keV gamma rays using NaI(Tl) detectors	5.49 ± 0.18
Biryukov et al. 1966	Triple coincidences between 810 keV gamma rays and the two β^+ annihilation gamma rays using 3 scintillation counters	5.48 ± 0.09
Williams 1970	Coincidences between gamma rays in Ge(Li) detector and β^+ in 4π Si(Li) arrangement	5.76 ± 0.04.

(* This result was obtained from the measured value of $P_{\beta+}$ using the decay scheme of Bambynek et al. (1968). Since the error in this measurement is greater than 10 per cent it is not included in the calculation of the weighted mean.)

The weighted mean of the results (excluding Grace et al.) is

$$\epsilon/\beta^+ = 5.71 \pm 0.05.$$

^{57}Ni

This isotope decays by positron emission and electron capture to several states in ^{57}Co. Measurements of the total ϵ/β^+ ratio have been carried out by Friedlander et al. (1950), Konijn et al. (1956 and 1958) and Bakhru and Preiss (1967).

Konijn et al. (1958) and Bakhru and Preiss have also measured the ϵ/β^+ ratios for each of the branches separately. The values of the ϵ/β^+ ratios obtained by these authors are shown below

Energy of excited state in ^{57}Co (MeV)	Konijn et al. 1958	Bakhru and Preiss 1967
1.37	0.805 ± 0.040	1 ± 0.1
1.46	-	2.5 ± 1
1.49	1.438 ± 0.059	1.5 ± 0.08
1.89	18 ± 6	-

In view of the very large error in the ϵ/β^+ ratio for the decay to the 1.89 MeV level this result is rejected.

The level at 1.46 MeV seen by Bakhru and Preiss (1967) has not been confirmed (Lingeman et al., 1967). The ϵ/β^+ ratio for the decay to this level reported by Bakhru and Preiss has, therefore, also been rejected.

The mean values of the ϵ/β^+ ratios for the decays to the 1.37 and 1.49 MeV levels are shown below.

Energy of excited state in ^{57}Co (MeV)	Mean ϵ/β^+
1.37	0.83 ± 0.07
1.49	1.46 ± 0.05.

^{61}Cu

This isotope decays to the ground state and several excited states of ^{61}Ni. The total K/β^+ ratio has been determined by Huber et al. (1949) and Bouchez (1950). Bouchez (1952) has summarized the experimental data and calculated the K/β^+ ratio for the transition to the ground state using the decay scheme of Owen et al. (1950).

Reference	(K/β^+) total	(K/β^+) ground state
Huber et al. 1949	0.32 ± 0.03	0.18 ± 0.03
Bouchez 1950	0.39 ± 0.05	0.22 ± 0.03
	0.44 ± 0.07	0.25 ± 0.03.

All these measurements have errors greater than 10 per cent and are, therefore, neglected.

^{64}Cu

This isotope decays by electron capture and β^+ emission to the ground state of ^{64}Ni, by electron capture to the first excited state of ^{64}Ni and by β^- emission to the ground state of ^{64}Zn.

The only measurement of the ϵ/β^+ ratio for the transition to the ^{64}Ni ground state comes from results obtained by Reynolds (1950) using a mass spectrometer. He measured the ratio of $Z \rightarrow Z - 1$ to $Z \rightarrow Z + 1$ transitions. The efficiency for the detection of electron capture events using this technique is the same as for positron events since the mass spectrometer detects the change $Z \rightarrow Z - 1$ for both. Calculation of the total ϵ/β^+ ratio requires knowledge of the ratio β^-/β^+. Reynolds used the mean of results obtained by Bradt et al. (1946) and Cook and Langer (1948 a) and found

$$(\epsilon/\beta^+)_{total} = 2.32 \pm 0.28.$$

This result is neglected since the error is greater than 10 per cent.

The various measurements of the total K/β^+ ratio are described below.

Reference	Technique	$(K/\beta^+)_{total}$
Cook and Langer 1948 b	K Auger electrons and positrons detected using magnetic spectrometer	3.5 ± 1.0 (ω_K not quoted)
Bouchez and Kayas 1949	β^+ annihilation radiation detected in ionization chamber and K x-rays in G-M counters	2.65 ± 0.40 (ω_K = 0.37)
Huber et al. 1949	x-rays and β^+ annihilation radiation detected in G-M counters	1.75 ± 0.2 (ω_K not quoted)
Plassmann and Scott 1951	As Cook and Langer 1948 b	2.18 ± 0.20 (ω_K = 0.45).

Of these results only that of Plassmann and Scott has an error less than 10 per cent. These authors used a value of 0.45 for the fluorescence yield. If the value due to Bambynek et al. (1972) is adopted (i.e. $\omega_K = 0.414 \pm 0.028$) their result becomes

$$(K/\beta^+)_{total} = 2.01 \pm 0.22.$$

The K/β^+ ratio for the transition to the ground state derived from this result using Reynolds' decay scheme is

$$K/\beta^+ = 1.99 \pm 0.22.$$

This result is retained although the error is greater than 10 per cent since the contribution to this error from the experimental result is less than 10 per cent.

^{65}Zn

^{65}Zn decays by electron capture to a 1.115 MeV excited state and by electron capture and positron emission to the ground state of ^{65}Cu. The early measurements are summarized by Yuasa (1952). These results are not included here since the agreement between the results is

extremely bad and the experimental accuracies are poor. Many of the measurements described below are of total K/β^+ ratios, the K/β^+ ratio for the transition to the ground state being calculated using the branching ratio of electron capture to the ground state and 1.14 MeV excited state.

Reference	Technique	$(K/\beta^+)_{total}$	$(K/\beta^+)_{ground\ state}$
Major 1952	Coincidences between K x-rays and positrons in G-M counters	39.5 ± 2.6	21.3 ± 1.4
Yuasa 1952	K Auger electrons and positrons detected using magnetic spectrometer	40.5 ± 5.0	21.8 ± 2.7
Perkins and Haynes 1953	As Yuasa (1952)	50.8 ± 5.8 (ω_K=0.44±0.04)	28.0 ± 3.2
Avignon 1956	Proportional counter with internal source	47 ± 5 (ω_K = 0.42)	26 ± 3
Hammer 1968	x-rays and annihilation gamma rays detected in NaI(Tl) detectors	-	27.7 ± 1.5 (ω_K = 0.4425)

Major (1952) and Yuasa (1952) do not state the value of fluorescence yield, ω_K, used to obtain their quoted results and these measurements are, therefore, neglected. The result quoted by Perkins and Haynes (1953) has an error greater than 10 per cent, however a large fraction of this error comes from the error in the value of ω_K they adopted. If the more recent value, $\omega_K = 0.445 \pm 0.009$ (Bambynek et al., 1972) is adopted, their result becomes

$$(K/\beta^+)_{ground\ state} = 28.0 \pm 1.8.$$

Avignon (1956) also quotes an error greater than 10 per cent but since

this arises solely from his experimental results and does not include any error in ω_K, this result is rejected.

The weighted mean of the results of Hammer (1968) and the revised Perkins and Haynes (1953) is

$$(K/\beta^+)_{\text{ground state}} = 27.8 \pm 1.2.$$

Gleason (1959) measured the ϵ/β^+ ratio for the transition to the ground state using NaI(Tl) detectors and found

$$\epsilon/\beta^+ = 27.6 \pm 2.4.$$

^{68}Ga

The K/β^+ ratios for the transitions to the ground state and first excited state (at 1.078 MeV) of ^{68}Zn have been measured by Ramaswamy (1959) using NaI(Tl) detectors. The values obtained are

$K/\beta^+ = 1.28 \pm 0.12$ for the transition to the 1.078 MeV state

and $K/\beta^+ = 0.10 \pm 0.02$ for the transition to the ground state.

This latter result is not considered further since it has an error greater than 10 per cent.

^{89}Zr

(i) Decay of ^{89}Zr to the 0.91 MeV level in ^{89}Y

The early measurements of the ϵ/β^+ ratio for this transition are reviewed by Monaro et al. (1961) but as the results show a wide range of values and the experimental accuracy is poor, they are not included here. Only the more recent results are described below.

Reference	Technique	ϵ/β^+
Monaro et al. 1961	Comparison of intensities of 0.91 and 0.511 MeV gamma rays in NaI(Tl) detector	3.54 ± 0.14
Van Patter and Shafroth 1964	As above including corrections to number of 0.91 MeV gamma for cascades following electron capture decays to higher levels	3.43 ± 0.10 *
Monaro et al. 1961 (revised)	Corrected by Van Patter and Shafroth for cascades contributing to the intensity of the 0.91 MeV gamma rays	3.48 ± 0.15 *
Hinrichsen 1968	Comparison of intensities of 0.91 and 0.511 MeV gamma rays in Ge(Li) detector - corrected for cascades	3.47 ± 0.21 *.

The weighted mean of the results marked * is

$$\epsilon/\beta^+ = 3.45 \pm 0.08.$$

(ii) Decay of ^{89m}Zr to the 1.51 MeV level in ^{89}Y

The measurements of the ϵ/β^+ ratio for this transition listed by Shore et al. (1953) have a mean value of $4.7 \, {}^{+\,2.3}_{-\,1.8}$. Because of the extremely large errors these results are not included here. In a more recent measurement, Van Patter and Shafroth (1964) observed a peak due to the summing of the 1.51 MeV gamma ray and a 0.511 MeV positron annihilation gamma ray in a NaI(Tl) detector. They determined the ϵ/β^+ ratio from the relative intensities of this sum peak and the 1.51 MeV photopeak. They found

$$\epsilon/\beta^+ = 3.76 \pm 0.19.$$

^{111}Sn

The decay scheme of this isotope has been studied extensively by Rivier and Moret (1971). ^{111}Sn decays by electron capture and positron emission to the ground state and several excited states in ^{111}In which decays by electron capture to ^{111}Cd. The measurements of the total ϵ/β^+ ratio for the decay of ^{111}Sn are listed below.

Reference	Technique	Total ϵ/β^+
McGinnis 1951	Positrons from ^{111}Sn and conversion electrons from the 247 keV transition in ^{111}Cd detected using magnetic spectrometer	2.50 ± 0.25
Snyder and Pool 1965	K x-rays and 0.511 MeV gamma rays observed in NaI(Tl) detector	2.7 ± 0.2
Rivier and Moret 1971	Coincidences between 511 keV and γ rays in NaI(Tl) detectors	2.44 ± 0.15.

The result of McGinnis is neglected because of its large error. Snyder and Pool measured the number of K x-rays and positrons but quote their result as a measurement of the ϵ/β^+ ratio rather than the K/β^+ ratio. Because of this uncertainty this result is also rejected.

The ϵ/β^+ ratio for the decay to the ^{111}In ground state derived from the total ϵ/β^+ ratio given by Rivier and Moret is

$$\epsilon/\beta^+ = 2.20 \pm 0.15.$$

^{115}Sb

^{115}Sb decays mainly to the 499 keV level in ^{115}Sn. Kiselev and Burmistrov (1969) measured the relative intensities of the 499 keV gamma ray and the 511 keV positron annihilation radiation. This

measurement enables the ϵ/β^+ ratio to be determined but Kiselev and Burmistrov give a value for the K/β^+ ratio ($K/\beta^+ = 1.22 \pm 0.06$) without stating how this result was obtained from the measurements they made. This result is, therefore, neglected.

^{118m}Sb

Bolotin et al. (1961) showed that ^{118m}Sb decays entirely to the 2.57 MeV level in ^{118}Sn, which decays with the emission of a 254 keV gamma ray. They measured the ϵ/β^+ ratio for this transition by taking triple coincidences between two 511 keV annihilation gamma rays and the 254 keV gamma rays. They found that (0.16 ± 0.01) per cent of the decays occur by positron emission. This leads to

$$\epsilon/\beta^+ = 620 \pm 40.$$

^{134}La, ^{140}Pr, ^{141}Nd and ^{143}Sm

These isotopes have been studied by Biryukov and Shimanskaya (1970) who measured the total K/β^+ ratio for each isotope using a 4π CsI(Tl) crystal. Two measurements were made with each source, one with the source surrounded with lead to stop all the positrons and enable the 511 keV β^+ annihilation gamma rays to be counted, and the other without the lead to count the K x-rays. The K/β^+ ratios were then derived probably using as values of the fluorescence yield the results of Wapstra et al. (1959) although this is not certain. They also studied the decay schemes of the isotopes to determine the K/β^+ ratios for the transition to the ground state of the daughter nucleus. The results they obtained are given below.

Isotope	K/β^+
^{134}La	0.40 ± 0.04
^{140}Pr	0.74 ± 0.03
^{141}Nd	28 ± 1
^{143}Sm	0.92 ± 0.09.

The reference (Biryukov and Shimanskaya, 1970) from which the results shown above were taken, is a review paper and does not give details or references for the individual experiments. Some references have been obtained by the present author(^{134}La : Biryukov et al., 1965, ^{140}Pr : Biryukov and Shimanskaya, 1962, ^{143}Sm : Belyanin et al., 1966) but not all the results given in these papers are as quoted in the 1970 review paper. It is possible that some of the results were revised and, therefore, the latest results (from Biryukov and Shimanskaya, 1970) have been adopted here.

The mean values of the K/β^+ and ϵ/β^+ ratios for allowed transitions described in this appendix are listed in chapter 3. Several measurements of K/β^+ and ϵ/β^+ have not been included in this review. These include results with errors greater than 10 per cent or with no errors quoted. Measurements of total K/β^+ or ϵ/β^+ ratios for isotopes with complicated or incompletely known decay schemes have also been omitted, e.g.

^{79}Kr (Langhoff et al., 1966), ^{108}Ag (Frevert et al., 1965), ^{107}Cd (Bradt et al., 1945), ^{155}Dy (Persson et al., 1963).

References

Alvarez, L.W., 1937, Phys. Rev. 52, 134.

Alvarez, L.W., 1938, Phys. Rev. 54, 486.

Avignon, P., 1956, Ann. de Phys. 1, 10.

Bahcall, J.N., 1962, Phys. Rev. Lett. 9, 500.

Bahcall, J.N., 1963a, Phys. Rev. 129, 2683.

Bahcall, J.N., 1963b, Phys. Rev. 131, 1756.

Bahcall, J.N., 1963c, Phys. Rev. 132, 362.

Bahcall, J.N., 1965, Nucl. Phys. 71, 267.

Bakhru, H. and Preiss, I.L., 1967, Phys. Rev. 154, 1091.

Bambynek, W., De Roost, E. and Funckh, E., 1968, Proc. Conference on Electron Capture and Higher Order Processes in Nuclear Decay, Debrecen (Budapest: Eötvös Lóránd Phys. Soc.) p.253.

Bambynek, W., Crasemann, B., Fink, R.W., Freund, H.-U., Mark, H., Swift, C.D., Price, R.E. and Venugopala Rao, P., 1972, Rev. Mod. Phys. 44, 716.

Band, I.M., Zyrianova, L.N. and Chen-Zhui, T., 1956, Izv. Akad. Nauk. SSSR, Ser. Fiz. 20, 1387.

Band, I.M., Zyrianova, L.N. and Suslov, Yu.P., 1958, Izv. Akad. Nauk. SSSR, Ser. Fiz. 22, 952.

Barker, P.H. and Connor, R.D., 1967, N.I.M. 57, 147.

Bearden, J.A., 1967, Rev. Mod. Phys. 39, 78.

Behrens, H. and Jänecke, J., 1969, Landolt-Börnstein, New Series, Group 1, Vol.4 (Berlin: Springer-Verlag).

Belyanin, Yu.I., Biryukov, E.I. and Shimanskaya, N.S., 1966, Izv. Akad. Nauk. SSSR, Ser. Fiz. 30, 1130 (1966, Bull Acad. Sci. USSR, Phys. Ser. 30, 1182).

Benoist-Gueutal, P., 1950, C.R. Acad. Sci., Paris 230, 624.

Benoist-Gueutal, P., 1953, Ann. de Phys. 8, 593.

Berenyi, D., 1963, Nucl. Phys. 48, 121.

Berenyi, D., 1968, Rev. Mod. Phys. 40, 390.

Campbell, J.L., Leiper, W., Ledingham, K.W.D. and Drever, R.W.P., 1967, Nucl. Phys. A96, 279.

Carlson, T.A., 1963, Phys. Rev. 132, 2239.

Casson, H., Goodman, L.S. and Krohn, V.E., 1953, Phys. Rev. 92, 1517.

Cook, C.S. and Langer, L.M., 1948a, Phys. Rev. 73, 601.

Cook, C.S. and Langer, L.M., 1948b, Phys. Rev. 74, 1241.

Cook, C.S. and Tomnovec, F.M., 1956, Phys. Rev. 104, 1407.

Cooper, J.A., Hollander, J.M., Kalkstein, M.I. and Rasmussen, J.O., 1965, Nucl. Phys. 72, 113.

Costa, S., Ferrero, F., Ferroni, S., Pasqualini, L. and Silva, E., 1965, Nucl. Phys. 72, 158.

Cretzu, T., Hohmuth, K. and Schintlmeister, J., 1965, Ann. der Phys. 16, 312.

Das, N.C., Pathak, B.P. and Mukherjee, S.K., 1969, Proc. Nucl. Phys. and Solid State Symposium, University of Rourkee, Dept. of Atomic Energy, Bombay, Vol.2, p.178.

Davisson, C.M., 1965, Alpha-, Beta- and Gamma-Ray Spectroscopy, ed. K. Siegbahn (Amsterdam: North-Holland).

De Barros, S., Maurenzig, P.R., Baptista, G, and Canto, L.F., 1970, Z. Naturforsch. 25a, 1250.

Del Bianco, W.E. and Stephens, W.E, 1962, Phys. 126, 709.

Depommier, P., Nguyen-Khac, U. and Bouchez, R., 1960, J. Phys. Radium 21, 456.

Dewey, R.D., Mapes, R.S. and Reynolds, T.W., 1969, Progress in Nuclear Energy, Series IX, Analytical Chemistry (Pergamon Press) Vol. 9.

Drever, R.W.P., Moljk, A. and Scobie, J.,1956, Phil. Mag. 1, 942.

Dzhelepov, B.S. and Zyrianova, L.N., 1956, Influence of Atomic Electric Fields on Beta Decay (Bull. Acad. Sci. USSR, Moscow - Leningrad).

Ebrey, T.G. and Gray, P.R., 1965, Nucl. Phys. 61, 479.

Engelbertink, G.A.P. and Brussaard, P.J., 1966, Nucl. Phys. 76, 442.

Endt, P.M. and Van Der Leun, C., 1967, Nucl. Phys. A105, 1.

Evans, R.D., 1955, The Atomic Nucleus, (McGraw-Hill).

Faessler, A., Huster, E., Krafft, O. and Krahn, F., 1970, Z. Phys. 238, 352.

Feenberg, E. and Trigg, G., 1950, Rev. Mod. Phys. 22, 399.

Fermi, E., 1934, Z. Phys. 88, 161.

Feynman, R.P. and Gell-Mann, M., 1958, Phys. Rev. 109, 193.

Fierz, M., 1937, Z. Phys. 104, 553.

Fink, R.W., 1968, Nucl. Phys. A110, 379.

Frauenfelder, H., Bobone, R., Von Goeler, E., Levine, N., Lewis, H.R., Peacock, R.N., Rossi, A. and DePasquali, G., 1957, Phys. Rev. 106, 386 and
Frauenfelder, H., Hansen, A.O., Levine, N., Rossi, A. and DePasquali, G., 1957, Phys. Rev. 107, 643.

Frauenfelder, H. and Steffen, R.M., 1965, Alpha-, Beta- and Gamma-Ray Spectroscopy, ed. K. Siegbahn (Amsterdam: North-Holland).

Freedman, M.S., Wagner Jr., F., Porter, F.T. and Bolotin, H.H., 1966, Phys. Rev. 146, 791.

Frevert, L., Schöneberg, R. and Flammersfeld, A., 1965, Z. Phys. 182, 439.

Friedlander, G., Perlman, M.L., Alburger, D.E. and Sunyar, A.W., 1950, Phys. Rev. 80, 30.

Froese, C., 1965, Phys. Rev. 137A, 1644.

Froese Fischer, C., 1969, Comp. Phys. Comm. 1, 151.

Gell-Mann, M., 1958, Phys. Rev. 111, 362.

Girgis, R.K. and Van Lieshout, R., 1959, Nucl. Phys. 12, 672.

Glaudemans, P.W.M., Weichers, G. and Brussaard, P.J., 1964, Nucl. Phys. 56, 529.

Gleason, G.I., 1959, Phys. Rev. 113, 287.

Goldhaber, M., Grodzins, L. and Sunyar, A.W., 1958, Phys. Rev. 109, 1015.

Good, W.M., Peaslee, D. and Deutsch, M., 1946, Phys. Rev. 69, 313.

Goulding, F.S., Walton, J. and Malone, D.F., 1969, N.I.M. 71, 273.

Gourlay, J.Y., 1971, Ph.D. Thesis, University of Glasgow.

Grace, M.A., Jones, G.A. and Newton, J.O., 1956, Phil. Mag. 1, 363.

Hammer, J.W., 1968, Z. Phys. 216, 355.

Haustein, P.E. and Voigt, A.F., 1971, J. Inorg. Nucl. Chem. 33, 289.

Herman, F. and Skillman, S., 1963, Atomic Structure Calculations, (Prentice-Hall).

Hesse, K. and Finckh, E., 1970, Nucl. Phys. A141, 417.

Hinrichsen, P.F., 1968, Nucl. Phys. A118, 538.

Huber, O., Rüetschi, R. and Scherrer, P., 1949, Helv. Phys. Acta 22, 375.

Huffaker, J.N. and Greuling, E., 1963, Phys. Rev. 132, 738.

Johnson, C.H., Pleasonton, F. and Carlson, T.A., 1963, Phys. Rev. 132, 1149.

Joshi, B.R. and Lewis, G.M., 1961, Proc. Phys. Soc. 78, 1056.

Katz, L., Baker, R.G. and Montalbetti, R., 1953, Can. J. Phys. 31, 250.

Kiselev, B.G. and Burmistrov, V.R., 1969, Yadern. Fiz. 10, 1105.

Konijn, J., Van Nooijen, B., Mostert, P. and Endt, P.M., 1956, Physica 22, 887.

Konijn, J., Hagedoorn, H.L. and Van Nooijen, B., 1958, Physica 24, 129.

Konijn, J., Van Nooijen, B., Hagedoorn, H.L. and Wapstra, A.H., 1958/59 Nucl. Phys. 9, 296.

Konijn, J., Lingeman, E.W.A. and De Wit, S.A., 1967a, Nucl. Phys. A90, 558.

Konijn, J., Lewin, W.H.G., Van Nooijen, B., Van Beek, H.F., De Wit, S.A. and Lingeman, E.W.A., 1967b, Nucl. Phys. A102, 129.

Konopinski, E.J. and Langer, L.M., 1953, Ann. Rev. Nucl. Sci. 2, 261.

Kramer, P., De Beer, A. and Blok, J., 1962, Physica 28, 587.

Landis, D.A., Goulding, F.S., Pehl, R.H. and Walton, J.T., 1971, IEEE Trans. Nucl. Sci. NS - 18, 115.

Landis, D.A., Goulding, F.S. and Jarrett, B.V., 1972, N.I.M. 101, 127.

Landau, L.D., 1957, Nucl. Phys. 3, 127.

Langhoff, H., Frevert, L., Schött, W. and Flammersfeld, A., 1966, Nucl. Phys. 79, 145.

Lederer, C.M., Hollander, J.M. and Perlman, I., 1967, Table of Isotopes, (John Wiley and Sons, Inc.).

Ledingham, K.W.D., Payne, J.A. and Drever, R.W.P., 1963, Proc. Int. Conf. on Role of Atomic Electrons in Nuclear Transformations (Warsaw), Vol. 2, p.359.

Ledingham, K.W.D., Gourlay, J.Y., Campbell, J.L., Fitzpatrick, M.L., Lynch, J.G. and McDonald, J., 1971, Nucl. Phys. A170, 663.

Lee, T.D. and Yang, C.N., 1956, Phys. Rev. 104, 254.

Leiper, W. and Drever, R.W.P., 1972, Phys. Rev. C6, 1132.

Leutz, H. and Wenninger, H., 1967, Nucl. Phys. A99, 55.

Levinger, J.S., 1960, Nuclear Photo-Disintegration, (Oxford University Press).

Lingeman, E.W.A., Konijn, J., Diederix, F. and Meijer, B.J., 1967, Nucl. Phys. A100, 136.

McCann, M.F. and Smith, K.M., 1969, J. Phys. A 2, 392.

McDonald, W.J., Bucholz, E. and Haslam, R.N.H., 1963, Can. J. Phys. 41, 180.

McGinnis, C.L., 1951, Phys. Rev. 81, 734.

MacMahon, T.D. and Baerg, A.P., 1970, Bull. Am. Phys. Soc., Ser II, Vol. 15, no. 6 and
1970, Physics in Canada, Vol. 26, no. 4.

Major, J.K., 1952, C.R.Acad. Sci., Paris 234, 2276.

Martin, M.J. and Blichert-Toft, P.H., 1970, Nucl. Data Tables A8, 1.

Massey, H.S.W. and Kestelman, H., 1964, Ancillary Mathematics (Pitman).

Matsuki, S., Nakamura, S., Hyakutake, M., Matoba, M., Yoshida, Y. and Kumabe, I., 1973, Nucl. Phys. A201, 608.

Moljk, A., Drever, R.W.P. and Curran, S.C., 1958, Proc. Int. Conf. on Radioisotopes in Scientific Research, Paris, p.596.

Møller, C., 1937, Phys. Rev. 51, 84.

Monaro, S., Vingiani, G.B. and Van Lieshout, R., 1961, Physica 27, 985.

Morinaga, H. and Bleuler, E., 1956, Phys. Rev. 103, 1423.

Mutsuro, N., Ohnuki, Y., Sato, K. and Kimura, M., 1959, J. Phys. Soc. Japan 14, 1649.

Neiler, J.H. and Bell, P.R., 1965, Alpha-, Beta- and Gamma-Ray Spectroscopy, ed. K. Siegbahn (Amsterdam: North-Holland).

Odiot, S. and Daudel, R., 1956, J. Phys. Radium 17, 60.

Owen, G.E., Cook, C.S. and Owen, P.H., 1950, Phys. Rev. 78, 686.

Pagden, I.M.H., Pearson, G.J. and Bewers, J.M., 1971, J. Radio. Anal. Chem. 8, 373.

Pahor, J., Kodre, A. and Moljk, A., 1968, Nucl. Phys. A109, 62.

Perkins, J.F. and Haynes, S.K., 1953, Phys. Rev. 92, 687.

Persson, L., Ryde, H. and Oelsner-Ryde. K., 1963, Nucl. Phys. 44, 653.

Plassmann, E. and Scott, F.R., 1951, Phys. Rev. 84, 156.

Powell, M.J.D., 1964, Computer J. 7, 155.

Ramaswamy, M.K., 1959, Nucl. Phys. 10, 205.

Ramaswamy, M.K., 1961, Indian J. Phys. 35, 610.

Reines, F. and Cowan, C.L., 1959, Phys. Rev. 113, 273.

Reynolds, J.H., 1950, Phys. Rev. 79, 789.

Ristinen, R.A., Bartlett, A.A. and Kraushaar, J.J., 1963, Nucl. Phys. 45, 321.

Rivier, J. and Moret, R., 1971, C.R. Acad. Sci., Paris B272, 1022.

Robinson, D.C., Freeman, J.M. and Thwaites, T.T., 1972, Nucl. Phys. A181, 645.

Rosenbrock, H.H., 1960, Computer J. 3, 175.

Routti, J.T. and Prussin, S.G., 1969, N.I.M. 72, 125.

Salam, A., 1957, Nuovo Cim. 5, 299.

Salem, S.I., Falconer, T.H. and Winchell, R.W., 1972, Phys. Rev. A6, 2147.

Schopper, H.F., 1966, Weak Interactions and Nuclear Beta Decay (Amsterdam: North-Holland).

Scobie, J. and Lewis, G.M., 1957, Phil. Mag. 2, 1089.

Sehr, R., 1954, Z. Phys. 137, 523.

Sherr, R. and Miller, R.H., 1954, Phys. Rev. 93, 1076.

Shore, F.J., Bendel, W.L., Brown, H.N. and Becker, R.A., 1953, Phys. Rev. 91, 1203.

Slivinsky, V.W. and Ebert, P.J., 1969, Phys. Lett. 29A, 463.

Smith Jr., F.B., Gove, N.B., Henry, R.W. and Becker, R.A., 1956, Phys. Rev. 104, 706.

Snyder, J.W. and Pool, M.L., 1965, Phys. Rev. 138B, 770.

Sterk, M.J., Wapstra, A.H. and Kropveld, R.F.W., 1953, Physica, 19, 135.

Suslov, Yu.P., 1968, Proc. Conference on Electron Capture and Higher Order Processes in Nuclear Decay, Debrecen (Budapest: Eötvös Lóránd Phys. Soc.) p.51.

Suslov, Yu.P., 1970, Izv. Akad. Nauk. SSSR, Ser. Fiz. 34, 97 (1970, Bull. Acad. Sci. USSR, Phys. Ser. 34, 91).

Topping, J., 1962, Errors of Observation and their Treatment (Chapman and Hall Ltd.).

Van Lieshout, R., 1965, Alpha-, Beta- and Gamma-Ray Spectroscopy, ed. K. Siegbahn (Amsterdam: North-Holland).

Van Patter, D.M. and Shafroth, S.M., 1964, Nucl. Phys. 50, 113.

Vatai, E., 1968, Proc. Conference on Electron Capture and Higher Order Processes in Nuclear Decay, Debrecen (Budapest: Eötvös Lóránd Phys. Soc.) p.71.

Vatai, E., 1970, Nucl. Phys. A156, 541.

Vatai, E., 1971, Phys. Lett. 34B, 395.

Vatai, E., Varga, D. and Uchrin, J., 1968, Nucl. Phys. A116, 637.

Wapstra, A.H., Nijgh, G.J. and Van Lieshout, R., 1959, Nuclear Spectroscopy Tables (Amsterdam: North-Holland).

Wapstra, A.H. and Gove, N.B., 1971, Nucl. Data Tables 9, 267.

Watson, R.E. and Freeman, A.J., 1961, Phys. Rev. 123, 521 and 1961, Phys. Rev. 124, 1117 and
Watson, R.E., 1960, Phys. Rev. 119, 1934.

Weinberg, S., 1958, Phys. Rev. 112, 1375.

Wilkinson, D.H., 1970, Phys. Lett. 31B, 447.

Wilkinson, D.H. and Alburger, D.E., 1971, Phys. Rev. Lett. 26, 1127.

Williams, A., 1964, Nucl. Phys. 52, 324.

Williams, A., 1970, Nucl. Phys. A153, 665.

Wilson, R.R., Bartlett, A.A., Kraushaar, J.J., McCullen, J.D. and Ristinen, R.A., 1962, Phys. Rev. 125, 1655.

Winter, G., 1968, Nucl. Phys. A113, 617.

Wu, C.S., Ambler, E., Hayward, R.W., Hoppes, D.D. and Hudson, R.P., 1957, Phys. Rev. 105, 1413.

Wu, C.S. and Moszkowski, S.A., 1966, Monographs and Texts in Physics and Astronomy, ed. R.E. Marshak, Vol. XVI, Beta Decay, (Interscience Publishers).

Yuasa, T., 1952, Physica 18, 1267.

Yukawa, H. and Sakata, S., 1936, Proc. Phys.-Math. Soc. Japan 18, 128.

Zweifel, P.F., 1957, Phys. Rev. 107, 329.

Zyrianova, L.N., 1963, Once Forbidden Beta Transitions (Pergamon Press) p.40.

Zyrianova, L.N. and Suslov, Yu.P., 1968, Proc. Conference on Electron Capture and Higher Order Processes in Nuclear Decay, Debrecen (Budapest: Eötvös Lóránd Phys. Soc.) p.234.

Zyrianova, L.N. and Suslov, Yu.P., 1970, Bull. Acad. Sci. USSR, Phys. Ser. 34, 95.